MICROBIAL COMMUNITY DYNAMICS WITHIN A SERPENTINIZATION-INFLUENCED AQUIFER: CHARACTERIZATION OF COMMUNITY ASSEMBLY PROCESSES AND RESPONSES TO DRILLING-INDUCED PERTURBATIONS

By

Lindsay Irene Putman

A DISSERTATION

Submitted to
Michigan State University
in partial fulfillment of the requirements
for the degree of

Environmental Geosciences—Doctor of Philosophy
Microbiology and Molecular Genetics—Dual Major

2021

ABSTRACT

MICROBIAL COMMUNITY DYNAMICS WITHIN A SERPENTINIZATION-INFLUENCED AQUIFER: CHARACTERIZATION OF COMMUNITY ASSEMBLY PROCESSES AND RESPONSES TO DRILLING-INDUCED PERTURBATIONS

By

Lindsay Irene Putman

Serpentinization is the hydrothermal alteration of ultramafic rock, which results in high pH, reducing fluids that are low in dissolved inorganic carbon, and have high levels of methane and hydrogen. While endemic microbial communities have been well-characterized from a variety of marine and terrestrial serpentinizing ecosystems, to date the ecological processes that contribute to microbial community assembly, community dynamics, and the impact of disturbances in serpentinizing environments have not yet been assessed.

The work in this dissertation was performed at the Coast Range Ophiolite Microbial Observatory, CA, USA, where a series of wells were drilled in 2011 to access serpentinization-influenced fluids directly from the subsurface. Geochemical and 16S rRNA gene amplicon datasets were collected directly from these wells and a series of microcosm experiments were performed on fluids from the site. Samples collected over the course of six years were used to assess community assembly processes and the biogeochemical impacts of drilling fluid injection into the subsurface. A series of microcosm experiments were also performed to better understand the response of microbial populations to geochemical changes observed *in situ* following drilling. Results from this work will inform studies of biogeochemical dynamics relevant to modern and ancient Earth and extraterrestrial sites such as Mars. These data further our understanding of microbial community responses to environmental perturbations and provide information that will aid in the development of future drilling and monitoring projects focused on learning about life in the deep subsurface.

This thesis is dedicated to my daughter, Adelaide.
May the beauty of the natural world always inspire curiosity within you.

ACKNOWLEDGEMENTS

The work within this dissertation would not have been possible without the support of many people in my life. I am thankful for the support and guidance I received during my degree from my scientific, professional, and personal relationships.

Firstly, I would like to thank my PhD advisor, Dr. Matthew Schrenk, for giving me the opportunity to work in your lab the summer of 2015, and continuing to guide me through my schooling, research, and career path. You have been a wonderful teacher, mentor, colleague, and friend. It was a true blessing to have an advisor who was always available to brainstorm, talk, review data, and edit proposals and manuscripts. More importantly, you always supported and advocated for, the research, teaching, service, personal goals, and decisions of your students. I will deeply miss working in your lab every day, but I look forward to continuing to work with you as a colleague in the future. Thank you for being such a wonderful role model.

I would like to thank the community of scientific support I received from Michigan State University, and the Rock Powered Life scientific team. Thank you to my guidance committee, Drs. Sarah Evans, Dalton Hardisty, Robert Hausinger, and Seth Jacobson. Your questions, critiques, and shared scientific experience have all helped mold me into the scientist I am today. I would like to thank former lab members and collaborators who were instrumental in helping me throughout my degree: Dr. Danielle Morgan-Smith, Dr. Katrina Twing, Dr. David Hyndman, Dr. William Brazelton, Michael Kubo, Mary Sabuda, Heather Miller, Osama Alian, and numerous undergraduate researchers who helped me with my work over the years. The support and help from the Schrenk lab and others made this experience a wonderful one and will hopefully continue in future friendship and collaboration.

I am grateful for the multitude of professional development activities I was able to participate in at Michigan State University. I would like to thank the Departments of Earth and Environmental Sciences and Microbiology and Molecular Genetics for their professional development activities over the years and their support of professional development activities outside of Michigan State University. I would like to thank Dr. Osvaldo Hernandez and Dr. David Long for their mentorship and guidance during my teaching experiences at Michigan State. Additionally, I would like to thank Dr. David Long for helping me complete the Certification in College Teaching by serving as my teaching project sponsor and mentor, and for being an excellent teacher and mentor to me during my time at Michigan State.

Finally, I would like to thank my family and friends for their never ending support during the five years of my graduate degree. I would like to thank my parents, Nancy and Steve Williams, and my sisters, Melissa and Natalie Williams, for always supporting my decision to pursue a PhD, and listening to my struggles despite being unsure exactly what it is I do. I would like to thank my daughter Adelaide. The news of your impending arrival to this world helped motivate me to finish my degree. Thank you for being a happy, calm baby who started sleeping through the night early on! I loved having you as my writing buddy during the early months of your life. Lastly, I would like to thank my best friend, husband, and the love of my life, Greg Putman. You have sacrificed time, energy, and opportunities over the last decade to help me pursue my dreams and this degree. You are a constant shoulder to lean on, my loudest cheerleader, a confidant, and my favorite person to spend time with. Thank you for changing the course of your life to be with me while I completed this degree.

TABLE OF CONTENTS

LIST OF TABLES vi

LIST OF FIGURES vii

KEY TO ABBREVIATIONS vii

CHAPTER 1 - Introduction 1
Serpentinization 1
Geomicrobiology of Continental Ophiolites 3
Site Description: Coast Range Ophiolite Microbial Observatory 8
Microbial Community Assembly 11
Disturbance Ecology and Effect of Drilling Perturbations on Microbial Communities 14
REFERENCES 18

CHAPTER 2 – Microbial communities in a serpentinizing aquifer are assembled through strong concurrent dispersal limitation and selection 32
Abstract 32
Importance 33
Introduction 33
Results 36
Geochemistry 36
Ecological Modeling Results 37
Physical Controls on Microbial Dispersal 45
Adaptations to Environmental Conditions 47
Discussion 53
Materials and Methods 58
Site Description and Sample Collection 58
Topographic Profile and Cross Section Construction 59
Estimation of Aquifer Properties 59
Tritium Sample Collection 60
Geochemical Analyses 60
Extraction of DNA and RNA 60
Sample Preparation, Sequencing, and Data Analysis of Metagenomes and Metatranscriptomes 61
16S rRNA Gene Amplicon Sequencing 61
16S rRNA Sequence Processing 61
Statistical Analyses 63
Ecological Modeling 64
Sequence Data Availability 65
Acknowledgements 66
APPENDIX 67
REFERENCES 103

CHAPTER 3 – Drilling activity in a serpentinization-influenced aquifer alters subsurface geochemistry and stimulates dominant microbial community members 113
Abstract 113
Introduction 114
Results 116
Geochemical Trends over Time 116
Microbial Community Diversity 118
Identification of Conditionally Rare Taxa 123
Microbial Populations Impacted by Drilling Activity 124
Discussion 129
Materials and Methods 135
Site Description and Sample Collection 135
Geochemical Analyses 136
Extraction of DNA 137
16S rRNA Gene Amplicon Sequencing 137
16S rRNA Sequence Processing 137
Statistical Analyses 138
Sequence Data Availability 139
Acknowledgements 139
APPENDIX 140
REFERENCES 147

CHAPTER 4 – Experimental insights into drilling-induced changes in microbial community structure and geochemistry in a serpentinizing aquifer 157
Abstract 157
Introduction 158
Results 160
Population Growth in Microcosm Experiments 160
Microcosm Geochemistry 162
Microbial Community Composition 168
Discussion 175
Materials and Methods 182
Sample Collection 182
Microcosm Experiment Set-Up and Subsampling Procedures 183
Geochemical Analyses 186
Cell Enumeration 187
Extraction of DNA 187
16S rRNA Gene Amplicon Sequencing 187
16S rRNA Sequence Processing 188
Statistical Analyses 189
Acknowledgements 190
APPENDIX 191
REFERENCES 202

CHAPTER 5 – Summary and Future Directions 212
Summary 212

Future Directions.....214
REFERENCES.....217

LIST OF TABLES

Table 2.1. Description of Community Assembly Processes Associated with Ecological Modeling Results 39

Table 2.2. PERMANOVA Results 47

Table A.1. Metadata 91

Table A.2. Ecological Modeling Results 94

Table A.3. Ecological Modeling and Metadata Mantel Test Results 95

Table A.4. May 2017 Tritium Results 96

Table A.5. Hydrologic Parameter Estimates 97

Table A.6. Alternative PERMANOVA Results 98

Table A.7. Linear Regression Model Results for Regressions of Gene Abundance vs. Environmental Data 99

Table A.8. Well Elevations and Geographic Coordinate System Locations 101

Table A.9. Sequencing Centers Used Through Project Lifetime 102

Table B.1. Metadata 142

Table B.2. Student's T-test Results on Bulk Geochemistry and Alpha Diversity Measures 144

Table B.3. Microbial Community PERMANOVA Results 145

Table B.4. Significant Regression Models on Dominant and CRT OTUs 146

Table C.1. Averaged Microcosm Metadata 194

Table C.2. Raw Microcosm Metadata 196

Table C.3. Drilling Experiment PERMANOVA Results 201

LIST OF FIGURES

Figure 2.1. Average Well Geochemical Parameters Plotted against Depth 36

Figure 2.2. Boxplots of the Distribution of βNTI and RCbray Values within Individual Wells Over Time and Between Wells Over Time 40

Figure 2.3. Bar Plots of Ecological Modeling Results in All Wells, and Neutral, Moderate, and Extreme pH Wells 44

Figure 2.4. Topographic Profile and Cross-Section of the CROMO Aquifer 46

Figure 2.5. Microbial Community Richness and Evenness vs. pH 49

Figure 2.6. Regression Plots of pH Adaptation Genes from Metagenomic and Metatranscriptomic Data against pH 51

Figure 3.1. Geochemistry Time Series Plots 117

Figure 3.2. Richness and Pielou's Evenness Time Series Plots 119

Figure 3.3. NMDS Plot of Bray-Curtis Dissimilarities.....121

Figure 3.4. Taxonomy of Dominant OTUs Over Time 122

Figure 3.5. Dominant and Conditionally Rare OTU Abundance Over Time.....125

Figure 3.6. Dominant and Conditionally Rare OTU Abundance Plotted Against Probe Chemistry 127

Figure 3.7. Dominant and Conditionally Rare OTU Abundance Plotted Against Aqueous Geochemistry 128

Figure 4.1. Subsampling Schematic Cartoon.....161

Figure 4.2. Cell Abundance Over Time.....162

Figure 4.3. Gas and Aqueous Geochemistry Over Time.....164

Figure 4.4. Richness and Pielou's Evenness Index of Microcosm Microbial Communities.....169

Figure 4.5. NMDS Plot Microcosm Microbial Communities.....171

Figure 4.6. Taxonomy of Dominant OTUs in T0 and Final Time Point Microbial Communities..... 173

Figure A.1. Stacked Bar Plot of the Relative Abundance of the 50 Most Abundant OTUs by Taxonomic Order 80

Figure A.2. Significant Regression Plots of βNTI Values against Environmental Data 81

Figure A.3. Significant Regression Plots of RCbray Values against Environmental Data 82

Figure A.4. Mantel Correlogram of Phylogenetic Distances against pH 83

Figure A.5. Plots of Significant Linear Regression Models of Metagenomic and Metatranscriptomic Data vs. Salinity and Depth 84

Figure A.6. Plots of Significant Linear Regression Models of Metagenomic and Metatranscriptomic Data vs. Oxidation Reduction Potential, Dissolved Inorganic Carbon, and Temperature 86

Figure A.7. Boxplot of Nearest Taxon Index across Wells (2011-2017) 88

Figure A.8. CROMO Merged Sequencing Center Multidimensional Scaling Plot with Samples Colored by Well 89

Figure A.9. Heatmap of Bray-Curtis Dissimilarities of Samples Sequenced at Multiple Sequencing Centers 90

Figure B.1. Additional Geochemistry Time Series Plots 141

Figure C.1. Control Cell Abundance and Geochemistry Plots 192

Figure C.2. Taxonomy of Dominant OTUs in T0 and Final Time Point Controls 193

KEY TO ABBREVIATIONS

CH_4	Methane
CO	Carbon Monoxide
CO_2	Carbon Dioxide
CRO	Coast Range Ophiolite
CROMO	Coast Range Ophiolite Microbial Observatory
CSW	Core Shed Well
DAPI	4’,6-diamidino-2-phenylindole
DGC	Distance-based Greedy Clustering
DIC	Dissolved Inorganic Carbon
DNA	Deoxyribonucleic Acid
DO	Dissolved Oxygen
ERT	Electrical Resistivity Tomography
H_2	Hydrogen
HDPE	High-density Polyethylene
HMC	Homestake Mining Company
LCHF	Lost City Hydrothermal Field
LCMS	Lost City *Methanosarcinales*
LSC	Liquid Scintillation Counting
MSU	Michigan State University
NAI	NASA Astrobiology Institute
NASA	National Aeronautics and Space Administration

NMDS	Nonmetric Multi-Dimensional Scaling
ORP	Oxidation Reduction Potential
OTU	Operational Taxonomic Unit
QV	Quarry Valley
rRNA	Ribosomal Ribonucleic Acid
RPL	Rock Powered Life
SEO	Santa Elena Ophiolite
SVC	Stonyford Volcanic Complex
UC-Davis	University of California Davis
UW-EIL	University of Waterloo Environmental Isotope Laboratory

CHAPTER 1

Introduction

Serpentinization

Serpentinization is the water-rock reaction where iron(II)-bearing minerals, olivine ($(Mg,Fe)_2SiO_4$) and orthopyroxene ($(Mg,Fe)_2Si_2O_6$), react with water to form serpentine minerals ($(Mg,Fe)_3(Fe,Si)_2O_5(OH)_4$), brucite ($(Mg,Fe)(OH)_2$), magnetite ($Fe_3O_4$), and molecular hydrogen (H_2) (1). The general reaction for this process is shown in equation 1:

$$(Mg,Fe)_2SiO_4 + (Mg,Fe)_2Si_2O_6 + wH_2O \rightarrow 1/2\ ((Mg,Fe)_3(Fe,Si)_2O_5(OH)_4 + x(Mg,Fe)(OH)_2 + y\ Fe_3O_4 + zH_2 \quad \text{(Eq. 1)}$$

In equation 1, modified from Preiner et al. (1), the stoichiometric coefficients *w*, *x*, *y*, and *z* are variable and depend on a variety of factors such as temperature and pressure of the local environment, and the relative proportions of mineral phases present within different ultramafic formations (1).

The above reaction (Eq. 1) oxidizes ferrous iron (Fe^{2+}) present in olivine and orthopyroxene to ferric iron (Fe^{3+}) which primarily forms magnetite as a product of the reaction. The oxidation of iron in the mineral phases during the reaction reduces water to H_2 gas and produces hydroxides, which raise fluid pH to hyperalkaline conditions (pH 9-11) (1–5). At these high pH conditions, dissolved inorganic carbon (DIC) speciates primarily as carbonate instead of bicarbonate (6). Calcium and magnesium ions released into solution during water-rock reactions readily combine with carbonate in solution and precipitate out as carbonate mineral assemblages, effectively removing bioavailable DIC from solution (5).

Ultramafic rocks commonly have elevated levels of trace metals, such as nickel (Ni), chromium (Cr), and cobalt (Co) (1,2,7–9). Early in the serpentinization process, while Fe(II) is still abundant in the minerals, FeNi alloys can form from the reduction of Fe(II) oxides and Ni(II) oxides in mineral assemblages by H_2 (1,2). This chemical process forms the commonly found mineral awaruite ($FeNi_3$), which has been shown to behave as a catalyst in H_2-dependent reductions of inorganic carbon (1,10). Awaruite may serve as the metal catalyst needed for Fischer-Tropsch type reactions between H_2 and DIC that produce methane (CH_4) and other simple organic compounds commonly found in serpentinizing environments (1,2,10,11). Synthesis of bioavailable organic carbon is important within serpentinizing systems, especially considering the low availability of DIC due to hyperalkaline fluid conditions (5).

Serpentinization can occur anywhere where water and ultramafic rock come in contact. Ultramafic deposits are common on modern Earth (8,12) and found in a variety of geologic settings including mid-ocean ridges, subduction zones, and continental ophiolites (5). Serpentinizing fluids often mix with fluids such as seawater or circumneutral ground or surface water, which creates natural chemical gradients and disequilibria of which chemosynthetic life can take advantage (13–15). Mixing of these fluids has important biological implications, as seawater and groundwater provide additional oxidants and electron acceptors that are often severely limited in serpentinizing environments (5,16).

Serpentinization is a common contemporary geological process and may have been even more pervasive on early Earth when ultramafic lithologies were likely more prevalent on the surface (1,2,17). Additionally, outcrops of serpentinite have been detected on the surface of Mars (18), indicating past or ongoing serpentinization (19). Chemical modeling using observational data from Enceladus and Europa, moons of Saturn and Jupiter, respectively, indicate that

serpentinization may be ongoing in the oceans beneath the icy surface (20,21). The unique geochemical disequilibria generated by serpentinization paired with the prevalence of the reaction throughout Earth's history and on other terrestrial planetary bodies, makes the study of serpentinization environments highly relevant to the ongoing study of the origins of life (1,10,17,22), astrobiology (19–22), contamination of agricultural soils and groundwater with trace metals (7–9), and carbon capture and sequestration (23–26). As such, it is imperative that we understand the geochemistry, microbiology, and ecology of this unique environment.

Geomicrobiology of Continental Ophiolites

One prominent environment where serpentinization occurs is within continental ophiolites, which are abundant along continental margins (12). Ophiolites are pieces of oceanic lithosphere that are emplaced onto the continental lithosphere by tectonic activity (12). This action preserves oceanic crust on the surface that would normally have been subducted into the mantle. The exact mechanics of obduction are not known (12,27), the process of emplacing dense oceanic crust onto less dense continental crust has remained enigmatic and likely requires very specific tectonic and rheological conditions (27). Despite this uncertainty, it seems clear that obduction is initiated when plate margin tectonics shift from tension or strike-slip motion to compression (12,27). Once emplaced on the continental lithosphere, ophiolites become subject to weathering and infiltration of meteoric water, primarily through tectonic fractures in the upper portion of the ophiolite (28). Meteoric water (i.e., water derived from precipitation) that percolates into the ultramafic subsurface becomes buffered by serpentine mineral assemblages (2) and could allow for further serpentinization to occur with fresh rock surfaces exposed in fractures. This process results in the

high pH, strongly reducing groundwater with abundant CH_4 and H_2 and low levels of DIC that is characteristic of serpentinizing fluids (3,29).

The geochemistry and microbiology of continental ophiolites has been investigated in numerous locations by accessing natural springs and seeps (29–33), or sampling groundwater from monitoring wells to access subsurface fluids (16,34). Ophiolites that have been investigated include the Tablelands Ophiolite in Newfoundland, Canada (30), the Santa Elena Ophiolite in Costa Rica (31), the Zambales Ophiolite in the Philippines (32), the Coast Range Ophiolite in California, USA (16,29), the Voltri Massif in Italy (33), and the Samail Ophiolite in Oman (34). While these ophiolites differ in age and local geologic and hydrologic setting, all sites show similarities in their general fluid composition. Sampled springs and groundwater from these sites are strongly reducing with moderate to extreme pH (pH 8-12), low dissolved oxygen (< 1 mg/L), moderate to high salinity (100-100,000 µM Na^+ and Cl^-), low to moderate levels of DIC (10-500 µM), moderate levels of dissolved H_2 (< 1- 150 µM), and abundant dissolved CH_4 (< 1-900 µM) (16,30,33–36). Variations in the fluid chemistry at these sites are likely due to differences in ophiolite age, the rate of fluid flow in the subsurface, connectivity to the surface and the influx of annual recharge, and the extent to which fresh ultramafic rock surfaces are still undergoing active serpentinization. Ophiolites with more saline fluids may have paleo seawater mixing with meteoric fluids passing through the formation (36,37). Trapped seawater not only increases the salinity of the fluids, but also serves as an important source of sulfate providing an additional electron acceptor to the environment that can be used for microbial metabolism (36).

Microbial communities within continental ophiolites are composed primarily of facultative and obligate anaerobic organisms (29–33,38). Due to the extreme pH, microbial community diversity is low (16,34) and microbial community richness (number of unique taxa in a

community) and evenness (how close in numbers taxa in a community are) has been shown to decrease with increasing pH (39). High pH conditions are challenging to live in and require that microorganisms expend additional energy to maintain intracellular pH homeostasis. To do so, microbes need to actively transport protons (H^+) back into the cell (40). Extracellular protons are scarce at high pH, so microorganisms employ sodium (Na^+) or potassium (K^+) cation/proton antiporters and Na^+ pumping V-type ATPases to maintain pH homeostasis and generate ATP under high pH conditions (40,41). In addition to physiological concerns related to pH, microbial community members must also contend with limited bioavailable DIC, requiring them to oxidize potentially more recalcitrant organic carbon sources during metabolism (5).

Serpentinization supplies abundant hydrogen to the subsurface environment (3) that can be easily used by microbial community members as an electron donor for a variety of metabolisms (33,42). Organisms capable of both hydrogen oxidation and hydrogen production via fermentation are prevalent within ophiolites and tend to be composed of members from Betaproteobacteria in more shallow hypoxic waters and Clostridia in the deep anoxic subsurface, respectively (42). Organisms from the candidate genus *Serpentinomonas* (class Betaproteobacteria) are dominant community members in most continental ophiolites, appearing to flourish at the hypoxic/anoxic transition zone within the subsurface (38). Organisms from the candidate genus *Serpentinomonas* are extremely versatile and can perform oxygen respiration, nitrate reduction, hydrogen oxidation, and the Calvin-Benson-Bassham cycle to fix carbon (38,43). The ability to utilize numerous metabolisms and to utilize both heterotrophy and autotrophy likely allow *Serpentinomonas* to flourish in such a challenging environment. Organisms in the subsurface use hydrogen oxidation to reduce sulfur, and nitrogen species (36), and fuel carbon fixation through the Wood-Ljungdahl pathway (43,44) and methanogenesis (29,33,35,45).

While hydrogen plays a major role in the metabolism of microbial communities in the serpentinizing subsurface, there are numerous other potential electron donors that microorganisms may use. Metagenomic and experimental evidence have shown that carbon monoxide (CO) (42,44), CH_4 (33,43), acetate (29,33,35), and formate (35,38,43,44) are also important electron donors within continental ophiolites. These alternative electron donors play important roles, as competition for H_2 is likely high, and the ability to oxidize CO, CH_4, acetate, or formate creates different metabolic niches that increase community diversity within the system. Acetate, formate, CO, and CH_4 can all be produced abiotically in ophiolites through Fischer-Tropsch type reactions (1,11), but acetate and CH_4 can also be produced biologically in serpentinites (43,45) making it difficult to determine the source of these organic carbon species in serpentinizing systems (46).

Assessing the role of methanogenesis has been of particular interest in continental ophiolite settings. CH_4 is an important electron donor and source of organic carbon in the deep subsurface. As such, understanding the biotic and abiotic processes of methane production is important to our understanding of carbon cycling in serpentinizing systems. The discovery of the Lost City Hydrothermal Field (LCHF) in the early 2000's, which spurred geomicrobiology research in serpentinizing systems in the following two decades, revealed both abundant dissolved CH_4 and methanogens of a single phylotype, identified as Lost City *Methanosarcinales* (LCMS), inhabiting the carbonate chimneys (47,48). Further investigation of LCHF chimney communities revealed vigorous methane production and oxidation occurring within the chimneys, indicating that methane cycling may be a primary biogeochemical process supporting life within serpentinizing environments (48). The characterization of continental ophiolites in the past decade revealed abundant H_2 and even more abundant CH_4 (16,30,33–36), potentially sourced from both Fischer-Tropsch type reactions (1,10,11) as well as methanogenesis. Potentially methanogenic archaea

have been detected in numerous continental ophiolites (29,32–35). Methyl coenzyme-M reductase (*mcrA*) genes, which encode the alpha subunit of the enzyme that forms methane in the final step of methanogenesis, have been detected at the Voltri Massif (33), the Samail Ophiolite (44,45), and the Santa Elena Ophiolite (35), and recent experimental and metatranscriptomic evidence have shown active methanogenesis at The Cedars (29) and Samail Ophiolite (44,45). Interestingly, methanogens do not appear to be present within all continental ophiolites. They have not been detected at the Tablelands Ophiolite (49) or the Coast Range Ophiolite, despite efforts to do so (16). Their apparent absence is likely related to physicochemical conditions unique to each location (35) and could also be indicative of competitive microbial relationships such as those seen between sulfate reducing bacteria and methanogens, where sulfate reducing bacteria outcompete methanogens for available H_2 (50). This competition could be a potential explanation in serpentinized ophiolites with abundant sulfate (36,51). Additionally, stable isotope compositions of CH_4 associated with serpentinization are distinct from thermogenic and microbial CH_4 signatures, indicating an abiotic origin and unique stable isotope signature potentially related to Fischer-Tropsch type formation of CH_4 (52,53). The lack of microbial signal in CH_4 stable isotope compositions, including at the Samail Ophiolite where active methanogens have been detected (44,45), is an interesting result when considering that active methanogens have been detected in some of these systems (29,44,45). Ultimately the factors that result in the presence or absence of methanogens in continental ophiolites and that generate a range of unique CH_4 stable isotope compositions are not well understood and require further investigation to improve our understanding of the methane cycle within serpentinizing ophiolites.

Future investigations into the biogeochemistry of serpentinizing ophiolites need to continue to address methane cycling and develop estimates of the global flux of CO_2 and CH_4

sequestered and released, respectively, from serpentinizing ophiolites. Current estimates from individual sites range from tens of kilograms per year to greater than one hundred tons of CH_4 released per year (52,54), and CO_2 sequestration rates of 1.9×10^{-5} mol/(m^2·min) (55). Generating global models for both processes from ophiolites will be important for improving global models of climate change and for carbon sequestration applications (23,52,55).

Site Description: Coast Range Ophiolite Microbial Observatory

The Coast Range Ophiolite Microbial Observatory (CROMO) is a series of observation wells drilled into the Coast Range Ophiolite (CRO). The CRO is a Jurassic age ophiolite that was emplaced on the west coast of the continental United States approximately 166-172 million years ago (56). The CRO is expansive, spanning approximately 600 km of the western California coast (56,57). CROMO lies within an area of the CRO known as the Stonyford Volcanic Complex (SVC). The SVC consists of four blocks of Jurassic aged seamount volcanics, primarily pillow basalts, intermixed with serpentinite mélange (56). CROMO and the SVC are bounded by the Franciscan Complex to the west, and the Great Valley Sequence to the east (56). The Franciscan Complex is an accretionary complex of varying metamorphic lithologies, while the Great Valley Sequence consists largely of turbidites and is representative of a forearc geologic setting (56). The research wells at CROMO are drilled into serpentinite mélange that is characteristic of the SVC section of the CRO (57).

CROMO is located within the University of California Davis (UC-Davis) Donald and Sylvia McLaughlin Natural Reserve near Lower Lake, CA. Homestake Mining Company (HMC) mined gold in the area during the late 20th century and agreed to work with UC-Davis to establish a serpentine habitat environmental reserve upon closure of the mine (58). Reclamation by HMC is

still ongoing at the site in conjunction with reserve activities and research. The CROMO wells were drilled in August of 2011 in two different locations, the core shed well (CSW) cluster and the quarry valley (QV) well cluster, which are 1.4 km apart (57). Five wells were drilled in 2011 at the CSW cluster (CSW1.1, CSW1.2, CSW1.3, CSW1.4, and CSW1.5), and three were drilled at the QV cluster (QV1.1, QV1.1, and QV1.3). One pre-existing HMC monitoring well lies at the CSW cluster (CSWold) and three pre-existing HMC monitoring wells are at the QV cluster (N08-A, N08-B, and N08-C). The QV cluster lies to the east of the HMC tailings pond in a drainage basin surrounded by a creek (59). The CSW cluster lies within a basin that is surrounded by serpentine valleys and is bounded by a spring to the south east (59). Between the well clusters is a valley created by a northwest-southeast running fault zone which is 400 m east of the QV well cluster (59).

Cores were obtained from the QV1.1 and CSW1.1 wells during drilling and X-ray diffraction was performed to infer mineralogy (57). X-ray diffraction analyses show that altered peridotite with relic olivine and pyroxene is prominent in the subsurface and identified serpentine, magnetite, carbonate and mixed clays dispersed throughout the core (57). Geophysical characterization of the subsurface using electrical resistivity tomography was performed at CROMO in 2016 to characterize the hydrological structure of the CROMO aquifer (59). This work identified three distinct hydrological units at CROMO: shallow perched aquifers in the upper three meters of the subsurface, a cemented serpentinite aquitard (~3-13 m), and a deep (> 13 m) confined serpentinite aquifer (59). Except for CSW1.4, which is 8.8 meters deep, all the wells at CROMO are greater than thirteen meters in depth and sample fluids from the confined serpentinite aquifer. Aquifer parameter estimation and tritium isotope analyses performed on CROMO fluids in May of 2017 indicate that fluid flow is slow, the wells have poor surface connectivity, and that modern

recharge (fluid < 50 years in age) is not present within the aquifer (60,61). Iodine ($^{129}I/I$) and chloride ($^{36}Cl/Cl$) isotope geochemistry performed in the Clear Lake region immediately north of CROMO in the early 1990's indicated that groundwater residence times in the region range from 37,000 to 100,000 years (62).

CROMO groundwater geochemistry displays strong signatures of serpentinization. The wells at CROMO span depths of 8.8 - 76.2 meters, accessing geochemical gradients within the subsurface. Changes in well chemistry are associated with depth (36). As well depth increases, fluids become more reducing (0.52 to -235.61 mV), pH increases (7.75 - 12.26), temperature increases (14.65 - 17.63 ℃), salinity increases (1.47 - 10.55 mS), CH_4 concentrations increase (1.13 - 1,316 µM), dissolved oxygen decreases (0.20 - 3.19 mg/L), and DIC decreases (58.25 - 4,301.35 µM) (16,36). The wells also contain low to moderate concentrations of H_2 (0.09 - 2.89 µM) and abundant sulfate (27.69 - 391.94 µM) (36). Measurements of sulfate and salinity at CROMO (36,51) align well with observations and isotope geochemistry performed on waters in the Clear Lake region by Peters (37) which showed that trapped Cretaceous seawater is a source water for different end-member fluids in the region (37). It is likely that paleo seawater at depth in the CROMO aquifer mixes with meteoric groundwater, introducing salinity and serving as a source of sulfate within the subsurface (36,51).

CROMO microbial communities are dominated by organisms from the orders Burkholderiales and Clostridiales and microbial communities decrease in diversity as pH increases (16,63). Metagenomic and 16S rRNA amplicon analyses on fluids from the CROMO wells show microbial communities are distinct within individual wells and that genes involved in H_2 and CO oxidation are prevalent (16). Further investigation of carbon metabolisms at the site showed that microbial community members use a variety of carbon fixation and assimilation methods including

methanotrophy, methylotrophy, the Calvin-Benson-Bassham cycle, the reverse tricarboxylic acid cycle, and the Wood Ljungdahl pathway (43). Vigorous biogeochemical cycling of sulfur through sulfide oxidation, sulfate reduction, and the oxidation, reduction and disproportionation of thiosulfate are also prevalent at CROMO and are driven by populations of the taxa *Dethiobacter*, *Desulfitispora*, and candidate genus *'Desulforudis'* (36). A recent geochemical and metagenomic investigation of gradients in the water column of the CSW1.1 well found a high abundance of genes involved in H_2 and CO oxidation, oxygen respiration, and nitrate reduction, despite low measured concentrations of these chemical species in the sampled fluids (64). This near-absence contrasted with abundant CH_4 present in the water column and low abundances of genes involved with methanotrophy, indicating that microbial populations actively draw down, and likely compete for, available H_2, CO, and oxygen in the water column, but are not fully utilizing available CH_4 for metabolic processes (64). The dominance of organisms from the genera *Serpentinomonas*, *Dethiobacter*, and *Truepera*, which are not capable of methanotrophy, in the water column may help explain the lack of methane utilization in the well (64).

Microbial Community Assembly

The ways in which microbial communities assemble has not yet been investigated within serpentine environments. Given the prevalence of serpentinizing systems on Earth (12) and throughout our solar system (20–22), and their relevance to numerous basic and applied fields of biogeochemical science (1,7–10,17,19–26) it is important that we understand the ecological forces that govern assembly in these unique environments. Understanding this process will aid in the prediction of microbial community composition and function (65,66) in newly investigated sites of serpentinization and will allow for improved anticipation of how serpentinite microbial communities respond to changing environmental conditions (67–71) and anthropogenic activities

(8,23–26). Since community assembly has not yet been assessed in serpentinized ophiolites and they represent both an extreme (pH, salinity, carbon limitation) and groundwater environment, the basics of community assembly and knowledge of community assembly processes in groundwater and extreme conditions are briefly reviewed.

Community assembly describes the processes that structure microbial communities and generate patterns underlying the diversity, composition, and function of different microbial communities (72,73). The field of microbial community ecology has advanced quickly in the last two decades with decreasing costs and improving sequencing technologies (74) allowing for in-depth characterization of the taxonomy and phylogeny (75) of microbial communities in a variety of environments. The seminal paper by Vellend (72) describes the four basic processes that structure microbial communities: speciation, selection, dispersal, and ecological drift (72,76). Importantly, the framework developed by Vellend (72) incorporates perspectives from both the niche (i.e. deterministic processes) and neutral (i.e. stochastic processes) theories of community ecology (77), which allows for a more nuanced assessment of assembly where stochastic and deterministic processes are likely both at play (72,73,77). The advent of taxonomic and phylogenetic null modeling techniques for microbial community data (78–81) has allowed for community assembly processes to be quantified in a variety of environments (69,80,82–92) revealing that a complex interplay between both stochastic and deterministic processes are important in structuring natural microbial communities (69,80,83,85,86,91–96).

Community assembly has been assessed in a handful of groundwater environments such as the Columbia River hyporheic zone (69,80,85,86,97), neutral near-surface aquifers in Ohio (88), and hard-rock aquifers in Pennsylvania (90) and Ontario, Canada (84). To date, studies of community assembly in these systems have shown that assembly tends to be dominated by

selection processes (80,86,98), where similar geochemical conditions in the aquifer drive microbial communities to a similar composition or differences in geochemical conditions select for different microbial community compositions in the subsurface (69,80,88,90). Additionally, changes in the abundance and speciation of dissolved organic carbon associated with seasonal groundwater surface water mixing in the hyporheic zone has been shown to alter community assembly processes and drive assembly towards more deterministic processes (69,97). While selection can play a dominant role in the subsurface, dispersal limitation and ecological drift are also important ecological drivers in groundwater systems (88,98,99), especially in isolated hard-rock environments that experience slower fluid flow in the subsurface (84,90). Given the importance of groundwater as one of the primary reservoirs of freshwater on Earth (61) and the great heterogeneity of groundwater environments in terms of physical and geochemical conditions, it is vital that we continue to characterize the biogeochemistry and microbial ecology of these systems.

Community assembly under extreme conditions has been assessed under desiccation stress (100) and drought (101), and in oligotrophic deep sea sediments (87), and acidic and alkaline pH soils (89). Not surprisingly, increased levels of stress due to extreme conditions imposes strong selection on microbial communities and drives communities towards more similar community composition (87,89,100,101). Investigations of acidic and alkaline soils by Tripathi and colleagues (89) further revealed a distinct difference in microbial community composition between acidic and alkaline soils, demonstrating that unique microbial taxa capable of withstanding acidic or alkaline pH extremes are selected for and persist under these conditions (89). Interestingly, work by Starnawski and colleagues (87) in oligotrophic deep sea sediments revealed that not only do extreme conditions impose a strong environmental filter on community composition, but that

mutations and further adaptation of microbial taxa in these sediments occur at rates slower than would normally be expected. This modest pace indicates that microbial taxa are not adapting to the extreme environment but were instead already well suited to observed environmental conditions prior to burial in the deep sea sediments, allowing them to persist while other poorly suited taxa perish (87).

Prior investigations of community assembly in groundwater and extreme environments reveal that deterministic processes (selection) play a dominant role in both settings, while stochastic processes (dispersal, ecological drift) play less prominent roles. Importantly, dispersal limitation and ecological drift appear to be more important factors in groundwater environments, especially hard-rock aquifers (84,88), where slow water flow in the subsurface can limit the transmission of microorganisms. Based on these observations, both selection and dispersal limitation likely play important roles in the assembly of microbial communities in serpentinizing ophiolites.

Disturbance Ecology and Effect of Drilling Perturbations on Microbial Communities

CROMO was established in 2011 as a subsurface scientific observatory to investigate the geochemistry and natural microbial communities present within serpentinizing ophiolites (57). It was the first scientific site of its kind to provide direct access to the serpentinizing subsurface and served as a template for drilling projects in the Samail Ophiolite (102), and the Atlantis Massif (103). Because CROMO is solely used for scientific investigation, filtered, ozonated water was used to drill wells to various depths to minimize subsurface contamination (57). Despite efforts to minimize disturbance in the subsurface at CROMO, shifts in geochemical conditions and microbial community composition following drilling were observed (**Chapter 3**). Characterizing these changes is vital to our understanding of the site, as research in other groundwater systems has

shown that the injection of fluid into the subsurface can introduce foreign fluid compositions and associated microbial communities that can substantially alter biogeochemistry and microbial community composition and function (104–107). To date, the impact of drilling activity on microbial community composition and function has not yet been assessed. Additionally, the response of serpentinite microbial communities to any kind of disturbance in their environment has not yet been studied. Due to the lack of literature on the topic in the fields of serpentinite and extremophile geomicrobiology, findings from investigations into disturbance ecology and the injection of water and substrates into the subsurface are briefly reviewed here.

Microbial communities are subject to a variety of natural (69,108–113) and anthropogenic changes (68,114–119) that can alter the habitability and resource landscape of their environments (120,121). As anthropogenic activities continue to influence and alter the natural environment it is important that we can anticipate how microbial communities may respond to these changes (120,121) and how likely microbial community composition and function and macroscale ecosystem functioning will be altered (65,66,71,122,123). The response of microbial communities to disturbances or environmental change can be assessed by quantifying microbial community stability (121). Stability is defined by two components, resistance and resilience, which mathematically describe a microbial community's ability to resist compositional or functional change or return to a pre-disturbance composition or functional state (120,121). The resistance and resilience of microbial communities to disturbances have been assessed in a variety of settings (114,115,117–119,124–129) revealing that most microbial communities are sensitive to disturbances in their environment (121), but that factors such as high community diversity (117,126), functional redundancy (117), dormancy dynamics and dispersal (118), and historical

contingency of disturbances (129) play important roles in the resistance and resilience responses of microbial communities.

Assessments of microbial community responses to disturbance in the subsurface have largely focused on the response of communities to the injection of exogenous substrates related to CO_2 sequestration (116,130–132) or hydrocarbon degradation (133) and the injection of water into the subsurface to aid in oil recovery at oil fields (104,106,107). Investigations on the effect of the injection of oxygen or CO_2 into subsurface reveal that following the injection of substrate, aquifer biogeochemistry is altered and microbial community diversity decreases while the overall abundance of microorganisms increases (116,132,133). Injections of oxygen, water, and CO_2 substantially alter aquifer redox conditions (105,133), the redox state and solubility of trace metals and elements (105,132), aquifer pH (116,130,132), and the speciation and mineralization of DIC (116,130,132). Studies in long-term water flooded oil reservoirs have shown that the injection of geochemically distinct waters, such as seawater, and their associated microbial communities can have a substantial impact on subsurface microbial community composition and biogeochemical cycling (106). Interestingly, the capacity of the microbial communities in injection fluids to flourish in the subsurface or replace native microbial populations in the subsurface is largely dependent on initial aquifer geochemical conditions and the extent to which injected fluids alter subsurface geochemistry (104,106,107). Unfortunately, most of these studies did not assess microbial community resilience or recovery following the subsurface disturbance (105,107,116,130,133), with the exception of the study performed by O'Mullan and colleagues (132). Their work showed that subsurface microbial abundances and community composition appeared to be approaching pre-disturbance conditions one year after the disturbance (132).

Investigations of microbial community stability in the face of environmental disturbances indicate that the microbial communities at CROMO were likely sensitive to the injection of aerobic drilling fluid into the anoxic subsurface. The capacity of microbial communities at CROMO to be resilient is uncertain. While microbial community members do display functional redundancy (43) and are likely capable of employing dormancy strategies due to the extreme conditions, microbial communities at CROMO have very low diversity and poor dispersal ability in the hard-rock subsurface, which may decrease the resilience capacity of these communities (117,118,126). On the other hand, many microbial populations at CROMO are not obligate anaerobes (16,36) and can perform a variety of metabolisms (16,36,43). This versatility may allow CROMO microbial communities to be resistant or resilient to the subsurface geochemical changes associated with drilling.

REFERENCES

REFERENCES

1. Preiner M., Xavier J.C., Sousa F.L., Zimorski V., Neubeck A., Lang S.Q., Greenwell H.C., Kleinermanns K., Tüysüz H., McCollom T.M., Holm N.G., Martin W.F. Serpentinization: Connecting Geochemistry, Ancient Metabolism and Industrial Hydrogenation. *Life*, 8(4) (2018). doi:10.3390/life8040041

2. Sleep N.H., Meibom A., Fridriksson Th., Coleman R.G., Bird D.K. H_2-rich fluids from serpentinization: Geochemical and biotic implications. *Proc Natl Acad Sci USA*, 101(35):12818–23 (2004). doi:10.1073/pnas.0405289101

3. McCollom T.M., Bach W. Thermodynamic constraints on hydrogen generation during serpentinization of ultramafic rocks. *Geochimica et Cosmochimica Acta*, 73(3):856–75 (2009). doi: 10.1016/j.gca.2008.10.032

4. Mayhew L.E., Ellison E.T., McCollom T.M., Trainor T.P., Templeton A.S. Hydrogen generation from low-temperature water-rock reactions. *Nature Geoscience*, 6(6):478–84 (2013). doi:10.1038/ngeo1825

5. Schrenk M.O., Brazelton W.J., Lang S.Q. Serpentinization, carbon, and deep life. *Reviews in Mineralogy and Geochemistry*, 75:575–606 (2013). doi:10.2138/rmg.2013.75.18

6. Frost R.B., Beard J.S. On silica activity and serpentinization. *Journal of Petrology*, 48(7):1351–68 (2007). doi:10.1093/petrology/egm021

7. Oze C., Bird D.K., Fendorf S. Genesis of hexavalent chromium from natural sources in soil and groundwater. *Proc Natl Acad Sci USA*, 104(16):6544–9 (2007). doi:10.1073/pnas.0701085104

8. Vithanage M., Kumarathilaka P., Oze C., Karunatilake S., Seneviratne M., Hseu Z-Y., Gunarathne V., Dassanayake M., Sik Ok Y., Rinklebe J. Occurrence and cycling of trace elements in ultramafic soils and their impacts on human health: A critical review. *Environment International*, 131(August 2018) (2019). doi:10.1016/j.envint.2019.104974

9. Porter S.S., Chang P.L., Conow C.A., Dunham J.P., Friesen M.L. Association mapping reveals novel serpentine adaptation gene clusters in a population of symbiotic Mesorhizobium. *The ISME Journal*,10 (2016). doi:10.1038/ismej.2016.88

10. Preiner M., Igarashi K., Muchowska K.B., Yu M., Varma S.J., Kleinermanns K., Nobu M.K., Kamagata Y., Tüysüz H., Moran J., Martin W.F. A hydrogen-dependent geochemical analogue of primordial carbon and energy metabolism. *Nature Ecology & Evolution*, 4(April) (2020). doi:10.1038/s41559-020-1125-6

11. McCollom T.M. Laboratory Simulations of Abiotic Hydrocarbon Formation in Earth's Deep Subsurface. *Reviews in Mineralogy & Geochemistry*, 75:467–94 (2013). doi:10.2138/rmg.2013.75.15

12. Vaughan A.P.M., Scarrow J.H. Ophiolite obduction pulses as a proxy indicator of superplume events? *Earth and Planetary Science Letters*, 213 (2003). doi:10.1016/S0012-821X(03)00330-3

13. Hoehler T.M., Amend J.P., Shock E.L. A "Follow the Energy" Approach for Astrobiology. *Astrobiology*, 7(6) (2007). doi:10.1089/ast.2007.0207

14. Deamer D., Weber A.L. Bioenergetics and Life's Origins. *Cold Spring Harbor Perspectives in Biology*, (2010). doi:10.1101/cshperspect.a004929

15. Jones R.M., Goordial J.M., Orcutt B.N. Low energy subsurface environments as extraterrestrial analogs. *Frontiers in Microbiology*, 9(JUL):1–18 (2018). doi:10.3389/fmicb.2018.01605

16. Twing K.I., Brazelton W.J., Kubo M.D.Y., Hyer A.J., Cardace D., Hoehler T.M., McCollom T.M., Schrenk M.O. Serpentinization-Influenced Groundwater Harbors Extremely Low Diversity Microbial Communities Adapted to High pH. *Frontiers in Microbiology*, 8:308 (2017). doi:10.3389/fmicb.2017.00308

17. Sleep N.H., Bird D.K., Pope E.C. Serpentinite and the dawn of life. *Philosophical Transactions of the Royal Society B*, 366 (2011). doi:10.1098/rstb.2011.0129

18. Ehlmann B.L., Mustard J.F., Murchie S.L. Geologic setting of serpentine deposits on Mars. *Geophysical Research Letters*, 37 (2010). doi:10.1029/2010GL042596

19. Michalski J.R., Cuadros J., Niles P.B., Parnell J., Rogers A.D., Wright S.P. Groundwater activity on Mars and implications for a deep biosphere. *Nature Geoscience*, 6(2):133–8 (2013). doi:10.1038/ngeo1706

20. Glein C.R., Baross J.A., Waite J.H. The pH of Enceladus' ocean. *Geochimica et Cosmochimica Acta*, 162:202–19 (2015). doi:10.1016/j.gca.2015.04.017

21. Vance S.D., Hand K.P., Pappalardo R.T. Geophysical controls of chemical disequilibria in Europa. *Geophysical Research Letters*, 43(10):4871–9 (2016). doi:10.1002/2016GL068547

22. Michalski J.R., Onstott T.C., Mojzsis S.J., Mustard J., Chan Q.H.S., Niles P.B., Johnson S.S. The Martian subsurface as a potential window into the origin of life. *Nature Geoscience*, (2017). doi:10.1038/s41561-017-0015-2

23. Kelemen P.B., Matter J., Streit E.E., Rudge J.F., Curry W.B., Blusztajn J. Rates and Mechanisms of Mineral Carbonation in Peridotite: Natural Processes and Recipes for Enhanced, in situ CO2 Capture and Storage. *Annual Review of Earth and Planetary Sciences*, (2011). doi: 10.1146/annurev-earth-092010-152509

24. Klein F., McCollom T.M. From serpentinization to carbonation: New insights from a CO2 injection experiment. *Earth and Planetary Science Letters*, 379:137–45 (2013). doi:10.1016/j.epsl.2013.08.017

25. Dichicco M.C., Laurita S., Paternoster M., Rizzo G., Sinisi R., Mongelli G. Serpentinite Carbonation for CO2 Sequestration in the Southern Apennines: Preliminary Study. *Energy Procedia*, 76:477–86 (2015). doi:10.1016/j.egypro.2015.07.888

26. Romão I.S., Gando-Ferreira L.M., da Silva M.M.V.G., Zevenhoven R. CO_2 sequestration with serpentinite and metaperidotite from Northeast Portugal. *Minerals Engineering*, 94:104–14 (2016). doi:10.1016/j.mineng.2016.05.009

27. Duretz T., Agard P., Yamato P., Ducassou C., Burov E.B., Gerya T.V. Thermo-mechanical modeling of the obduction process based on the Oman Ophiolite case. *Gondwana Research*, 2016;32:1–10 (2016). doi:10.1016/j.gr.2015.02.002

28. Dewandel B., Lachassagne P., Boudier F., Al-Hattali S., Ladouche B., Pinault J., Al-Suleimani Z. A conceptual hydrogeological model of ophiolite hard-rock aquifers in Oman based on a multiscale and a multidisciplinary approach. *Hydrogeology Journal* (2005). doi:10.1007/s10040-005-0449-2

29. Kohl L., Cumming E., Cox A., Rietze A., Morrissey L., Lang S.Q., Richter A., Suzuki S., Nealson K.H., Morrill P.L. Exploring the metabolic potential of microbial communities in ultra-basic, reducing springs at The Cedars, CA, USA: Experimental evidence of microbial methanogenesis and heterotrophic acetogenesis. *Journal of Geophysical Research: Biogeosciences*, 121(4):1203–20 (2016). doi: 10.1002/2015JG003233

30. Brazelton W.J., Morrill P.L., Szponar N., Schrenk M.O. Bacterial communities associated with subsurface geochemical processes in continental serpentinite springs. *Applied and Environmental Microbiology*, 79(13):3906–16 (2013). doi:10.1128/AEM.00330-13

31. Sánchez-Murillo R., Gazel E., Schwarzenbach E.M., Crespo-Medina M., Schrenk M.O., Boll J., Gill B.C. Geochemical evidence for active tropical serpentinization in the Santa Elena Ophiolite, Costa Rica: An analog of a humid early Earth? *Geochemistry, Geophysics, Geosystems*, 15(5):1783–800 (2014). doi:10.1002/2013GC005213

32. Woycheese K.M., Meyer-Dombard D.R., Cardace D., Argayosa A.M., Arcilla C.A. Out of the dark: Transitional subsurface-to-surface microbial diversity in a terrestrial serpentinizing seep (Manleluag, Pangasinan, the Philippines). *Frontiers in Microbiology*, 6 (2015). doi:10.3389/fmicb.2015.00044

33. Brazelton W.J., Thornton C.N., Hyer A., Twing K.I., Longino A.A., Lang S.Q., Lilley M.D., Früh-Green G.L., Schrenk M.O. Metagenomic identification of active methanogens and methanotrophs in serpentinite springs of the Voltri Massif, Italy. *PeerJ*, (2017). doi:10.7717/peerj.2945

34. Rempfert K.R., Miller H.M., Bompard N., Nothaft D., Matter J.M., Kelemen P., Fierer N., Templeton A.S. Geological and geochemical controls on subsurface microbial life in the Samail Ophiolite, Oman. *Frontiers in Microbiology*, 8 (2017). doi:10.3389/fmicb.2017.00056

35. Crespo-Medina M., Twing K.I., Sánchez-Murillo R., Brazelton W.J., McCollom T.M., Schrenk M.O. Methane dynamics in a tropical serpentinizing environment: The Santa Elena Ophiolite, Costa Rica. *Frontiers in Microbiology*, 8(MAY):1–14 (2017). doi:10.3389/fmicb.2017.00916

36. Sabuda M.C., Brazelton W.J., Putman L.I., McCollom T.M., Hoehler T.M., Kubo M.D.Y., Cardace D., Schrenk M.O. A dynamic microbial sulfur cycle in a serpentinizing continental ophiolite. *Environmental Microbiology*, 22:2329–45 (2020). doi:10.1111/1462-2920.15006

37. Peters E.K. D-^{18}0 enriched waters of the Coast Range Mountains, northern California: Connate and ore-forming fluids. *Geochimica et Cosmochimica Acta*, 57:1093–104 (1993). doi:10.1016/0016-7037(93)90043-V

38. Suzuki S., Kuenen J.G., Schipper K., van der Velde S., Ishii S., Wu A., Sorokin D.Y., Tenney A., Meng X., Morrill P.L., Kamagata Y., Muyzer G., Nealson K.H. Physiological and genomic features of highly alkaliphilic hydrogen-utilizing Betaproteobacteria from a continental serpentinizing site. *Nature Communications*, 5 (2014). doi:10.1038/ncomms4900

39. Putman L.I., Sabuda M.C., Brazelton W.J., Kubo M.D., Hoehler T.M., McCollom T.M., Cardace D., Schrenk M.O. Microbial communities in a serpentinizing aquifer are assembled through strong concurrent dispersal limitation and selection. *mSystems*, (2021). doi:10.1128/mSystems.00300-21

40. Krulwich T.A., Sachs G., Padan E. Molecular aspects of bacterial pH sensing and homeostasis. *Nature Reviews Microbiology*, 9(5):330–43 (2011). doi:10.1038/nrmicro2549

41. Miller H.M., Matter J.M., Kelemen P., Ellison E.T., Conrad M.E., Fierer N., Ruchala T., Tominaga M., Templeton A.S. Modern water/rock reactions in Oman hyperalkaline peridotite aquifers and implications for microbial habitability. *Geochimica et Cosmochimica Acta*, 179:217–41 (2016). doi:10.1016/j.gca.2016.01.033

42. Brazelton W.J., Nelson B., Schrenk M.O. Metagenomic evidence for H_2 oxidation and H_2 production by serpentinite-hosted subsurface microbial communities. *Frontiers in Microbiology*, 2 (2012). doi:10.3389/fmicb.2011.00268

43. Seyler L.M., Brazelton W.J., McLean C., Putman L.I., Hyer A., Kubo M.D.Y., Hoehler T., Cardace D., Schrenk M.O. Carbon Assimilation Strategies in Ultrabasic Groundwater: Clues from the Integrated Study of a Serpentinization-Influenced Aquifer. *mSystems*, 5(2):1–17 (2020. doi:10.1128/mSystems.00607-19

44. Fones E.M., Colman D.R., Kraus E.A., Nothaft D.B., Poudel S., Rempfert K.R., Spear J.R., Templeton A.S., Boyd E.S. Physiological adaptations to serpentinization in the Samail Ophiolite, Oman. *The ISME Journal* (2019). doi:10.1038/s41396-019-0391-2

45. Kraus E.A., Nothaft D., Stamps B.W., Rempfert K.R., Ellison E.T., Matter J.M., Templeton A.S., Boyd E.S., Spear J.R. Molecular Evidence for an Active Microbial Methane Cycle in

Subsurface Serpentinite-Hosted Groundwaters in the Samail Ophiolite, Oman. *Applied and Environmental Microbiology*, (August 2020):1–18 (2021). doi:10.1128/AEM.02068-20

46. Wang D.T., Gruen D.S., Sherwood Lollar B., Hinrichs K-U., Stewart L.C., Holden J.F., Hristov A.N., Pohlman J.W., Morrill P.L., Könneke M., Delwiche K.B., Reeves E.P., Sutcliffe C.N., Ritter D.J., Seewald J.S., McIntosh J.C., Hemond H.F., Kubo M.D., Cardace D., Hoehler T.M., Ono S. Nonequilibrium clumped isotope signals in microbial methane. *Science*, 348(6233):428–31 (2015). doi:10.1126/science.aaa4326

47. Kelley D.S., Karson J.A., Früh-green G.L., Yoerger D.R., Shank T.M., Butterfield D.A., Hayes J.M., Schrenk M.O., Olson E.J., Proskurowski G., Jakuba M., Bradley A., Larson B., Ludwig K., Glickson D., Buckman K., Bradley A.S., Brazelton W.J., Roe K., Elend M.J. Delacour A., Bernasconi S.M., Lilley M.D., Baross J.A., Summons R.E., Sylva S.P. A Serpentinite-Hosted Ecosystem: The Lost City Hydrothermal Field. *Science*, 307 (2005). doi:10.1126/science.1102556

48. Brazelton W.J., Mehta M.P., Kelley D.S., Baross J.A. Physiological differentiation within a single-species biofilm fueled by serpentinization. *mBio*, 2(4):e00127-11 (2011). doi:10.1128/mBio.00127-11

49. Morrill P.L., Brazelton W.J., Kohl L., Rietze A., Miles S.M., Kavanagh H., Schrenk M.O., Ziegler S.E., Lang S.Q. Investigations of potential microbial methanogenic and carbon monoxide utilization pathways in ultra-basic reducing springs associated with present-day continental serpentinization: The Tablelands, NL, CAN. *Frontiers in Microbiology*, 5(NOV):1–13 (2014). doi:10.3389/fmicb.2014.00613

50. Hedderich R., Whitman W.B. Physiology and Biochemistry of the Methane-Producing Archaea. *Prokaryotes*, 2:1050–79 (2006). doi:10.1007/0-387-30741-9

51. Glombitza C., Putman L.I., Rempfert K.R., Kubo M.D., Schrenk M.O., Templeton A.S., Hoehler T.M. Active microbial sulfate reduction in fluids of serpentinizing peridotites of the continental subsurface. *Communications Earth & Environment*, 2(84):1-9 (2021). doi:10.1038/s43247-021-00157-z

52. Etiope G., Sherwood Lollar B. Abiotic methane on earth. *Reviews of Geophysics*, 51(2):276–99 (2013). doi:10.1002/rog.20011

53. Etiope G. Abiotic methane in continental serpentinization sites: an overview. *Procedia Earth and Planetary Science*, 17:9–12 (2017). doi:10.1016/j.proeps.2016.12.006

54. Etiope G., Schoell M., Hosgörmez H. Abiotic methane flux from the Chimaera seep and Tekirova ophiolites (Turkey): Understanding gas exhalation from low temperature serpentinization and implications for Mars. *Earth and Planetary Science Letters*, 310(1–2):96–104 (2011). doi:10.1016/j.epsl.2011.08.001

55. Morrissey L.S., Morrill P.L. Flux of methane release and carbon dioxide sequestration at Winterhouse Canyon, Gros Morne, Newfoundland, Canada: a site of continental

serpentinization. *Canadian Journal of Earth Sciences*, 54(3):257–62 (2017). doi:10.1139/cjes-2016-0123

56. Shervais J.W., Murchey B.L., Kimbrough D.L., Renne P.R. Radioisotopic and biostratigraphic age relations in the Coast Range Ophiolite, northern California: Implications for the tectonic evolution of the Western Cordillera. *GSA Bulletin*, 117(5):633–53 (2005). doi:10.1130/B25443.1

57. Cardace D., Hoehler T., Mccollom T., Schrenk M., Carnevale D., Kubo M., Twing, K. Establishment of the Coast Range ophiolite microbial observatory (CROMO): drilling objectives and preliminary outcomes. *Scientific Drilling*, 16:45–55 (2013). doi:10.5194/sd-16-45-2013

58. University of California Davis Natural Reserve System. Human History. In: Natural History of the McLaughlin Reserve. 2003. p. 3–10.

59. Ortiz E., Tominaga M., Cardace D., Schrenk M.O., Hoehler T.M., Kubo M.D., Rucker D.F. Geophysical Characterization of Serpentinite Hosted Hydrogeology at the McLaughlin Natural Reserve, Coast Range Ophiolite. *Geochemistry, Geophysics, Geosystems*, 19(1):114–31 (2018). doi:10.1002/2017GC007001

60. Newman B.D., Osenbrück K., Aeschbach-Hertig W., Solomon D.K., Cook P., Różański K., Kipfer R. Dating of "young" groundwaters using environmental tracers: advantages, applications, and research needs. *Isotopes in Environmental and Health Studies*, 46(3):259–78 (2010). doi:10.1080/10256016.2010.514339

61. Gleeson T., Befus K.M., Jasechko S., Luijendijk E., Cardenas M.B. The global volume and distribution of modern groundwater. *Nature Geoscience* (2016). doi:10.1038/NGEO2590

62. Fehn U., Peters E.K., Tullai-Fitzpatrick S., Kubik P.W., Sharma P., Teng R.T.D., Grove H.E., Elmore D. ^{129}I and ^{36}Cl concentrations in waters of the eastern Clear Lake area, California: Residence times and source ages of hydrothermal fluids. *Geochimica et Cosmochimica Acta*, 56(5):2069–79 (1992). doi:10.1016/0016-7037(92)90330-L

63. Crespo-Medina M., Twing K.I., Kubo M.D.Y., Hoehler T.M., Cardace D., McCollom T., Schrenk M.O. Insights into environmental controls on microbial communities in a continental serpentinite aquifer using a microcosm-based approach. *Frontiers in Microbiology*, 5:604 (2014). doi:10.3389/fmicb.2014.00604

64. Sabuda M.C., Putman L.I., Hoehler T.M., Kubo M.D., Brazelton W.J., Schrenk M.O. Biogeochemical Gradients in a Serpentinization-Influenced Aquifer: Implications for Gas Exchange between the Subsurface and Atmosphere. *Journal of Geophysical Research: Biogeosciences*, 126, e2020JG006209 (2021). doi:10.1029/2020JG006209

65. Knelman J.E., Nemergut D.R. Changes in community assembly may shift the relationship between biodiversity and ecosystem function. *Frontiers in Microbiology*, 5(August):1–4 (2014). doi:3389/fmicb.2014.00424

66. Graham E.B., Knelman E.K., Schindlbacher A., Siciliano S., Breulmann M., Yannarell A., Beman J.M., Abell G., Philippot L., Prosser J., Foulquier A., Yuste J.C., Glanville H.C., Jones D.L., Angel R., Salminen J., Newton R.J., Bürgmann H., Ingram L.J., Hamer U., Siljanen H.M.P., Peltoniemi K., Potthast K., Bañeras L., Hartmann M., Banerjee S., Yu R-Q., Nogaro G., Richter A., Koranda M., Castle S.C., Goberna M., Song B., Chatterjee A., Nunes O.C., Lopes A.R., Cao Y., Kaisermann A., Hallin S., Strickland M.S., Garcia-Pausas J., Barba J., Kang H., Isobe K., Papaspyrou S., Pastorelli R., Lagomarsino A., Lindström E.S., Basiliko N., Nemergut D.R. Microbes as Engines of Ecosystem Function: When Does Community Structure Enhance Predictions of Ecosystem Processes? *Frontiers in Microbiology*, 7(February):1–10 (2016). doi:10.3389/fmicb.2016.00214

67. Singh B.K., Bardgett R.D., Smith P., Reay D.S. Microorganisms and climate change: terrestrial feedbacks and mitigation options. *Nature Reviews Microbiology*, 8(November):779–90 (2010). doi:10.1038/nrmicro2439

68. Evans S.E., Wallenstein M.D. Climate change alters ecological strategies of soil bacteria. *Ecology Letters*, 17:155–64 (2014). doi:10.1111/ele.12206

69. Stegen J.C., Fredrickson J.K., Wilkins M.J., Konopka A.E., Nelson W.C., Arntzen E.V., Chrisler W.B., Chu R.K., Danczak R.E., Fansler S.J., Kennedy D.W., Resch C.T., Tfaily M. Groundwater–surface water mixing shifts ecological assembly processes and stimulates organic carbon turnover. *Nature Communications*, 7 (2016). doi:10.1038/ncomms11237

70. Urban M.C., Bocedi G., Hendry A.P., Mihoub J-B., Pe'er G., Singer A., Bridle J.R., Crozier L.G., De Meester L., Godsoe W., Gonzalez A., Hellmann J.J., Holt R.D., Huth A., Johst K., Krug C.B., Leadley P.W., Palmer S.C.F., Pantel J.H., Schmitz A., Zollner P.A., Travis J.M.J. Improving the forecast for biodiversity under climate change. *Science*, 353(6304) (2016). doi:10.1126/science.aad8466

71. Shade A. Understanding Microbiome Stability in a Changing World. *MSystems*, 3(2):e00157-17 (2018). doi:10.1128/mSystems.00157-17

72. Vellend M. Conceptual synthesis in community ecology. *The Quarterly Review of Biology*, 85(2):183–206 (2010). doi:10.1086/652373

73. Nemergut D.R., Schmidt S.K., Fukami T., O'Neill S.P., Bilinski T.M., Stanish L.F., Knelman J.E., Darcy J.L., Lynch R.C., Wickey P., Ferrenberg S. Patterns and Processes of Microbial Community Assembly. *Microbiology and Molecular Biology Reviews*, 77(3):342–56 (2013). doi:10.1128/MMBR.00051-12

74. Medini D., Serruto D., Parkhill J., Relman D.A., Donati C., Moxon R., Falkow S., Rappuoli R. Microbiology in the post-genomic era. *Nature Reviews Microbiology*, 6 (2008). doi:10.1038/nrmicro1901

75. Cavender-Bares J., Kozak K.H., Fine P.V.A., Kembel S.W. The merging of community ecology and phylogenetic biology. *Ecology Letters*, 12:693–715 (2009). doi:10.1111/j.1461-0248.2009.01314.x

76. Nemergut D., Shade A., Violle C. When, where and how does microbial community composition matter? *Frontiers in Microbiology*. 5(SEP):2012–4 (2014). doi:10.3389/fmicb.2014.00497

77. Leibold M.A., McPeek M.A. Coexistence of the niche and neutral perspectives in community ecology. *Ecology*, 87(6):1399–410 (2006). doi:10.1890/0012-9658(2006)87[1399:cotnan]2.0.co;2

78. Chase J.M., Myers J.A. Disentangling the importance of ecological niches from stochastic processes across scales. *Philosophical Transactions of the Royal Society B*, 2351–63 (2011). doi:10.1098/rstb.2011.0063

79. Chase J.M., Kraft N.J.B., Smith K.G., Vellend M., Inouye B.D. Using null models to disentangle variation in community dissimilarity from variation in α-diversity. *Ecosphere*, 2(2) (2011). doi:10.1890/ES10-00117.1

80. Stegen J.C., Lin X., Konopka A.E., Fredrickson J.K. Stochastic and deterministic assembly processes in subsurface microbial communities. *The ISME Journal*, 6(10):1653–64 (2012). doi:10.1038/ismej.2012.22

81. Stegen J.C., Lin X., Fredrickson J.K., Konopka A.E. Estimating and mapping ecological processes influencing microbial community assembly. *Frontiers in Microbiology*, 6(MAY):1–15 (2015). doi:10.3389/fmicb.2015.00370

82. Caruso T., Chan Y., Lacap D.C., Lau M.C.Y., Mckay C.P., Pointing S.B. Stochastic and deterministic processes interact in the assembly of desert microbial communities on a global scale. *The ISME Journal*, (2011). doi:10.1038/ismej.2011.21

83. Zhou J., Liu W., Deng Y., Jiang Y., Xue K., He Z., Van Nostrand J.D., Wu L., Yang Y., Wang A. Stochastic Assembly Leads to Alternative Communities with Distinct Functions in a Bioreactor Microbial Community. *mBio*, 4(2):1–8 (2013). doi:10.1128/mBio.00584-12.Editor.

84. Beaton E.D., Stevenson B.S., King-Sharp K.J., Stamps B.W., Nunn H.S., Stuart M. Local and Regional Diversity Reveals Dispersal Limitation and Drift as Drivers for Groundwater Bacterial Communities from a Fractured Granite Formation. *Frontiers in Microbiology*, 7 (2016). doi:10.3389/fmicb.2016.01933

85. Graham E.B., Crump A.R., Resch C.T., Fansler S., Arntzen E., Kennedy D.W., Fredrickson J.K., Stegen J.C. Coupling Spatiotemporal Community Assembly Processes to Changes in Microbial Metabolism. *Frontiers in Microbiology*, 7 (2016). doi:10.3389/fmicb.2016.01949

86. Graham E.B., Crump A.R., Resch C.T., Fansler S., Arntzen E., Kennedy D.W., Fredrickson J.K., Stegen J.C. Deterministic influences exceed dispersal effects on hydrologically-connected microbiomes. *Environmental Microbiology*, 19:1552–67 (2017). doi:10.1111/1462-2920.13720

87. Starnawski P., Bataillon T., Ettema T.J.G., Jochum L.M., Schreiber L., Chen X., Lever M.A., Polz M.F., Jørgensen B.B., Schramm A., Kjeldsen K.U. Microbial community assembly and evolution in subseafloor sediment. *Proc Natl Acad Sci USA*, (2017). doi:10.1073/pnas.1614190114

88. Danczak R.E., Johnston M.D., Kenah C., Slattery M., Wilkins M.J. Microbial Community Cohesion Mediates Community Turnover in Unperturbed Aquifers. *mSystems*, 3(4):e00066-18 (2018). doi:10.1128/mSystems.00066-18

89. Tripathi B.M., Stegen J.C., Kim M., Dong K., Adams J.M., Lee Y.K. Soil pH mediates the balance between stochastic and deterministic assembly of bacteria. *The ISME Journal* (2018). doi:10.1038/s41396-018-0082-4

90. Danczak R.E., Daly R.A., Borton M.A., Stegen J.C., Roux S., Wrighton K.C., Wilkins M.J. Ecological assembly processes are coordinated between bacterial and viral communities in fractured shale ecosystems. *mSystems*, 5(2):1–13 (2020). doi:10.1128/mSystems.00098-20

91. Liu W., Graham E.B., Zhong L., Zhang J., Li W., Li Z., Lin X., Feng Y. Dynamic microbial assembly processes correspond to soil fertility in sustainable paddy agroecosystems. *Functional Ecology*, 34(February):1244–56 (2020). doi:10.1111/1365-2435.13550

92. Liu W., Graham E.B., Dong Y., Zhong L., Zhang J., Qiu C., Chen R., Lin X., Feng Y. Balanced stochastic versus deterministic assembly processes benefit diverse yet uneven ecosystem functions in representative agroecosystems. *Environmental Microbiology*, 23:391–404 (2021). doi:10.1111/1462-2920.15326

93. Ofiteru I.D., Lunn M., Curtis T.P., Wells G.F., Criddle C.S., Francis C.A., Sloan W.T. Combined niche and neutral effects in a microbial wastewater treatment community. *Proc Natl Acad Sci USA*, 107(35) (2010). doi:10.1073/pnas.1000604107

94. Dini-Andreote F., Stegen J.C., Dirk van Elsas J., Falcão Salles J. Disentangling mechanisms that mediate the balance between stochastic and deterministic processes in microbial succession. *Proc Natl Acad Sci USA*, 112(11) (2015). doi:10.1073/pnas.1414261112

95. Zhou J., Ning D. Stochastic Community Assembly: Does It Matter in Microbial Ecology? *Microbiology and Molecular Biology Reviews*, 81(4):1–32 (2017). doi:10.1128/MMBR.00002-17

96. Fodelianakis S., Valenzuela-Cuevas A., Barozzi A., Daffonchio D. Direct quantification of ecological drift at the population level in synthetic bacterial communities. *The ISME Journal*, (2020). doi:10.1038/s41396-020-00754-4

97. Stegen J.C., Johnson T., Fredrickson J.K., Wilkins M.J., Konopka A.E., Nelson W.C., Arntzen E.V., Chrisler W.B., Chu R.K., Fansler S.J., Graham E.B., Kennedy D.W., Resch C.T., Tfaily M., Zachara J. Influences of organic carbon speciation on hyporheic corridor biogeochemistry and microbial ecology. *Nature Communications*, 9(1):1–11 (2018). doi:10.1038/s41467-018-02922-9

98. Stegen J.C., Lin X., Fredrickson J.K., Chen X., Kennedy D.W., Murray C.J., Rockhold M.L., Konopka A. Quantifying community assembly processes and identifying features that impose them. *The ISME Journal*, 7(11):2069–79 (2013). doi:10.1038/ismej.2013.93

99. Graham E.B., Stegen J.C. Dispersal-Based Microbial Community Assembly Decreases Biogeochemical Function. *Processes*, 5(65) (2017). doi:10.3390/pr5040065

100. Valverde A., Makhalanyane T.P., Cowan D.A. Contrasting assembly processes in a bacterial metacommunity along a desiccation gradient. *Frontiers in Microbiology*, 5 (2014). doi:10.3389/fmicb.2014.00668

101. Chase J.M. Drought mediates the importance of stochastic community assembly. *Proc Natl Acad Sci USA*, 104(44) (2007). doi:10.1073/pnas.0704350104

102. Conze R., Coggon J.A., Matter J. ICDP Oman Drilling Project: News from the Scientific Drilling in the Samail Ophiolite Sultanate of Oman. *ECORD Newsletter*, 28 (2017). doi:10.14379/OmanDP.proc.2020

103. Früh-Green G.L., Orcutt B.N., Green S., Cotterill C., Expedition 357 Scientists. Expedition 357 Preliminary Report: Atlantis Massif Serpentinization and Life. *International Ocean Discovery Program*, (2016). doi:10.14379/iodp.pr.357.2016

104. Zhang F., She Y-H., Chai L-J., Banat I.M., Zhang X-T., Shu F-C., Wang Z-L., Yu L-J., Hou D-J. Microbial diversity in long-term water-flooded oil reservoirs with different in situ temperatures in China. *Scientific Reports*, 2:1–10 (2012). doi:10.1038/srep00760

105. Ginige M.P., Kaksonen A.H., Morris C., Shackelton M., Patterson B.M. Bacterial community and groundwater quality changes in an anaerobic aquifer during groundwater recharge with aerobic recycled water. *FEMS Microbiology Ecology*, 85(3):553–67 (2013). doi:10.1111/1574-6941.12137

106. Piceno Y.M., Reid F.C., Tom L.M., Conrad M.E., Bill M., Hubbard C.G., Fouke B.W., Graff C.J., Han J., Stringfellow W.T., Hanlon J.S., Hu P., Hazen T.C., Andersen G.L. Temperature and injection water source influence microbial community structure in four Alaskan North Slope hydrocarbon reservoirs. *Frontiers in Microbiology*, 5(AUG):1–13 (2014). doi:10.3389/fmicb.2014.00409

107. Ren H., Xiong S., Gao G., Song Y., Cao G., Zhao L., Zhang X. Bacteria in the injection water differently impacts the bacterial communities of production wells in high-temperature petroleum reservoirs. *Frontiers in Microbiology*, 6(MAY) (2015). doi:10.3389/fmicb.2015.00505

108. Fuhrman J.A., Hewson I., Schwalbach M.S., Steele J.A., Brown M.V., Naeem S. Annually reoccurring bacterial communities are predictable from ocean conditions. *Proc Natl Acad Sci USA*, 103(35):13104–9 (2006). doi:10.1073/pnas.0602399103

109. Cermeño P., de Vargas C., Abrantes F., Falkowski P.G. Phytoplankton Biogeography and Community Stability in the Ocean. *PLoS ONE*, 5(4) (2010). doi:10.1371/journal.pone.0010037

110. Creamer C.A., de Menezes A.B., Krull E.S., Sanderman J., Newton-Walters R., Farrell M. Microbial community structure mediates response of soil C decomposition to litter addition and warming. *Soil Biology and Biochemistry*, 80:175–88 (2015). doi:10.1016/j.soilbio.2014.10.008

111. Fuhrman J.A., Cram J.A., Needham D.M. Marine microbial community interpretation. *Nature Reviews Microbiology*, 13(March) (2015). doi:10.1038/nrmicro3417

112. Bastida F., Torres I.F., Hernández T., García C. The impacts of organic amendments: Do they confer stability against drought on the soil microbial community? *Soil Biology and Biochemistry*, 113:173–83 (2017). doi:10.1016/j.soilbio.2017.06.012

113. Gravuer K., Eskelinen A. Nutrient and rainfall additions shift phylogenetically estimated traits of soil microbial communities. *Frontiers in Microbiology*, 8(JUL):1–16 (2017). doi:10.3389/fmicb.2017.01271

114. de Vries F.T., Shade A. Controls on soil microbial community stability under climate change. *Frontiers in Microbiology*, 4(September):1–16 (2013). doi:10.3389/fmicb.2013.00265

115. Lee S-H., Sorensen J.W., Grady K.L., Tobin T.C., Shade A. Divergent extremes but convergent recovery of bacterial and archaeal soil communities to an ongoing subterranean coal mine fire. *The ISME Journal*, 11(6):1447–59 (2017). doi:10.1038/ismej.2017.1

116. Trias R., Ménez B., le Campion P., Zivanovic Y., Lecourt L., Lecoeuvre A., Schmitt-Kopplin P., Uhl J., Gislason S.R., Alfredsson H.A., Mesfin K.G., Snaebjörnsdóttir S.O., Aradóttir E.S., Gunnarsson I., Matter J.M., Stute M., Oelkers E.H., Gérard E. High reactivity of deep biota under anthropogenic CO_2 injection into basalt. *Nature Communications*, 8(1) (2017). doi:10.1038/s41467-017-01288-8

117. Herold M., Martínez Arbas S., Narayanasamy S., Sheik A.R., Kleine-Borgmann L.A.K., Lebrun L.A., Kunath B.J., Roume H., Bessarab I., Williams R.B.H., Gillece J.D., Schupp J.M., Keim P.S., Jäger C., Hoopmann M.R., Moritz R.L., Ye Y., Li S., Tang H., Heintz-Buschart A., May P., Muller E.E.L., Laczny C.C. Wilmes P. Integration of time-series meta-omics data reveals how microbial ecosystems respond to disturbance. *Nature Communications*, 11 (2020). doi:10.1038/s41467-020-19006-2

118. Sorensen J.W., Shade A. Dormancy dynamics and dispersal contribute to soil microbiome resilience. *Philosophical Transactions of the Royal Society B*, 375 (2020). doi:10.1098/rstb.2019.0255

119. Wilpiszeski R.L., Gionfriddo C.M., Wymore A.M., Moon J-W., Lowe K.A., Podar M., Rafie S., Fields M.W., Hazen T.C., Ge X., Poole F., Adams M.W.W., Chakraborty R., Fan Y., Van Nostrand J.D., Zhou J., Arkin A.P., Elias D.A. In-field bioreactors demonstrate

dynamic shifts in microbial communities in response to geochemical perturbations. *PLoS ONE*, 15(9):1–18 (2020). doi:10.1371/journal.pone.0232437

120. Allison S.D., Martiny J.B.H. Resistance, resilience, and redundancy in microbial communities. *Proc Natl Acad Sci USA*, 105 (2008). doi:10.1073/pnas.0801925105

121. Shade A., Peter H., Allison S.D., Baho D.L., Berga M., Bürgmann H., Huber D.H., Langenheder S., Lennon J.T., Martiny J.B.H., Matulich K.L., Schmidt T.M., Handelsman J. Fundamentals of microbial community resistance and resilience. *Frontiers in Microbiology*, 3(DEC):1–19 (2012). doi:10.3389/fmicb.2012.00417

122. Hall E.K., Bernhardt E.S., Bier R.L., Bradford M.A., Boot C.M., Cotner J.B., del Giorgio P.A., Evans S.E., Graham E.B., Jones S.E., Lennon J.T., Locey K.J., Nemergut D., Osborne B.B., Rocca J.D., Schimel J.P., Waldrop M.P., Wallenstein M.D. Understanding how microbiomes influence the systems they inhabit. *Nature Microbiology*, 3(September):977–82 (2018). doi:10.1038/s41564-018-0201-z

123. Widder S., Allen R.J., Pfeiffer T., Curtis T.P., Wiuf C., Sloan W.T., Cordero O.X., Brown S.P., Momeni B., Shou W., Kettle H., Flint H.J., Haas A.F., Laroche B., Kreft J-U., Rainey P.B., Freilich S., Schuster S., Milferstedt K., van der Meer J.R., Groβkopf T., Huisman J., Free A., Picioreanu C., Quince C., Klapper I., Labarthe S., Smets B.F., Wang H., Isaac Newton Institute Fellows, Soyer O.S. Challenges in microbial ecology: building predictive understanding of community function and dynamics. *The ISME Journal*, 10(November 2015):2557–68 (2016). doi:10.1038/ismej.2016.45

124. Shade A., Read J.S., Welkie D.G., Kratz T.K., Wu C.H., McMahon K.D. Resistance, resilience and recovery: aquatic bacterial dynamics after water column disturbance. *Environmental Microbiology*, 13:2752–67 (2011). doi:10.1111/j.1462-2920.2011.02546.x

125. Shade A., Read J.S., Youngblut N.D., Fierer N., Knight R., Kratz T.K., Lottig N.R., Roden E.E., Stanley E.H., Stombaugh J., Whitaker R.J., Wu C.H., McMahon K.D. Lake microbial communities are resilient after a whole-ecosystem disturbance. *The ISME Journal*, 6(12):2153–67 (2012). doi:10.1038/ismej.2012.56

126. Erkus O., de Jager V.C.L., Spus M., van Alen-Boerrigter I.J., van Rijswijck I.M.H., Hazelwood L., Janssen P.W.M., van Hijum S.A.F.T., Kleerebezem M., Smid E.J. Multifactorial diversity sustains microbial community stability. *The ISME Journal*, 7(11):2126–36 (2013). doi:10.1038/ismej.2013.108

127. Lu H-P., Shao Y-H., Wu J-H., Hsieh C-H. System Performance Corresponding to Bacterial Community Succession after a Disturbance in an Autotrophic Nitrogen Removal Bioreactor. *mSystems*, (July):1–12 (2020). doi:10.1128/mSystems.00398-20

128. Kurkjian H.M., Akbari M.J., Momeni B. The impact of interactions on invasion and colonization resistance in microbial communities. *PLoS Computational Biology*, (2021). doi:10.1371/journal.pcbi.1008643

129. Song H-S., Stegen J.C., Graham E.B., Scheibe T.D. Historical Contingency in Microbial Resilience to Hydrologic Perturbations. *Frontiers in Water*, 3(February):1–10 (2021). doi:10.3389/frwa.2021.590378

130. Mu A., Boreham C., Leong H.X., Haese R.R., Moreau J.W. Changes in the deep subsurface microbial biosphere resulting from a field-scale CO_2 geosequestration experiment. *Frontiers in Microbiology*, 5(May):1–11 (2014). doi:10.3389/fmicb.2014.00209

131. Mu A., Moreau J.W. The geomicrobiology of CO_2 geosequestration: a focused review on prokaryotic community responses to field-scale CO_2 injection. *Frontiers in Microbiology*, 6(April):1–13 (2015). doi:10.3389/fmicb.2015.00263

132. O'Mullan G. Dueker M.E., Clauson K., Yang Q., Umemoto K., Zakharova N., Matter J., Stute, M., Takahashi T., Goldberg D. Microbial stimulation and succession following a test well injection simulating CO_2 leakage into a shallow Newark basin aquifer. *PLoS ONE*, 10(1):1–25 (2015). doi:10.1371/journal.pone.0117812

133. Cai M., Yu C., Wang R., Si Y., Masakorala K., Yuan H., Yao J., Zhang J. Effects of oxygen injection on oil biodegradation and biodiversity of reservoir microorganisms in Dagang oil field, China. *International Biodeterioration and Biodegradation*, 98:59–65 (2015). doi:10.1016/j.ibiod.2014.12.003

CHAPTER 2

Microbial communities in a serpentinizing aquifer are assembled through strong concurrent dispersal limitation and selection[1]

Abstract

In recent years, our appreciation of the extent of habitable environments in Earth's subsurface has greatly expanded, as has our understanding of the biodiversity contained within. Most studies have relied on single sampling points, rather than considering the long-term dynamics of subsurface environments and their microbial populations. One such habitat are aquifers associated with the aqueous alteration of ultramafic rocks through a process known as serpentinization. Ecological modeling performed on a multi-year time series of microbiology, hydrology, and geochemistry in an ultrabasic aquifer within the Coast Range Ophiolite reveals that community assembly is governed by undominated assembly (i.e., neither stochastic (random) nor deterministic (selective) processes alone govern assembly). Controls on community assembly were further assessed by characterizing aquifer hydrogeology and microbial community adaptations to the environment. These analyses show that low permeability rocks in the aquifer restrict the transmission of microbial populations between closely situated wells. Alpha and beta diversity measures and metagenomic and metatranscriptomic data from microbial communities indicate that high pH and low dissolved inorganic carbon levels impose strong environmental selection on microbial communities within individual wells. Here, we find that the interaction between strong selection imposed by extreme pH and enhanced ecological drift due to dispersal limitation imposed by slow fluid flow results in the undominated assembly signal observed

[1] Work presented in this chapter has been published as Putman L.I., Sabuda M.C., Brazelton W.J., Kubo M.D., Hoehler T.M., McCollom T.M., Cardace D., Schrenk M.O. Microbial communities in a serpentinizing aquifer are assembled through strong concurrent dispersal limitation and selection. *mSystems*, (2021). doi:10.1128/mSystems.00300-21

throughout the site. Strong environmental selection paired with extremely low dispersal in the subsurface results in low diversity microbial communities that are well-adapted to extreme pH conditions and subject to enhanced stochasticity introduced by ecological drift over time.

Importance

Microbial communities existing under extreme or stressful conditions have long been thought to be structured primarily by deterministic processes. The application of macroecology theory and modeling to microbial communities in recent years has spurred assessment of assembly processes in microbial communities, revealing that both stochastic and deterministic processes are at play to different extents within natural environments. We show that low-diversity microbial communities in a hard-rock serpentinizing aquifer are assembled under the influence of strong selective processes, imposed by high pH, and enhanced ecological drift that occurs as the result of dispersal limitation due to the slow movement of water in the low permeability aquifer. This study demonstrates the important roles that both selection and dispersal limitation play in terrestrial serpentinites, where extreme pH assembles a microbial metacommunity well-adapted to alkaline conditions, and dispersal limitation drives compositional differences in microbial community composition between local communities in the subsurface.

Introduction

Recent estimates of the distribution of biomass on Earth indicate that bacteria are the second largest reservoir of biomass (~ 70 gigatons of carbon), and that the majority of bacterial and archaeal biomass is hosted within subsurface environments (~64 gigatons of carbon) (1). In the last decade, several deep subsurface environments have been studied and characterized in

detail, allowing us to improve our understanding of the composition and function of microbial communities in this biome and the important roles they play in global biogeochemical cycling (2–4). One type of deep subsurface habitat that has become the subject of intensive study over the last decade is serpentinized peridotite. Serpentinization is a geochemical reaction that hydrates ultramafic rock (peridotite) (5) and generates high pH, reducing fluids with abundant hydrogen (H_2) (6). In recent years, the microbiology of serpentinizing systems has been studied in a variety of marine (7–9) and terrestrial (6,10–16) environments. This work has confirmed the presence of endemic, low diversity, microbial communities capable of tolerating the extreme pH (15,16) and utilizing available hydrogen (17,18), carbon monoxide (17,19), methane (14,20), acetate (6,14,21), formate (18–21), and sulfur compounds (22) for both dissimilatory and assimilatory metabolic processes. Combined, this work has provided ample evidence that distinct communities of microorganisms inhabit serpentinizing environments and that they play active roles in these ecosystems.

To date, the ecological forces that structure microbial communities and drive turnover within and between microbial communities in serpentinizing systems have yet to be investigated. Community assembly describes the stochastic (dispersal and ecological drift) and deterministic (environmental and/or biological selection) ecological processes that structure observed microbial communities (23,24). Advances in DNA sequencing technology in the last two decades (25), paired with the more recent implementation of community assembly theory and modeling of sequencing data from microbial ecosystems has provided new insights into the mechanisms that structure microbial communities in a variety of conditions (24,26–36). Assessments of community assembly in groundwater systems have shown that selection and dispersal processes play an extremely important role in structuring both the environmental resource landscape as well as

microbial communities (29,31,32,34,37). Due to accessibility, much of this work has been performed in neutral pH, near surface, groundwaters with connectivity to the surface (31,32,37). Relatively little work has been done in isolated hard-rock aquifers within the deep subsurface (29,34). Old groundwaters (> 100 years), which are often hosted within hard-rock aquifers in the deep subsurface, are a substantial reservoir of globally available freshwater (38). As these systems are likely dispersal limited, it is important that we understand the ecological forces that structure microbial communities in hard-rock aquifers (29,34) to better account for the controls on microbial community composition and function within these large reservoirs of valuable water resources (39).

In this study, we apply a null modeling ecological framework (28) that uses the β-nearest taxon index (βNTI) and the abundance-weighted Raup-Crick (RCbray) metric to quantify microbial community assembly processes in an isolated serpentinizing aquifer. We apply the modeling framework to the longest running and highest resolution time series dataset collected from a serpentinizing system to date, to better understand the forces that drive assembly and microbial community turnover within these unique systems. Additionally, we integrate an aqueous geochemistry dataset collected alongside microbial samples to better understand environmental drivers of microbial community composition. We perform basic hydrologic modeling to estimate aquifer hydraulic properties to better understand the movement of water and the physical environment that microbial communities experience in the subsurface. Our data show that pH imposes a strong selective force on microbial community composition but that, overall, slow fluid flow and poor connectivity in the subsurface isolates microbial communities from one another.

This isolation introduces a significant amount of stochasticity by enhancing ecological drift within and between these alkaliphilic microbial communities.

Results

Geochemistry

Fluids were sampled from twelve wells of varying depth (7-76 m) that access a high pH aquifer in the serpentinizing ophiolite at the Coast Range Ophiolite Microbial Observatory

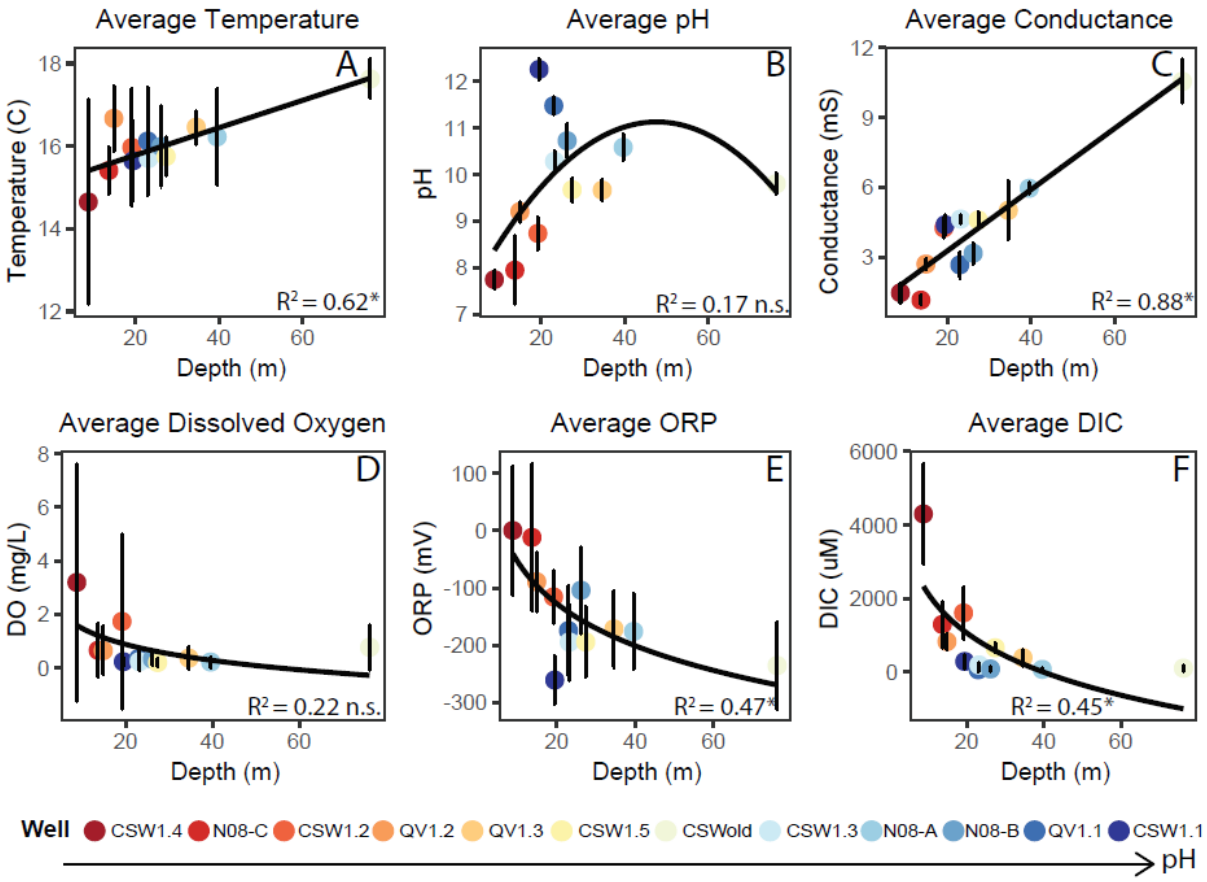

Figure 2.1. Average Well Geochemical Parameters Plotted against Depth.

Average measurements for temperature (A), pH (B), specific conductance (C), dissolved oxygen (D), oxidation reduction potential (E), and dissolved inorganic carbon (F) in each well plotted against depth. Averages were calculated using data from 2011-2017. R^2 coefficients from regression models are listed in the bottom right corner of each plot, where * indicates a significant correlation ($p \leq 0.05$) and n.s. indicates an insignificant correlation. Wells are organized from lowest to highest average pH in the legend.

(CROMO) in Northern California (40). Fluids were sampled two to three times per year over the course of six years. Sampled fluids, which are pumped under positive pressure via permanently installed submersible pumps, traveled directly through a chamber with a multiprobe meter to measure temperature, pH, dissolved oxygen (DO), oxidation-reduction potential (ORP), and specific conductance (11,15). Luer-lock syringes were attached directly to the pump outflow tubing for anoxic sampling of fluids to support subsequent chemical analyses, as described in the **Appendix**. Analysis of the fluid chemistry (**Table A.1** at https://doi.org/10.6084/m9.figshare.14983851) over the duration of the study shows that CROMO fluids generally become more reducing, increase in temperature, salinity, and pH, and decrease in DO and dissolved inorganic carbon (DIC) concentrations with depth (**Fig. 2.1 A-F**).

Ecological Modeling Results

DNA and RNA were extracted from microbial communities that were captured on 0.22 µm Sterivex filter cartridges (Millipore, Billerica, MA, USA) during sampling trips from 2011-2017 as described below and in the **Appendix**. The following diversity and ecological modeling results are based on a dataset generated from gene amplicon sequencing of the V4 region of the 16S rRNA gene. The dataset utilized for these analyses consists of 104 samples, 5,974,056 sequence reads, and 13,444 operational taxonomic units (OTUs) clustered at a 3% distance threshold, as described below. The 16S rRNA gene amplicon dataset represents 51 different phyla and community composition is largely dominated by members of the Betaproteobacteriales and Clostridiales orders (**Fig. A.1**). The OTU count table (CROMO_Filtered_FINAL_counts.xlsx) utilized for the

following analyses and ecological modeling are published on FigShare (https://figshare.com/projects/Community_Assembly_in_Serpentinizing_Ophiolites/101648).

Ecological modeling of the microbial communities was carried out to characterize the relative contributions of different community assembly processes, using the framework developed by Stegen and colleagues (28). This framework employs null modeling techniques to generate randomized communities that can be compared with observed microbial community composition to determine if microbial communities are more or less similar to each other than would be expected if communities assembled by random chance. First, βNTI values are calculated to differentiate between deterministic (selective) and stochastic (random) processes. Significant βNTI values indicate that deterministic processes are responsible for observed differences between microbial communities in a pairwise comparison (37). Non-significant βNTI values indicate that stochastic processes are responsible for observed differences between microbial communities (28). Stochastic assembly processes are further characterized using the RCbray metric to characterize the roles of dispersal and ecological drift (28). A detailed description of each community assembly process associated with ecological modeling results (28) can be found in **Table 2.1**. βNTI (CROMO_weighted_bNTI_matrix.csv) and RCbray (CROMO_RCbray_matrix.xlsx) matrices used for the following analyses are available on FigShare (https://figshare.com/projects/Community_Assembly_in_Serpentinizing_Ophiolites/101648).

Community assembly processes were assessed within individual wells over time (**Fig. 2.2A & B**) and between wells over time (**Fig. 2.2C & D**). Within individual wells, selection processes

Process	Description	Deterministic or Stochastic	Model Result
Variable Selection	Communities are more different from each other than can be expected by random chance (i.e., different physical/chemical conditions in samples drive differingcommunity composition)	Deterministic	βNTI > 2
Homogeneous Selection	Communities are more similar to each other than can be expected by random chance (i.e., similar physical/chemical conditions in samples drive community composition to be similar)	Deterministic	βNTI < -2
Dispersal Limitation	Microbial communities between samples are unable to interact due to separation by space or time. When communities cannot interact, variation in composition caused by ecological drift over time results in communities that are less similar to each other than expected by chance.	Stochastic	|βNTI| < 2 and RCbray > 0.95
Homogenizing Dispersal	Microbial communities between samples can freely interact, free and easy mixing between communities results in communities that are more similar to each other than expected by chance.	Stochastic	|βNTI| < 2 and RCbray < -0.95
Undominated	While both deterministic and stochastic processes are at play, differences in observed community composition between samples cannot be explained by either selection or random processes (i.e., Insignificant βNTI and RCbray result)	Both	|βNTI| < 2 and |RCbray| < 0.95

Table 2.1. Description of Community Assembly Processes Associated with Ecological Modeling Results.

do play an important role and can account for 9-66% of microbial community turnover observed between samples as a function of time (**Table A.2** at https://doi.org/10.6084/m9.figshare.14983857). However, individual wells with more neutral pH conditions (7.5-9) display stochastic assembly signatures (|βNTI| < 2), with some influence of variable selection (βNTI > 2) between certain timepoints (**Fig. 2.2A**). The neutral pH well N08-C shows a particularly strong influence of variable selection (25%) over time, indicating that local geochemical conditions may fluctuate enough within the well to drive greater than expected microbial community turnover (**Table A.2** at https://doi.org/10.6084/m9.figshare.14983857).

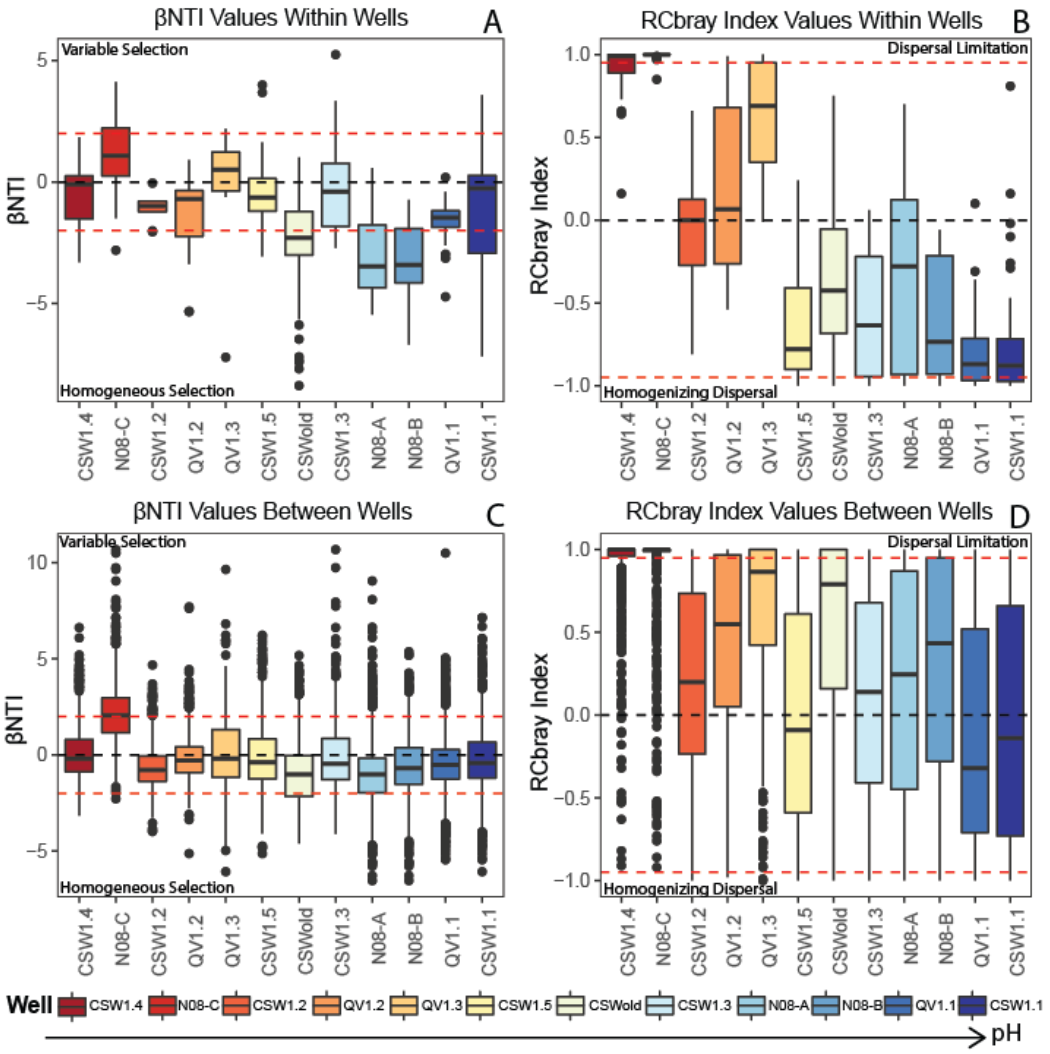

Figure 2.2. Boxplots of the Distribution of βNTI and RCbray Values within Individual Wells Over Time and Between Wells Over Time.

Boxplots showing the distribution of βNTI (A) and RCbray (B) values within individual wells over time, and the distribution of βNTI (C) and RCbray (D) values between wells over time. Boxplots represent pairwise comparisons within individual wells over time (A & B), and pairwise comparisons between samples from each individual well and all other wells (C & D). The dashed black line in plots represents the null expectation. Dashed red lines in each plot represent significance thresholds for both the βNTI and RCbray metrics. Plotted RCbray values (B & D) do not include values from pairwise comparisons that have significant βNTI values. See Table 2.1 for further clarification and interpretation of model results. Wells are organized from lowest to highest average pH in boxplots. Boxplots display the distribution of the data, where the main colored box displays the interquartile range (25th to 75th percentile) of the data. Solid lines within the boxes represent the median of the data. Whiskers on the plot display the maximum and minimum expected values of the data distribution, and black colored points represent outlier data points with respect to the plotted distribution.

Moderate pH (9-10.5) wells are primarily influenced by stochastic processes over time with some influence of both variable and homogeneous selection processes between certain timepoints (**Fig. 2.2A**). Extreme pH (10.5-12) wells become more strongly influenced by homogeneous selection (βNTI < -2) (**Fig. 2.2A**), although stochastic processes still play a significant role within these wells, accounting for 34-91% of assembly within an individual well (**Table A.2** at https://doi.org/10.6084/m9.figshare.14983857). In general, no single assembly process was able to explain variation in microbial community composition between timepoints (14-84% undominated processes) (**Fig. 2.2B; Table A.2** at https://doi.org/10.6084/m9.figshare.14983857), indicating that no single assembly process can explain variation in microbial community composition between timepoints (undominated assembly).

In pairwise comparisons between individual wells, βNTI mean and median values lie close to zero, indicating that stochastic processes dominate (**Fig. 2.2C**). Nevertheless, selection processes still have some influence on between-well comparisons. Variable selection strongly influences pairwise comparisons between the neutral pH (7.5-9) wells CSW1.4 and N08-C with other higher pH (9-12) wells at the site, while homogeneous selection plays a stronger role in pairwise comparisons between the deepest wells at the site N08-A (39.6 m) and CSWold (76.2 m) and other medium to deep wells (20-35 m) with moderate to extreme pH (9-12) (**Fig. 2.2C**). Further characterization of stochastic processes at play in comparisons between wells reveals that dispersal limitation plays a larger role as compared to within well comparisons, but that overall, no single assembly process dominates between well comparisons (undominated assembly) (**Fig. 2.2B & D**). Mean and median RCbray values trend more towards dispersal limitation, with numerous samples within the distribution of pairwise comparisons crossing the significance threshold (RCbray > 0.95) (**Fig. 2.2D**). A small proportion of between well pairwise comparisons

cross the significance threshold for being under the influence of homogenizing dispersal (RCbray < -0.95), suggesting that microbial communities associated with those specific wells are mixing and interacting with each other (**Fig. 2.2D**). These comparisons are primarily associated with the two partially cased wells at the site, CSW1.1 and QV1.1, and nearby wells at similar depths. Discussion of the increased influence of homogenizing dispersal in CSW1.1 and QV1.1 can be found in the **Appendix**.

Mantel tests were used to assess correlations between ecological modeling metrics and measured environmental parameters (**Table A.3** at https://doi.org/10.6084/m9.figshare.14983860). Environmental variables were transformed into Euclidean distance matrices so they could be correlated with ecological modeling matrices. βNTI values were significantly correlated with pH (R = 0.29), ORP (R = 0.23), and DIC (R = 0.14) (**Fig. A.2**). This correlation indicates that greater differences in environmental measurements of pH, ORP, and DIC are associated with variable selection (i.e. more positive values of βNTI). Samples that are more different from each other with respect to pH, ORP, and DIC conditions are likely to be influenced by variable selection, whereas samples with similar pH, ORP, and DIC conditions are likely to be influenced by homogeneous selection. RCbray values were significantly correlated with well depth (R = 0.32), temperature (R = 0.15), pH (R = 0.27), specific conductance (R = 0.34), ORP (R = 0.30), and DIC (R = 0.33) (**Fig. A.3**). That is, samples with greater differences in environmental conditions are more likely to be influenced by dispersal limitation (high RCbray), while samples with more similar environmental conditions are more likely to show influences of homogenizing dispersal. The relative strength of selection processes on microbial communities

seem to be tightly linked to pH, ORP, and DIC conditions, while the influence of stochastic processes are correlated with a wider range of environmental conditions.

Finally, the contribution of each community assembly process was quantified by compiling the number of significant pairwise comparisons for each process and dividing these numbers by the total number of pairwise comparisons. Overall, half of the comparisons could not be attributed to a single assembly process (50% undominated processes), with the other half distributed among dispersal limitation (20%), homogeneous selection (16%), variable selection (12%), and homogenizing dispersal (2%) (**Fig. 2.3; Table A.2** at https://doi.org/10.6084/m9.figshare.14983857). Due to the importance of pH in structuring ecological niches in the system (**Fig. A.4**), community assembly processes were also quantified for all pairwise comparisons between neutral pH (7.5-9) wells (CSW1.4, N08-C, CSW1.2, QV1.2), moderate pH (9-10.5) wells (QV1.3, CSW1.5, CSWold, CSW1.3) and extreme pH (10.5-12) wells (N08-A, N08-B, QV1.1, CSW1.1). When separated into discrete pH ranges, trends in the influence of community assembly processes with pH are evident. As pH increases, the role of variable selection decreases (from 17 to 2%), the role of homogeneous selection increases (from 4 to 25%), the role of dispersal limitation decreases (from 48 to 0%), the role of homogenizing dispersal increases (from 0 to 8%), and the role of undominated processes increase (from 31 to 63%) (**Fig. 2.3 A-E, Table A.2** at https://doi.org/10.6084/m9.figshare.14983857). The increasing role of homogeneous selection indicates that microbial communities are more like each other than expected by chance as pH conditions become more extreme (**Fig. 2.3B**). The shift from dispersal

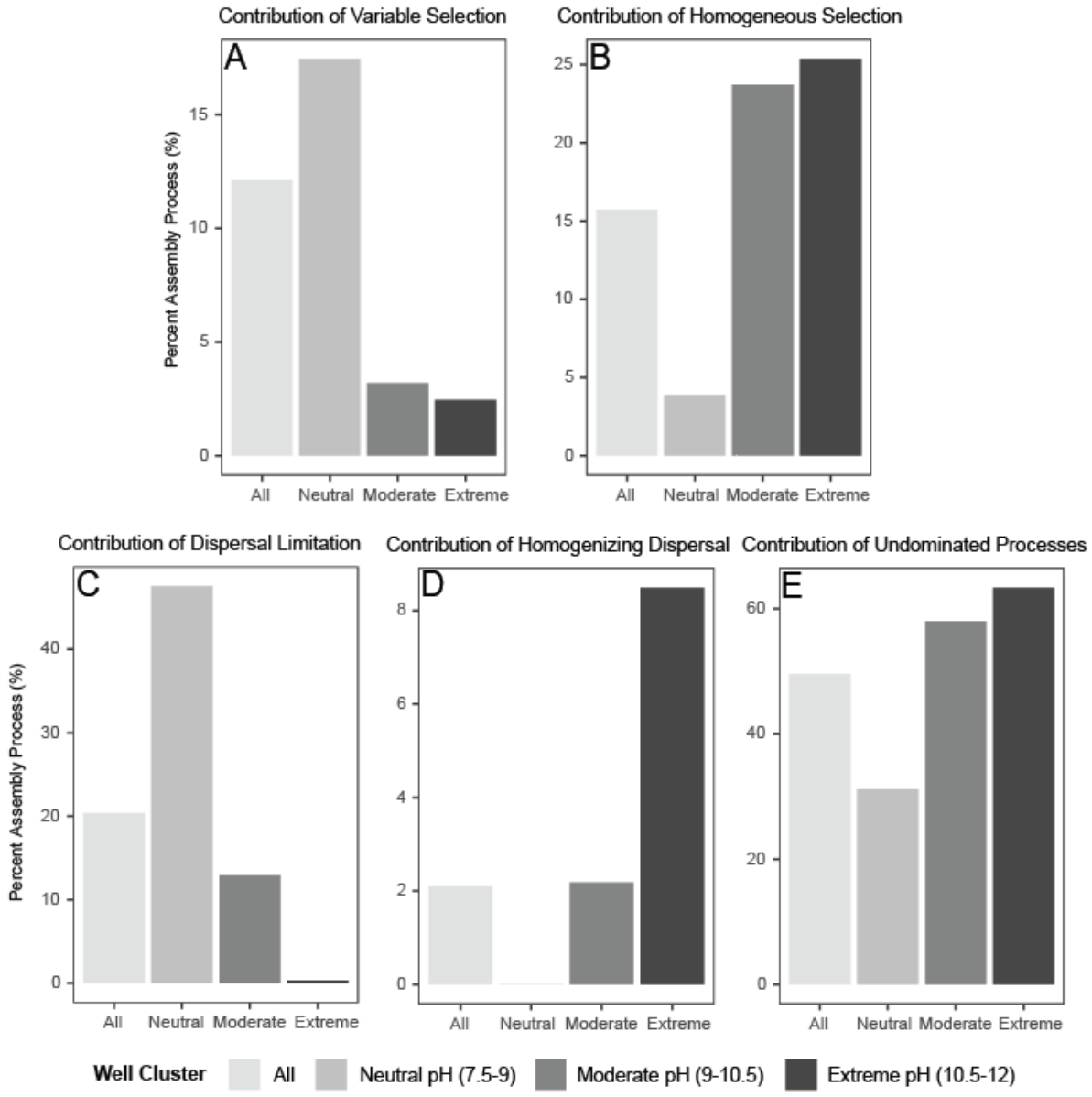

Figure 2.3. Bar Plots of Ecological Modeling Results in All Wells, and Neutral, Moderate, and Extreme pH Wells.

Bar plots showing the overall contribution of variable selection (A), homogeneous selection (B), dispersal limitation (C), homogenizing dispersal (D), and undominated processes (E) for all wells, neutral pH wells (pH 7.5-9), moderate pH wells (pH 9-10.5), and extreme pH wells (pH 10.5-12). The contribution (%) of each assembly process was calculated within each grouping of samples by dividing the number of significant pairwise comparisons for each assembly process by the total number of pairwise comparisons within the sample grouping. Pairwise comparisons include within well comparisons and between well comparisons for all wells and wells within each pH category.

limitation (**Fig. 2.3C**) to homogenizing dispersal (**Fig. 2.3D**) with increasing pH indicates that microbial communities are less isolated from one another, and interact more, at high pH.

Physical Controls on Microbial Dispersal

Ecological modeling results revealed that CROMO microbial communities are overwhelmingly assembled through undominated processes (50% undominated processes; **Table A.2** at https://doi.org/10.6084/m9.figshare.14983857), where neither stochastic nor deterministic processes entirely govern assembly (**Table 2.1**). Since model results indicate that half the data analyzed in the model is governed by a mixture of stochastic and deterministic processes that cannot be well defined by the model (**Table 2.1**) alternative assessments of dispersal and environmental selection (following section) were performed to better understand physicochemical drivers of assembly at CROMO. Connectivity of the aquifer to the surface and estimation of aquifer hydraulic properties were assessed to better understand dispersal within the subsurface.

Characterization of the CROMO aquifer's connectivity to the surface and aquifer hydraulic properties were carried out for this study using tritium analyses and pumping tests as described below. Previous work by Ortiz and colleagues (41) indicated that the main aquifer at CROMO is confined. Tritium analyses (**Table A.4** at https://doi.org/10.6084/m9.figshare.14983863)

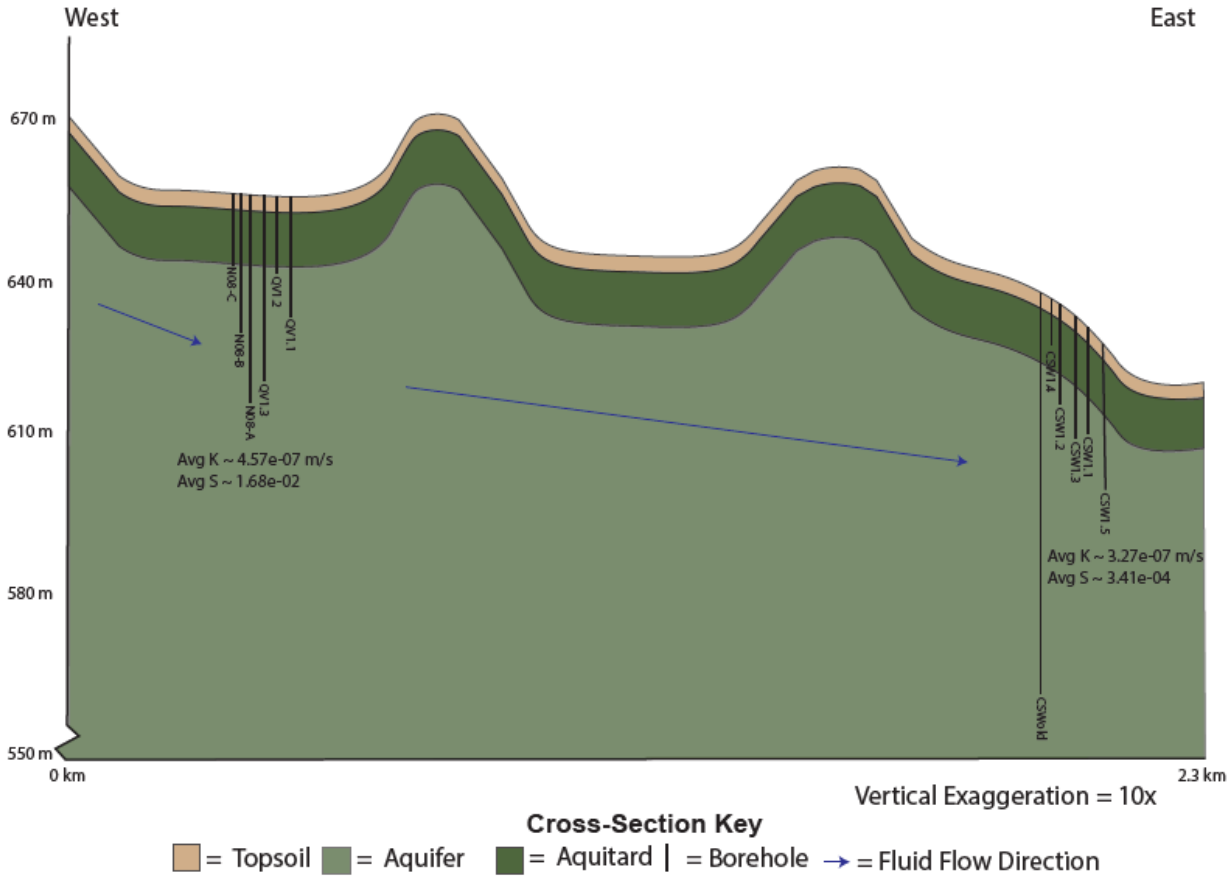

Figure 2.4. Topographic Profile and Cross-Section of the CROMO Aquifer.

Cross-section with 10x vertical exaggeration showing the topographic profile of the landscape around the CROMO wells. Well locations are scattered close to the cross-section line, so well locations were estimated in their approximate order from west to east. Wells are drawn to accurate depth based on the surface elevation within the profile. The depths of the topsoil and aquitard layers were estimated based on geophysical mapping done by Ortiz and colleagues (41). Given that the same units were present at both the CSW and QV clusters and were about the same thickness, we made the simplifying assumption that the topsoil and aquitard layers are laterally continuous and of even thickness between well cluster locations. We estimated that the main aquifer was 76.2 m thick. It needed to accommodate the depth of CSWold, but we do not have a good estimate as to the depth where basement rock begins. The general direction of groundwater flow is shown within the diagram, and average estimates for hydraulic conductivity (K) and storativity (S) at each well cluster are included from Table A.5. (https://doi.org/10.6084/m9.figshare.14983866).

performed on samples collected in May of 2017 were below detection (0.8 tritium unit (T.U.)) in all wells except for a shallow well, N08-C, where tritium was detected at 0.9 T.U.

Pumping tests used to estimate aquifer hydraulic conductivity (K) indicate that water flows through the subsurface at a slow rate (K = 10^{-7} m/s) (**Fig. 2.4; Table A.5** at https://doi.org/10.6084/m9.figshare.14983866). Estimates of K and other hydraulic properties (**Table A.5** at https://doi.org/10.6084/m9.figshare.14983866) are in line with estimates obtained at the Samail ophiolite, Sultanate of Oman (42) and Koniambo massif in New Caledonia (43).

Adaptations to Environmental Conditions

Given the distinct geochemical trends observed at CROMO (**Fig. 2.1**), a PERMANOVA analysis was performed on Bray-Curtis dissimilarities and measured environmental data to determine how much variance in the community dissimilarity data can be explained by measured environmental data (**Table 2.2**). Results from this analysis show that well location (i.e. corresponding subsurface location) (R^2 = 0.468) is the primary driver of differences in microbial

Variable	Degrees of Freedom	Sum of Squares	Mean Squares	F Score	R^2	p-value
Well	11	16.239	1.47626	8.0442	0.46783	**0.001**
Days	1	1.018	1.01783	5.5461	0.02932	**0.001**
Temperature (°C)	1	0.145	0.14524	0.7914	0.00418	0.702
pH	1	0.355	0.35524	1.9357	0.01023	**0.028**
Conductance (mS)	1	0.274	0.27357	1.4907	0.00788	0.113
DO (mg/L)	1	0.376	0.37644	2.0512	0.01084	**0.014**
ORP (mV)	1	0.274	0.27357	1.4907	0.00788	0.09
DIC (µM)	1	0.431	0.43122	2.3497	0.01242	**0.006**
Residuals	85	15.599	0.18352		0.4494	
Total	103	34.711			1	

Table 2.2. PERMANOVA Results.

Results from PERMANOVA analysis on Bray-Curtis dissimilarities and associated sample metadata. R^2 values indicate the percent variation in community dissimilarity that can be described by an individual variable.

community composition. Significant differences in microbial community composition are also seen over time (R^2 = 0.029) and are driven by differences in DIC (R^2 = 0.012), DO (R^2 = 0.011), and pH (R^2 =0.010) to a lesser extent (**Table 2.2**). PERMANOVA results also indicate that a significant amount of variation in microbial community composition is unexplained (Residuals R^2 = 0.44) (**Table 2.2**). It is important to note that community composition changes related to changes in time, DIC, DO, and pH may already be accounted for as a portion of the large amount of variance explained by individual well location. This observation could explain why the amount of variation described by each individual variable is quite low (R^2 of 0.01 to 0.029). We performed an additional PERMANOVA analysis without the well location variable to further explore this result. While less of the overall variance in community composition is explained (Residuals R^2=0.69), more variance in community composition is associated with geochemical metadata, especially pH (R^2=0.13) (**Table A.6** at https://doi.org/10.6084/m9.figshare.14983869). The increased variance accounted for in the data when considering the well location variable likely includes both measured and unmeasured physicochemical data specific to each well location (**Table 2.2**).

Since pH appears to play an important role in structuring ecological niches at CROMO (**Fig. A.4; Table 2.2; Table A.6** at https://doi.org/10.6084/m9.figshare.14983869), as well as microbial communities in a variety of environments (24,33), the influence of pH in structuring CROMO microbial communities was further assessed. While DO and DIC concentrations were also found to drive changes in community composition (**Table 2.2**), DO was not found to be significantly correlated with ecological model βNTI values, which assess the role of environmental selection (**Fig. A.2, Table A.3** at https://doi.org/10.6084/m9.figshare.14983860). DIC was significantly correlated with βNTI values but is not assessed here since pH has been shown to

govern the amount of available DIC in serpentinizing systems (44). Due to this, environmental selection due to changes in DIC availability should ultimately be controlled by pH conditions.

Community richness (number of unique taxa in a community) and evenness (how close in numerical abundance taxa in a community are; measured by Pielou's evenness index) decrease as pH increases (**Fig. 2.5A & B**). This result supports previous reports that pH is a major driver of microbial community diversity at the site (15), as has been seen in numerous other environments (24,33). To further assess this point, metagenomic and metatranscriptomic data collected during the 2011-2013 field campaigns and again in 2016 were screened for genes associated with adaptations to high pH (https://doi.org/10.6084/m9.figshare.14372030). It is known through physiological studies of alkaliphilic cultures at high pH that a proton (H^+) gradient exists from cell

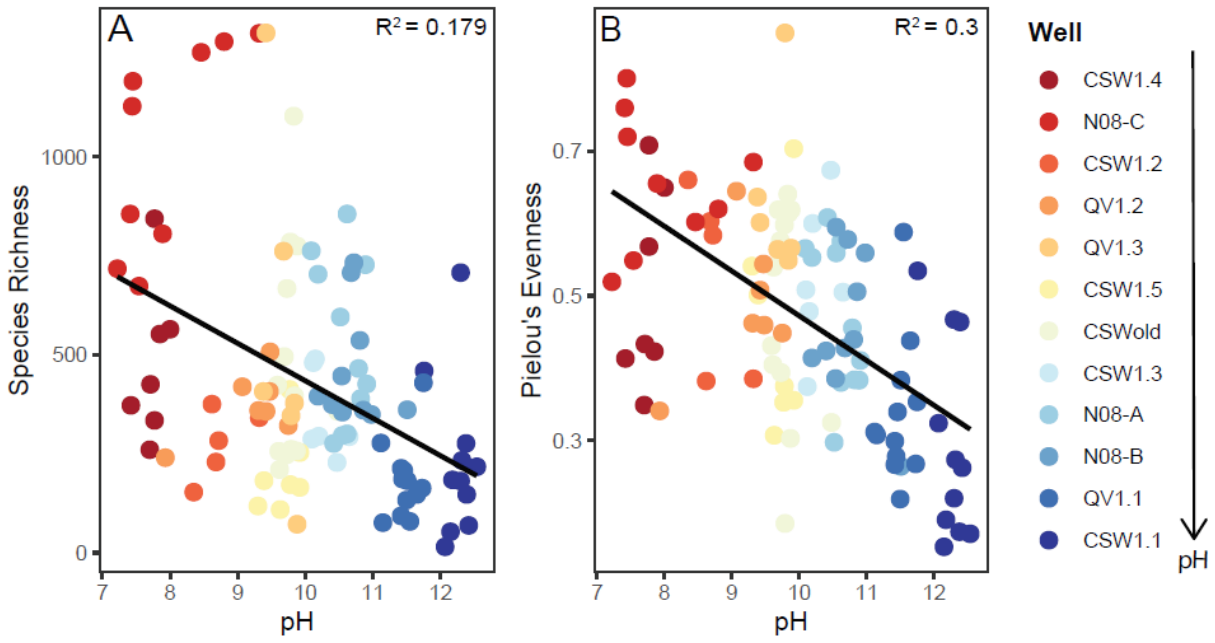

Figure 2.5. Microbial Community Richness and Evenness vs. pH.

Microbial community richness (A) and evenness (B) plotted against pH. Points represent individual microbial community samples, which are colored are by well location. Wells are organized from lowest to highest average pH in the legend. Linear regression lines are plotted in black. Significant ($p \leq 0.05$) regression R^2 values are displayed in the upper right corner of plots.

cytoplasm to cell exterior that can drive loss of protons from the cell (45). To combat this issue, microorganisms must actively transport protons back into the cell (45). The use of cation/proton antiporters, which can transport sodium (Na^+) or potassium (K^+) ions out of the cell while transporting protons into the cell, as well as Na^+ pumping V-type ATPases, which pump Na^+ ions across the cell membrane to generate ATP, are common mechanisms used by microorganisms growing in alkaline pH conditions (45,46). We find that CROMO metagenomes have abundant Na^+/H^+ and K^+/H^+ antiporters, and Na^+ pumping V-type ATPases (https://doi.org/10.6084/m9.figshare.14372030). The abundance and transcription of genes encoding carbonic anhydrases cynT/can and cah and sporulation genes spoVAA and spoVAB decrease with increasing pH (**Fig. 2.6 A, F, M, & N**), while the abundance and transcription of genes associated with motility, pili for motility and adhesion, Na^+/H^+ antiporters, Na^+ dependent V-type ATPases, Na^+ dependent bicarbonate transporters, and the sporulation gene spoVR increase with increasing pH (**Fig. 2.6 B-E, G-L, O-P**). The abundance and transcription of genes associated with motility and adhesion, Na^+/H^+ antiporters, Na^+ dependent bicarbonate transporters, Na^+ pumping V-type ATPases, sporulation, and survival related transcription factors increase with increasing salinity and depth (**Fig. A.5 A-R**). Despite a great abundance of sporulation genes at depth, poor transcription of these genes paired with evidence for the transcription of other maintenance and metabolic genes (20,22), indicate that microbial community members were not actively employing this strategy to cope with extreme environmental conditions at the time of sampling. The abundance and transcription of genes associated with sporulation, Na^+/H^+ antiporters, and Na^+ pumping V-type ATPases decrease with increasing ORP (**Fig. A.6 A-F**). The abundance and transcription of genes associated with carbonic anhydrases increase with increasing concentrations of DIC (**Fig. A.6 G & L**), while the abundance of genes associated with

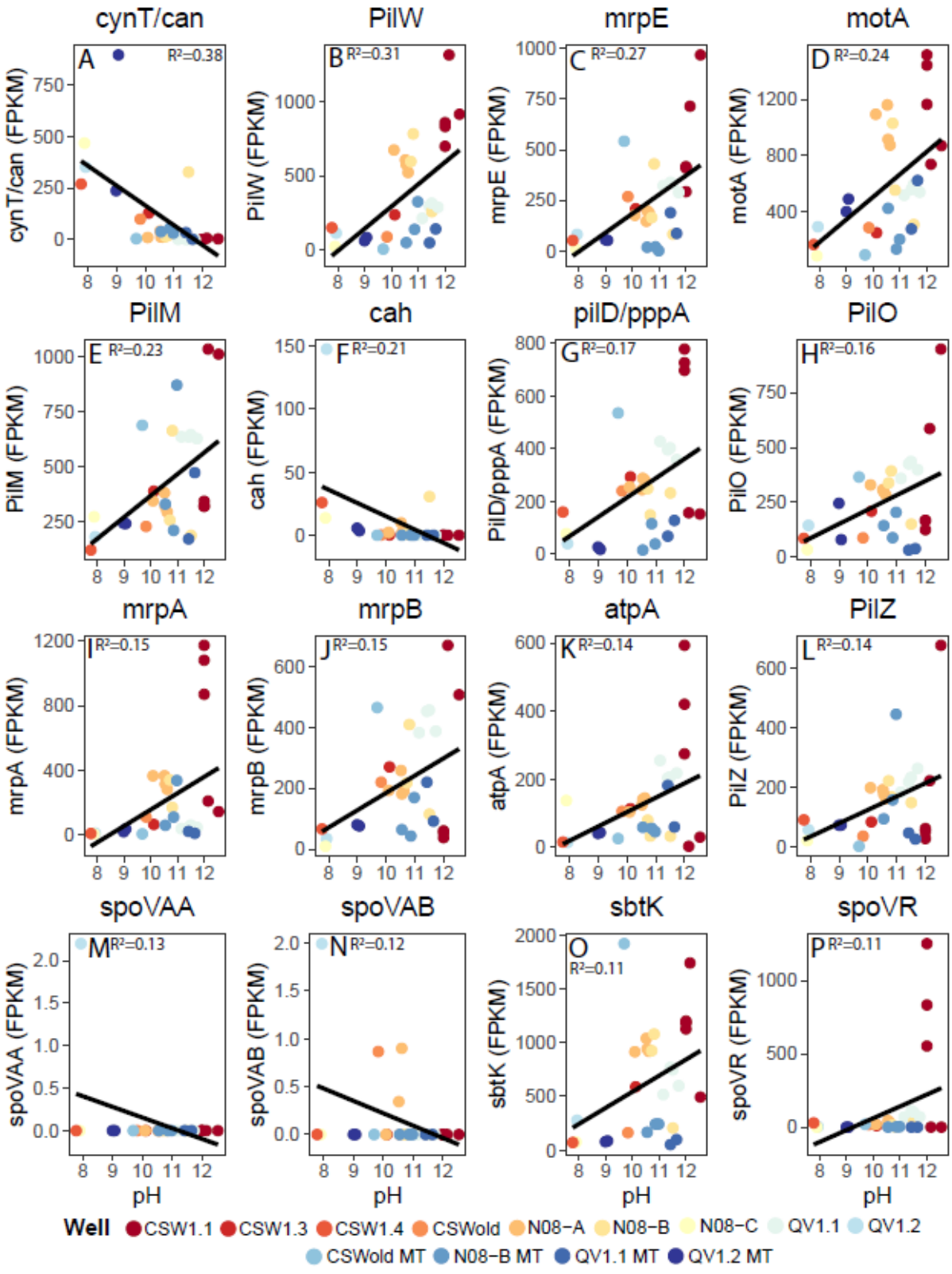

Figure 2.6. Regression Plots of pH Adaptation Genes from Metagenomic and Metatranscriptomic Data against pH.

Figure 2.6. continued.

Significant linear regression plots of the normalized abundance of metagenomic and metranscriptomic data in fragments per kilobase per million reads (FPKM) for the genes cynT/can (A), PilW (B), mrpE (C), motA (D), PilM (E), cah (F), pilD/pppA (G), PilO (H), mrpA (I), mrpB (J), atpA (K), PilZ (L), spoVAA (M), spoVAB (N), sbtK (O), and spoVR (P) plotted against pH. Solid black lines represent a linear trendline. Linear regression R^2 values are included at the top of each plot. Samples of metagenomic and metatranscriptomic data are colored by well location. Metatranscriptomic samples are labeled with an MT following the well name in the legend. Functions associated with genes are as follows: motility/adhesion (PilW, motA, PilM, pilD/pppA, PilO, PilZ), sodium:hydrogen antiporters (mrpE, mrpA, mrpB), sporulation (spoVAA, spoVAB, spoVR), sodium dependent bicarbonate transporters (sbtK), sodium dependent V-type ATPase (atpA), carbonic anhydrase (cynT/can, cah).

Na^+/H^+ antiporters, and motility and adhesion decrease with increasing concentrations of DIC (**Fig. A.6 H-K**). The abundance and transcription of genes associated with motility and adhesion, sporulation, Na^+ pumping V-type ATPases, Na^+ dependent bicarbonate transporters, and K^+/H^+ symporters increase with increasing temperature (**Fig. A.6 M-V**). Linear model results for significant and insignificant regressions can be found in **Table A.7** (https://doi.org/10.6084/m9.figshare.14983872) and an additional table published on FigShare (https://doi.org/10.6084/m9.figshare.14939202), respectively.

In addition to the community diversity, metagenomic, and metatranscriptomic evidence provided, phylogenetic analysis of these communities using the nearest taxon index (a within sample, or alpha diversity, variation of the βNTI metric used for ecological modeling) indicate that CROMO microbial communities are composed of closely related organisms and demonstrate significant phylogenetic clustering (**Fig. A.7**). Phylogenetic clustering indicates that environmental filtering and the conservation of adaptive traits have likely occurred as the result of habitat specialization (47).

Discussion

Given the extreme pH conditions at CROMO, we anticipated that deterministic processes would be dominant, as has been observed in other systems under extreme or stressful environmental conditions (33,48–52). Ecological modeling results revealed that community assembly at CROMO instead occurs through a combination of deterministic and stochastic processes that cannot be well defined (undominated assembly; **Table A.2** at https://doi.org/10.6084/m9.figshare.14983857). Because the model cannot define the stochastic and deterministic processes at work when undominated assembly governs pairwise comparisons we employed alternative methods to assess the roles of dispersal (**Fig. 2.4; Table A.4** at https://doi.org/10.6084/m9.figshare.14983863) and selection (**Figs. 2.5, 2.6, A.5, A.6, A.7; Table 2.2**) within the CROMO aquifer. Here we explore the combined results and aim to describe the stochastic and deterministic processes at work within the undominated fraction of data identified by the ecological model. We discuss the roles of dispersal and selection in the CROMO aquifer, incorporating results and interpretations from the multiple data streams reported here, as well as previous reports and interpretations of community assembly relevant to observations in this study.

While most assembly processes at CROMO cannot be well defined (undominated assembly), dispersal limitation (20%) and homogeneous selection (16%) are the two primary quantifiable processes at work within the aquifer (**Fig. 2.3; Table A.2** at https://doi.org/10.6084/m9.figshare.14983857). Evidence of dispersal limitation is clear when looking at the hydrogeology of the system (**Fig. 2.4**). Tritium levels below detection in well fluids (**Table A.4** at https://doi.org/10.6084/m9.figshare.14983863) indicate that the main aquifer is not well connected to the surface and that modern recharge (fluid <50 years in age) does not contribute appreciably to the subsurface reservoir (38,53). When considered alongside hydraulic conductivity

estimates (**Table A.5** at https://doi.org/10.6084/m9.figshare.14983866), these results indicate that the CROMO aquifer is a confined system receiving no detectable modern recharge and is characterized by poor connectivity between wells and low rates of fluid flow (**Fig. 2.4**). Differences in compositional beta diversity (Bray-Curtis dissimilarity; **Table 2.2**) provide additional evidence of dispersal limitation. The mean Bray-Curtis dissimilarity at the site when considering all pairwise comparisons is extremely high (0.8), indicating that compositional diversity of microbial communities have little overlap (54,55). Differences in well location (and conditions – see results relevant to **Table 2.2 & Table A.6** at https://doi.org/10.6084/m9.figshare.14983869) alone account for nearly 50% of observed variation in community dissimilarity, while changes in community composition over time follows at a much lower level of explained variance (~3%) (**Table 2.2**). Additionally, 44% of the variation in microbial community composition could not be explained by environmental variables during PERMANOVA analysis. The unexplained variation in community composition could be the result of stochastic changes in community composition due to ecological drift. Isolation of microbial communities due to dispersal limitation could certainly introduce enough ecological drift within each well location to generate such high levels of microbial community compositional dissimilarity (56–59). Environmental heterogeneity and differences in community size could be another potential explanation for the observed high beta diversity (58). However, hydrologic data paired with the fact that the null ecological modeling method accounts for differences in alpha diversity (60) indicate that model results are accurate and high observed beta diversity is the result of ecological drift.

The influence of selection is also clear throughout the site. The metacommunity (average sitewide NTI=1.73), as well as local communities sampled through time, show significant

phylogenetic clustering, indicating that microorganisms within the aquifer are highly adapted to environmental conditions (**Fig. A.7**). While it is unlikely that this observation is solely due to high pH adaptations, pH is known to be a significant driver of microbial community composition (33,61), and high pH conditions and the physiological adaptations required to survive in these conditions likely played a significant role in structuring the observed microbial communities at CROMO. Microbial community diversity measures are also significantly affected by pH conditions (**Fig. 2.5**), and metagenomic and metatranscriptomic data indicate that pH homeostasis mechanisms used in alkaline conditions are prevalent and actively transcribed within the wells (**Fig. 2.6;** https://doi.org/10.6084/m9.figshare.14372030). The increased abundance and transcription of genes associated with motility at high pH, including flagellar synthesis genes, and Type IV pili (**Fig. 2.6 B, D-E, G-H, & L**) potentially represents a means to improve access to both limited available DIC and oxidants in the deep subsurface, or to enable the attachment of organisms to minerals to form biofilms and/or aid in electron transport to mineral surfaces. Improved access to substrates via motility or adhesion, and the capability to form biofilms that can lower pH within the microenvironment (62) may be key survival strategies that allow microbial populations to persist under hyperalkaline conditions in the deep subsurface. Additionally, factors such as DO concentrations (**Table 2.2**), redox conditions (**Fig. A.6 A-F**), salinity (**Fig. A.5 A-I**), temperature (**Fig. A.6 M-V**), DIC concentrations (**Table 2.2; Fig. A.6 G-L**), which are likely controlled by pH, and other unmeasured variables likely play a smaller role in driving community composition differences across the wells (**Table 2.2; Table A.6** at https://doi.org/10.6084/m9.figshare.14983869). While ecological modeling results did not identify homogeneous selection as the dominant assembly process across the site (**Table A.2** at https://doi.org/10.6084/m9.figshare.14983857), other measures of microbial community diversity

(**Fig. 2.5; Table A.2** at https://doi.org/10.6084/m9.figshare.14983857**; Table A.6** at https://doi.org/10.6084/m9.figshare.14983869), phylogeny (**Figs. A.4 & A.7**), and physiology (**Fig. 2.6;** https://doi.org/10.6084/m9.figshare.14372030) indicate that pH plays a major role in structuring microbial community composition in the CROMO aquifer.

Given the strong evidence for selection and dispersal limitation within the physicochemical and microbial community data, the preponderance of undominated processes at the site was initially surprising. However, recent studies in soil (33) and a fractured shale aquifer (34) using the Stegen et al. (28) ecological modeling framework provide some insight. Tripathi and colleagues (33) showed that while pH plays a significant role in structuring soil microbial communities, selection imposed by pH only accounted for ~17% of observed assembly. As in our study, this low value indicates that other assembly processes still play a substantial role in structuring microbial communities under extreme pH conditions. Recent work by Danczak and colleagues (34) in a fractured shale aquifer highlighted how strong concurrent homogeneous selection and variable selection counteract to result in an undominated community assembly signal. While this same mechanism is not observed at CROMO, results from Danczak and colleagues (34) demonstrate that an undominated assembly signal can be the result of strong counteracting processes. Extreme pH and slow fluid flow at CROMO consistently impose strong counteracting deterministic and stochastic processes, resulting in the undominated assembly signal observed across the site (**Fig. 2.3E**).

Our observations at CROMO are also supported by recent computational and experimental work that has shown that dispersal conditions and microbial community size affect the importance of selection in structuring microbial communities (30,59). Strong environmental selection can result in low diversity and low biomass communities that are inherently prone to enhanced drift as

theorized by Vellend (23) and observed in computational modeling experiments by Evans and colleagues (30). Ecological drift in communities assembled under strong selection can be further enhanced under low dispersal conditions (30,59), resulting in microbial communities composed of a small number of highly abundant species, with large variation in the birth and death rates of rare taxa within the communities (59). Microbial communities characterized in serpentinizing systems to date have notoriously low diversity and are primarily composed of a few dominant taxa and many highly variable low abundance species (6,15,16,22,44), which likely makes serpentinite microbial communities inherently prone to enhanced ecological drift.

Finally, we propose a more nuanced mechanism of assembly within the serpentinizing subsurface, relevant to the geological history (63) and long groundwater residence times in the region (64). Poor connectivity to the surface (**Table A.4** at https://doi.org/10.6084/m9.figshare.14983863) and slow fluid flow in the subsurface (**Fig. 2.4; Table A.5** at https://doi.org/10.6084/m9.figshare.14983866) indicate that dispersal of microorganisms into and out of the region is extremely slow. Microorganisms present within the serpentinizing subsurface were therefore potentially transported to the terrestrial surface when the ophiolite was obducted and continued to grow and persist (22,65), or were introduced to the system by persisting hundreds or thousands of years along slow regional groundwater flow pathways, similar to observations of community assembly patterns in deep seafloor sediments (52). In either case, extreme pH conditions buffered by the presence of serpentine minerals present throughout much of the ophiolite (66) impose strong environmental filtering and likely selects for well-adapted alkaliphilic microorganisms long before they reach the subsurface localities observed in this study (52). Within this geologic context we suggest that homogeneous selection imposed by extreme pH structures a low diversity alkaliphilic metacommunity within the larger region of the

CROMO aquifer from which the observed local communities in this study are assembled. Within observed local communities' homogeneous selection maintains the persistence of dominant alkaliphilic microbial community members. At the same time, poor dispersal between local communities and variability in the birth and death rates of the large pool of rare community members results in enhanced ecological drift over space and time (23,30,59). Overall, these results highlight the important roles and complex interplay that occurs between selection, dispersal, and ecological drift in structuring subsurface microbial communities. Given the great heterogeneity observed in subterranean environments, it is critical to continue to assess community assembly processes in these systems to better constrain how different physical and environmental conditions structure microbial communities within the expansive subsurface biosphere.

Materials and Methods

Site Description and Sample Collection

CROMO is located within the McLaughlin Natural Reserve near Lower Lake, CA. This site lies within the Coast Range Ophiolite and consists of 4 wells drilled >30 years ago, and 8 wells drilled in August of 2011. The latter set of wells was drilled using techniques designed to minimize and quantify subsurface contamination (40). Initial characterization of CROMO fluids indicated a strong influence of serpentinization (low Eh, pH>11) and microbial communities that share similarity to other characterized serpentinite springs (11,15,40). The main aquifer is confined by a well-cemented aquitard (41), and tritium analyses, described below, indicate no mixing of modern surface water within the aquifer (53,67). CROMO has been sampled 2-3 times per year since the site was established in 2011, resulting in a high-resolution time series dataset of geochemistry and microbial biodiversity. The sampling procedure utilized to collect fluids from CROMO wells has

been previously described (11,15). Geochemical and microbial sample collection methods are described in detail in the **Appendix**.

Topographic Profile and Cross Section Construction

A topographic profile and cross-section of the study area (**Fig. 2.4**) were created using ArcMap (Esri, Redlands, CA, USA), and Adobe Illustrator (Adobe, San Jose, CA, USA). Well-head locations and elevations were obtained as described in the **Appendix** and drawn into the cross section at their proper location and depth. Well-head coordinate and elevation data are listed in **Table A.8** (https://doi.org/10.6084/m9.figshare.14983893). A detailed description of topographic profile methods, and assumptions made in the construction of the cross-section can be found in the **Appendix**. Detailed maps displaying the location of McLaughlin Reserve in California, a geologic map of the CROMO site, and the location of each well cluster at the site can be found in Ortiz et al. (41).

Estimation of Aquifer Properties

Aquifer properties were estimated using the program AQTESOLV (68). Drawdown/Recovery analysis was performed within AQTESOLV to obtain estimates of transmissivity (T), and storativity (S) to calculate hydraulic conductivity (K) using T and aquifer thickness (b) according to the following equation: $T = K \times b$ (**Table A.5** at https://doi.org/10.6084/m9.figshare.14983866). Detailed description of data collection, model parameters, and fitting model solutions can be found in the **Appendix**.

Tritium Sample Collection

Water samples for tritium analyses were collected in June of 2017. Water was collected into 0.5 L narrow-mouth high-density polyethylene bottles. Samples were air-tight and bottle mouths were wrapped with parafilm to prevent evaporation or leakage from the bottles. Samples were stored at room temperature and shipped to University of Waterloo Environmental Isotope Laboratory (UW-EIL, Waterloo, ON, Canada). Detailed methods of tritium analyses performed by UW-EIL are described in the **Appendix**. Measured tritium values for each well are included in **Table A.4** (https://doi.org/10.6084/m9.figshare.14983863).

Geochemical Analyses

Analytical methods used to measure DIC have been previously described (11,15). Briefly, fluid samples were acidified to convert all forms of DIC to carbon dioxide (CO_2), which could partition into the headspace of the sealed sample vial. Subsequently, the concentration of CO_2 in the headspace gas was quantified by gas chromatography with flame ionization detection (SRI 8610C; SRI Instruments, Torrance, CA, USA), using an inline methanizer to convert liberated CO_2 to methane prior to passage through the FID. All analyses were performed in duplicate. Geochemical data used for analyses can be found in **Table A.1** (https://doi.org/10.6084/m9.figshare.14983851).

Extraction of DNA and RNA

Extractions of DNA and RNA from 0.22 um Sterivex© filter cartridges were performed as previously described by Twing and colleagues (15) and Sabuda and colleagues (22), respectively. A brief description can be found in the **Appendix**.

Sample Preparation, Sequencing, and Data Analysis of Metagenomes and Metatranscriptomes

Metagenomic and metatranscriptomic sequences were previously reported (15,20,22). Sample preparation and sequencing of metagenomes and metatranscriptomes were carried out as previously described (22). The assemblies and predicted protein annotations reported here were performed as previously described by Sabuda and colleagues (22).

16S rRNA Gene Amplicon Sequencing

Throughout the course of the project, samples were submitted for amplicon sequencing of the V4 region of the 16S rRNA gene at three different sequencing centers: Department of Energy Joint Genome Institute (JGI), Marine Biological Laboratory's (MBL) Josephine Bay Paul Center, and the Michigan State University (MSU) Genomics Core Facility (**Table A.9** at https://doi.org/10.6084/m9.figshare.14983896). Sequences generated by the JGI were reported by Twing and colleagues (15). Sequences generated by the MBL were reported by Crespo-Medina and colleagues (11). Samples sequenced at the MSU Genomics Core were submitted for sequencing of the V4 region of the 16S rRNA gene. Amplification, quantification, and sequencing procedures performed by the MSU Genomics Core have been previously described (22). Blanks and extraction blanks collected alongside samples in this dataset could not be quantified or amplified and were not submitted for sequencing.

16S rRNA Sequence Processing

Sequences generated by JGI, MBL, and the MSU Genomics Core were processed using mothur v1.39.5 (69) as previously described (11,15,22). Quality-trimmed fasta files and count tables for sequences from each sequencing center were concatenated together and clustered into

OTUs at a 3% distance threshold using the *de novo* distance-based greedy clustering (DGC) method as implemented in mothur v1.39.5 (70). *De novo* clustering has successfully been used to compile and re-analyze 16S rRNA data from multiple sources for large meta-analysis studies of the human microbiome (71,72). Continued discussion on the successful use of DGC to cluster sequences from different sequencing centers and analyses of sequences clustered using this method are included in the **Appendix**. Clustered OTUs were aligned to the SILVA SSURef alignment (v132), and taxonomic classifications were assigned using mothur.

Following the successful merger of the 16S rRNA datasets (23,994 OTUs and 6,210,850 reads), count data from sample replicates were averaged and rounded to the nearest whole count number to avoid statistical issues that can arise from pseudoreplication (73,74). Singletons, which rounded to zero when present within a set of replicates, were removed (8,526 OTUs), and sequences identified as eukaryotes (58 OTUs and 1,475 reads), archaea (138 OTUs and 7,271 reads) mitochondria (46 OTUs and 1,295 reads), chloroplasts (94 OTUs and 7,881 reads), and unknown (842 OTUs and 9,127 reads) by SILVA were removed. Following this process, the 16S rRNA sequences were screened for potential contaminants associated with DNA extraction reagents and for human skin and fecal-derived organisms previously identified in deep subsurface samples by Sheik and colleagues (75). Following analysis of the taxonomy and distribution of each potential contaminant within the dataset, sequences that were likely contaminants were removed from the dataset (792 OTUs and 111,576 reads). In addition to this cleanup, two human contaminant microorganisms, *Simkania negevensis* (76) and *Akkermansia muciniphila* (77), were removed that were identified at high abundance in a handful of samples. These organisms from families cvE6 and Akkermansiaceae accounted for a maximum of 39% and 48% of the reads in the affected samples, respectively, and 1.6% of total reads from the dataset. There were no patterns

in sample contamination by these two organisms when looking at sample collection, or sample extraction logs. A similar approach to removing contaminant sequences from a deep subsurface dataset was successfully used by Fullerton and colleagues (78). The final 16S rRNA dataset used for analysis consisted of 13,444 OTUs and retained 96% of the original reads (5,974,056 reads). Following dataset filtering, a phylogenetic tree was generated using FastTree v2.1.3 (79).

Excel files containing raw count table data, averaged and contaminant filtered data, and count and taxonomy information for removed OTUs (https://doi.org/10.6084/m9.figshare.14879535 and https://doi.org/10.6084/m9.figshare.14371964) are available on FigShare along with R code used to identify and screen potential contaminant OTUs (https://figshare.com/projects/Community_Assembly_in_Serpentinizing_Ophiolites/101648).

Statistical Analyses

Basic statistical analyses and data exploration of the community data and associated metadata were performed using the R packages phyloseq and vegan (80,81). These packages were used to combine and organize 16S rRNA tag sequencing data with corresponding sample metadata and to perform basic data visualization and data analysis. Correlations between the ecological modeling matrices and environmental variables were performed using Mantel tests, using the command mantel.rtest() from the R package ade4 (82). PERMANOVA analyses were performed in vegan using the adonis() function (28). PERMANOVA results were used to define significant relationships between community data and environmental variables. Sample richness was calculated using the function specnumber() from the R package vegan (81). Pielou's evenness was calculated by dividing the Shannon diversity index, calculated using the function diversity() in

vegan (81), by sample richness, which was previously calculated. Geochemical data, richness and Pielou's evenness data, and metagenomic and metatranscriptomic data were plotted in ggplot() and linear regression models were calculated using the lm() function.

Ecological Modeling

Ecological modeling of community and phylogenetic turnover within the system was performed according to the framework developed by Stegen and colleagues (28). A basic assumption of the framework is that there is significant phylogenetic signal (i.e., closely related organisms have similar habitat preferences) at short phylogenetic distances, making the use of the βNTI metric, which assesses phylogenetic turnover between close relatives, an ideal measure for the framework (60). Mantel correlograms were used to test for phylogenetic signal at different phylogenetic distance classes. Positive, significant correlations at short phylogenetic distances were observed when pH environmental niches were assessed (**Fig. A.4**), indicating that the community assembly framework developed by Stegen and colleagues (28) was an appropriate choice for the dataset analyzed here.

The framework developed by Stegen and colleagues uses two different metrics to quantify the contributions of selection, dispersal, and ecological drift that contribute towards an observed assembled community (28). This model can quantify all processes except for speciation/diversification as has been outlined in Vellend's seminal paper that conceptualizes the processes of community assembly (23). The Stegen et al. framework (28) first assesses the role of selection by assessing changes in phylogenetic distance using βMNTD and βNTI for all pairwise comparisons within the dataset. Once the role of selective processes have been assessed, pairwise comparisons that were not significant with the βNTI metric are assessed with the RCbray metric

to look at the role of the stochastic processes of dispersal and drift (28). Detailed description of the model and how each metric is calculated is included within the **Appendix**.

All R scripts, excel, and csv files used in analyses are available on Figshare at https://figshare.com/projects/Community_Assembly_in_Serpentinizing_Ophiolites/101648

Sequence Data Availability

The 16S rRNA gene sequence data used in this work are publicly available in the NCBI Sequence Read Archive (SRA) under the Bioproject accession number: PRJNA690585. CROMO metagenome sequences previously published by Twing and colleagues (15) are publicly available in the JGI IMG/M database under the project IDs: 1021918, 1021921, 1021924 and 1021927; and in the MG-RAST database under the following sample IDs: 4569549.3, 4569550.3, 4569551.3 and 4569552.3. Metagenome sequences previously published by Seyler and colleagues (20) are publicly available under the Bioproject IDs: PRJNA410019, PRJNA410020, PRJNA410022, PRJNA410035, PRJNA410037, PRJNA410553, PRJNA410555, PRJNA410036, PRJNA410024, PRJNA410028, PRJNA410025, PRJNA410023, PRJNA410027, and PRJNA410026. Metagenomic sequences collected in 2016 are publicly available in the NCBI Sequence Read Archive (SRA) database under the following Accession IDs: SRX9385611, SRX9385612, SRX9385613. CROMO metatranscriptome sequences previously published by Sabuda and colleagues (22) are publicly available in the SRA under the following Accession IDs: SRX3339504, SRX3339503, SRX3339089, SRX3331179, SRX3331177, SRX3330963, SRX3330943, and SRX3330753.

Acknowledgments

We thank Cathy Koehler and Paul Aigner, Co-directors of the University of California - Davis McLaughlin Reserve for their support and help in establishing CROMO and continued field work at the site. Thanks to Kate Fullerton (UTK) for advice and examples of the contaminant filtering process and Brent Heerspink (MSU) for guidance and feedback on hydrological modeling work. Special thanks to Katrina Twing and Melitza Crespo-Medina for their involvement in this project and sample collection during the early years of this project. This work was supported by the NASA Astrobiology Institute CAN-7 Rock Powered Life Grant #NNA15BB02A.

APPENDIX

Materials & Methods

Sample collection

Fluids were pumped to the surface using permanently emplaced positive displacement Teflon bladder pumps (Geotech Environmental Equipment, Denver, CO, USA), and flushed through a YSI 3059 flow-through cell attached to a YSI multiprobe (Yellowsprings, OH, USA). The flow-through cell measured pH, oxidation-reduction potential (ORP), dissolved oxygen (DO), specific conductance, and temperature (11,15). Fluid sampling from tubing attached directly to the flow-through cell began following the stabilization of fluid temperature and DO. Fluid samples to measure dissolved inorganic carbon (DIC) were collected by attaching syringes directly to the tubing attached to the flow-through cell, allowing for anoxic sampling of the fluids. DIC samples were filtered through a 0.22 μm syringe filter into an acid washed serum vial filled with N_2 and a pre-set volume of phosphoric acid (11,15). Fluids for molecular microbiology samples were collected in a sterile 4 L cubitainer, filtered through 0.22 μm Sterivex© filters (Merck Millipore, Billerica, MA, USA) using a Masterflex E/S portable sampler (Masterflex, Gelsenkirchen, Germany) and compatible sterile tubing and adaptors, and flash frozen in liquid nitrogen in the field. Upon return to the lab flash frozen Sterivex filters were stored at -80°C (15).

Wellhead GPS Measurements

Elevation and GPS coordinates were collected in January of 2016 for all twelve CROMO wells to obtain accurate measurements for spatial analyses. A Trimble GNSS system (California Surveying and Drafting Supply (CSDS), Dublin, CA) was attached to a

tripod balanced precisely over the center of each well head for 20 minutes. Elevation and GPS coordinates were also collected for nearby creek beds at each well cluster. Data obtained by the unit was post-processed by CSDS using CORS site P206 CRAZYCREEK and US State Plane 1983 Datum California Zone 2 using Geoid 12B. Elevation measurements were adjusted accordingly to account for well monument height above the ground and any additional space between the monument head and the tripod. Collected elevation and location data were used in the development of a topographic profile of the aquifer and surrounding landscape, and in the estimation of aquifer properties. Elevation and coordinate data are listed in **Table A.8** (https://doi.org/10.6084/m9.figshare.14983893).

Topographic Profile and Cross Section Construction:

Well-head locations and elevations were obtained as described above. These data were used to create a shape file of well locations within ArcMap (Esri, Redlands, CA, USA). Following this, an ArcMap compatible version of the Jericho Valley Quadrangle California 7.5 Minute Series (Topographic) map was obtained from the U.S. Geological Survey (USGS) Data Catalog (USGS, Reston, VA, USA). A digital elevation model (DEM) was available for this location, but at extremely low resolution. Due to this, the historic USGS quadrangle map was used instead. The CROMO well clusters are located within a V-shaped valley and lie approximately 1.4 km away from each other. A 2.3 km cross-section line was drawn from west to east between start and end point features in ArcMap across the valley, intersecting the well cluster locations. Point features were added along the line each time it intersected a topographic line and well locations were added to

the line as well. The wells did not all fall directly on the topographic line, so their location was approximated on the line based on their order from west to east. The map data were projected using the North American 1983 geographic coordinate system and datum. The map was then exported from ArcMap as an Adobe Illustrator (Adobe, San Jose, CA, USA) file.

In Adobe Illustrator, the base map was deleted, and the cross section line and intersecting points were grouped together as a single object. This object was then rotated to lie horizontally to create a topographic profile. The grid function was used to generate a uniform grid on the file to create an accurate profile. A vertical exaggeration of 10x was chosen for the vertical axis to display the topographic profile as well as geologic layers and well depths most accurately in the subsurface. Topographic profile points were drawn at the proper elevation on the profile based on their horizontal location on the original cross-section line. Lines were drawn between the points to mimic the natural shape of the landscape.

Following the creation of the profile, subsurface geological layers were added to the cross-section. Ortiz and colleagues (41) characterized the relevant water-bearing units within the subsurface at both CROMO well cluster sites using electrical resistivity tomography (ERT). The subsurface ERT maps indicate a shallow topsoil water-bearing unit, followed by an aquitard, and then a main serpentine aquifer (41). While the thickness of the topsoil layer varied by a few meters between the two well cluster locations, the thickness of the aquitard and serpentine unit below appear to be relatively uniform in thickness at both locations (41). Given the uniform presence of all three layers at both locations, it was assumed that the upper soil layer, aquitard, and serpentine unit were

laterally continuous and of uniform thickness throughout the extent of the cross-section. The main aquifer was assumed to be 76.2 m in thickness, accommodating the deepest well at the site. The depth at which basement rock lies in the area is unknown, but it is assumed that basement rock likely serves as an aquitard at the bottom of the main serpentine aquifer unit (41). Lines were drawn to accurate lengths to represent individual wells. The lines were then emplaced in the proper location on the topographic profile, providing accurate representation of the well's relationships to each other in the subsurface in the context of the natural topography of the landscape. Fluid flow direction lines were placed in the main aquifer unit moving from west to east. It is assumed that groundwater flow generally moves from topographic high to topographic low and moves down elevation within the valley from the QV well cluster to the CSW well cluster. Hydraulic conductivity estimates (K) (see methods below) are included at each well cluster.

Estimation of Aquifer Properties

Displacement data during pumping and recovery was obtained from measurements collected by ODYSSEY temperature and pressure transducers emplaced within the wells (Dataflow Systems Ltd., Christchurch, New Zealand). Water elevation data obtained by the transducers was pulled from the timeframe during pumping and for 24 hours following pumping. Water elevation data was converted to displacement data, compatible for analyses in AQTESOLV (68), by subtracting elevation data from the starting depth to water elevation level, prior to when the system was disturbed by pumping activity. The time in minutes from the start of pumping was also calculated for each displacement measurement. Time and displacement data were then imported into AQTESOLV.

Model parameters are as follows: aquifer thickness was assumed to be 76.2 m. The hydraulic conductivity anisotropy ratio was set at 0.1 based on average estimates obtained by Marechal and colleagues (83) on a variety of hard rock aquifers. The radius of the positive displacement Teflon bladder pump (Geotech Environmental Equipment, Denver, CO, USA) is 2.01 cm, based on the reported diameter of the pumps from the manufacturer. The inner radius of fully cased wells (CSW1.2, CSW1.3, CSW1.4, CSW1.5, QV1.2, and QV1.3) is 2.53 cm, and the radius of the entire well, including PVC piping is 3.13 cm, based on the thickness of Sch40 PVC piping used to case the wells. The inner radii of the partially cased wells are 6.34 cm and 5.06 cm for CSW1.1 and QV1.1, respectively, and the radii of the wells are 6.94 cm and 5.67 cm for CSW1.1 and QV1.1, respectively. Since the main aquifer being sampled lies beneath an aquitard, wells were characterized as vertical partial penetration wells. Wells were then characterized based on their depth from the top of the aquifer layer to the top of the screened interval. The top of the aquifer was set to 13 m in the subsurface based on thickness estimates of the topsoil layer and aquitard from Ortiz and colleagues (41). In cased wells, the screened interval is 1.5 m, except for CSW1.3 which has a screened interval of 2.6 m. In the partially cased wells, the uncased portion was assumed to be the screened interval and is 4.27 m and 10 m from the top of the aquifer in CSW1.1 and QV1.1, respectively. Pumping rates (L/min) were calculated using the length of pumping cycles used at each well for a given sampling trip, the total time pumping at each well, and total volume of water removed while pumping. The total volume of water removed was divided by the number of pump cycles completed during the total sampling time to obtain a pump rate (L/min). This pump rate was set for the duration of

the timeframe sampling occurred and served as the drawdown portion of the test. The pumping rate for recovery data is set to 0 L/min.

Following the input of well and aquifer parameter data and time-displacement data, a time-displacement graph was generated to fit a model solution. The Theis(1935)/Hantush(1961) solution (84,85) for non-leaky confined aquifers was used to fit time-displacement curves for all the wells. While this aquifer does contain fractured rock, a solution for fractured rock aquifers was not used, as the type and extent of fracturing has not been characterized at CROMO. The aquifer also contains interbedded layers of clay material (40), so the simplest solution for a confined aquifer was used as the model solution. Curve fit solutions provide estimates for transmissivity (T) and storativity (S). T and aquifer thickness (b) were then used to calculate hydraulic conductivity (K) using the equation $T = K \times b$ (**Table A.5** at https://doi.org/10.6084/m9.figshare.14983866).

Tritium Analysis

The University of Waterloo Environmental Isotope Laboratory (UW-EIL) performed enriched tritium analyses on water samples from each well in June of 2017. Water samples were enriched fifteen times via electrolysis and then tritium was quantified using the liquid scintillation counting technique. The detection limit with these methods is 0.8 ± 0.8 T.U. at low levels, where 1 T.U. is equivalent to one tritiated water molecule per 10^{18} water molecules (86). UW-EIL runs three background samples with each batch of samples: a natural groundwater with no detectable tritium, lab deionized water, and a standard traceable to NIST-4926-E. Measured tritium values for each well are listed in **Table A.4** (https://doi.org/10.6084/m9.figshare.14983863).

DNA and RNA Extraction

Cells on filter cartridges for DNA extraction were lysed by using freeze/thaw cycles and lysozyme/Proteinase K treatment and purified using a series of phenol/chloroform extractions. DNA was precipitated using ethanol and purified using the Genomic DNA Clean & Concentrate kit (Zymo Research, Irvine, CA, USA) (15). Genomic DNA was quantified using the High Sensitivity dsDNA Assay Kit on a Qubit fluorometer (Invitrogen, Carlsbad, CA, USA). RNA extractions were performed as previously described (22), using a modified phenol/chloroform extraction method. RNA was precipitated using ethanol, suspended in RNAse-free water, and quantified using a Qubit fluorometer (Invitrogen, Carlsbad, CA, USA) (22).

Ecological Modeling Framework

The ecological modeling framework developed by Stegen and colleagues (28) was used to quantify the role that selection, dispersal, and drift processes play at CROMO. Null modeling results using the β-nearest taxon index (βNTI) and the modified Raup-Crick (RCbray) metric, described below, result in distance matrix-like output where pairwise βNTI and RCbray values have been calculated between all samples included within the dataset. This resulted in square distance matrix-like objects that consisted of 104 rows and 104 columns for this dataset. As is seen in the calculation of other distance matrices, the upper and lower triangles of the distance matrix are identical, and the diagonal is populated by values of 0 or 1 indicating that samples are identical to one another when a sample is compared with itself. The βNTI and RCbray distance matrices obtained from ecological modeling are available for download on FigShare

(https://figshare.com/projects/Community_Assembly_in_Serpentinizing_Ophiolites/101648).

Selection processes are distinguished from stochastic (random) processes first in the model and are quantified using the β-mean nearest taxon distance (βMNTD) and βNTI metrics. First, βMNTD is calculated for all pairwise comparisons within the dataset to assess phylogenetic contributions to differences in community composition across the dataset. Following this, a null modeling approach permutes taxa locations on the phylogenetic tree 999 times, generating a distribution of βMNTD values under random assembly (i.e., under completely random assembly, we would assume that community members are randomly related to each other). Following this, βNTI is calculated by comparing observed βMNTD values to the null βMNTD distribution and determining the deviation of the observed βMNTD from the null expectation. βNTI results are compiled for each pairwise comparison and are used to assess phylogenetic turnover between wells and over time. Values of $|\beta NTI| > 2$ indicate that deterministic (selective) processes are responsible for the differences in community composition between two locations/timepoints, while $|\beta NTI| < 2$ indicates that stochastic processes are responsible for differences between the two samples (37). Values of $|\beta NTI| > 2$ can be further analyzed by assessing the raw results, which can range from $\beta NTI \geq 2$ or $\beta NTI \leq -2$. $\beta NTI \geq 2$ indicates variable selection, which indicates that differing conditions between two locations select for different microbial community composition. $\beta NTI \leq -2$ indicates homogeneous selection, where environmental conditions drive communities to more similar compositions (28). Both environmental conditions and biotic interactions can impose selection on microbial communities (24). Pairwise comparisons of $|\beta NTI| < 2$,

which implicate the role of stochastic processes, are further analyzed using an abundance weighted Raup-Crick measure to quantify the roles of the stochastic processes of dispersal and ecological drift (28).

Stochastic processes are quantified using the RCbray metric, which incorporates species abundance data to the metric originally developed by Chase and colleagues (26,60). The stochastic or random processes of microbial community assembly that are quantified here are dispersal and ecological drift (24). Dispersal here is considered passive and depends upon how environmental conditions allow for the transport or lack of transport of microorganisms through a natural environment. Ecological drift is the result of random changes in the death and replication rate of microorganisms, which ultimately leads to variance in the presence and abundance of different microorganisms (56). A null modeling approach permutes community composition 999 times and calculates a Bray-Curtis dissimilarity for each pairwise comparison. This generates a null distribution of Bray-Curtis values based on OTU richness and diversity within each sample. Observed Bray-Curtis values are compared to the null distribution to determine how the observed value deviates from the null expectation. Results are normalized for all pairwise comparisons to generate an RCbray metric that ranges from +1 to -1 (60). Values of |RCbray| >0.95 for any given pairwise comparison indicates that either homogenizing dispersal or dispersal limitation paired with ecological drift drives differences in observed community composition. Dispersal limitation (RCbray > 0.95) occurs when turnover between communities is greater than would be expected when considering ecological drift alone. This indicates that lack of interaction between communities due to dispersal limitation paired with ecological drift is driving differences in observed community compositions

(60). Homogenizing dispersal (RCbray < -0.95) occurs when turnover between communities is less than would normally be expected. This can occur when dispersal of microbial community members is high and local selection in an area is low. Continual transport of microorganisms between two locations ultimately generates community compositions that are more similar to each other than would be expected by chance (56,60). Only pairwise comparisons that were not significant with the βNTI metric (|βNTI| < 2) were analyzed with the RCbray metric. This leaves out pairwise comparisons dominated by selection (|βNTI| > 2) and uses the RCbray metric to quantify the stochastic process in pairwise comparisons that are not driven by selection processes (|βNTI| < 2).

Model results where both βNTI and RCbray are insignificant (|βNTI| < 2 and |RCbray| < 0.95) are defined as undominated, where values for βNTI and RCbray do not cross the significance threshold. In this scenario, both deterministic and stochastic processes are at work, but neither can be deemed entirely responsible for observed differences in pairwise comparisons of communities. Undominated assembly has been posited to occur under weak selection and moderate dispersal (28,56) and has also been observed to be the result of strong interactions between variable and homogeneous selective processes (34). Importantly, undominated assembly does not indicate that neither stochastic or deterministic processes are at play, instead it reveals that no single ecological process can explain the observed variation between communities and that assembly occurs through a mixture of stochastic and deterministic processes that cannot be well defined by the model. Ecological modeling results are presented in **Table A.2** (https://doi.org/10.6084/m9.figshare.14983857).

Discussion

Homogenizing Dispersal in Partially Uncased Wells

Wells CSW1.1 (4.26 m of 19.5 m uncased) and QV1.1 (21.2 m of 23 m uncased) are partially cased wells. Wells are generally cased with an impermeable material (PVC piping) to help support the sides of the borehole and to allow for water to be pumped from a discrete depth range at the bottom of the well, called the screened interval. The screened interval (commonly 1-3 m) allows fluid to enter the borehole and be pumped out of the well. Due to their uncased nature, hydraulic gradients generated during pumping activity in CSW1.1 and QV1.1 likely pull and mix fluids from the top of the uncased portion down to the bottom of the well where fluids are being pumped (87). Samples collected from these wells likely represent a greater depth range in the formation as compared to fluids collected from the more discrete 1.5 m screened intervals present on cased wells at the site. As a result, sampled communities from the partially uncased wells likely represent a mixed microbial community, representative of a much larger depth range. This results in a homogenizing dispersal signal ($RC_{bray} < -0.95$) between the uncased wells and cased wells at nearby depths (1-10 m shallower or deeper).

This phenomenon also likely alters interpretation of results seen in **Figure 2.3D**. CSW1.1 and QV1.1 are both included within the extreme pH well grouping and are consistently characterized by extremely high pH (**Fig. 2.1B**). Enhanced homogenizing dispersal observed in these wells that is the result of top-down fluid dynamics in the uncased portion of these wells (87) results in an increased contribution of homogenizing dispersal in extreme pH wells that is not in line with hydrological data obtained from the site (**Table A.5** at https://doi.org/10.6084/m9.figshare.14983866).

Use of Distance-based Greedy Clustering in 16S rRNA Sequence Processing

Distance-based Greedy Clustering (DGC) was chosen because it uses the distance between sequences within a dataset to cluster them into operational taxonomic units (OTUs), as opposed to comparing the distance of sequences to that of sequences in a reference database, as is done when using closed-reference clustering methods (70). The DGC clustering method prevented sequences from different sequencing centers from clustering separately from each other. *De novo* clustering methods have been successfully used to cluster OTUs using data compiled from different sequencing platforms (71,72). Samples sequenced at the different sequencing centers cluster together by each different well, as has been seen with smaller subsets of the dataset generated at a single sequencing center in the past (15,22). Evidence of this can be seen in **Figure A.8**. This is further supported by the fact that several samples were sequenced at two of the three sequencing centers (**Fig. A.9; Table A.9** at https://doi.org/10.6084/m9.figshare.14983896) used in this study. These samples overlap with each other by sample (**Fig. A.8**) and show high community compositions similarity (**Fig. A.9**) as would be expected for the same sample, and did not differ from each other based on the sequencing center (**Figs. A.8 & A.9**).

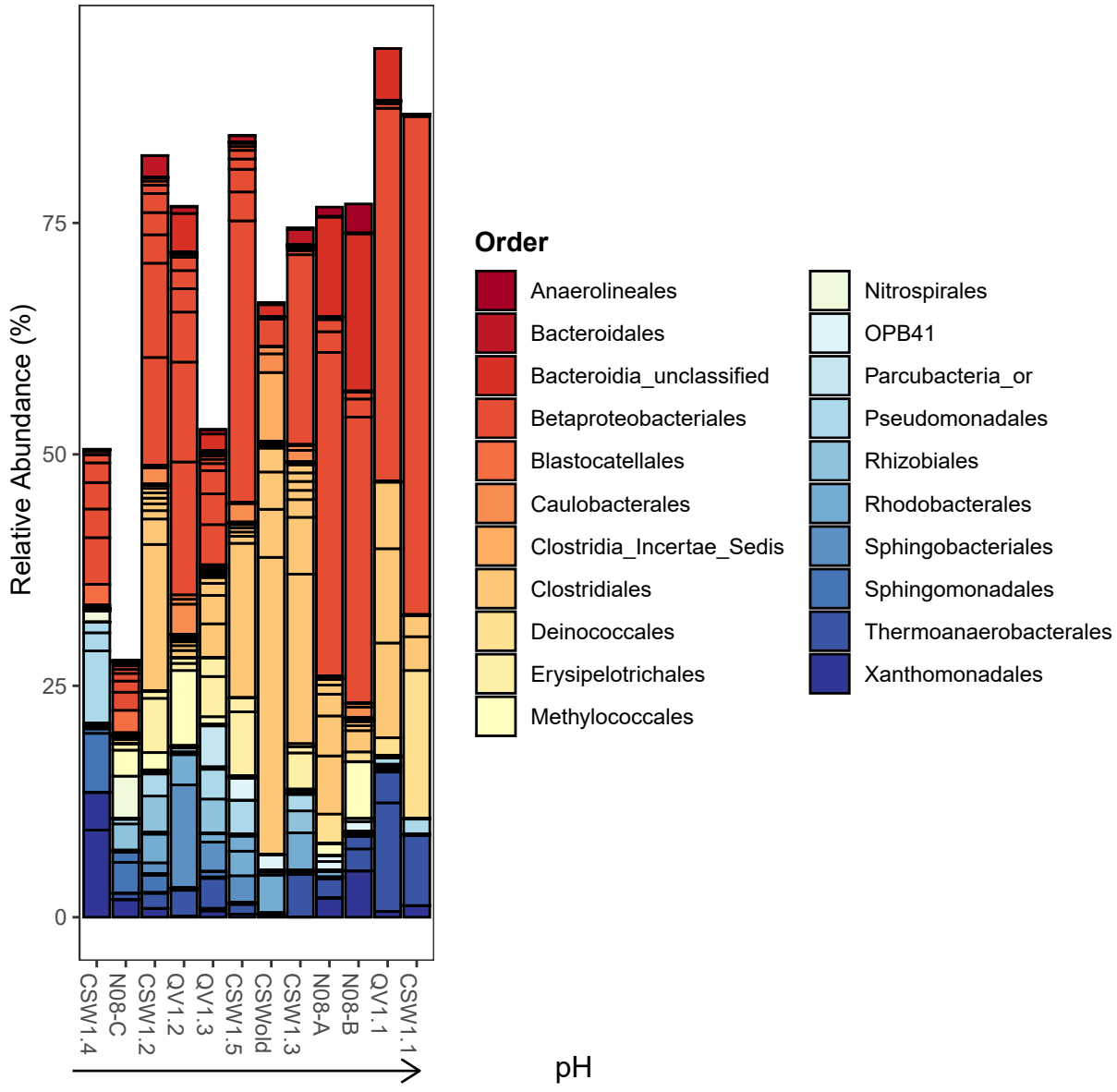

Figure A.1. Stacked Bar Plot of the Relative Abundance of the 50 Most Abundant OTUs by Taxonomic Order.

Stacked bar plot showing average relative abundance of each taxonomic order represented in the 50 most abundant OTUs in the dataset. Normalized community composition was averaged across all samples for an individual well to determine the 'general' community composition within each well. Wells are organized from lowest to highest average pH.

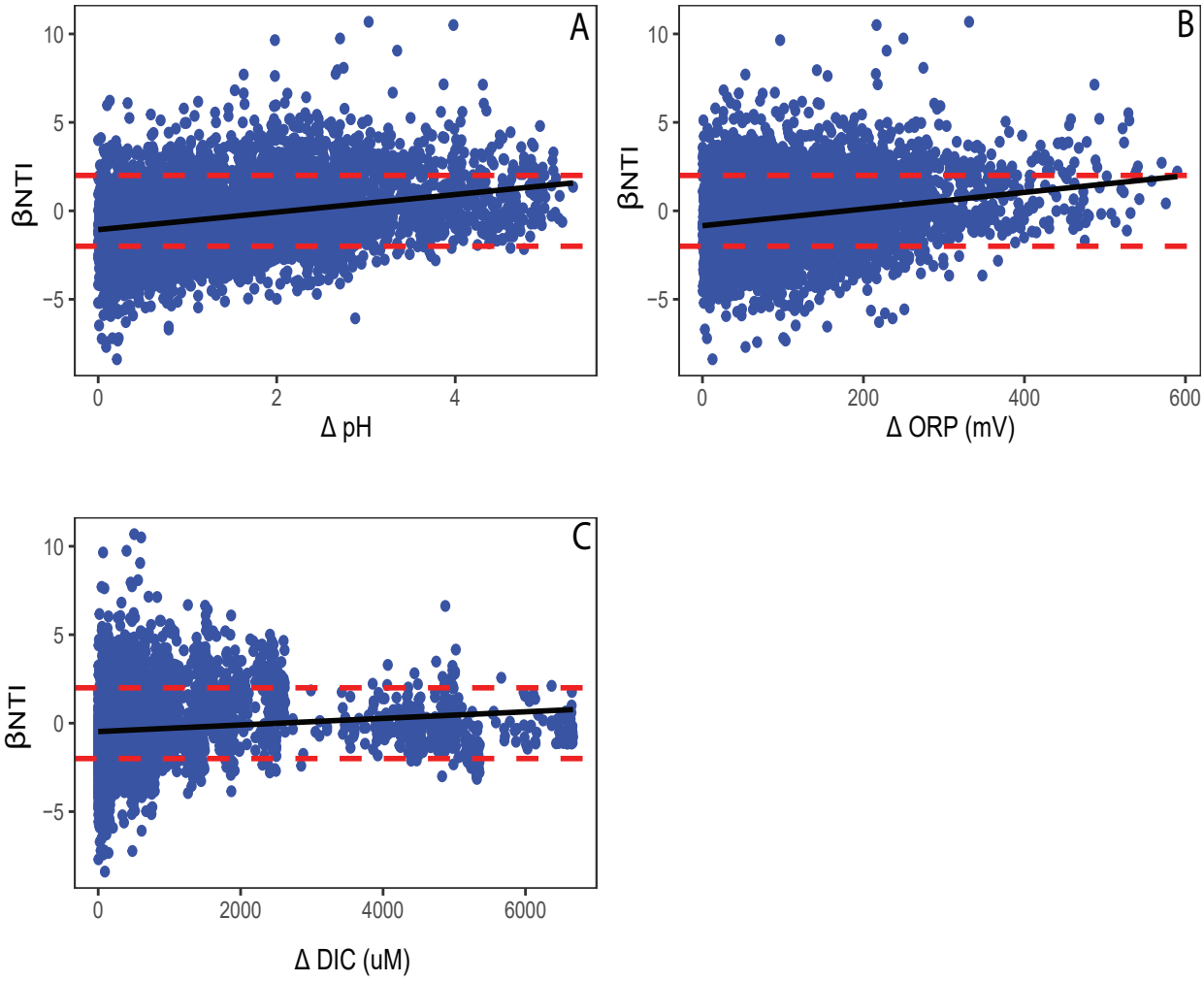

Figure A.2. Significant Regression Plots of βNTI Values against Environmental Data.

βNTI plotted as a function of the difference in pH (A), oxidation reduction potential (ORP) (B), and dissolved inorganic carbon (DIC) (C). Solid black lines in plots represent fitted regression trend lines based on significant Mantel test correlations (Table A.3 at https://doi.org/10.6084/m9.figshare.14983860). Horizontal red lines at βNTI values of 2 and -2 represent the significance threshold for the βNTI metric which indicate that homogeneous selection (βNTI < -2) or variable selection (βNTI > 2) govern assembly.

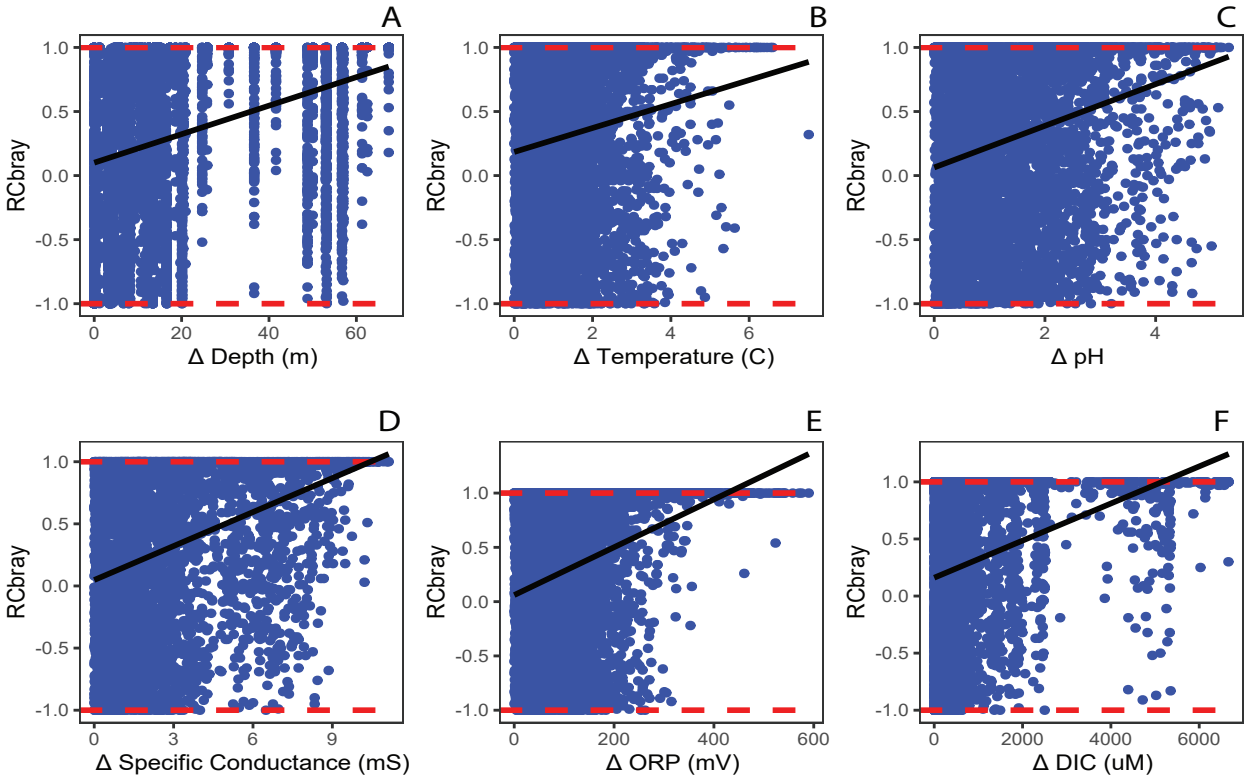

Figure A.3. Significant Regression Plots of RCbray Values against Environmental Data.

RCbray plotted as a function of the difference in depth (A), temperature (B), pH (C), specific conductance (D), oxidation reduction potential (ORP) (E), and dissolved inorganic carbon (DIC) (F). Solid black lines in plots represent fitted regression trend lines based on significant Mantel test correlations (Table A.3 at https://doi.org/10.6084/m9.figshare.14983860). Horizontal red lines at RCbray values of 0.95 and -0.95 represent the significance threshold for the RCbray metric which indicate that dispersal limitation (RCbray > 0.95) or homogenizing dispersal (RCbray < -0.95) govern assembly.

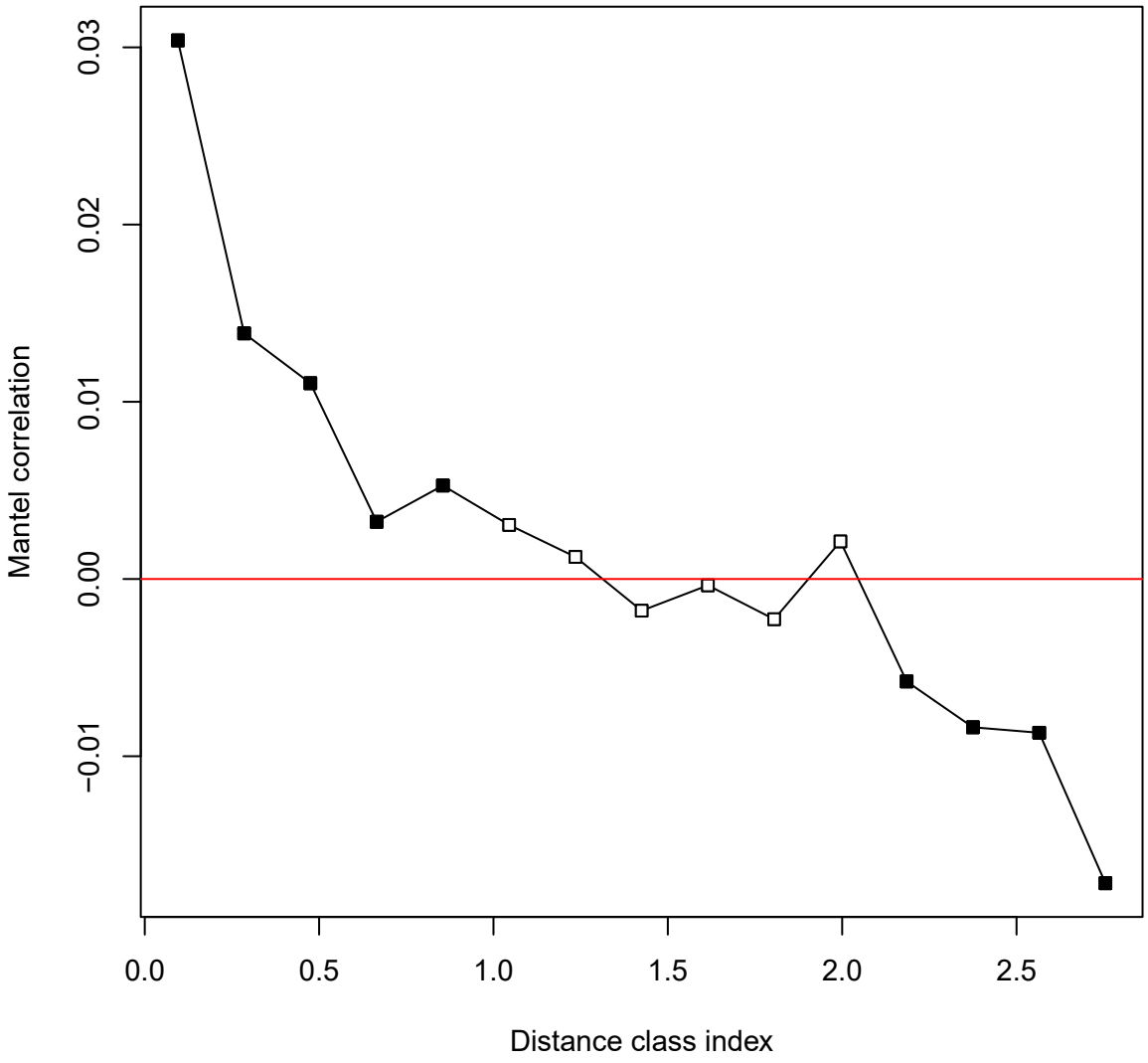

Figure A.4. Mantel Correlogram of Phylogenetic Distances against pH.

Mantel correlogram showing significant phylogenetic signal at short phylogenetic distances. The correlogram plots the phylogenetic distance of each OTU in the dataset against the average pH niche value calculated for each OTU. Solid boxes represent significant correlations and open boxes represent insignificant correlations. Significant correlations at short phylogenetic distances indicate that phylogenetic signal occurs at small phylogenetic distances, making it appropriate to assess phylogenetic turnover amongst closely related organisms.

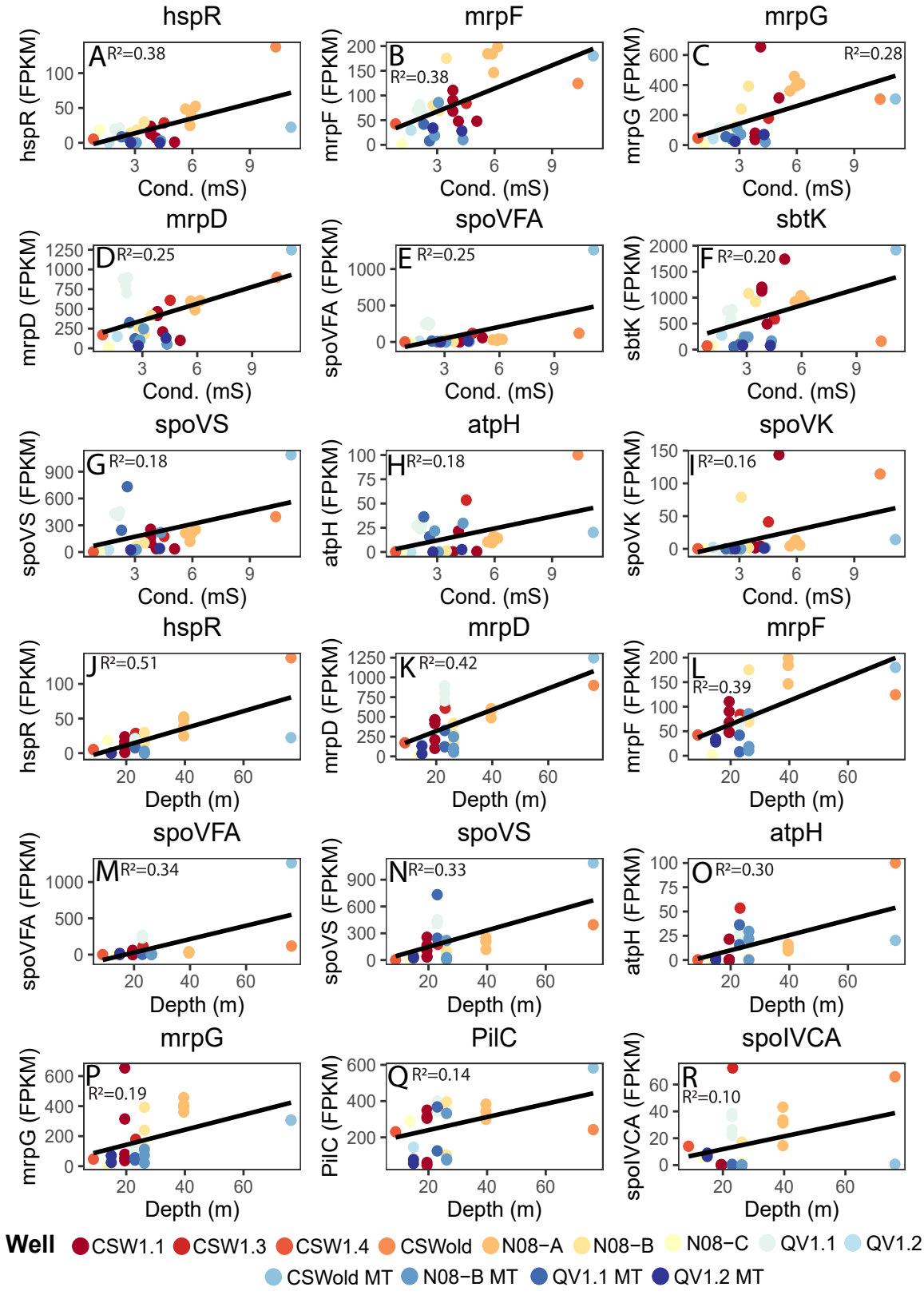

Figure A.5. Plots of Significant Linear Regression Models of Metagenomic and Metatranscriptomic Data vs. Salinity and Depth

Figure A.5. (cont'd).

Significant linear regression plots of the normalized abundance of metagenomic and metranscriptomic data in fragments per kilobase per million reads (FPKM) for the genes hspR (A), mrpF (B), mrpG (C), mrpD (D), spoVFA (E), sbtK (F), spoVS (G), atpH (H), and spoVK (I) plotted against specific conductance (Cond. (mS)), and genes hspR (J), mrpD (K), mrpF (L), spoVFA (M), spoVS (N), atpH (O), mrpG (P), PilC (Q), and spoIVCA (R) plotted against depth. Solid black lines represent a linear trend line. Linear regression R^2 values are included at the top of each plot. Samples of metagenomic and metatranscriptomic data are colored by well location. Metatranscriptomic samples are labeled with an MT following the well name in the legend. Functions associated with genes are as follows: motility/adhesion (PilC), sodium:hydrogen antiporters (mrpF, mrpG, mrpD), sporulation (spoVFA, spoVS, spoVK, spoIVCA), sodium dependent bicarbonate transporters (sbtK), sodium dependent V-type ATPase (atpH), survival transcription factors (hspR).

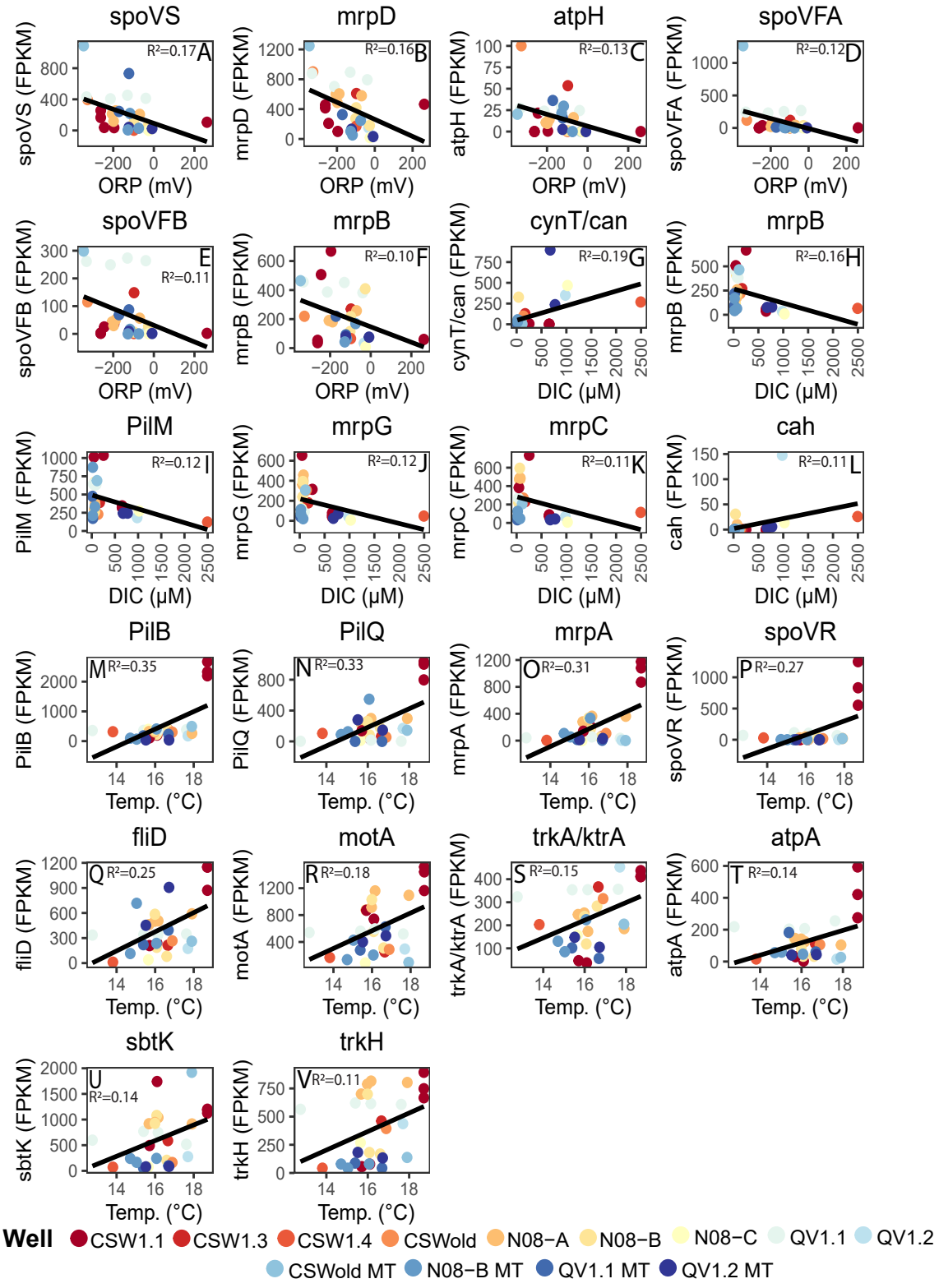

Figure A.6. Plots of Significant Linear Regression Models of Metagenomic and Metatranscriptomic Data vs. Oxidation Reduction Potential, Dissolved Inorganic Carbon, and Temperature.

Figure A.6. (cont'd).

Significant linear regression plots of the normalized abundance of metagenomic and metranscriptomic data in fragments per kilobase per million reads (FPKM) for the genes spoVS (A), mrpD (B), atpH (C), spoVFA (D), spoVFB (E), and mrpB (F) plotted against oxidation reduction potential (ORP (mV)), genes cynT/can (G), mrpB (H), PilM (I), mrpG (J), mrpC (K), and cah (L) plotted against dissolved inorganic carbon (DIC (μM)), and genes PilB (M), PilQ (N), mrpA (O), spoVR (P), fliD (Q), motA (R), trkA/ktrA (S), atpA (T), sbtK (U), and trkH (V) plotted against temperature (Temp. (°C)). Solid black lines represent a linear trend line. Linear regression R^2 values are included at the top of each plot. Samples of metagenomic and metatranscriptomic data are colored by well location. Metatranscriptomic samples are labeled with an MT following the well name in the legend. Functions associated with genes are as follows: motility/adhesion (PilM, PilB, PilQ, motA, fliD), sodium:hydrogen antiporters (mrpD, mrpB, mrpG, mrpC, mrpA), sporulation (spoVS, spoVFA, spoVFB, spoVR), sodium dependent bicarbonate transporters (sbtK), sodium dependent V-type ATPase (atpH, atpA), potassium:hydrogen symporters (trkA/ktrA, trkH), carbonic anhydrase (cynT/can, cah).

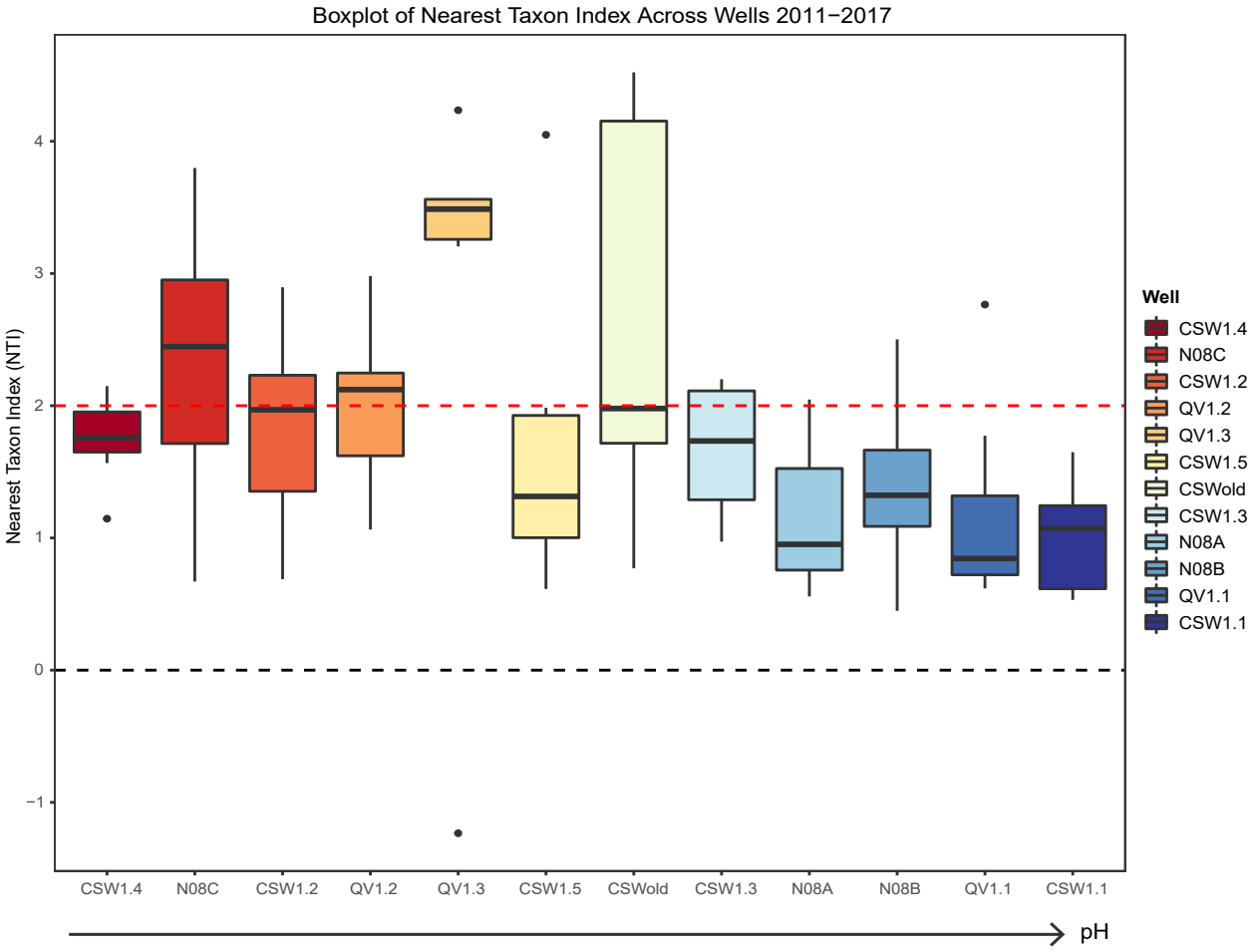

Figure A.7. Boxplot of Nearest Taxon Index across Wells (2011-2017).

Nearest Taxon Index (NTI) plotted within individual wells. NTI values are obtained by comparing observed Mean Nearest Taxon Distance (MNTD) values to those generated within a null distribution. The black dashed line represents the null expectation, and the red dashed line is representative of the significance threshold. Positive values crossing the significance threshold indicate that microbial communities are phylogenetically clustered.

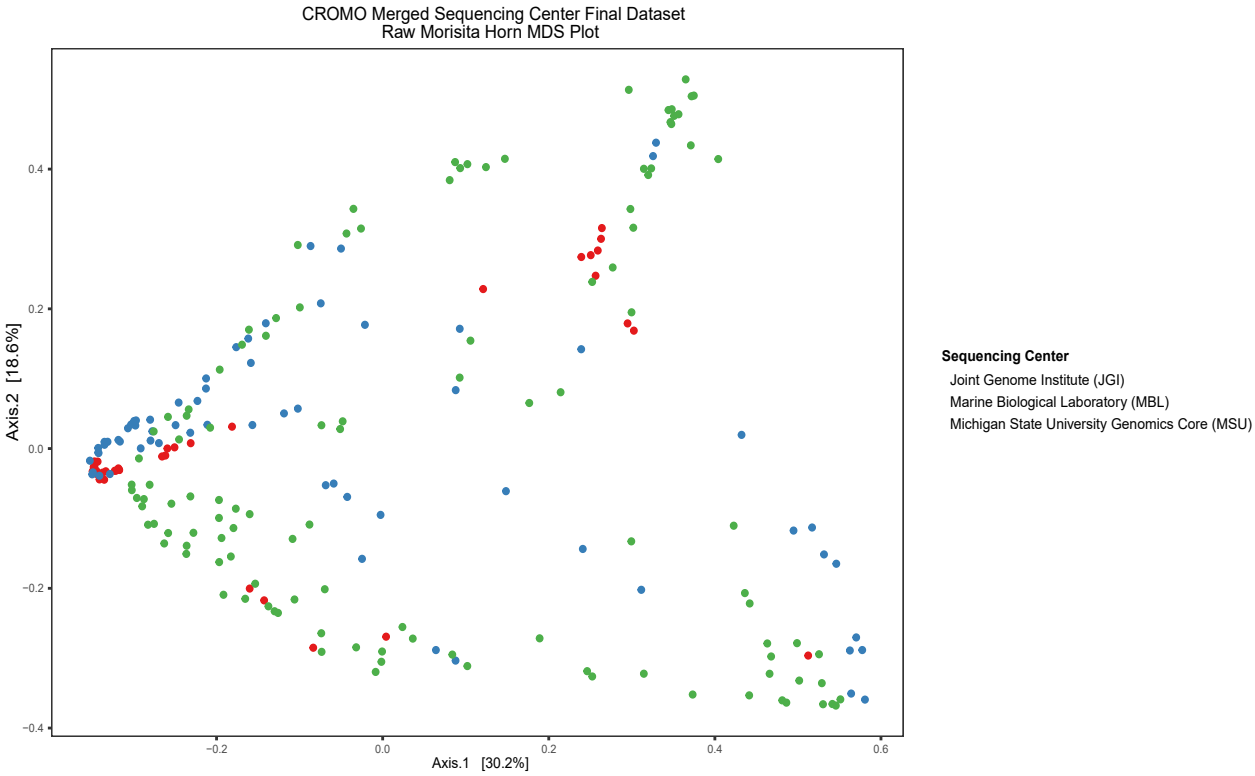

Figure A.8. CROMO Merged Sequencing Center Multidimensional Scaling Plot with Samples Colored by Well.

Multidimensional scaling plot of CROMO 16S rRNA microbial community samples using Morisita-Horn distances. Points represent individual samples and are colored by the sequencing center they were sequenced at. Points that lie closer together are more similar to each other while points further apart are more dissimilar. The overlap and consistent intermixing of samples from different sequencing centers indicate that samples are not biased based on the sequencing center they were sequenced at and are representative of the samples themselves.

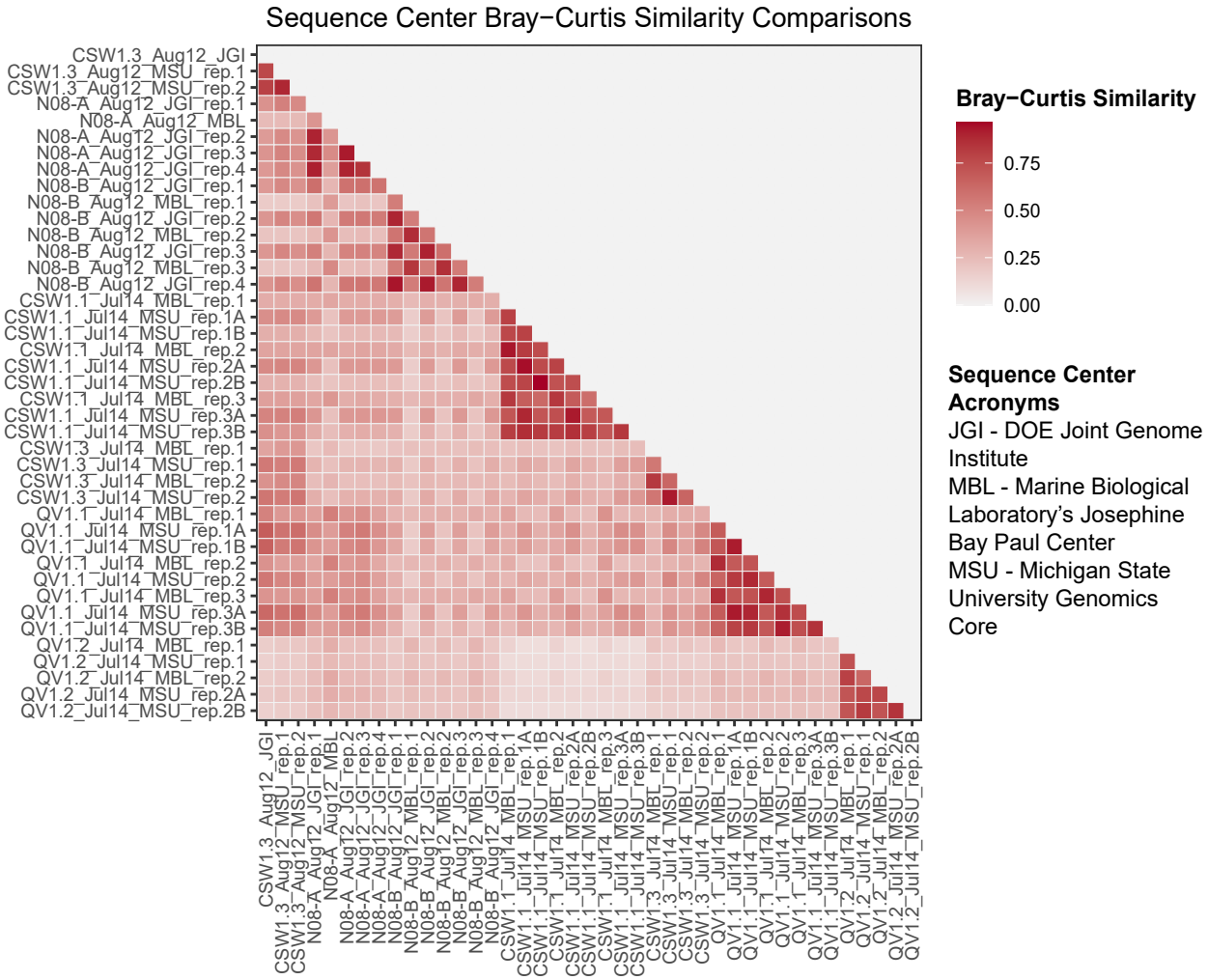

Figure A.9. Heatmap of Bray-Curtis Dissimilarities of Samples Sequenced at Multiple Sequencing Centers.

Heatmap displaying Bray-Curtis similarity data between samples where technical replicates were sequenced at more than one sequencing center. Dark red colors indicate high similarity while light red colors indicate low similarity in community composition. Comparisons between technical replicates from the same sampling trip and same well can be seen along the diagonal of the heatmap. Dark red values, indicating high community composition similarity, are observed along the diagonal, indicating that community composition and taxonomic structure of technical replicates from the same well were not significantly altered based on the sequencing center the sample was sequenced at.

Table A.1. Metadata.

Well	Date Sampled	Drilled Depth (m)	Temperature (°C)	pH	Specific Conductance (mS)	Dissolved Oxygen (mg/L)	ORP (mV)	DIC (μM)
CSW1.1	11/1/2011	19.50	15.71[a]	12.54	4.11[a]	0.64	-244.44[a]	46.40
CSW1.1	3/16/2012	19.50	13.66	12.38	4.67	0.03	-298.90	130.03
CSW1.1	6/26/2012	19.50	14.99	12.30	5.10	0.32	-287.90	86.76
CSW1.1	8/21/2012	19.50	16.10	12.15	5.07	0.00	-195.80	253.42
CSW1.1	3/27/2013	19.50	14.78	12.18	4.54	0.28	-293.60	209.74
CSW1.1	8/6/2013	19.50	16.21	12.39	4.49	0.18	-258.40	194.19
CSW1.1	7/22/2014	19.50	16.31	12.32	4.45	0.43	-297.00	232.38
CSW1.1	8/26/2015	19.50	16.71	11.76	4.21	0.17	-243.10	316.23
CSW1.1	1/26/2016	19.50	14.83	12.42	4.13	0.19	-276.50	435.10
CSW1.1	5/31/2016	19.50	16.28	12.07	3.81	0.16	-279.50	654.65
CSW1.1	5/29/2017	19.50	16.51	12.30	3.77	0.10	-179.00	572.21
CSW1.2	8/21/2012	19.20	18.16	9.32	3.71	0.45	-61.80	604.87
CSW1.2	3/27/2013	19.20	14.80	8.68	3.81	7.57	-140.80	1448.81
CSW1.2	1/28/2016	19.20	14.71	8.62	4.57	0.15	-176.20	1938.07
CSW1.2	5/30/2016	19.20	16.32	8.72	4.60	0.41	-124.00	1513.54
CSW1.2	5/29/2017	19.20	15.85	8.35	4.60	0.09	-75.20	2523.35
CSW1.3	8/21/2012	23.20	16.66	10.12	4.52	0.07	-97.30	171.89
CSW1.3	3/27/2013	23.20	15.17	10.10	4.36	0.93	-170.60	152.58
CSW1.3	8/7/2013	23.20	16.42	10.20	4.71	0.03	-246.60	153.70
CSW1.3	7/23/2014	23.20	15.64	10.15	4.84	0.16	-204.80	229.02
CSW1.3	1/28/2016	23.20	14.73	10.47	4.62	0.13	-286.40	121.68
CSW1.3	5/29/2017	23.20	15.58	10.65	4.78	0.06	-162.00	314.8[b]
CSW1.4	12/5/2011	8.80	13.10[a]	7.70[a]	0.75[a]	3.44[a]	-103.27[a]	901.60
CSW1.4	3/17/2012	8.80	13.81	7.77	0.83	0.86	-98.20	2494.60
CSW1.4	8/22/2012	8.80	15.22	8.00	1.60	0.27	-22.50	5046.20
CSW1.4	3/27/2013	8.80	14.24	7.77	1.52	11.85	-126.20	5374.35
CSW1.4	1/28/2016	8.80	11.78	7.85	1.78	3.06	63.40	5045.17
CSW1.4	5/30/2016	8.80	19.30	7.71	1.99	2.74	181.30	4564.11
CSW1.4	5/28/2017	8.80	15.09	7.42	1.85	0.14	5.30	6683.40
CSW1.5	8/21/2012	27.40	16.37	9.63	4.17	0.06	-110.20	544.85
CSW1.5	3/27/2013	27.40	15.32	9.30	4.05	0.37	-165.20	816.61
CSW1.5	7/23/2014	27.40	15.80	9.77	4.79	0.16	-285.20	833.82
CSW1.5	8/26/2015	27.40	16.15	9.39	4.76	0.19	-211.60	638.54
CSW1.5	1/28/2016	27.40	15.16	9.92	4.78	0.09	-249.10	546.99
CSW1.5	5/30/2016	27.40	16.04	9.78	4.78	0.42	-202.70	505.58
CSW1.5	5/29/2017	27.40	15.42	9.92	4.87	0.09	-137.10	709.59

Table A.1. (cont'd).

Well	Date Sampled	Drilled Depth (m)	Temperature (°C)	pH	Specific Conductance (mS)	Dissolved Oxygen (mg/L)	ORP (mV)	DIC (µM)
CSWold	6/1/2011	76.20	18.38[a]	9.62[a]	9.81[a]	1.31[a]	-314.06[a]	42.37[a]
CSWold	7/7/2011	76.20	17.45[a]	9.84	9.64[a]	0.46[a]	-210.72[a]	187.59[a]
CSWold	8/1/2011	76.20	16.89[a]	9.83[a]	10.35[a]	0.25[a]	-326.59[a]	136.68[a]
CSWold	11/2/2011	76.20	17.80[a]	9.88	11.88[a]	1.03	-187.05[a]	27.70
CSWold	3/17/2012	76.20	17.99[a]	9.79[a]	10.03[a]	0.85[a]	-133.48[a]	24.20[a]
CSWold	3/27/2013	76.20	17.04	9.72	10.40	3.31	-181.40	62.72
CSWold	8/7/2013	76.20	18.24	9.78	10.94	0.02	-278.00	42.30
CSWold	12/13/2013	76.20	17.90	9.69	11.15	0.22	-346.00	113.55
CSWold	7/22/2014	76.20	17.43	9.73	11.53	0.26	-279.90	185.16[b]
CSWold	8/26/2015	76.20	17.24	9.59	11.11	0.55	-213.90	70.22
CSWold	1/28/2016	76.20	17.95	9.87	11.00	0.08	-294.90	63.41
CSWold	5/31/2016	76.20	17.70	9.61	11.00	0.98	-165.40	54.55
CSWold	5/29/2017	76.20	17.14	10.48	8.32	0.63	-125.40	314.8[b]
N08A	4/21/2011	39.60	15.68[a]	10.62[a]	5.64[a]	0.17[a]	-205.58[a]	55.95
N08A	7/7/2011	39.60	15.98[a]	10.55	6.16[a]	0.46[a]	-188.16[a]	67.40
N08A	8/1/2011	39.60	17.91[a]	10.09[a]	5.87[a]	0.04[a]	-198.23[a]	74.94[a]
N08A	8/22/2012	39.60	16.16	10.52	5.95	0.17	-69.70	70.92
N08A	3/26/2013	39.60	14.51	10.79	5.68	0.64	-184.00	38.01
N08A	8/6/2013	39.60	16.78	10.42	5.92	0.02	-161.10	58.18
N08A	12/15/2013	39.60	15.29	10.19	6.44	0.03	-229.60	68.61[b]
N08A	7/24/2014	39.60	16.85	10.89	6.34	0.09	-249.50	185.16[b]
N08A	1/29/2016	39.60	14.78	10.62	5.94	0.31	-207.30	61.92[b]
N08A	5/29/2016	39.60	16.45	10.82	5.89	0.23	-218.20	35.33
N08A	5/28/2017	39.60	18.09	10.91	5.76	0.21	-89.50	50.56
N08B	4/21/2011	26.20	15.99[a]	10.72[a]	3.48[a]	0.56[a]	-98.31[a]	63.25
N08B	7/7/2011	26.20	16.60	11.51	2.78[a]	0.36[a]	-101.39[a]	40.90
N08B	8/22/2012	26.20	16.08	10.81	3.10	0.34	-27.10	57.78
N08B	3/26/2013	26.20	14.71	10.86	2.87	0.31	-127.70	21.48
N08B	8/6/2013	26.20	16.07	10.98	3.07	0.32	-74.60	21.33
N08B	12/14/2013	26.20	15.04	10.55	4.35	0.10	-117.90	68.61[b]
N08B	7/24/2014	26.20	16.12	10.68	3.13	0.76	-197.60	185.16[b]
N08B	1/29/2016	26.20	14.87	10.54	2.98	0.21	-191.10	68.73
N08B	6/1/2016	26.20	18.04	10.19	3.05	0.15	-117.50	89.90
N08B	5/28/2017	26.20	16.40	10.40	2.90	0.14	21.20	190.65

Table A.1. (cont'd).

Well	Date Sampled	Drilled Depth (m)	Temperature (°C)	pH	Specific Conductance (mS)	Dissolved Oxygen (mg/L)	ORP (mV)	DIC (μM)
N08C	7/7/2011	13.70	16.30	7.44	0.95[a]	0.18[a]	44.84[a]	627.84[a]
N08C	8/22/2012	13.70	15.65	7.89	1.15	0.11	-25.40	1023.40
N08C	3/26/2013	13.70	14.59	7.41	0.79	3.14	-127.70	1830.84
N08C	8/6/2013	13.70	14.94	7.45	1.14	0.17	243.90	1144.02
N08C	12/15/2013	13.70	15.08	9.32	1.31	0.10	-164.90	970.71
N08C	7/24/2014	13.70	15.53	8.46	1.37	0.42	-153.10	1576.56
N08C	1/27/2016	13.70	15.30	8.80	1.14	0.79	-13.40	691.67
N08C	6/1/2016	13.70	16.12	7.22	1.39	0.11	30.70	1129.57
N08C	5/28/2017	13.70	15.18	7.54	1.21	0.87	60.70	2641.28
QV1.1	11/2/2011	23.00	16.12[a]	11.55	2.67[a]	0.67	-174.51[a]	21.80
QV1.1	3/18/2012	23.00	12.75	11.73	2.14	0.12	-213.80	75.19
QV1.1	6/25/2012	23.00	16.15	11.50	1.95	0.12	-331.80	37.11
QV1.1	8/21/2012	23.00	17.62	11.15	2.09	0.12	-39.60	95.93
QV1.1	12/4/2012	23.00	15.40	11.42	2.20	1.40	-130.00	41.57
QV1.1	3/26/2013	23.00	15.39	11.42	2.30	0.54	-171.50	23.81
QV1.1	8/7/2013	23.00	16.69	11.65	2.60	0.05	-122.70	15.50
QV1.1	7/22/2014	23.00	17.52	11.51	2.85	0.28	-233.50	185.16[b]
QV1.1	8/26/2015	23.00	17.27	11.12	3.08	0.33	-139.40	52.39[b]
QV1.1	1/26/2016	23.00	15.90	11.75	3.27	0.18	-218.30	61.92[b]
QV1.1	6/1/2016	23.00	16.67	11.44	3.38	0.15	-203.90	57.01[b]
QV1.1	5/29/2017	23.00	16.01	11.46	3.54	0.17	-115.10	31.60
QV1.2	8/21/2012	14.90	17.70	7.93	1.63	0.05	-32.90	979.43
QV1.2	3/26/2013	14.90	14.94	9.42	2.43	2.52	-110.60	541.01
QV1.2	8/7/2013	14.90	16.72	9.07	2.78	0.76	-8.50	675.57
QV1.2	7/22/2014	14.90	17.09	9.47	3.04	0.40	-142.70	982.19
QV1.2	1/27/2016	14.90	16.78	9.48	3.01	0.42	-77.10	706.31
QV1.2	5/29/2016	14.90	16.88	9.31	3.00	0.22	-149.50	804.16
QV1.2	5/29/2017	14.90	16.58	9.75	3.06	0.12	-103.60	1099.03
QV1.3	8/22/2012	34.60	16.88	9.42	3.10	0.05	-51.70	696.62
QV1.3	3/26/2013	34.60	15.80	9.38	5.59	1.19	-153.30	216.56
QV1.3	7/24/2014	34.60	16.60	9.68	6.51	0.26	-223.60	526.40
QV1.3	1/27/2016	34.60	16.25	9.88	5.96	0.17	-229.30	116.97
QV1.3	5/29/2016	34.60	16.37	9.79	4.76	0.22	-208.70	210.81
QV1.3	5/30/2017	34.60	16.85	9.84	4.17	0.27	-163.00	551.87

[a] = data was not collected. Value was permuted based on mean and s.d. of existing data

[b] = DIC sample was below detection limit. Value represents detection limit.

Table A.2. Ecological Modeling Results.

	Ecological Process (2011-2017 CROMO Samples)				
	Variable Selection	Homogeneous Selection	Homogenizing Dispersal	Dispersal Limitation	Undominated
All Wells	12%	16%	2%	20%	50%
Neutral pH Wells	17%	4%	0%	48%	31%
Moderate pH Wells	3%	24%	2%	13%	58%
Extreme pH Wells	2%	25%	8%	0%	63%

	Ecological Process (2011-2017 CROMO Samples)				
	Variable Selection	Homogeneous Selection	Homogenizing Dispersal	Dispersal Limitation	Undominated
CSW1.4	0%	9%	0%	55%	37%
N08-C	25%	2%	0%	59%	14%
CSW1.2	0%	16%	0%	0%	84%
QV1.2	0%	30%	0%	9%	62%
QV1.3	6%	6%	0%	18%	71%
CSW1.5	8%	12%	12%	0%	67%
CSWold	0%	54%	5%	0%	41%
CSW1.3	11%	17%	17%	0%	56%
N08-A	0%	64%	5%	0%	31%
N08-B	0%	66%	6%	0%	28%
QV1.1	0%	20%	21%	0%	59%
CSW1.1	5%	33%	17%	0%	45%

The percent contribution of each process was calculated by dividing the number of significant pairwise comparisons for each process by the total number of pairwise comparisons. This was done for all comparisons within the study, neutral, moderate, and extreme pH wells, and within each individual well over time.

Table A.3. Ecological Modeling and Metadata Mantel Test Results.

Ecological Modeling Metric	Environmental Variable	Correlation	p-value
βNTI	pH	0.29	1.00E-04
	ORP (mV)	0.23	5.00E-04
	DIC (μM)	0.14	0.04
Rcbray	Well Depth (m)	0.31	1.00E-04
	Temperature (°C)	0.15	5.70E-03
	pH	0.27	1.00E-04
	Specific Conductance (mS)	0.34	1.00E-04
	ORP (mV)	0.30	1.00E-04
	DIC (μM)	0.33	1.00E-04

Table A.4. May 2017 Tritium Results.

Well	Date Collected	^{3}H Result (TU)* ± 0.8 TU	± 1σ (TU) ± 0.8 TU
CSW1.1	5/29/2017	<0.8	0.3
CSW1.2	5/29/2017	<0.8	0.3
CSW1.3	5/29/2017	<0.8	0.3
CSW1.4	5/28/2017	<0.8	0.3
CSW1.5	5/29/2017	<0.8	0.3
CSWold	5/29/2017	<0.8	0.3
N08-A	5/28/2017	<0.8	0.3
N08-B	5/28/2017	<0.8	0.3
N08-C	5/28/2017	0.9	0.4
QV1.1	5/29/2017	<0.8	0.4
QV1.2	5/29/2017	<0.8	0.3
QV1.3	5/30/2017	<0.8	0.3

Detection Limit: 0.8 ± 0.8 TU

*1 tritium unit (TU) = 1 molecule ^{3}HHO per 10^{18} molecules H_2O

Table A.5. Hydrologic Parameter Estimates.

Well	Aquifer Thickness (b) (m)	Kv/Kh Ratio	Storativity (S)	Transmissivity (T) (m^2/s)	Hydraulic Conductivity (K) (m/s)
CSW1.1	76.2	0.1	1.06E-03	1.22E-05	1.60E-07
CSW1.2	76.2	0.1	9.91E-06	1.11E-05	1.46E-07
CSW1.3	76.2	0.1	2.97E-04	3.80E-05	4.99E-07
CSW1.4	10	0.01	3.05E-06	5.05E-06	5.05E-07
QV1.1	76.2	0.1	1.23E-05	8.61E-06	1.13E-07
QV1.2	76.2	0.1	5.04E-02	4.31E-05	5.65E-07
QV1.3	76.2	0.1	2.51E-05	5.28E-05	6.93E-07
CSW Cluster Avg.			3.41E-04	1.66E-05	3.27E-07
QV Cluster Avg.			1.68E-02	3.48E-05	4.57E-07
Sitewide Avg.			7.40E-03	2.44E-05	3.83E-07

Table A.6. PERMANOVA Results without Well Location Variable.

Variable	Degrees of Freedom	Sum of Squares	Mean Squares	F Score	R^2	p-value
Days	1	1.065	1.065	4.2641	0.03068	0.001
Temperature (°C)	1	0.979	0.9794	3.9211	0.02821	0.001
pH	1	4.536	4.5365	18.1628	0.13069	0.001
Conductance (mS)	1	2.529	2.5286	10.1239	0.07285	0.001
DO (mg/L)	1	0.399	0.3987	1.5964	0.01149	0.066
ORP (mV)	1	0.428	0.4277	1.7124	0.01232	0.049
DIC (µM)	1	0.797	0.7973	3.1922	0.02297	0.001
Residuals	96	23.978	0.2498		0.69078	
Total	103	34.711			1	

Results from PERMANOVA analysis without the well location variable on Bray-Curtis dissimilarities and associated sample metadata. R^2 values indicate the percent variation in community dissimilarity that can be described by an individual variable.

Table A.7. Linear Regression Model Results for Regressions of Gene Abundance vs. Environmental Data.

Environmental Variable	KEGG ID	Gene	Linear Regression R^2	p-value
pH	K01673	cynT, can	0.38	2.20E-04
	K02672	PilW	0.31	1.08E-03
	K05569	mrpE	0.27	2.09E-03
	K02556	motA	0.24	4.06E-03
	K02662	PilM	0.23	5.06E-03
	K01674	cah	0.21	6.64E-03
	K02654	pilD, pppA	0.17	1.43E-02
	K02664	PilO	0.16	1.83E-02
	K05565	mrpA	0.15	2.21E-02
	K05566	mrpB	0.15	2.34E-02
	K02117	atpA	0.14	2.42E-02
	K02676	PilZ	0.14	2.45E-02
	K06403	spoVAA	0.13	3.23E-02
	K06404	spoVAB	0.12	3.48E-02
	K07086	sbtK	0.11	4.31E-02
	K06415	spoVR	0.11	4.78E-02
Specific Conductance (mS)	K13640	hspR	0.38	2.05E-04
	K05570	mrpF	0.38	2.23E-04
	K05571	mrpG	0.28	1.89E-03
	K05568	mrpD	0.25	3.27E-03
	K06410	spoVFA	0.25	3.28E-03
	K07086	sbtK	0.20	8.41E-03
	K06416	spoVS	0.18	1.23E-02
	K02107	atpH	0.18	1.32E-02
	K06413	spoVK	0.16	1.90E-02
Depth (m)	K13640	hspR	0.51	8.56E-06
	K05568	mrpD	0.42	8.82E-05
	K05570	mrpF	0.39	1.57E-04
	K06410	spoVFA	0.34	5.60E-04
	K06416	spoVS	0.33	7.26E-04
	K02107	atpH	0.30	1.28E-03
	K05571	mrpG	0.19	1.10E-02
	K02653	PilC	0.14	2.81E-02
	K06400	spoIVCA	0.10	4.96E-02
Oxidation Reduction Potential (mV)	K06416	spoVS	0.17	1.42E-02
	K05568	mrpD	0.16	1.70E-02
	K02107	atpH	0.13	3.38E-02
	K06410	spoVFA	0.12	3.45E-02
	K06411	spoVFB	0.11	4.82E-02
	K05566	mrpB	0.10	4.89E-02

Table A.7. (cont'd).

Environmental Variable	KEGG ID	Gene	Linear Regression R^2	p-value
Dissolved Inorganic Carbon (µM)	K01673	cynT, can	0.19	1.08E-02
	K05566	mrpB	0.16	1.80E-02
	K02662	PilM	0.12	3.43E-02
	K05571	mrpG	0.12	3.94E-02
	K05567	mrpC	0.11	4.20E-02
	K01674	cah	0.11	4.55E-02
Temperature (°C)	K02652	PilB	0.35	4.65E-04
	K02666	PilQ	0.33	6.71E-04
	K05565	mrpA	0.31	9.23E-04
	K06415	spoVR	0.27	2.10E-03
	K02407	fliD	0.25	3.42E-03
	K02556	motA	0.18	1.33E-02
	K03499	trkA; ktrA	0.15	2.15E-02
	K02117	atpA	0.14	2.67E-02
	K07086	sbtK	0.14	2.68E-02
	K03498	trkH	0.11	4.04E-02

Table A.8. Well Elevations and Geographic Coordinate System Locations.

Point ID	Elevation (meters)	Latitude Global	Longitude Global
CSW1.1	639.7901352	38.86184	-122.41428
CSW1.2	639.839208	38.86182	-122.41442
CSW1.3	639.9080928	38.86184	-122.41442
CSW1.4	639.9044352	38.86182	-122.41445
CSW1.5		38.86185	-122.41418
CSWold	639.8142144	38.86187	-122.41449
N08-A	649.8912072	38.86184	-122.43052
N08-B	649.6924776	38.86186	-122.43053
N08-C	649.7311872	38.86188	-122.43054
QV1.1	649.6068288	38.86205	-122.43043
QV1.2	650.312136	38.86207	-122.43043
QV1.3	650.174976	38.86208	-122.43044
CSW (BRIDGE) CREEK	637.0896072	38.86189	-122.4139
QV CREEK	648.1843272	38.86188	-122.43032

Table A.9. Sequencing Centers Used Through Project Lifetime.

Sampling Trip	DOE Joint Genome Institute	Marine Biological Laboratory's Josephine Bay Paul Center	Michigan State University Genomics Core
December 2011	X		
March 2012	X	X	
June 2012	X	X	
August 2012	X	X	
December 2012	X		
March 2013	X	X	
August 2013	X	X	
December 2013		X	
July 2014		X	X
August 2015			X
January 2016			X
June 2016			X
June 2017			X

REFERENCES

REFERENCES

1. Bar-On Y.M., Phillips R., Milo R. The biomass distribution on Earth. *Proc Natl Acad Sci USA*. (2018). doi:10.1073/pnas.1711842115

2. Flynn T.M., Sanford R.A., Ryu H., Bethke C.M., Levine A.D., Ashbolt N.J., Santo Domingo J.W. Functional microbial diversity explains groundwater chemistry in a pristine aquifer. *BMC Microbiology*, 13 (2013). doi:10.1186/1471-2180-13-146

3. Anantharaman K., Brown C.T., Hug L.A., Sharon I., Castelle C.J., Probst A.J., Thomas B.C., Singh A., Wilkins M.J., Karaoz U., Brodie E.L., Williams K.H., Hubbard S.S., Banfield J.F. Thousands of microbial genomes shed light on interconnected biogeochemical processes in an aquifer system. *Nature Communications*, 7 (2016). doi:10.1038/ncomms13219

4. Lau M.C.Y., Kieft T.L., Kuloyo O., Linage-Alvarez B., van Heerden E., Lindsay M.R., Magnabosco C., Wang W., Wiggins J.B., Guo L., Perlman D.H., Kyin S., Shwe H.H., Harris R.L., Oh Y., Yi M.J., Purtschert R., Slater G.F., Ono S., Wei S., Li L., Lollar B.S., Onstott T.C. An oligotrophic deep-subsurface community dependent on syntrophy is dominated by sulfur-driven autotrophic denitrifiers. *Proc Natl Acad Sci USA*, (2016). doi:10.1073/pnas.1612244113

5. McCollom T.M., Bach W. Thermodynamic constraints on hydrogen generation during serpentinization of ultramafic rocks. *Geochimica et Cosmochimica Acta*, 73(3):856–75 (2009). doi: 10.1016/j.gca.2008.10.032

6. Kohl L., Cumming E., Cox A., Rietze A., Morrissey L., Lang S.Q., Richter A., Suzuki S., Nealson K.H., Morrill P.L. Exploring the metabolic potential of microbial communities in ultra-basic, reducing springs at The Cedars, CA, USA: Experimental evidence of microbial methanogenesis and heterotrophic acetogenesis. *Journal of Geophysical Research: Biogeosciences*, 121(4):1203–20 (2016). doi: 10.1002/2015JG003233

7. Schrenk M.O., Kelley D.S., Bolton S.A., Baross J.A. Low archaeal diversity linked to subseafloor geochemical processes at the Lost City Hydrothermal Field, Mid-Atlantic Ridge. *Environmental Microbiology*, 6(10):1086–95 (2004). doi:10.1111/j.1462-2920.2004.00650.x

8. Brazelton W.J., Mehta M.P., Kelley D.S., Baross J.A. Physiological differentiation within a single-species biofilm fueled by serpentinization. *mBio,* 2(4):e00127-11 (2011). doi:10.1128/mBio.00127-11

9. Quéméneur M., Bes M., Postec A., Mei N., Hamelin J., Monnin C., Chavagnac V., Payri C., Pelletier B., Guentas-Dombrowsky L., Gérard M., Pisapia C., Gérard E., Ménez B., Ollivier B., Erauso G. Spatial distribution of microbial communities in the shallow submarine alkaline hydrothermal field of the Prony Bay, New Caledonia. *Environmental Microbiology Reports*, 6:665–74 (2014). doi:10.1111/1758-2229.12184

10. Tiago I., Veríssimo A. Microbial and functional diversity of a subterrestrial high pH groundwater associated to serpentinization. *Environmental Microbiology*, 15(6):1687–706 (2013). doi:10.1111/1462-2920.12034

11. Crespo-Medina M., Twing K.I., Kubo M.D.Y., Hoehler T.M., Cardace D., McCollom T., Schrenk M.O. Insights into environmental controls on microbial communities in a continental serpentinite aquifer using a microcosm-based approach. *Frontiers in Microbiology*, 5:604 (2014). doi:10.3389/fmicb.2014.00604

12. Sánchez-Murillo R., Gazel E., Schwarzenbach E.M., Crespo-Medina M., Schrenk M.O., Boll J., Gill B.C. Geochemical evidence for active tropical serpentinization in the Santa Elena Ophiolite, Costa Rica: An analog of a humid early Earth? *AGU Publications Geochemistry, Geophysics, Geosystems*, 15(5):1783–800 (2014). doi:10.1002/2013GC005213

13. Woycheese K.M., Meyer-Dombard D.R., Cardace D., Argayosa A.M., Arcilla C.A. Out of the dark: Transitional subsurface-to-surface microbial diversity in a terrestrial serpentinizing seep (Manleluag, Pangasinan, the Philippines). *Frontiers in Microbiology*, 6 (2015). doi:10.3389/fmicb.2015.00044

14. Brazelton W.J., Thornton C.N., Hyer A., Twing K.I., Longino A.A., Lang S.Q., Lilley M.D., Früh-Green G.L., Schrenk M.O. Metagenomic identification of active methanogens and methanotrophs in serpentinite springs of the Voltri Massif , Italy. *PeerJ*, (2017). doi:10.7717/peerj.2945

15. Twing K.I., Brazelton W.J., Kubo M.D.Y., Hyer A.J., Cardace D., Hoehler T.M., McCollom T.M., Schrenk M.O. Serpentinization-Influenced Groundwater Harbors Extremely Low Diversity Microbial Communities Adapted to High pH. *Frontiers in Microbiology*, 8:308 (2017). doi:10.3389/fmicb.2017.00308

16. Rempfert K.R., Miller H.M., Bompard N., Nothaft D., Matter J.M., Kelemen P., Fierer N., Templeton A.S. Geological and geochemical controls on subsurface microbial life in the Samail Ophiolite, Oman. *Frontiers in Microbiology*, 8 (2017). doi:10.3389/fmicb.2017.00056

17. Brazelton W.J., Nelson B., Schrenk M.O. Metagenomic evidence for H_2 oxidation and H_2 production by serpentinite-hosted subsurface microbial communities. *Frontiers in Microbiology*, 2 (2012). doi:10.3389/fmicb.2011.00268

18. Suzuki S., Kuenen J.G., Schipper K., van der Velde S., Ishii S., Wu A., Sorokin D.Y., Tenney A., Meng X., Morrill P.L., Kamagata Y., Muyzer G., Nealson K.H. Physiological and genomic features of highly alkaliphilic hydrogen-utilizing Betaproteobacteria from a continental serpentinizing site. *Nature Communications*, 5 (2014). doi:10.1038/ncomms4900

19. Fones E.M., Colman D.R., Kraus E.A., Nothaft D.B., Poudel S., Rempfert K.R., Spear J.R., Templeton A.S., Boyd E.S. Physiological adaptations to serpentinization in the Samail Ophiolite, Oman. *The ISME Journal* (2019). doi:10.1038/s41396-019-0391-2

20. Seyler L.M., Brazelton W.J., McLean C., Putman L.I., Hyer A., Kubo M.D.Y., Hoehler T., Cardace D., Schrenk M.O. Carbon Assimilation Strategies in Ultrabasic Groundwater: Clues from the Integrated Study of a Serpentinization-Influenced Aquifer. *mSystems*, 5(2):1–17 (2020. doi:10.1128/mSystems.00607-19

21. Crespo-Medina M., Twing K.I., Sánchez-Murillo R., Brazelton W.J., McCollom T.M., Schrenk M.O. Methane dynamics in a tropical serpentinizing environment: The Santa Elena Ophiolite, Costa Rica. *Frontiers in Microbiology*, 8(MAY):1–14 (2017). doi:10.3389/fmicb.2017.00916

22. Sabuda M.C., Brazelton W.J., Putman L.I., McCollom T.M., Hoehler T.M., Kubo M.D.Y., Cardace D., Schrenk M.O. A dynamic microbial sulfur cycle in a serpentinizing continental ophiolite. *Environmental Microbiology*, 22:2329–45 (2020). doi:10.1111/1462-2920.15006

23. Vellend M. Conceptual synthesis in community ecology. *The Quarterly Review of Biology*, 85(2):183–206 (2010). doi:10.1086/652373

24. Nemergut D.R., Schmidt S.K., Fukami T., O'Neill S.P., Bilinski T.M., Stanish L.F., Knelman J.E., Darcy J.L., Lynch R.C., Wickey P., Ferrenberg S. Patterns and Processes of Microbial Community Assembly. *Microbiology and Molecular Biology Reviews*, 77(3):342–56 (2013). doi:10.1128/MMBR.00051-12

25. Medini D., Serruto D., Parkhill J., Relman D.A., Donati C., Moxon R., Falkow S., Rappuoli R. Microbiology in the post-genomic era. *Nature Reviews Microbiology*, 6 (2008). doi:10.1038/nrmicro1901

26. Chase J.M., Kraft N.J.B., Smith K.G., Vellend M., Inouye B.D. Using null models to disentangle variation in community dissimilarity from variation in α-diversity. *Ecosphere*, 2(2) (2011). doi:10.1890/ES10-00117.1

27. Zhou J., Liu W., Deng Y., Jiang Y., Xue K., He Z., Van Nostrand J.D., Wu L., Yang Y., Wang A. Stochastic Assembly Leads to Alternative Communities with Distinct Functions in a Bioreactor Microbial Community. *mBio*, 4(2):1–8 (2013). doi:10.1128/mBio.00584-12.Editor

28. Stegen J.C., Lin X., Fredrickson J.K., Konopka A.E. Estimating and mapping ecological processes influencing microbial community assembly. *Frontiers in Microbiology*, 6(MAY):1–15 (2015). doi:10.3389/fmicb.2015.00370

29. Beaton E.D., Stevenson B.S., King-Sharp K.J., Stamps B.W., Nunn H.S., Stuart M. Local and Regional Diversity Reveals Dispersal Limitation and Drift as Drivers for Groundwater Bacterial Communities from a Fractured Granite Formation. *Frontiers in Microbiology*, 7 (2016). doi:10.3389/fmicb.2016.01933

30. Evans S., Martiny J.B.H., Allison S.D. Effects of dispersal and selection on stochastic assembly in microbial communities. *The ISME Journal*, 11(1):176–85 (2016). doi:10.1038/ismej.2016.96

31. Stegen J.C., Fredrickson J.K., Wilkins M.J., Konopka A.E., Nelson W.C., Arntzen E.V., Chrisler W.B., Chu R.K., Danczak R.E., Fansler S.J., Kennedy D.W., Resch C.T., Tfaily M. Groundwater–surface water mixing shifts ecological assembly processes and stimulates organic carbon turnover. *Nature Communications*, 7 (2016). doi:10.1038/ncomms11237

32. Danczak R.E., Johnston M.D., Kenah C., Slattery M., Wilkins M.J. Microbial Community Cohesion Mediates Community Turnover in Unperturbed Aquifers. *mSystems*, 3(4):e00066-18 (2018). doi:10.1128/mSystems.00066-18

33. Tripathi B.M., Stegen J.C., Kim M., Dong K., Adams J.M., Lee Y.K. Soil pH mediates the balance between stochastic and deterministic assembly of bacteria. *The ISME Journal* (2018). doi:10.1038/s41396-018-0082-4

34. Danczak R.E., Daly R.A., Borton M.A., Stegen J.C., Roux S., Wrighton K.C., Wilkins M.J. Ecological assembly processes are coordinated between bacterial and viral communities in fractured shale ecosystems. *mSystems*, 5(2):1–13 (2020). doi:10.1128/mSystems.00098-20

35. Liu W., Graham E.B., Zhong L., Zhang J., Li W., Li Z., Lin X., Feng Y. Dynamic microbial assembly processes correspond to soil fertility in sustainable paddy agroecosystems. *Functional Ecology*, 34(February):1244–56 (2020). doi:10.1111/1365-2435.13550

36. Liu W., Graham E.B., Dong Y., Zhong L., Zhang J., Qiu C., Chen R., Lin X., Feng Y. Balanced stochastic versus deterministic assembly processes benefit diverse yet uneven ecosystem functions in representative agroecosystems. *Environmental Microbiology*, 23:391–404 (2021). doi:10.1111/1462-2920.15326

37. Stegen J.C., Lin X., Konopka A.E., Fredrickson J.K. Stochastic and deterministic assembly processes in subsurface microbial communities. *The ISME Journal*, 6(10):1653–64 (2012). doi:10.1038/ismej.2012.22

38. Gleeson T., Befus K.M., Jasechko S., Luijendijk E., Cardenas M.B. The global volume and distribution of modern groundwater. *Nature Geoscience* (2016). doi:10.1038/NGEO2590

39. Lall U., Josset L., Russo T. A Snapshot of the World's Groundwater Challenges. *Annu. Rev. Environ. Resour.*, 45:171–96 (2020). doi:10.1146/annurev-environ-102017-025800

40. Cardace D., Hoehler T., Mccollom T., Schrenk M., Carnevale D., Kubo M., Twing, K. Establishment of the Coast Range ophiolite microbial observatory (CROMO): drilling objectives and preliminary outcomes. *Scientific Drilling*, 16:45–55 (2013). doi:10.5194/sd-16-45-2013

41. Ortiz E., Tominaga M., Cardace D., Schrenk M.O., Hoehler T.M., Kubo M.D., Rucker D.F. Geophysical Characterization of Serpentinite Hosted Hydrogeology at the McLaughlin Natural Reserve, Coast Range Ophiolite. *Geochemistry, Geophysics, Geosystems*, 19(1):114–31 (2018). doi:10.1002/2017GC007001

42. Dewandel B., Lachassagne P., Boudier F., Al-Hattali S., Ladouche B., Pinault J., Al-Suleimani Z. A conceptual hydrogeological model of ophiolite hard-rock aquifers in Oman based on a multiscale and a multidisciplinary approach. *Hydrogeology Journal* (2005). doi:10.1007/s10040-005-0449-2

43. Jeanpert J., Iseppi M., Adler P.M., Genthon P., Sevin B., Thovert J.-F., Dewandel B., Join J.-L. Fracture controlled permeability of ultramafic basement aquifers. Inferences from the Koniambo massif, New Caledonia. *Engineering Geology*, 256(May):67–83 (2019). doi:10.1016/j.enggeo.2019.05.006

44. Schrenk M.O., Brazelton W.J., Lang S.Q. Serpentinization, carbon, and deep life. *Reviews in Mineralogy and Geochemistry*, 75:575–606 (2013). doi:10.2138/rmg.2013.75.18

45. Krulwich T.A., Sachs G., Padan E. Molecular aspects of bacterial pH sensing and homeostasis. *Nature Reviews Microbiology*, 9(5):330–43 (2011). doi:10.1038/nrmicro2549

46. Miller H.M., Matter J.M., Kelemen P., Ellison E.T., Conrad M.E., Fierer N., Ruchala T., Tominaga M., Templeton A.S. Modern water/rock reactions in Oman hyperalkaline peridotite aquifers and implications for microbial habitability. *Geochimica et Cosmochimica Acta*, 179:217–41 (2016). doi:10.1016/j.gca.2016.01.033

47. Fine P.V.A, Kembel S.W. Phylogenetic community structure and phylogenetic turnover across space and edaphic gradients in western Amazonian tree communities. *Ecography*, 34(4):552–65 (2011). doi:10.1111/j.1600-0587.2010.06548.x

48. Chase J.M. Drought mediates the importance of stochastic community assembly. *Proc Natl Acad Sci USA*, 104(44) (2007). doi:10.1073/pnas.0704350104

49. Ofiteru I.D., Lunn M., Curtis T.P., Wells G.F., Criddle C.S., Francis C.A., Sloan W.T. Combined niche and neutral effects in a microbial wastewater treatment community. *Proc Natl Acad Sci USA*, 107(35) (2010). doi:10.1073/pnas.1000604107

50. Caruso T., Chan Y., Lacap D.C., Lau M.C.Y., Mckay C.P., Pointing S.B. Stochastic and deterministic processes interact in the assembly of desert microbial communities on a global scale. *The ISME Journal*, (2011). doi:10.1038/ismej.2011.21

51. Valverde A., Makhalanyane T.P., Cowan D.A. Contrasting assembly processes in a bacterial metacommunity along a desiccation gradient. *Frontiers in Microbiology*, 5 (2014). doi:10.3389/fmicb.2014.00668

52. Starnawski P., Bataillon T., Ettema T.J.G., Jochum L.M., Schreiber L., Chen X., Lever M.A., Polz M.F., Jørgensen B.B., Schramm A., Kjeldsen K.U. Microbial community assembly and evolution in subseafloor sediment. *Proc Natl Acad Sci USA*, (2017). doi:10.1073/pnas.1614190114

53. Newman B.D., Osenbrück K., Aeschbach-Hertig W., Solomon D.K., Cook P., Różański K., Kipfer R. Dating of "young" groundwaters using environmental tracers: advantages, applications, and research needs. *Isotopes in Environmental and Health Studies*, 46(3):259–78 (2010). doi:10.1080/10256016.2010.514339

54. Graham E.B., Crump A.R., Resch C.T., Fansler S., Arntzen E., Kennedy D.W., Fredrickson J.K., Stegen J.C. Deterministic influences exceed dispersal effects on hydrologically-connected microbiomes. *Environmental Microbiology*, 19:1552–67 (2017). doi:10.1111/1462-2920.13720

55. Graham E.B., Crump A.R., Resch C.T., Fansler S., Arntzen E., Kennedy D.W., Fredrickson J.K., Stegen J.C. Coupling Spatiotemporal Community Assembly Processes to Changes in Microbial Metabolism. *Frontiers in Microbiology*, 7 (2016). doi:10.3389/fmicb.2016.01949

56. Zhou J., Ning D. Stochastic Community Assembly: Does It Matter in Microbial Ecology? *Microbiology and Molecular Biology Reviews*, 81(4):1–32 (2017). doi:10.1128/MMBR.00002-17

57. Graham E.B., Stegen J.C. Dispersal-Based Microbial Community Assembly Decreases Biogeochemical Function. *Processes*, 5(65) (2017). doi:10.3390/pr5040065

58. Liu J., Vellend M., Wang Z., Yu M. High beta diversity among small islands is due to environmental heterogeneity rather than ecological drift. *Journal of Biogeography*, (45):2252–61 (2018). doi:10.1111/jbi.13404

59. Fodelianakis S., Valenzuela-Cuevas A., Barozzi A., Daffonchio D. Direct quantification of ecological drift at the population level in synthetic bacterial communities. *The ISME Journal*, (2020). doi:10.1038/s41396-020-00754-4

60. Stegen J.C., Lin X., Fredrickson J.K., Chen X., Kennedy D.W., Murray C.J., Rockhold M.L., Konopka A. Quantifying community assembly processes and identifying features that impose them. *The ISME Journal*, 7(11):2069–79 (2013). doi:10.1038/ismej.2013.93

61. Nemergut D., Shade A., Violle C. When, where and how does microbial community composition matter? *Frontiers in Microbiology*. 5(SEP):2012–4 (2014). doi:10.3389/fmicb.2014.00497

62. Yin W., Wang Y., Liu L., He J. Biofilms: The Microbial "Protective Clothing" in Extreme Environments. *International Journal of Molecular Sciences*, (2019). doi:10.3390/ijms20143423

63. Shervais J.W., Murchey B.L., Kimbrough D.L., Renne P.R. Radioisotopic and biostratigraphic age relations in the Coast Range Ophiolite, northern California: Implications for the tectonic evolution of the Western Cordillera. *GSA Bulletin*, 117(5):633–53 (2005). doi:10.1130/B25443.1

64. Fehn U., Peters E.K., Tullai-Fitzpatrick S., Kubik P.W., Sharma P., Teng R.T.D., Grove H.E., Elmore D. ^{129}I and ^{36}Cl concentrations in waters of the eastern Clear Lake area, California: Residence times and source ages of hydrothermal fluids. *Geochimica et Cosmochimica Acta*, 56(5):2069–79 (1992). doi:10.1016/0016-7037(92)90330-L

65. Inagaki F., Hinrichs K.-U., Kubo Y., Bowles M.W., Heuer V.B., Hong W.-L., Hoshino T., Ijiri A., Imachi H., Ito M., Kaneko M., Lever M.A., Lin Y.-S., Methé B.A., Morita S.,

Morono Y., Tanikawa W., Bihan M., Bowden S.A., Elvert M., Glombitza, C., Gross, D., Harrington G.J., Hori T., Li K., Limmer D., Liu C.-H., Murayama M., Ohkouchi N., Ono S., Park Y.-S., Phillips S.C., Prieto-Mollar X., Purkey M., Riedinger N., Sanada Y., Sauvage J., Snyder G., Susilawati R., Takano Y., Tasumi E., Terada T., Tomaru H., Trembath-Reichert E., Wang D.T., Yamada Y. Exploring deep microbial life in coal-bearing sediment down to ~2.5 km below the ocean floor. *Science*, 349(6246):16–21 (2015). doi:10.1126/science.aaa6882

66. Sleep N.H., Meibom A., Fridriksson T., Coleman R.G., Bird D.K. H2-rich fluids from serpentinization: geochemical and biotic implications. *Proc Natl Acad Sci USA*, 101(35):12818–23 (2004). doi:10.1073/pnas.0405289101

67. Kralik M. How to Estimate Mean Residence Times of Groundwater. *Procedia Earth and Planetary Science*, 13:301-6 (2015). doi:10.1016/j.proeps.2015.07.070

68. Duffield G.M. AQTESOLV for Windows User's Guide. Version 4.5. Hydrosolve Inc., Reston, VA, USA, (2007).

69. Schloss P.D., Westcott S.L., Ryabin T., Hall J.R., Hartmann M., Hollister E.B., Lesniewski R.A., Oakley B.B., Parks D.H., Robinson C.J., Sahl J.W., Stres B., Thallinger G.G., Van Horn D.J., Weber C.F. Introducing mothur: Open-source, platform-independent, community-supported software for describing and comparing microbial communities. *Applied and Environmental Microbiology*, 75(23):7537–41 (2009). doi:10.1128/AEM.01541-09

70. Westcott S.L., Schloss P.D. De novo clustering methods outperform reference-based methods for assigning 16S rRNA gene sequences to operational taxonomic units. *PeerJ*, 3:e1487 (2015). doi:10.7717/peerj.1487

71. Koren O., Knights D., Gonzalez A., Waldron L., Segata N., Knight R., Huttenhower C., Ley R.E. A Guide to Enterotypes across the Human Body: Meta-Analysis of Microbial Community Structures in Human Microbiome Datasets. *PLoS Computational Biology*, 9(1) (2013). doi:10.1371/journal.pcbi.1002863

72. Duvallet C., Gibbons S.M., Gurry T., Irizarry R.A., Alm E.J. Meta-analysis of gut microbiome studies identifies disease-specific and shared responses. *Nature Communications*, 8(1784) (2017). doi:10.1038/s41467-017-01973-8

73. Davies G.M., Gray A. Don't let spurious accusations of pseudoreplication limit our ability to learn from natural experiments (and other messy kinds of ecological monitoring). *Ecology and Evolution*, 5(22):5295–304 (2015). doi:10.1002/ece3.1782

74. Lazic S.E., Mellor J.R., Ashby M.C., Munafo M.R. A Bayesian predictive approach for dealing with pseudoreplication. *Scientific Reports*, 10(1):1–10 (2020). doi:10.1038/s41598-020-59384-7

75. Sheik C.S., Reese B.K., Twing K.I., Sylvan J.B., Grim S.L., Schrenk M.O., Sogin M.L., Colwell F.S. Identification and removal of contaminant sequences from ribosomal gene

databases: Lessons from the Census of Deep Life. *Frontiers in Microbiology*, 9(APR):1–14 (2018). doi:10.3389/fmicb.2018.00840

76. Vouga M., Baud D., Greub G. *Simkania negevensis*, an insight into the biology and clinical importance of a novel member of the *Chlamydiales* order. *Critical Reviews in Microbiology*, 7828 (2017). doi:10.3109/1040841X.2016.1165650

77. Geerlings S.Y., Kostopoulos I., de Vos W.M., Belzer C. *Akkermansia muciniphila* in the Human Gastrointestinal Tract: When, Where, and How? *Microorganisms*, (2018). doi:10.3390/microorganisms6030075

78. Fullerton K.M., Schrenk M.O., Yücel M., Manini E., Basili M., Rogers T.J., Fattorini D., Di Carlo M., d'Errico G., Regoli F., Nakagawa M., Vetriani C., Smedile F., Ramírez C., Miller H., Morrison S.M., Buongiorno J., Jessen G.L., Steen A.D., Martínez, M., Maarten de Moor J., Barry P.H., Giovannelli D., Lloyd K.G. Effect of tectonic processes on biosphere-geosphere feedbacks across a convergent margin. *Nature Geoscience*, 14(MAY) (2021). doi:10.1038/s41561-021-00725-0

79. Price M.N., Dehal P.S., Arkin A.P. FastTree: Computing Large Minimum Evolution Trees with Profiles instead of a Distance Matrix. *Molecular Biology and Evolution*, (2009). doi:10.1093/molbev/msp077

80. McMurdie P.J., Holmes S. Phyloseq: An R Package for Reproducible Interactive Analysis and Graphics of Microbiome Census Data. *PLoS ONE*, 8(4) (2013). doi:10.1371/journal.pone.0061217

81. Oksanen J., Blanchet F.G., Friendly M., Kindt R., Legendre P., McGlinn D., Minchin P.R., O'Hara R.B., Simpson G.L., Solymos P., Stevens M.H.H., Szoecs E., Wagner H. vegan: Community Ecology Package. R package version 25-5 (2019). Available from: https://cran.r-project.org/package=vegan

82. Chessel D., Dufour A.B., Thioulouse J. The ade4 package - I: One-table methods. *R News*, 4(June):5–10 (2004).

83. Marechal J.C., Dewandel B., Subrahmanyam K. Use of hydraulic tests at different scales to characterize fracture network properties in the weathered-fractured layer of a hard rock aquifer. *Water Resources Research*, 40:1–17 (2004). doi:10.1029/2004WR003137

84. Theis C.V. The relation between the lowering of the piezometric surface and the rate and duration of discharge of a well using groundwater storage. *US Geological Survey*, 16:519-24 (1935).

85. Hantush M.S. Aquifer Tests on Partially Penetrating Wells. *Journal of the Hydraulics Division*, 87(5):171–95 (1961).

86. Phillips F.M., Castro M.C. Groundwater Dating and Residence-Time Measurements. *Treatise on Geochemistry: Second Edition*, (2013). doi:10.1016/B978-0-08-095975-7.00513-1

87. Jones I., Lerner D.N. Level-determined sampling in an uncased borehole. Journal of Hydrology, 171:291–317 (1995).

CHAPTER 3

Drilling activity in a serpentinization-influenced aquifer alters subsurface geochemistry and stimulates dominant microbial community members

Abstract

Reservoirs of groundwater in the deep subsurface are extremely valuable resources and diverse ecosystems, hosting complex and enigmatic microbial communities and biogeochemical cycles. To preserve and manage these resources for continued future use it is vital that we understand extant microbial communities and biogeochemical cycles in these systems and their capacity to respond to enhanced use and future environmental change. Here we report observations from a time series dataset collected from a serpentinization-influenced aquifer following drilling and installation of boreholes to access the subsurface in 2011. Results show that fluids became more oxidizing, and that dissolved oxygen, hydrogen, and acetate concentrations were higher during the first two years following drilling. Organisms from the genera *Serpentinomonas* and *Dethiobacter*, which are commonly observed at sites of serpentinization, flourished immediately after drilling and gradually decreased in relative abundance over time. Interestingly, rare taxa played a small role in microbial community responses to change, contrasting with prior observations where rare microbial taxa play an important role in microbial community responses to perturbation. The metabolic versatility of both *Serpentinomonas* and *Dethiobacter* likely allowed these organisms to thrive under changing geochemical conditions following drilling activity at the site. The response of dominant microbial community members to an environmental disturbance has important implications for future studies in serpentine and other hard-rock environments as well as applications such as carbon capture and sequestration.

Introduction

Microbial communities in natural environments play important roles in mediating biogeochemical cycles of organic and inorganic chemical species (1–5). In addition to their important roles in mediating ecosystem processes microbial communities are subject to both natural and anthropogenic changes that can alter microbial community composition and function (4,6–13). One such disturbance that will likely become more common in the future as shallow groundwater reservoirs are depleted and subjected to anthropogenic contaminations is drilling into the subsurface to access deep groundwater resources that are relatively 'untouched' in comparison (14). While microbial community responses to drilling activity have not been previously assessed, the most geochemically disruptive portion of the process, the injection of drilling fluid into the subsurface, has previously been investigated. Investigations of the injection of exogenous substrates and water into the subsurface have primarily been related to carbon dioxide sequestration (11,15–17) and water flooding of oil fields to enhance oil recovery (18–20). This work has revealed that the injection of water or exogenous substrates into the subsurface can substantially alter aquifer geochemistry and microbial community composition and function (11,15–21).

Continental ophiolites are common hard-rock environments (22). These environments host microbial communities that are well-adapted to strongly reducing, ultrabasic fluids, with limited available dissolved inorganic carbon (DIC) and abundant dissolved hydrogen (H_2) which are the result of serpentinization reactions that occur between water and iron bearing minerals in ultramafic rocks (23–25). Investigations of microbial community composition and function in these environments revealed low biomass, low diversity microbial communities consisting of metabolically versatile alkaliphiles capable of using H_2, carbon monoxide (CO), methane (CH_4),

DIC, sulfur compounds, and small organic acids (26–41). Interest in the biogeochemistry of the serpentinizing subsurface has spurred three scientific drilling projects in the last decade (42–44), providing the unique opportunity to investigate how drilling activity, and the injection of drilling fluid into the subsurface, affect the geochemistry and microbial communities of serpentinizing systems. To date, the capacity of serpentinite microbial communities to respond to environmental perturbations has not yet been assessed. Understanding microbial community stability and microbial community responses to environmental change (45,46) in these systems is vital to our overall understanding of these environments and the potential feasibility for applications such as carbon capture and sequestration (11,47–49).

Here, I report results from the analysis of a geochemistry and 16S rRNA gene amplicon time series dataset collected from the Coast Range Ophiolite Microbial Observatory (CROMO) near Lower Lake, CA, USA over the course of five years after drilling to install observational boreholes was completed at the site in August of 2011. Drilling was performed using sterile water as a drilling fluid to minimize subsurface contamination (42,50). Analysis of geochemistry and the relative abundance of microbial populations over time reveal dominant microbial community members from the candidate genus *Serpentinomonas* (41) and the genus *Dethiobacter* were the primary responders to increased concentrations of dissolved oxygen (DO), H_2, and acetate following the injection of water drilling fluid into the subsurface. Our data also show that rare taxa play a negligible role in serpentine microbial community responses to environmental disturbances. Instead, impressive functional diversity possessed by *Serpentinomonas* and *Dethiobacter* populations allow these organisms to reach extremely high relative abundances during the initial two years following drilling. Results highlight the role of these dominant microbial populations in the overall response of microbial communities in this system with important implications for

microbial community stability in other serpentinization-influenced aquifers, hard rock aquifers, and extreme environments.

Results

Geochemical Trends over Time

High pH, reducing fluids were collected from the CSW1.1 (19.5 m), QV1.1 (23.0 m), and N08-B (26.2 m) wells in the serpentinization-influenced CROMO aquifer two to three times per year over the course of five years to measure pH, temperature, specific conductance, DO, and oxidation reduction potential (ORP) using a YSI flow through cell and multiprobe as previously described (33,51). Additionally, aqueous samples were collected to measure dissolved H_2, carbon monoxide (CO), CH_4, DIC, and acetate.

Analysis of fluid chemistry (**Table B.1**) over time showed increased DO concentrations and less reducing ORP measurements in the initial two years of sampling (**Fig. 3.1 A & B**). Additionally, large peaks in observed H_2 and acetate concentrations were observed in the first two years after drilling (**Fig. 3.1 C & D**). Increases in DO and H_2 were substantial in QV1.1 in comparison to CSW1.1 and N08-B, and CSW1.1 experienced a large increase in acetate concentrations in comparison to QV1.1 and N08-B (**Fig. 3.1 A, C & D**). ORP measurements were highly variable but were generally less reducing in the initial two years after drilling (**Fig. 3.1 B**). Specific conductance and pH measurements differed between each of the three wells but remained relatively stable over time (**Fig. B.1 A & B**). Fluid temperature has gradually increased over time in general, although sharp decreases in temperature were observed in CSW1.1 and QV1.1 in March of 2012 (**Table B.1; Fig. B.1 C**). CO concentrations were variable although they appear to be higher in the initial two years of sampling (**Fig. B.1 D**). CH_4 concentrations did not display an

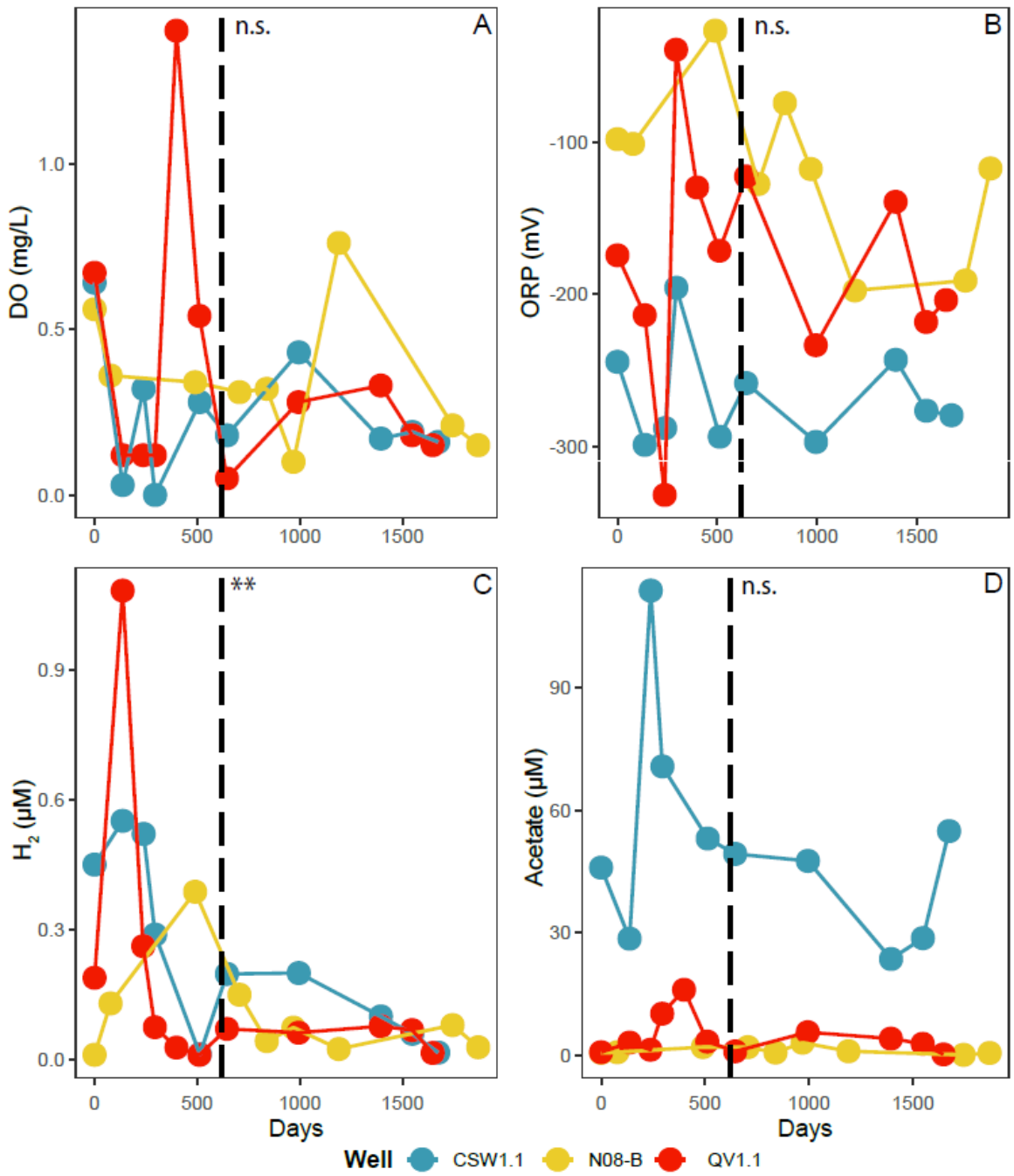

Figure 3.1. Geochemistry Time Series Plots.

Dissolved oxygen (A), oxidation reduction potential (B), dissolved hydrogen (C), and acetate (D) plotted over time. Individual samples are represented by points and connected by lines. Points and connecting lines are colored by well location. The vertical dashed line is placed between the March 2013 and August 2013 samples, when observed geochemistry starts to become more stable. Student's t-tests were used to assess the difference in mean geochemical values between samples collected from 2011 to March 2013 and samples collected from August 2013 to May 2016. ** $p < 0.05$ significance, * $p < 0.1$, n.s. not significant.

obvious trend and were highly variable over time (**Fig. B.1 E**), while DIC concentrations increased over time, especially in CSW1.1 (**Fig. B.1 F**). Mean temperature ($p < 0.05$) and concentration of H_2 ($p < 0.05$) and DIC ($p < 0.1$) were significantly different between samples collected before and after March of 2013 (**Table B.2**).

Microbial Community Diversity

DNA was extracted from CSW1.1, N08-B, and QV1.1 fluid microbial communities captured on 0.22 μm Sterivex filter cartridges (Millipore, Billerica, MA, USA) from 2011 to 2016 as described below. The taxonomic and diversity measures discussed here are based on a dataset generated from gene amplicon sequencing of the V4 region of the 16S rRNA gene. The 16S rRNA gene amplicon dataset analyzed here contains 29 samples consisting of 1,651,065 reads and 3,078 operational taxonomic units (OTUs) clustered at a 3% distance threshold as described below. The OTU count table, table with OTU taxonomic classifications, and R script used for the following analyses have been deposited on FigShare (https://figshare.com/projects/Drilling_Disturbance_in_a_Serpentinizing_Ophiolite/113898).

Given observed spikes in the concentration of DO, H_2, and acetate (**Fig. 3.1 A, C & D**) trends in microbial community richness (number of unique OTUs) and evenness (extent to which the abundance of OTUs is similar in a sample; assessed using Pielou's evenness index) were assessed over time to determine if changes in geochemical conditions altered local microbial community diversity (**Fig. 3.2 A & B**). No obvious trends were observed in microbial community richness over time (**Fig. 3.2 A**). In general, microbial community richness was greater in N08-B than in CSW1.1 and QV1.1, although a large spike in microbial community richness was observed in CSW1.1 in June of 2012 where 658 unique OTUs were observed. Microbial community

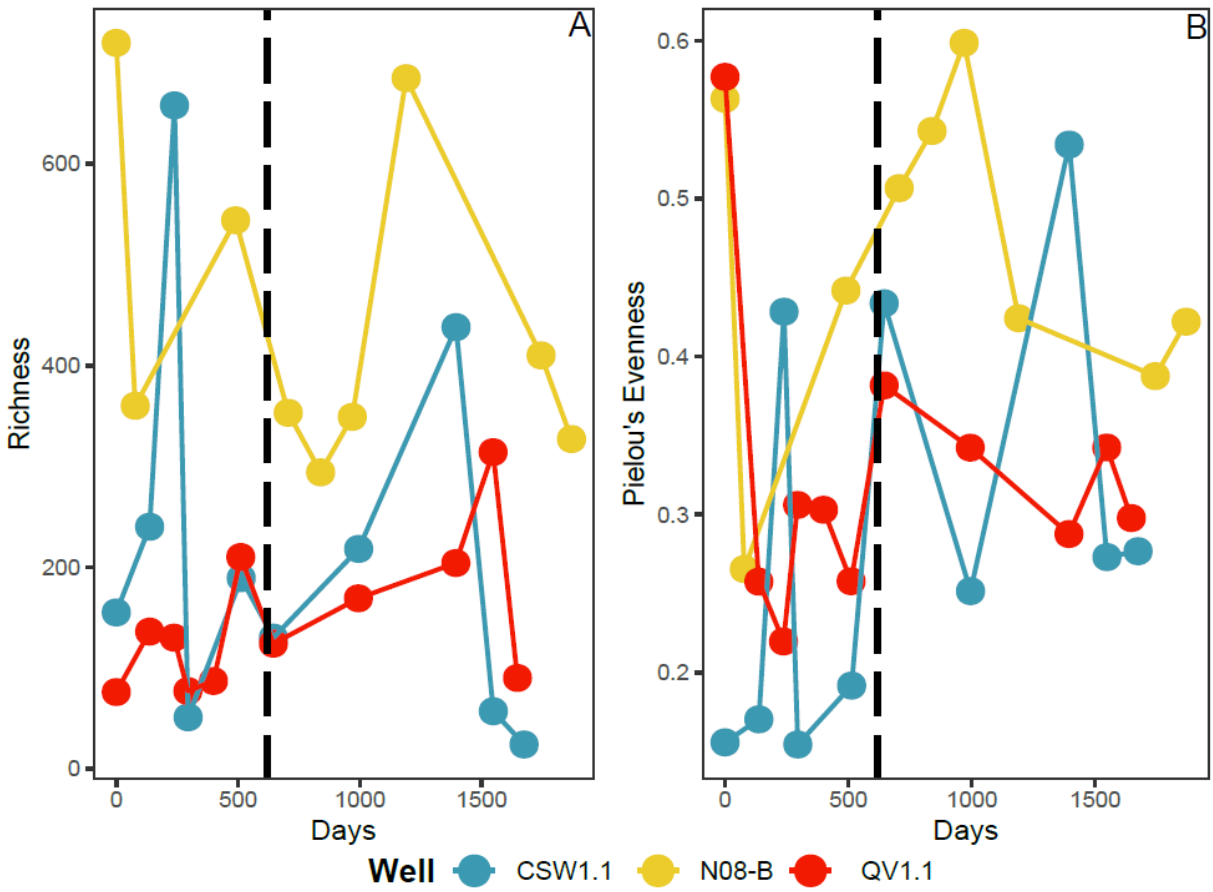

Figure 3.2. Richness and Pielou's Evenness Time Series Plots.

Microbial community richness (A) and evenness (B) plotted over time. Individual samples are represented by points and connected by lines. Points and connecting lines are colored by well location. The vertical dashed line is placed between the March 2013 and August 2013 samples, when observed geochemistry started to become more stable (Fig. 3.1).

evenness appeared to increase over time, especially in samples collected from CSW1.1 and QV1.1, with the exception of a QV1.1 sample from November of 2011 where evenness was 0.58 (**Fig. 3.2 B**). Microbial community evenness was more variable and did not display as much of an increasing trend in N08-B as compared to observations in CSW1.1 and QV1.1 (**Fig. 3.2 B**). There was no significant difference ($p < 0.05$) between mean richness and evenness values for samples collected before March of 2013 and samples collected after March of 2013 (**Table B.2**).

A PERMANOVA analysis was performed on Bray-Curtis dissimilarities and measured environmental data to determine environmental factors that drive changes in microbial community

composition (**Table B.3**). Since spikes and generally higher concentrations of DO, H_2, and acetate (**Fig. 3.1 A, C & D**) were observed prior to March of 2013 a 'Perturbance' variable was created. Samples collected from April of 2011 to March of 2013 were considered 'perturbed' and samples collected after March of 2013 were considered 'recovering'. Bray-Curtis dissimilarities were ordinated using non-metric multidimensional scaling (NMDS) and significant environmental variables identified in PERMANOVA analysis were overlain on the plot as vectors (**Fig. 3.3**). Results from this analysis showed that differences in well location (R^2=0.34) were a primary driver of differences in microbial community composition, as has previously been observed (30,33). Additionally, the 'Perturbance' variable and differences in fluid salinity accounted for 13.5% and 6.8% of the variation in microbial communities, respectively. PERMANOVA results also indicate that a large portion of the variance observed between microbial communities could not be described by measured environmental data (Residuals R^2=0.32) (**Table B.3**). Samples from individual wells generally cluster close to one another on the plot, indicating greater similarity in microbial community compositions, except for a few samples that overlap from CSW1.1 and QV1.1 (**Fig. 3.3**). Interestingly, samples collected from 'perturbed' time points from all wells lie in the center of the plot closer to one another, while samples collected from 'recovering' time points lie near the edge of the plot (**Fig. 3.3**). This indicates that while microbial communities in individual wells are distinct (**Table B.3**), community composition in all three wells was more similar during 'perturbed' time points and moved to more distinct and less similar community compositions in 'recovering' time points.

Finally, the taxonomy of microbial populations was visualized in samples collected from each well over time. Since CROMO microbial communities tend to be dominated by a small number of microbial populations (30,33), the relative abundance of the twenty five most abundant

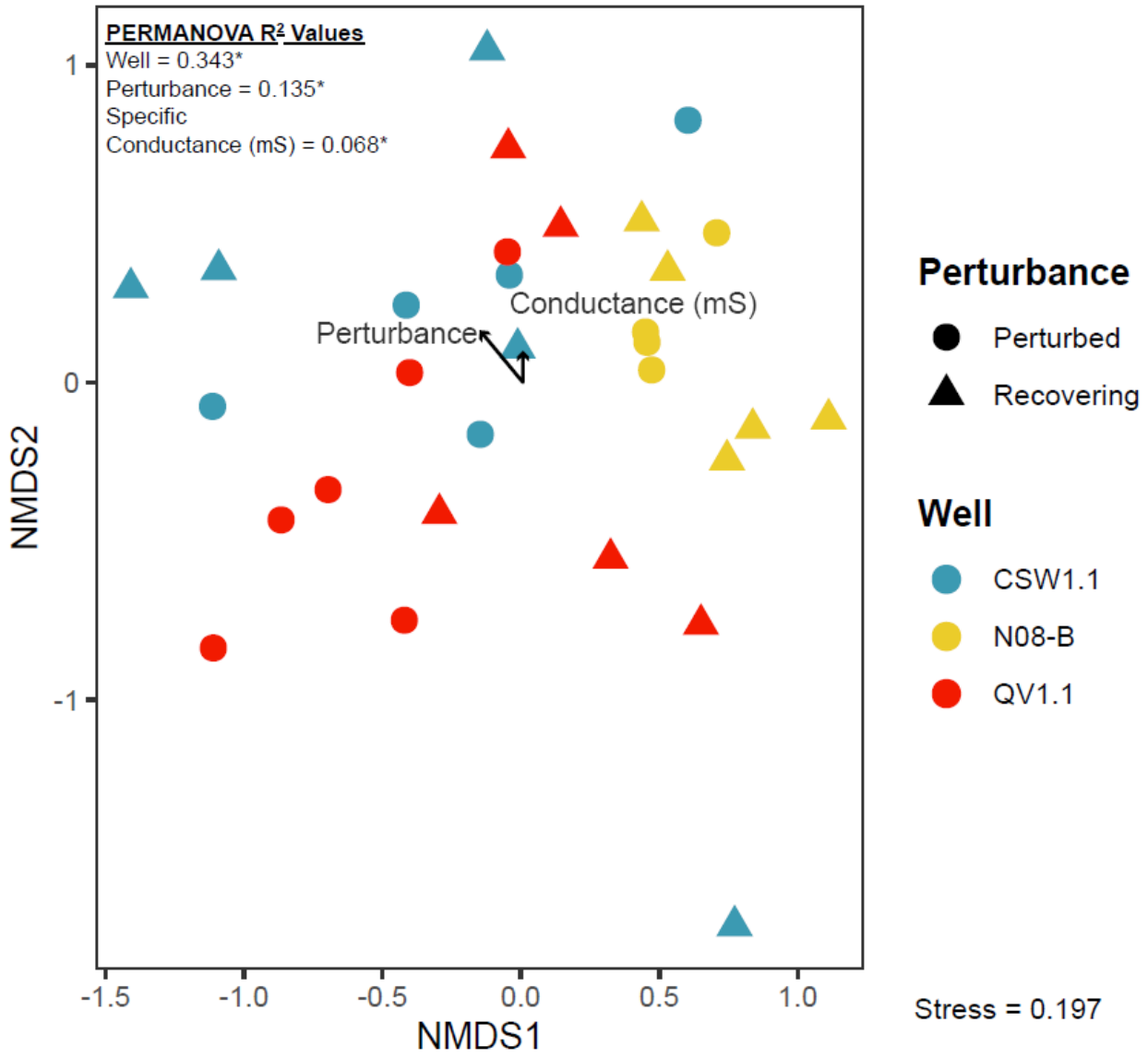

Figure 3.3. NMDS Plot of Bray-Curtis Dissimilarities.

Non-metric multidimensional scaling (NMDS) plot of microbial community 16S rRNA gene relative abundances using Bray-Curtis dissimilarities with significant environmental variables ($p \leq 0.05$) identified during PERMANOVA analysis overlain as vectors. Points on the plot are representative of individual microbial community samples and are colored by well. Points that plot close to each other are more similar in microbial community composition than to points plotted farther away.

OTUs in the dataset was assessed (**Fig. 3.4 A-C**). The twenty five most abundant OTUs in the dataset account for 75 to >90% of community composition in most time points. N08-B samples are composed of a more diverse array of OTUs as compared to CSW1.1 and QV1.1 samples and

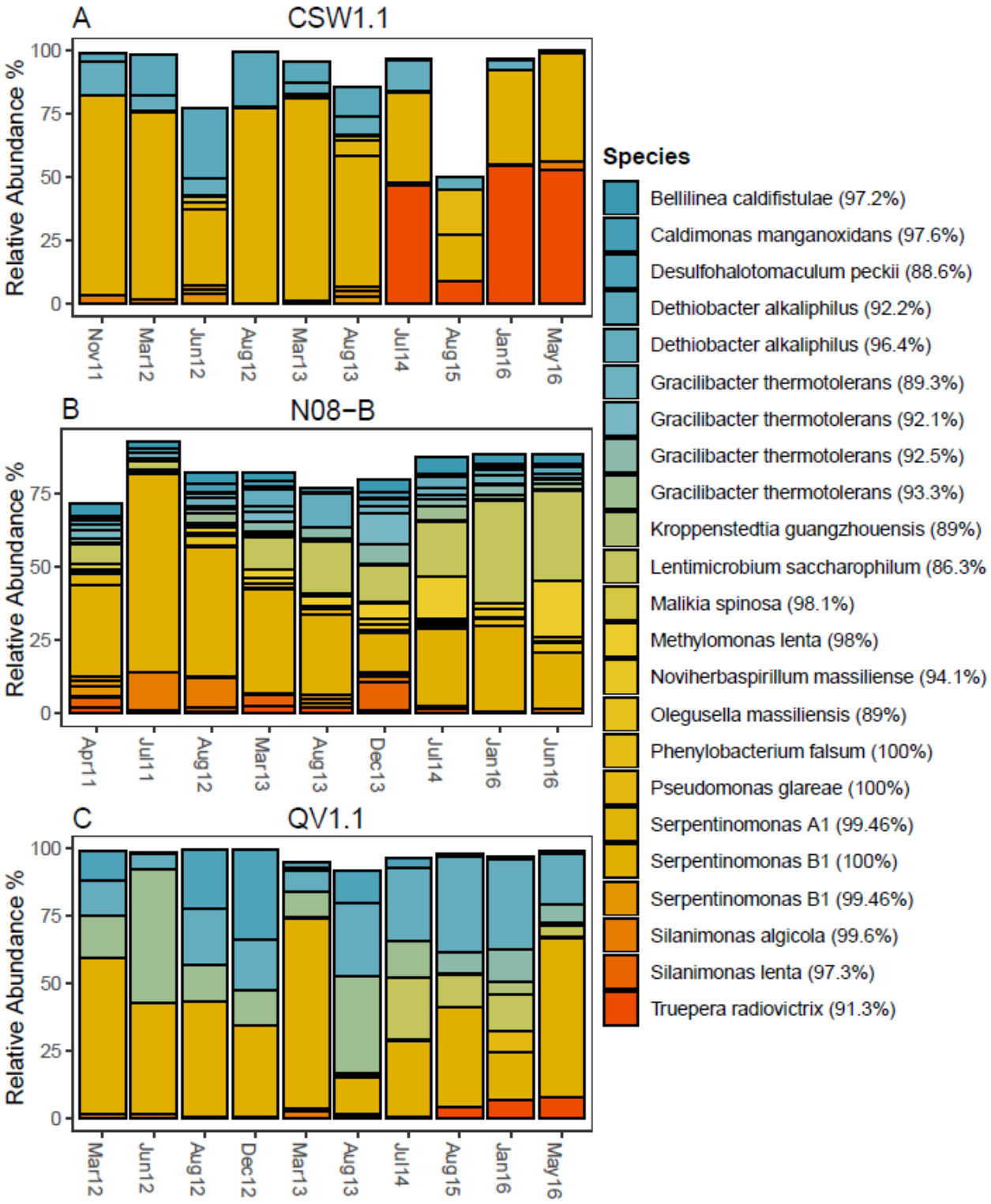

Figure 3.4. Taxonomy of Dominant OTUs Over Time.

Figure 3.4. (cont'd).

Stacked bar plots showing the closest known species taxonomic classifications for the twenty five most abundant OTUs in CSW1.1 (A), N08-B (B), and QV1.1 (C) over time as determined by assessing the normalized abundance of OTUs in the 16S rRNA gene amplicon dataset. Species classifications were determined using MegaBLAST. The closest known species name classification is listed for each OTU along with the percent pairwise identity of the sequence in question in parentheses following the species name.

contain a greater proportion of less abundant OTUs in all samples (**Fig. 3.4 B**). A microbial population closely related to *Serpentinomonas* strain B1 is dominant in all three wells in most samples, although the relative abundance appears to decrease over time (**Fig. 3.4 A-C**). Populations of organisms closely related to *Dethiobacter alkaliphilus* were abundant in the CSW1.1 and QV1.1 wells, visibly decreasing over time in CSW1.1 (**Fig. 3.4 A & C**). A microbial population closely related to *Truepera radiovictrix* was present at low abundance in all wells and increased in abundance to account for nearly 50% of community composition in CSW1.1 (**Fig. 3.4 A**).

Identification of Conditionally Rare Taxa

Since rare microbial populations have been observed to play important roles in ecosystem functioning (52) and rare taxa have been observed to play an important role in microbial community responses to stress (53) conditionally rare taxa (CRT) were identified in the dataset according to the method developed by Shade and colleagues (53). The analysis identified forty eight OTUs as conditionally rare taxa. Interestingly, eight of these CRT were also identified as being one of the twenty five most abundant OTUs in the dataset indicating that the relative abundance of certain OTUs in the dataset varied enough over time that despite being identified as conditionally rare these OTUs reached a great enough abundance at one or more time points to also be dominant within the dataset based on average relative abundance within the entire dataset.

The relative abundance and taxonomic classification of OTUs identified as CRT is published on FigShare under the following digital object identified: https://doi.org/10.6084/m9.figshare.14751744

Microbial Populations Impacted by Drilling Activity

Since microbial community composition was significantly different between samples collected during 'perturbed' and 'recovering' timepoints (**Fig. 3.3**) and the relative abundance of the twenty five most abundant OTUs (eight of which are also CRT) in the dataset was qualitatively observed to vary over time (**Fig. 3.4**) linear regression models were developed to identify OTUs whose abundance increased or decreased significantly over time (**Table B.4; Fig. 3.5**). Nine OTUs were found to be significantly correlated with time (**Fig. 3.5 A-I**). OTUs characterized as *Serpentinomonas* strain B1 (OTU_16687) and *Dethiobacter alkaliphilus* (OTU_15534) decreased in relative abundance over time (**Fig. 3.5 E & F**). *Serpentinomonas* is a dominant taxon throughout the entire dataset, while the OTU identified as *Dethiobacter alkaliphilus* was identified as a CRT as well as a dominant OTU in the dataset (**Fig. 3.4**). OTUs characterized as a distant relative of *Lentimicrobium saccharophilum* (OTU_29), a close relative of *Truepera radiovictrix* (OTU_148), a close relative of *Gracilibacter thermotolerans* (OTU_5809), *Methylomonas lenta* (OTU_10476), *Phenylobacterium falsum* (OTU_589), a close relative of *Desulfofundulus kuznetsovii* (OTU_5054), and a close relative of *Noviherbaspirillum massiliense* (OTU_8099) all increased in relative abundance over time (**Fig. 3.5 A-D & G-I**). OTUs identified as *Gracilibacter thermotolerans* and *Methylomonas lenta* were identified as both CRT and dominant OTUs within the dataset. OTUs identified as *Lentimicrobium saccharophilum* and *Truepera radiovictrix* were identified as dominant OTUs in the dataset, while OTUs identified as *Phenylobacterium falsum*,

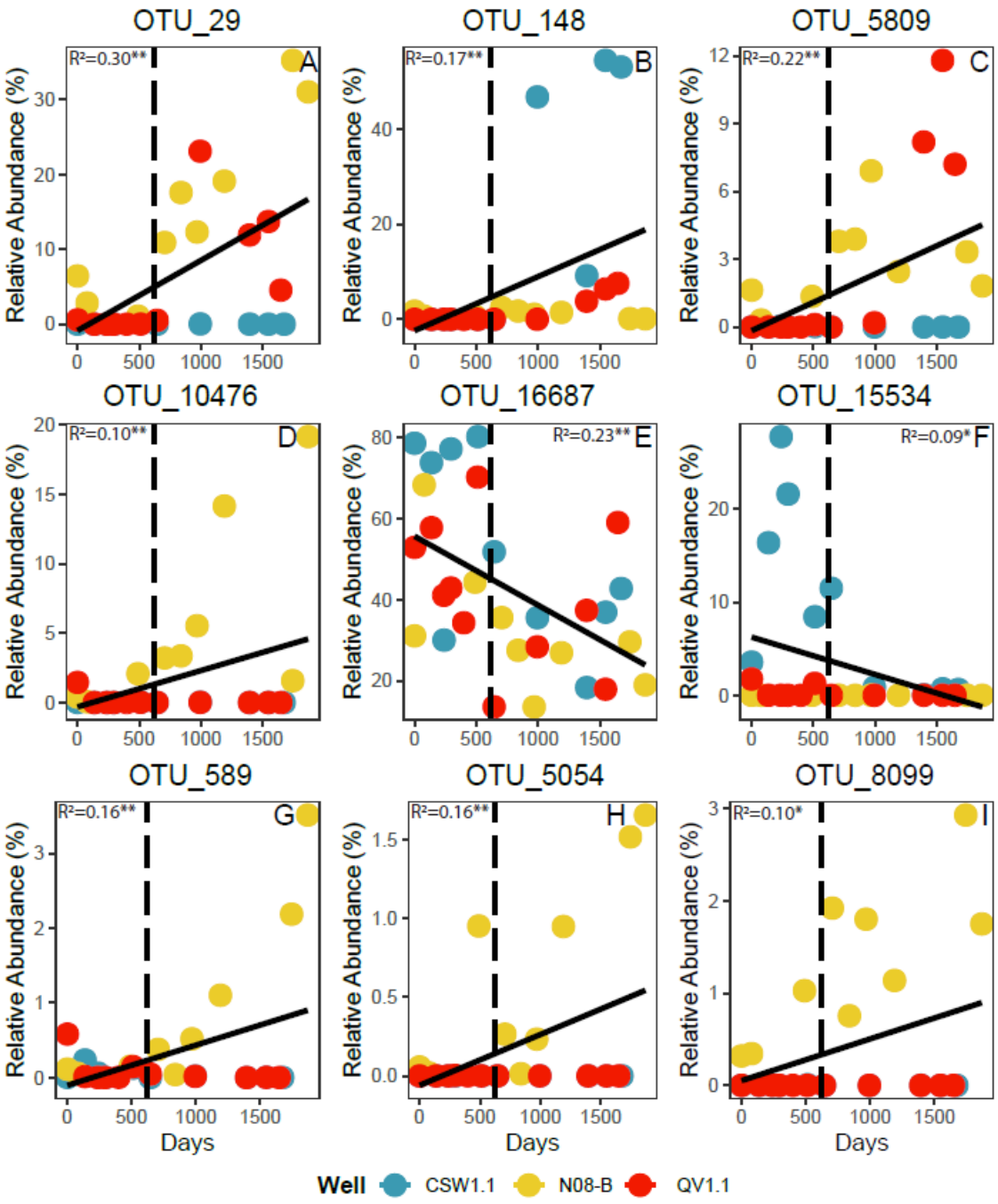

Figure 3.5. Dominant and Conditionally Rare OTU Abundance Over Time.

Plots displaying the relative abundance of dominant taxa OTU_29 (A), OTU_148 (B), OTU_5809 (C), OTU_10476 (D), and OTU_16687 (E) over time, and conditionally rare taxa OTU_15534 (F), OTU_589 (G), OTU_5054 (H), and OTU_8099 (I) over time. Points are representative of individual microbial community samples and are colored by well. Black linear regression lines are shown on the plot with linear regression model R^2 coefficients printed at the top of plots. ** $p < 0.05$ model significance, * < 0.1 model significance. Species classifications for each OTU are listed in Table B.4.

Desulfofundulus kuznetsovii, and *Noviherbaspirillum massiliense* were identified solely as CRT within the dataset. Populations of *Methylomonas lenta, Phenylobacterium falsum, Desulfofundulus kuznetsovii*, and *Noviherbaspirillum massiliense* were primarily observed within N08-B (**Fig. 3.5 D, G-I**).

OTUs significantly correlated with time in the dataset were further characterized by determining their relationship with measured probe geochemical data (**Table B.4; Fig. 3.6 A-N**) and aqueous geochemistry measure (**Table B.4; Fig. 3.7 A-K**). Results from these analyses revealed that all OTUs were significantly correlated with pH (**Fig. 3.6 A-I**). OTUs identified as *Lentimicrobium saccharophilum* (OTU_29), a close relative of *Gracilibacter thermotolerans* (OTU_5809), *Methylomonas lenta* (OTU_10476), *Phenylobacterium falsum* (OTU_589), a close relative of *Desulfofundulus kuznetsovii* (OTU_5054), and a close relative of *Noviherbaspirillum massiliense* (OTU_8099) all decreased in abundance with increasing pH (**Fig. 3.6 A, C, D, G-I**). N08-B generally has the lowest pH of the three wells assessed here (**Fig. B.1 B**), which fits well with the observation that these taxa were most abundant within samples collected from N08-B (**Fig. 3.6 A, C, D, G-I**). OTUs identified as *Serpentinomonas* strain B1 (OTU_16687) and *Dethiobacter alkaliphilus* (OTU_15534), and a close relative of *Truepera radiovictrix* (OTU_148) all increased in abundance with increasing pH (**Fig. 3.6 B, E & F**) and are most abundant within QV1.1 and CSW1.1 which have higher pH (**Fig. B.1 B**). The OTU identified as *Noviherbaspirillum massiliense* (OTU_8099) increased in abundance as redox conditions became more oxidizing (**Fig. 3.6 L**), while OTUs identified as *Dethiobacter alkaliphilus* (OTU_15534), and *Truepera radiovictrix* (OTU_148) increased in abundance as redox conditions became more reducing (**Fig. 3.6 J & K**). *Serpentinomonas* strain B1 (OTU_16687) decreased in abundance with increasing temperature (**Fig. 3.6 M**) and *Dethiobacter alkaliphilus* (OTU_15534) increased in

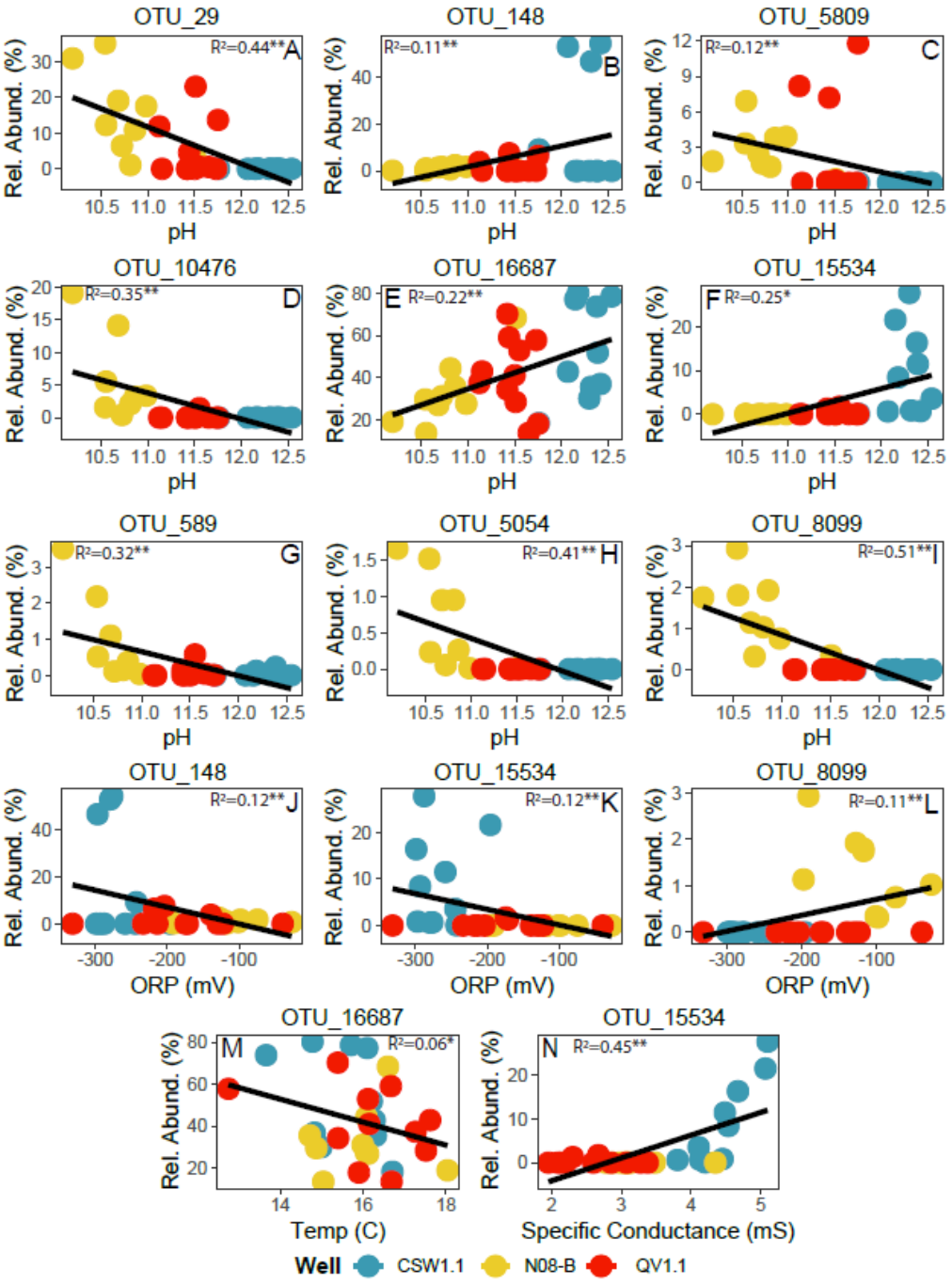

Figure 3.6. Dominant and Conditionally Rare OTU Abundance Plotted Against Probe Chemistry.

Plots displaying the relative abundance of dominant and conditionally rare taxa plotted against pH (A-I), ORP (J-L), temperature (M), and specific conductance (N). Points are representative of individual microbial community samples and are colored by well. Black linear regression lines are shown on the plot with linear regression model R^2 coefficients printed at the top of plots. ** $p < 0.05$ model significance, * < 0.1 model significance. Species classifications for each OTU are listed in Table B.4.

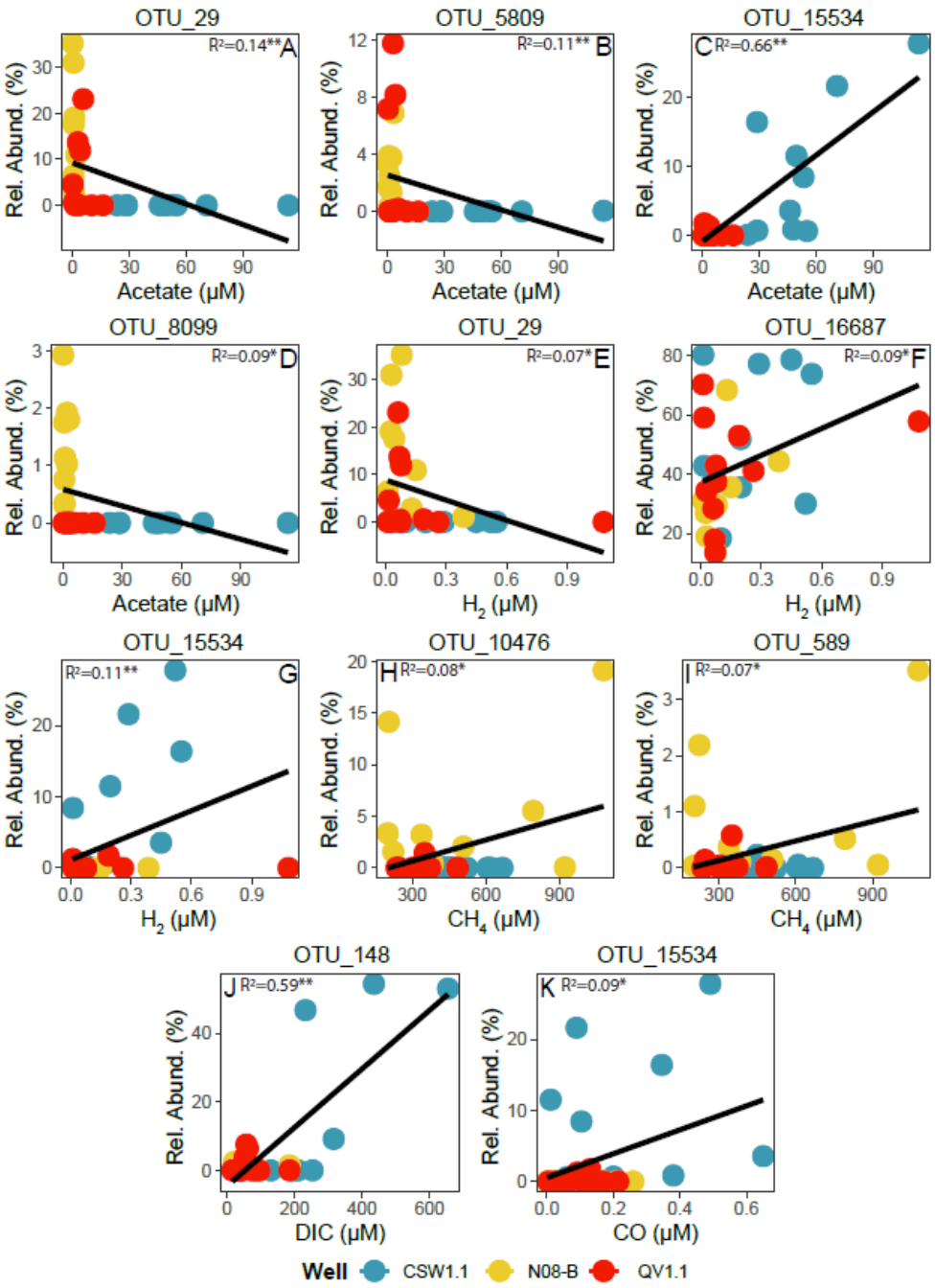

Figure 3.7. Dominant and Conditionally Rare OTU Abundance Plotted Against Aqueous Geochemistry.

Plots displaying the relative abundance of dominant and conditionally rare taxa plotted against acetate (A-D), H_2 (E-G), CH_4 (H-I), DIC (J), and CO (K). Points are representative of individual microbial community samples and are colored by well. Black linear regression lines are shown on the plot with linear regression model R^2 coefficients printed at the top of plots. ** $p < 0.05$ model significance, * < 0.1 model significance. Species classifications for each OTU are listed in Table B.4.

abundance with increasing specific conductance, or salinity (**Fig. 3.6 N**). *Dethiobacter alkaliphilus* (OTU_15534) was also found to increase in relative abundance with increasing concentrations of acetate, H_2, and CO (**Fig. 3.7 C, G & K**). The abundance of *Lentimicrobium saccharophilum* (OTU_29) was negatively correlated with acetate and H_2 concentrations (**Fig. 3.7 A & E**). The abundance of *Gracilibacter thermotolerans* (OTU_5809) and *Noviherbaspirillum massiliense* (OTU_8099) decreased with increasing acetate concentrations (**Fig. 3.7 B & D**). The abundance of *Serpentinomonas* strain B1 (OTU_16687) increased with increasing H_2 concentrations (**Fig. 3.7 F**). *Methylomonas lenta* (OTU_10476) and *Phenylobacterium falsum* (OTU_589) were positively correlated with increasing CH_4 concentrations (**Fig. 3.7 H & I**). The abundance of *Truepera radiovictrix* (OTU_148) was correlated with increasing concentrations of DIC (**Fig. 3.7 J**).

Discussion

Results from this work revealed that the injection of sterile water as a drilling fluid into the subsurface resulted in more oxidizing conditions and spikes in the concentration of DO, H_2, and acetate. Given the geologic setting and known microbial community composition at the site, the source of increased H_2 concentrations is unclear. H_2 could have been generated through water-rock reactions during drilling (23,24,54,55) or due to enhanced microbial activity of fermentative organisms capable of producing H_2 as a fermentation product (26,33). Similarly, increased concentrations of acetate could be the result of Fischer Tropsch type reactions catalyzed by serpentinization derived iron nickel minerals and alloys between hydrogen and inorganic carbon species resulting in the production of small organic carbon molecules, including acetate (24,56,57). Alternatively, microbial populations capable of acetogenesis through fermentation or the Wood-Ljungdahl pathway are prevalent at many terrestrial sites of serpentinization (32,58).

Microbial populations from the genera *Serpentinomonas* and *Dethiobacter* were observed at high relative abundances immediately after drilling (**Fig. 3.5 E & F**) and gradually decreasing in abundance over time. Organisms from the candidate genus *Serpentinomonas* (41) have been identified as dominant microbial community members previously at CROMO (28,31,33,51) and other terrestrial sites of serpentinization around the world including the Tablelands Ophiolite, Newfoundland, Canada (27,41), the Voltri Massif, Italy (34), the Samail Ophiolite, Sultanate of Oman (36,59), the Cabeço de Vide intrusive ultramafic massif (41,60), and the nearby Cedars ultramafic massif from which the organism was isolated (41). Characterization of *Serpentinomonas* isolates using culture-dependent and metagenomic sequencing has revealed that *Serpentinomonas* is a facultative anaerobe capable of autotrophic and mixotrophic growth using H_2, CO, oxygen, carbonate DIC species, and a variety of fatty acids including acetate (28,41). Metagenome assembled genomes (MAGs) of CROMO populations of *Serpentinomonas* reveal organisms with the same capabilities (28). Close relatives of *Dethiobacter alkaliphilus* are also common at CROMO and have previously been implicated as important in the transformation of intermediate sulfur compounds in the biogeochemical cycling of sulfur at the site (31). *Dethiobacter alkaliphilus* is a strict anaerobe capable of fixing carbon using the Wood-Ljungdahl pathway of acetogenesis and using H_2 and CO as electron donors (61). MAGs of CROMO populations related to *Dethiobacter alkaliphilus* have the same capabilities and also possess superoxide dismutase genes (SOD), which manage oxidative stress, and a portion of the genes required to build oxidative respiration enzymes (28), likely allowing them to persist in the presence of increased oxygen concentrations. CROMO populations of *Serpentinomonas* and *Dethiobacter* were significantly correlated with increasing concentrations of H_2 measured at the site (**Fig. 3.7 F & G**). Additionally, *Dethiobacter* populations were significantly correlated with increasing

concentrations of both acetate and CO (**Fig. 3.7 C & K**). These observations are in line with increased observed concentrations of H_2, CO, and acetate in the initial two years after drilling (**Fig. 3.1 C & D, Fig. B.1 D**), indicating that *Serpentinomonas* and *Dethiobacter* populations likely took advantage of increased concentrations of electron donors H_2 and CO to flourish and grow to greater abundances. Given the capability of CROMO *Dethiobacter* populations to perform acetogenesis via the Wood-Ljungdahl pathway, these populations may have utilized available H_2 and CO to perform acetogenesis (28), resulting in increased concentrations of acetate measured at the site.

Results from analyses also revealed that OTUs identified as *Lentimicrobium saccharophilum, Truepera radiovictrix, Gracilibacter thermotolerans, Methylomonas lenta, Phenylobacterium falsum, Desulfofundulus kuznetsovii*, and *Noviherbaspirillum massiliense* increased in relative abundance significantly over time, indicating that these organisms did not fare well under geochemical conditions observed initially after drilling and were better suited to conditions in more recent years. This hypothesis fits with current knowledge of *Lentimicrobium saccharophilum, Gracilibacter thermotolerans,* and *Desulfofundulus kuznetsovii*. These organisms are all obligate anaerobes (62–64) and *Lentimicrobium saccharophilum* and *Gracilibacter thermotolerans* are fermentative organisms capable of producing acetate and H_2 (62,64). Given the more oxidizing conditions present in the subsurface in the initial two years after drilling these organisms were likely inactive and may have employed sporulation or other dormancy responses to persist in the environment until fluids became more reducing and conditions were favorable again (13,65,66). Metagenomic and metatranscriptomic assessments of CROMO microbial community physiological adaptations to extreme conditions in the subsurface revealed a great abundance of sporulation genes in metagenomes with relatively low active transcription (**Table A.4**), indicating that active microbial populations can employ this survival

strategy when necessary to persist in this extreme environment (30). Interestingly, isolates of the organisms *Truepera radiovictrix*, *Methylomonas lenta*, *Phenylobacterium falsum*, and *Noviherbaspirillum massiliense* are all aerobic organisms capable of heterotrophic metabolisms (67–70). Given the known preferences of these organisms, it would seem more likely that they would have thrived when oxygen and acetate concentrations were higher the initial two years after drilling, as opposed to afterwards when conditions were more reducing with less abundant acetate. One potential explanation is that these organisms may have needed to compete for available increased concentrations of oxygen and acetate. *Serpentinomonas* is capable of both aerobic respiration and mixotrophic growth using acetate (28,41). Large populations of *Serpentinomonas* in samples from the initial two years after drilling could may have been able to outcompete these populations for available oxygen and acetate, limiting their growth.

An additional factor assessed in this work was the role of CRT in the microbial community response to environmental stress. Serpentinite microbial communities are low biomass, low diversity communities, composed of a few extremely well-adapted dominant community members (28,31,33,37,40,71). Under normal conditions we can expect that normally dominant taxa would maintain abundant populations and are not likely susceptible to being displaced by rare or newly immigrated microorganisms that enter the local environment, especially considering the strong selective force imposed by pH in this system (30). Following a disturbance to the system, and changes in the resource landscape of an environment, turnover in community structure and function (46,72) and the rapid growth of rare or previously dormant taxa have been observed (13,53,65,66). Based on prior observations, we wanted to assess if CRT played an important role in the microbial community response to injected drilling fluid. In general, CRT did not contribute greatly to the microbial community response to drilling fluid. In fact, all identified CRT increased

in relative abundance when collected samples and geochemistry were considered 'recovering' (**Fig. 3.5 C-D, G-I**), except for one CRT OTU identified as *Dethiobacter alkaliphilus*, which increased in relative abundance when samples were considered 'perturbed' (**Fig. 3.5 F**). One potential explanation for the identification of CRT in 'recovering' samples collected from 2013 to 2016 could be that instead of flourishing in response to environmental stress, these CRT instead utilized dormancy strategies to handle changes in environmental conditions and later 'bloomed' to high abundances when favorable conditions returned in the subsurface (13,65,66). Although the CRT did not respond by 'blooming' during environmental stress, the effective differences in their relative abundances were still detected and determined to be significant using the method developed by Shade and colleagues (53). The apparent response of the CRT OTU identified as *Dethiobacter alkaliphilus* to geochemical changes following drilling was also curious. Organisms from the genus *Dethiobacter* are commonly detected at CROMO and are abundant community members in the deeper more saline wells at CROMO (31). While microbial populations from the genus *Dethiobacter* are commonly abundant organisms at CROMO, this particular population seems to have responded dramatically to the changes in environmental conditions at CROMO during this time, especially within the CSW1.1 well (**Fig. 3.5 F**). Overall, results reveal that CRT did not play an important role in the microbial community response to the injection of drilling fluid. Instead, dominant community members from the genera *Serpentinomonas* and *Dethiobacter* were the primary populations that responded to changes in environmental conditions (**Fig. 3.5 E & F**).

Observations at CROMO are also consistent with recently published work assessing the role of dominant and rare microbial populations in microbial community responses to environmental change in soils (73–75). These studies revealed that dominant microbial

populations are equally as likely, if not more likely, to flourish in response to environmental disturbances, especially when these taxa are habitat generalists and metabolically versatile (74,75). Commonly observed organisms in serpentinization-influenced environments often have an impressive amount of metabolic versatility allowing them to persist in extreme and oligotrophic conditions (32,33,35,41). Both *Serpentinomonas* and *Dethiobacter alkaliphilus* have been shown to utilize autotrophic and heterotrophic growth in culture and can use a variety of electron donors and acceptors (41,61). The metabolic versatility of these organisms and capacity to withstand harsh environmental conditions make both organisms well-suited to flourish within the serpentinizing subsurface under a variety of conditions.

Overall, results from this study reveal that the injection of drilling fluid into a serpentinization-influenced aquifer resulted in more oxidizing conditions and spikes in the concentrations of DO, H_2, and acetate. Microbial populations from the genera *Serpentinomonas* and *Dethiobacter*, which are common and abundant microbial community members, flourished under these conditions appearing at high relative abundances in samples collected during the initial two years following drilling and gradually decreasing in relative abundance over time. CRT were identified in the dataset, but generally were not found to have flourished immediately after drilling. Instead, the CRT method that calculates a coefficient of bimodality based on abundance data (53) may have identified dormancy dynamics in taxa poorly suited to the more oxidizing conditions. In this scenario the OTUs identified as CRT were poorly detected while employing dormancy strategies from 2011 to 2013 and were observed to increase in abundance in samples from 2013 to 2016 when conditions became more favorable. These results corroborate recent findings in soils that show that dominant microbial community members that are metabolically diverse can be primary responders to environmental disturbance, contributing to the overall capacity of microbial

communities to be resistant or resilient (73–75). These results contrast with a variety of other studies showing that members from the rare biosphere often respond to disturbances and play large roles in overall microbial community stability (46,52,53,76,77). The results shown here have important implications for future investigations in the serpentinizing subsurface revealing that serpentine microbial communities are sensitive to environmental disturbances, but that dominant and metabolically versatile microbial community members are most likely to respond to changes in environmental conditions, as opposed to unknown opportunistic members of the rare biosphere. If this observation holds true at other sites of serpentinization, careful characterization of the functional capacities of dominant microbial communities using culture dependent and independent methods should allow for effective modeling and anticipation of changes in microbial community composition and structure when these systems are subjected to a variety environmental changes, including applications such as carbon capture and sequestration (11,47–49).

Materials and Methods

Site Description and Sample Collection

CROMO lies within McLaughlin Natural Reserve near Lower Lake, CA, USA. CROMO consists of 8 wells that were drilled into serpentinite mélange of the Coast Range Ophiolite in August of 2011 using sterile water as drilling fluid during drilling (42). Geochemical and molecular biology samples were collected from two wells drilled in August of 2011, CSW1.1 and QV1.1, and one reference well drilled > 30 years ago, N08-B 1-3 times per year from 2011 to 2016 to characterize the geochemistry and native microbial communities of serpentinizing subsurface at the site (30,31,33,51). CROMO is a low permeability confined aquifer (30,78) that hosts microbial communities that are well adapted to high pH, strongly reducing fluids (30,33). Fluid

sampling procedures have been previously described (33,51), and are briefly described again below.

Fluid samples to measure dissolved H_2 and CH_4 were collected anoxically in a 60 mL syringe attached via a luer-lock stopcock attached to pump tubing. 10 mL of instrument grade nitrogen is then injected into the syringe and the syringe is vigorously shaken for one minute to allow dissolved gases to partition into the nitrogen gas (33,51). The nitrogen gas is then extracted and injected into an exetainer containing 20% v/v sodium chloride solution, displacing a portion of the solution (38). Exetainers are stored upside down at room temperature to minimize the loss of gas via diffusion prior to analysis (38). Samples to measure DIC and acetate in well fluids were collected anoxically by a syringe connected directly to well tubing (30,33,51). DIC samples were filtered through a 0.2 µm syringe filter into acid washed, nitrogen filled serum vials dosed with phosphoric acid as previously described (30,51). Acetate samples were filtered through a 0.2 µm syringe filter into acid washed and ashed I-Chem™ vials as previously described (51). Acidified DIC samples were stored upside down at room temperature prior to analysis and acetate samples were frozen and stored in the dark prior to analysis. Molecular microbiology samples for the extraction of DNA were filtered through 0.22 µm Sterivex© filters (Merck Millipore, Billerica, MA, USA) using a Masterflex E/S portable pump (Masterflex, Gelsenkirchen, Germany) and compatible sterile tubing and adaptors. Filters were flash frozen in liquid nitrogen in the field and stored at -80°C upon return to the lab (30,31,33).

Geochemical Analyses

Analysis of dissolved H_2, CO, and CH_4 were performed using gas chromatography (GC) with a reduced gas detector (H_2 and CO) and a flame ionizing detector (FID) as previously

described (51). DIC samples, acidified to liberate CO_2, were analyzed using GC-FID with a methanizer to convert CO_2 to CH_4 prior to arrival at the FID, as previously described (30,51). Acetate samples were analyzed using high performance liquid chromatography as previously described (51).

Extraction of DNA

DNA extractions from 0.22 µm Sterivex© filters were performed as previously described (30,31,33).

16S rRNA Gene Amplicon Sequencing

Amplification, quantification, and sequencing of the V4 region of the 16S rRNA gene for CROMO samples used in this work at the Department of Energy Joint Genome Institute (JGI), Marine Biological Laboratory's (MBL) Josephine Bay Paul Center, and Michigan State University (MSU) Genomics Core have been previously described by Twing and colleagues (33), Crespo-Medina and colleagues (51), and Sabuda and colleagues (31), respectively (**Table A.9**).

16S rRNA Sequence Processing

Sequences generated by MBL, JGI, and the MSU Genomics Core were analyzed, merged, and clustered into OTUs at a 3% distance threshold as previously described (30). Clustered OTUs were aligned to the SILVA SSURef alignment (v138) and taxonomic classifications were assigned using mothur v1.39.5 (79).

After merging the 16S rRNA datasets (19,155 OTUs and 10,847,024 reads) count data from sample replicates were averaged and rounded to the nearest whole number as previously

described (30). OTUs with an abundance of zero (8,215 OTUs) after averaging (the result of singletons within a set of replicates) were removed along with sequences classified as archaea (34 OTUs and 7,213 reads), eukaryotes (22 OTUs and 1,439 reads), unknown (318 OTUs and 5,244 reads), chloroplasts (44 OTUs and 3,953 reads), and mitochondria (36 OTUs and 710 reads) by SILVA. After this initial filtering, sequences were screened for common human-associated and DNA extraction contaminants identified in deep subsurface samples by Sheik and colleagues (80), as previously described (28,30,81). This analysis resulted in the removal of 724 OTUs (213,587 reads) that were likely contaminants in the dataset. The removed potential contaminant OTUs accounted for 1.97% of total reads in the original dataset and 3.78% of OTUs present in the original dataset. There were no patterns in sample contamination with any of the contaminant OTUs. The final dataset used in analyses consisted of 3,078 OTUs and 1,651,065 reads. Samples from an associated dataset (8,963,813 reads of the 10,614,878 reads) were processed alongside these samples and were not retained for analyses described here. Once dataset filtering was complete, species taxonomic classifications were performed on the final fasta file using MegaBLAST (82), and species classification was assigned based on the closest known relative that could be identified for each sequence.

R scripts used to average and contaminant filter 16S rRNA sequence data along with raw, averaged, and contaminant filtered count, taxonomy, and fasta files are available on FigShare (https://figshare.com/projects/Drilling_Disturbance_in_a_Serpentinizing_Ophiolite/113898).

Statistical Analyses

Basic data exploration and statistical analyses performed on microbial community data and associated metadata were performed in R (83) using the R packages phyloseq (84) and vegan (85).

Geochemistry plots were made using the package ggplot2 (86). Student's T-test values were calculated using the basic R package stats (83) and linear models were calculated using the R package base (83). Species richness and Pielou's evenness were calculated as described by Putman and colleagues (30). PERMANOVA analysis, NMDS ordination of Bray-Curtis dissimilarities, and plotting of variables identified in PERMANOVA analyses on an NMDS plot were performed as previously described (30). Bar plots displaying the normalized abundance of OTUs by taxonomic classification were plotted using the plot_bar() function in phyloseq (84). CRT were identified as previously described, using the R Script provided by Shade and colleagues (53).

Data files and R scripts used for analyses are available on FigShare (https://figshare.com/projects/Drilling_Disturbance_in_a_Serpentinizing_Ophiolite/113898).

Sequence Data Availability

The 16S rRNA gene amplicon data used in this work were previously published by Putman and colleagues (30) under the Bioproject accession number: PRJNA690585.

Acknowledgements

We thank Cathy Koehler and Paul Aigner, Co-directors of the University of California - Davis McLaughlin Reserve for their support and help in establishing CROMO and continued field work at the site. Special thanks to Katrina Twing and Melitza Crespo-Medina for their work in the field and lab during the first few years of this project. This work was supported by the NASA Astrobiology Institute CAN-7 Rock Powered Life Grant #NNA15BB02A.

APPENDIX

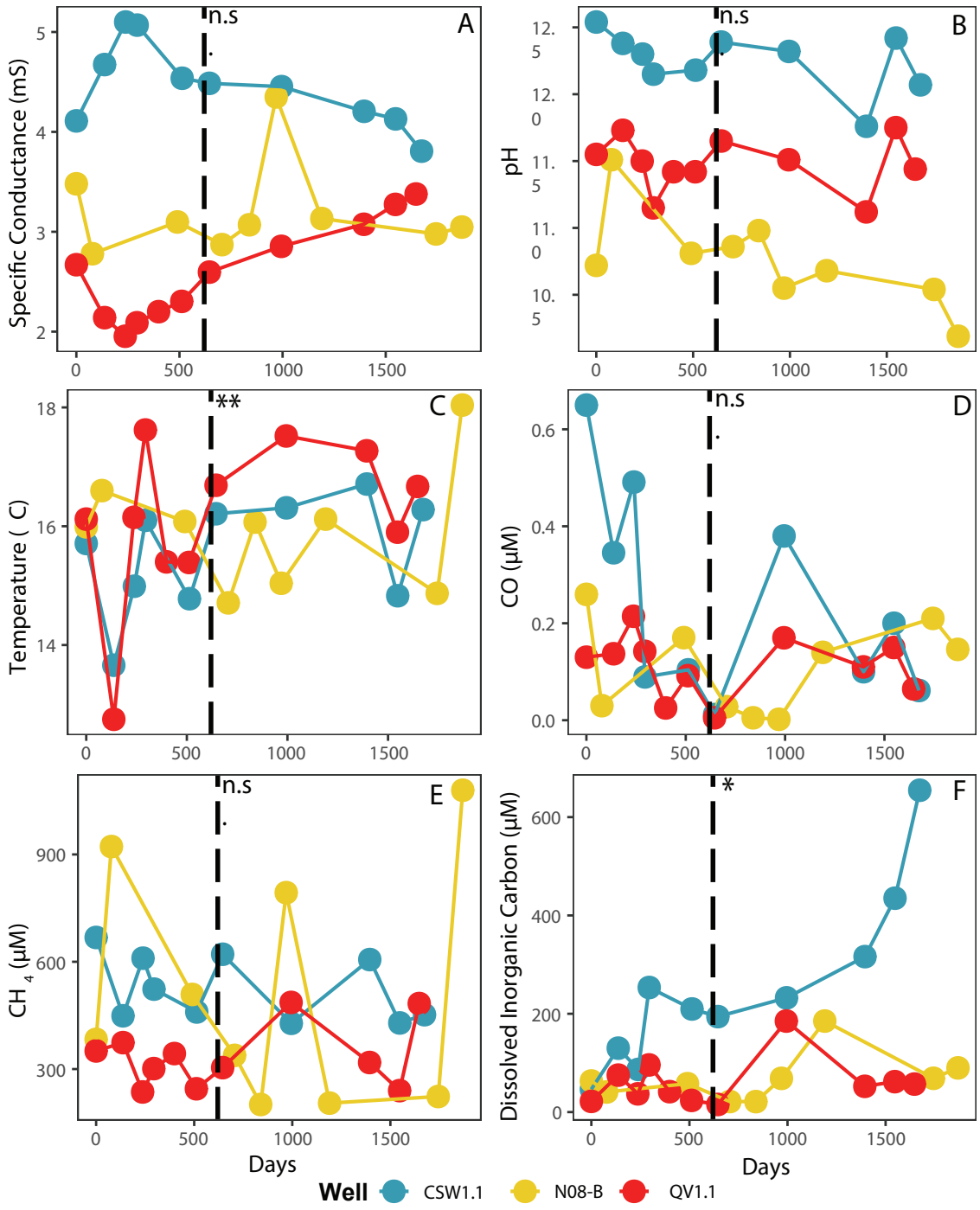

Figure B.1. Additional Geochemistry Time Series Plots.

Plots of specific conductance (A), pH (B), temperature (C), CO (D), CH4 (E), and DIC (F) plotted over time. Points and connecting lines are colored by well location. The vertical dashed line is placed between the March 2013 and August 2013 samples, when observed geochemistry starts to become more stable. ** $p < 0.05$ significance, * $p < 0.1$, n.s. not significant represent results from Student's T-Tests.

Table B.1. Metadata.

Well	Date Sampled*	Drilled Depth (m)*	Temperature (°C)*	pH*	Specific Conductance (mS)*	Dissolved Oxygen (mg/L)*	ORP (mV)*	DIC (μM)*	Acetate (μM)	H_2 (μM)	CO (μM)	CH_4 (μM)
CSW1.1	11/1/2011	19.50	15.71[a]	12.54	4.11[a]	0.64	-244.44[a]	46.40	45.99	0.45[a]	0.65[a]	667.92[a]
CSW1.1	3/16/2012	19.50	13.66	12.38	4.67	0.03	-298.90	130.03	28.58	0.55	0.35	448.90
CSW1.1	6/26/2012	19.50	14.99	12.30	5.10	0.32	-287.90	86.76	113.89	0.52	0.49	610.00
CSW1.1	8/21/2012	19.50	16.10	12.15	5.07	0.00	-195.80	253.42	70.79	0.29	0.09	523.50
CSW1.1	3/27/2013	19.50	14.78	12.18	4.54	0.28	-293.60	209.74	53.11	0.01	0.10	459.60
CSW1.1	8/6/2013	19.50	16.21	12.39	4.49	0.18	-258.40	194.19	49.35	0.20	0.01	621.00
CSW1.1	7/22/2014	19.50	16.31	12.32	4.45	0.43	-297.00	232.38	47.63[a]	0.2[a]	0.38[a]	427.94[a]
CSW1.1	8/26/2015	19.50	16.71	11.76	4.21	0.17	-243.10	316.23	23.60[a]	0.10[a]	0.10[a]	606.10[a]
CSW1.1	1/26/2016	19.50	14.83	12.42	4.13	0.19	-276.50	435.10	28.71a	0.06[a]	0.2[a]	428.87[a]
CSW1.1	5/31/2016	19.50	16.28	12.07	3.81	0.16	-279.50	654.65	54.94[a]	0.02	0.06	452.00
N08B	4/21/2011	26.20	15.99[a]	10.72[a]	3.48[a]	0.56[a]	-98.31[a]	63.25	0.62	0.01	0.26	383.00
N08B	7/7/2011	26.20	16.60	11.51	2.78[a]	0.36[a]	-101.39[a]	40.90	0.75[b]	0.13[a]	0.03[a]	922.00
N08B	8/22/2012	26.20	16.08	10.81	3.10	0.34	-27.10	57.78	2.01[b]	0.39	0.17	508.60
N08B	3/26/2013	26.20	14.71	10.86	2.87	0.31	-127.70	21.48	1.99[b]	0.15	0.03	338.30
N08B	8/6/2013	26.20	16.07	10.98	3.07	0.32	-74.60	21.33	0.67	0.04	0.005[b]	201.00
N08B	12/14/2013	26.20	15.04	10.55	4.35	0.10	-117.90	68.61[b]	3.08[b]	0.07	0.00	793.18
N08B	7/24/2014	26.20	16.12	10.68	3.13	0.76	-197.60	185.16[b]	0.98[a]	0.02	0.14[a]	204.79[a]
N08B	1/29/2016	26.20	14.87	10.54	2.98	0.21	-191.10	68.73	0.10[a]	0.08[a]	0.21[a]	223.23[a]
N08B	6/1/2016	26.20	18.04	10.19	3.05	0.15	-117.50	89.90	0.57[a]	0.03	0.15	1079.49

Table B.1. (cont'd).

Well	Date Sampled*	Drilled Depth (m)*	Temperature (°C)*	pH*	Specific Conductance (mS)*	Dissolved Oxygen (mg/L)*	ORP (mV)*	DIC (μM)*	Acetate (μM)	H_2 (μM)	CO (μM)	CH_4 (μM)
QV1.1	11/2/2011	23.00	16.12[a]	11.55	2.67[a]	0.67	-174.51[a]	21.80	0.75[b]	0.19[a]	0.13[a]	350.65[a]
QV1.1	3/18/2012	23.00	12.75	11.73	2.14	0.12	-213.80	75.19	3.12[b]	1.08	0.14	373.90
QV1.1	6/25/2012	23.00	16.15	11.50	1.95	0.12	-331.80	37.11	1.35[b]	0.26	0.21	236.00
QV1.1	8/21/2012	23.00	17.62	11.15	2.09	0.12	-39.60	95.93	10.2	0.08	0.14	301.30
QV1.1	12/4/2012	23.00	15.40	11.42	2.20	1.40	-130.00	41.57	16.05	0.03	0.03	343.30
QV1.1	3/26/2013	23.00	15.39	11.42	2.30	0.54	-171.50	23.81	3.36	0.01	0.09	244.90
QV1.1	8/7/2013	23.00	16.69	11.65	2.60	0.05	-122.70	15.50	0.96	0.07	0.005[b]	304.00
QV1.1	7/22/2014	23.00	17.52	11.51	2.85	0.28	-233.50	185.16[b]	5.66[a]	0.06[a]	0.17[a]	486.29[a]
QV1.1	8/26/2015	23.00	17.27	11.12	3.08	0.33	-139.40	52.39[b]	4.08[a]	0.08[a]	0.11[a]	318.34[a]
QV1.1	1/26/2016	23.00	15.90	11.75	3.27	0.18	-218.30	61.92[b]	2.82[a]	0.07[a]	0.15[a]	239.73[a]
QV1.1	6/1/2016	23.00	16.67	11.44	3.38	0.15	-203.90	57.01[b]	0.22[a]	0.02	0.06	483.11

*= data previously reported by Putman and colleagues (2021).

[a] = data was not collected. Value was permuted based on mean and s.d. of existing data

[b] = Sample below detection limit. Value represents detection limit.

Table B.2. Student's T-test Results on Bulk Geochemistry and Alpha Diversity Measures.

Condition	Metadata Metric	Mean	T-test p-value
Perturbed	Temperature (°C)	15.47	
Recovering	Temperature (°C)	16.30	**0.04198**
Perturbed	pH	11.61	
Recovering	pH	11.42	0.4375
Perturbed	Specific Conductance (mS)	3.27	
Recovering	Specific Conductance (mS)	3.52	0.4665
Perturbed	Dissolved Oxygen (mg/L)	0.39	
Recovering	Dissolved Oxygen (mg/L)	0.24	0.1723
Perturbed	Oxidation Reduction Potential (mV)	-182.42	
Recovering	Oxidation Reduction Potential (mV)	-198.07	0.6128
Perturbed	Dissolved H2 (uM)	0.28	
Recovering	Dissolved H2 (uM)	0.07	**0.01851**
Perturbed	Dissolved CO (uM)	0.19	
Recovering	Dissolved CO (uM)	0.12	0.1618
Perturbed	Dissolved CH4 (uM)	447.46	
Recovering	Dissolved CH4 (uM)	457.94	0.8945
Perturbed	Dissolved Inorganic Carbon (uM)	80.34	
Recovering	Dissolved Inorganic Carbon (uM)	175.88	**0.06794**
Perturbed	Acetate (uM)	23.50	
Recovering	Acetate (uM)	14.89	0.4054
Perturbed	Species Richness	265.73	
Recovering	Species Richness	255.53	0.8883
Perturbed	Pielou's Evenness	0.32	
Recovering	Pielou's Evenness	0.39	0.1682

Table B.3. Microbial Community PERMANOVA Results.

PERMANOVA Results						
Variable	**Degrees of Freedom**	**Sum of Squares**	**Mean Squares**	**F Score**	**R^2**	**p-value**
Well	2	1.7513	0.87565	7.9772	0.34	**0.001**
Binomial Perturbation	1	0.6913	0.69132	6.298	0.14	**0.001**
Days	1	0.0315	0.03148	0.2868	0.01	0.969
Temperature (°C)	1	0.0188	0.01878	0.1711	0	0.994
pH	1	0.0872	0.08715	0.7939	0.02	0.571
Conductance (mS)	1	0.3451	0.34506	3.1435	0.07	**0.008**
DO (mg/L)	1	0.0708	0.07079	0.6449	0.01	0.736
ORP (mV)	1	0.1276	0.12758	1.1622	0.02	0.319
H_2 (µM)	1	0.0442	0.04421	0.4028	0.01	0.912
CO (µM)	1	0.0298	0.02977	0.2712	0.01	0.963
CH_4 (µM)	1	0.094	0.09403	0.8566	0.02	0.559
DIC (µM)	1	0.0871	0.08709	0.7934	0.02	0.588
Acetate (µM)	1	0.0854	0.0854	0.778	0.02	0.601
Residuals	15	1.6465	0.10977		0.32	
Total	29	5.1105			1	

Table B.4. Significant Regression Models on Dominant and CRT OTUs.

Environmental Variable	Organism	Linear Regression R^2	p-value
Time	OTU_29 - Lentimicrobium saccharophilum (86.3%)	0.30	1.05E-03
	OTU_148 - Truepera radiovictrix (91.3%)	0.17	1.46E-02
	OTU_5809 - Gracilibacter thermotolerans (92.5%)	0.22	5.16E-03
	OTU_10476 - Methylomonas lenta (98%)	0.10	4.73E-02
	OTU_16687 - Serpentinomonas B1 (100%)	0.23	4.25E-03
	OTU_15534 - Dethiobacter alkaliphilus (92.2%)	0.09	6.28E-02
	OTU_589 - Phenylobacterium falsum (100%)	0.16	1.72E-02
	OTU_5054 - Desulfofundulus kuznetsovii (91%)	0.16	1.74E-02
	OTU_8099 - Noviherbaspirillum massiliense (94.1%)	0.10	5.31E-02
pH	OTU_29 - Lentimicrobium saccharophilum (86.3%)	0.44	3.74E-05
	OTU_148 - Truepera radiovictrix (91.3%)	0.11	4.18E-02
	OTU_5809 - Gracilibacter thermotolerans (92.5%)	0.12	3.39E-02
	OTU_10476 - Methylomonas lenta (98%)	0.35	3.76E-04
	OTU_16687 - Serpentinomonas B1 (100%)	0.22	5.27E-03
	OTU_15534 - Dethiobacter alkaliphilus (92.2%)	0.25	2.88E-03
	OTU_589 - Phenylobacterium falsum (100%)	0.32	6.93E-04
	OTU_5054 - Desulfofundulus kuznetsovii (91%)	0.41	8.90E-05
	OTU_8099 - Noviherbaspirillum massiliense (94.1%)	0.51	5.50E-06
Acetate (µM)	OTU_29 - Lentimicrobium saccharophilum (86.3%)	0.14	2.23E-02
	OTU_5809 - Gracilibacter thermotolerans (92.5%)	0.11	4.37E-02
	OTU_15534 - Dethiobacter alkaliphilus (92.2%)	0.66	2.92E-08
	OTU_8099 - Noviherbaspirillum massiliense (94.1%)	0.09	5.76E-02
Dissolved Hydrogen (µM)	OTU_29 - Lentimicrobium saccharophilum (86.3%)	0.07	7.79E-02
	OTU_16687 - Serpentinomonas B1 (100%)	0.09	6.21E-02
	OTU_15534 - Dethiobacter alkaliphilus (92.2%)	0.11	3.97E-02
Oxidation Reduction Potential (mV)	OTU_148 - Truepera radiovictrix (91.3%)	0.12	3.62E-02
	OTU_15534 - Dethiobacter alkaliphilus (92.2%)	0.12	3.14E-02
	OTU_8099 - Noviherbaspirillum massiliense (94.1%)	0.11	4.29E-02
Dissolved Methane (µM)	OTU_10476 - Methylomonas lenta (98%)	0.08	7.28E-02
	OTU_589 - Phenylobacterium falsum (100%)	0.07	8.01E-02
Temperature (ºC)	OTU_16687 - Serpentinomonas B1 (100%)	0.06	9.98E-02
Dissolved CO (µM)	OTU_15534 - Dethiobacter alkaliphilus (92.2%)	0.09	5.44E-02
Specific Conductance (mS)	OTU_15534 - Dethiobacter alkaliphilus (92.2%)	0.45	3.12E-05
Dissolved Inorganic Carbon (µM)	OTU_148 - Truepera radiovictrix (91.3%)	0.59	4.06E-07

REFERENCES

REFERENCES

1. Lin C., Larsen E.I., Larsen G.R., Cox M.E., Smith J.J. Bacterially mediated iron cycling and associated biogeochemical processes in a subtropical shallow coastal aquifer: implications for groundwater quality. *Hydrobiologia*, (2012). doi:10.1007/s10750-012-1184-z.

2. Anantharaman K., Brown C.T., Hug L.A., Sharon I., Castelle C.J., Probst A.J., Thomas B.C., Singh A., Wilkins M.J., Karaoz U., Brodie E.L., Williams K.H., Hubbard S.S., Banfield J.F. Thousands of microbial genomes shed light on interconnected biogeochemical processes in an aquifer system. *Nature Communications*, 7 (2016). doi:10.1038/ncomms13219

3. Lau M.C.Y., Kieft T.L., Kuloyo O., Linage-Alvarez B., van Heerden E., Lindsay M.R., Magnabosco C., Wang W., Wiggins J.B., Guo L., Perlman D.H., Kyin S., Shwe H.H., Harris R.L., Oh Y., Yi M.J., Purtschert R., Slater G.F., Ono S., Wei S., Li L., Lollar B.S., Onstott T.C. An oligotrophic deep-subsurface community dependent on syntrophy is dominated by sulfur-driven autotrophic denitrifiers. *Proc Natl Acad Sci USA*, (2016). doi:10.1073/pnas.1612244113

4. Stegen J.C., Fredrickson J.K., Wilkins M.J., Konopka A.E., Nelson W.C., Arntzen E.V., Chrisler W.B., Chu R.K., Danczak R.E., Fansler S.J., Kennedy D.W., Resch C.T., Tfaily M. Groundwater–surface water mixing shifts ecological assembly processes and stimulates organic carbon turnover. *Nature Communications*, 7 (2016). doi:10.1038/ncomms11237

5. Hall E.K., Bernhardt E.S., Bier R.L., Bradford M.A., Boot C.M., Cotner J.B., del Giorgio P.A., Evans S.E., Graham E.B., Jones S.E., Lennon J.T., Locey K.J., Nemergut D., Osborne B.B., Rocca J.D., Schimel J.P., Waldrop M.P., Wallenstein M.D. Understanding how microbiomes influence the systems they inhabit. *Nature Microbiology*, 3(September):977–82 (2018). doi:10.1038/s41564-018-0201-z

6. Creamer C.A., de Menezes A.B., Krull E.S., Sanderman J., Newton-Walters R., Farrell M. Microbial community structure mediates response of soil C decomposition to litter addition and warming. *Soil Biology and Biochemistry*, 80:175–88 (2015). doi:10.1016/j.soilbio.2014.10.008

7. Bastida F., Torres I.F., Hernández T., García C. The impacts of organic amendments: Do they confer stability against drought on the soil microbial community? *Soil Biology and Biochemistry*, 113:173–83 (2017). doi:10.1016/j.soilbio.2017.06.012

8. Gravuer K., Eskelinen A. Nutrient and rainfall additions shift phylogenetically estimated traits of soil microbial communities. *Frontiers in Microbiology*, 8(JUL):1–16 (2017). doi:10.3389/fmicb.2017.01271

9. de Vries F.T., Shade A. Controls on soil microbial community stability under climate change. *Frontiers in Microbiology*, 4(September):1–16 (2013). doi:10.3389/fmicb.2013.00265

10. Lee S.-H., Sorensen J.W., Grady K.L., Tobin T.C., Shade A. Divergent extremes but convergent recovery of bacterial and archaeal soil communities to an ongoing subterranean coal mine fire. *The ISME Journal*, 11(6):1447–59 (2017). doi:10.1038/ismej.2017.1

11. Trias R., Ménez B., le Campion P., Zivanovic Y., Lecourt L., Lecoeuvre A., Schmitt-Kopplin P., Uhl J., Gislason S.R., Alfredsson H.A., Mesfin K.G., Snaebjörnsdóttir S.O., Aradóttir E.S., Gunnarsson I., Matter J.M., Stute M., Oelkers E.H., Gérard E. High reactivity of deep biota under anthropogenic CO_2 injection into basalt. *Nature Communications*, 8(1) (2017). doi:10.1038/s41467-017-01288-8

12. Evans S.E., Wallenstein M.D. Climate change alters ecological strategies of soil bacteria. *Ecology Letters*, 17:155–64 (2014). doi:10.1111/ele.12206

13. Sorensen J.W., Shade A. Dormancy dynamics and dispersal contribute to soil microbiome resilience. *Philosophical Transactions of the Royal Society B*, 375 (2020). doi:10.1098/rstb.2019.0255

14. Lall U., Josset L., Russo T. A Snapshot of the World's Groundwater Challenges. *Annu. Rev. Environ. Resour.*, 45:171–96 (2020). doi:10.1146/annurev-environ-102017-025800

15. Mu A., Moreau J.W. The geomicrobiology of CO_2 geosequestration: a focused review on prokaryotic community responses to field-scale CO_2 injection. *Frontiers in Microbiology*, 6(April):1–13 (2015). doi:10.3389/fmicb.2015.00263

16. Mu A., Boreham C., Leong H.X., Haese R.R., Moreau J.W. Changes in the deep subsurface microbial biosphere resulting from a field-scale CO_2 geosequestration experiment. *Frontiers in Microbiology*, 5(May):1–11 (2014). doi:10.3389/fmicb.2014.00209

17. O'Mullan G. Dueker M.E., Clauson K., Yang Q., Umemoto K., Zakharova N., Matter J., Stute, M., Takahashi T., Goldberg D. Microbial stimulation and succession following a test well injection simulating CO_2 leakage into a shallow Newark basin aquifer. *PLoS ONE*, 10(1):1–25 (2015). doi:10.1371/journal.pone.0117812

18. Zhang F., She Y-H., Chai L-J., Banat I.M., Zhang X-T., Shu F-C., Wang Z-L., Yu L-J., Hou D-J. Microbial diversity in long-term water-flooded oil reservoirs with different in situ temperatures in China. *Scientific Reports*, 2:1–10 (2012). doi:10.1038/srep00760

19. Piceno Y.M., Reid F.C., Tom L.M., Conrad M.E., Bill M., Hubbard C.G., Fouke B.W., Graff C.J., Han J., Stringfellow W.T., Hanlon J.S., Hu P., Hazen T.C., Andersen G.L. Temperature and injection water source influence microbial community structure in four Alaskan North Slope hydrocarbon reservoirs. *Frontiers in Microbiology*, 5(AUG):1–13 (2014). doi:10.3389/fmicb.2014.00409

20. Ren H., Xiong S., Gao G., Song Y., Cao G., Zhao L., Zhang X. Bacteria in the injection water differently impacts the bacterial communities of production wells in high-temperature petroleum reservoirs. *Frontiers in Microbiology*, 6(MAY) (2015). doi:10.3389/fmicb.2015.00505

21. Ginige M.P., Kaksonen A.H., Morris C., Shackelton M., Patterson B.M. Bacterial community and groundwater quality changes in an anaerobic aquifer during groundwater recharge with aerobic recycled water. *FEMS Microbiology Ecology*, 85(3):553–67 (2013). doi:10.1111/1574-6941.12137

22. Vaughan A.P.M., Scarrow J.H. Ophiolite obduction pulses as a proxy indicator of superplume events? *Earth and Planetary Science Letters*, 213 (2003). doi:10.1016/S0012-821X(03)00330-3

23. McCollom T.M., Bach W. Thermodynamic constraints on hydrogen generation during serpentinization of ultramafic rocks. *Geochimica et Cosmochimica Acta*, 73(3):856–75 (2009). doi: 10.1016/j.gca.2008.10.032

24. Preiner M., Xavier J.C., Sousa F.L., Zimorski V., Neubeck A., Lang S.Q., Greenwell H.C., Kleinermanns K., Tüysüz H., McCollom T.M., Holm N.G., Martin W.F. Serpentinization: Connecting Geochemistry, Ancient Metabolism and Industrial Hydrogenation. *Life*, 8(4) (2018). doi:10.3390/life8040041

25. Schrenk M.O., Brazelton W.J., Lang S.Q. Serpentinization, carbon, and deep life. *Reviews in Mineralogy and Geochemistry*, 75:575–606 (2013). doi:10.2138/rmg.2013.75.18

26. Brazelton W.J., Nelson B., Schrenk M.O. Metagenomic evidence for H_2 oxidation and H_2 production by serpentinite-hosted subsurface microbial communities. *Frontiers in Microbiology*, 2 (2012). doi:10.3389/fmicb.2011.00268

27. Brazelton W.J., Morrill P.L., Szponar N., Schrenk M.O. Bacterial communities associated with subsurface geochemical processes in continental serpentinite springs. *Applied and Environmental Microbiology*, 79(13):3906–16 (2013). doi:10.1128/AEM.00330-13

28. Sabuda M.C., Putman L.I., Hoehler T.M., Kubo M.D., Brazelton W.J., Schrenk M.O. Biogeochemical Gradients in a Serpentinization-Influenced Aquifer: Implications for Gas Exchange between the Subsurface and Atmosphere. *Journal of Geophysical Research: Biogeosciences*, 126, e2020JG006209 (2021). doi:10.1029/2020JG006209

29. Crespo-Medina M., Twing K.I., Sánchez-Murillo R., Brazelton W.J., McCollom T.M., Schrenk M.O. Methane dynamics in a tropical serpentinizing environment: The Santa Elena Ophiolite, Costa Rica. *Frontiers in Microbiology*, 8(MAY):1–14 (2017). doi:10.3389/fmicb.2017.00916

30. Putman L.I., Sabuda M.C., Brazelton W.J., Kubo M.D., Hoehler T.M., McCollom T.M., Cardace D., Schrenk M.O. Microbial communities in a serpentinizing aquifer are assembled through strong concurrent dispersal limitation and selection. *mSystems*, (2021). doi:10.1128/mSystems.00300-21

31. Sabuda M.C., Brazelton W.J., Putman L.I., McCollom T.M., Hoehler T.M., Kubo M.D.Y., Cardace D., Schrenk M.O. A dynamic microbial sulfur cycle in a serpentinizing continental ophiolite. *Environmental Microbiology*, 22:2329–45 (2020). doi:10.1111/1462-2920.15006

32. Seyler L.M., Brazelton W.J., McLean C., Putman L.I., Hyer A., Kubo M.D.Y., Hoehler T., Cardace D., Schrenk M.O. Carbon Assimilation Strategies in Ultrabasic Groundwater: Clues from the Integrated Study of a Serpentinization-Influenced Aquifer. *mSystems*, 5(2):1–17 (2020. doi:10.1128/mSystems.00607-19

33. Twing K.I., Brazelton W.J., Kubo M.D.Y., Hyer A.J., Cardace D., Hoehler T.M., McCollom T.M., Schrenk M.O. Serpentinization-Influenced Groundwater Harbors Extremely Low Diversity Microbial Communities Adapted to High pH. *Frontiers in Microbiology*, 8:308 (2017). doi:10.3389/fmicb.2017.00308

34. Brazelton W.J., Thornton C.N., Hyer A., Twing K.I., Longino A.A., Lang S.Q., Lilley M.D., Früh-Green G.L., Schrenk M.O. Metagenomic identification of active methanogens and methanotrophs in serpentinite springs of the Voltri Massif, Italy. *PeerJ*, (2017). doi:10.7717/peerj.2945

35. Fones E.M., Colman D.R., Kraus E.A., Nothaft D.B., Poudel S., Rempfert K.R., Spear J.R., Templeton A.S., Boyd E.S. Physiological adaptations to serpentinization in the Samail Ophiolite, Oman. *The ISME Journal* (2019). doi:10.1038/s41396-019-0391-2

36. Kraus E.A., Nothaft D., Stamps B.W., Rempfert K.R., Ellison E.T., Matter J.M., Templeton A.S., Boyd E.S., Spear J.R. Molecular Evidence for an Active Microbial Methane Cycle in Subsurface Serpentinite-Hosted Groundwaters in the Samail Ophiolite, Oman. *Applied and Environmental Microbiology*, (August 2020):1–18 (2021). doi:10.1128/AEM.02068-20

37. Rempfert K.R., Miller H.M., Bompard N., Nothaft D., Matter J.M., Kelemen P., Fierer N., Templeton A.S. Geological and geochemical controls on subsurface microbial life in the Samail Ophiolite, Oman. *Frontiers in Microbiology*, 8 (2017). doi:10.3389/fmicb.2017.00056

38. Glombitza C., Putman L.I., Rempfert K.R., Kubo M.D., Schrenk M.O., Templeton A.S., Hoehler T.M. Active microbial sulfate reduction in fluids of serpentinizing peridotites of the continental subsurface. *Communications Earth & Environment*, 2(84):1-9 (2021). doi:10.1038/s43247-021-00157-z

39. Woycheese K.M., Meyer-Dombard D.R., Cardace D., Argayosa A.M., Arcilla C.A. Out of the dark: Transitional subsurface-to-surface microbial diversity in a terrestrial serpentinizing seep (Manleluag, Pangasinan, the Philippines). *Frontiers in Microbiology*, 6 (2015). doi:10.3389/fmicb.2015.00044

40. Kohl L., Cumming E., Cox A., Rietze A., Morrissey L., Lang S.Q., Richter A., Suzuki S., Nealson K.H., Morrill P.L. Exploring the metabolic potential of microbial communities in ultra-basic, reducing springs at The Cedars, CA, USA: Experimental evidence of microbial methanogenesis and heterotrophic acetogenesis. *Journal of Geophysical Research: Biogeosciences*, 121(4):1203–20 (2016). doi: 10.1002/2015JG003233

41. Suzuki S., Kuenen J.G., Schipper K., van der Velde S., Ishii S., Wu A., Sorokin D.Y., Tenney A., Meng X., Morrill P.L., Kamagata Y., Muyzer G., Nealson K.H. Physiological and genomic features of highly alkaliphilic hydrogen-utilizing Betaproteobacteria from a continental serpentinizing site. *Nature Communications*, 5 (2014). doi:10.1038/ncomms4900

42. Cardace D., Hoehler T., Mccollom T., Schrenk M., Carnevale D., Kubo M., Twing, K. Establishment of the Coast Range ophiolite microbial observatory (CROMO): drilling objectives and preliminary outcomes. *Scientific Drilling*, 16:45–55 (2013). doi:10.5194/sd-16-45-2013

43. Conze R., Coggon J.A., Matter J. ICDP Oman Drilling Project: News from the Scientific Drilling in the Samail Ophiolite Sultanate of Oman. *ECORD Newsletter*, 28 (2017). doi:10.14379/OmanDP.proc.2020

44. Früh-Green G.L., Orcutt B.N., Green S., Cotterill C., Expedition 357 Scientists. Expedition 357 Preliminary Report: Atlantis Massif Serpentinization and Life. *International Ocean Discovery Program*, (2016). doi:10.14379/iodp.pr.357.2016

45. Allison S.D., Martiny J.B.H. Resistance, resilience, and redundancy in microbial communities. *Proc Natl Acad Sci USA*, 105 (2008). doi:10.1073/pnas.0801925105

46. Shade A., Peter H., Allison S.D., Baho D.L., Berga M., Bürgmann H., Huber D.H., Langenheder S., Lennon J.T., Martiny J.B.H., Matulich K.L., Schmidt T.M., Handelsman J. Fundamentals of microbial community resistance and resilience. *Frontiers in Microbiology*, 3(DEC):1–19 (2012). doi:10.3389/fmicb.2012.00417

47. Dichicco M.C., Laurita S., Paternoster M., Rizzo G., Sinisi R., Mongelli G. Serpentinite Carbonation for CO2 Sequestration in the Southern Apennines: Preliminary Study. *Energy Procedia*, 76:477–86 (2015). doi:10.1016/j.egypro.2015.07.888

48. Kelemen P.B., Matter J. In situ carbonation of peridotite for CO2 storage. *Proc Natl Acad Sci USA*, 105 (2008). doi:10.1073/pnas.0805794105

49. Kelemen P.B., Matter J., Streit E.E., Rudge J.F., Curry W.B., Blusztajn J. Rates and Mechanisms of Mineral Carbonation in Peridotite: Natural Processes and Recipes for Enhanced, in situ CO2 Capture and Storage. *Annual Review of Earth and Planetary Sciences*, (2011). doi: 10.1146/annurev-earth-092010-152509

50. Wilkins M.J., Daly R.A., Mouser P.J., Trexler R., Sharma S., Cole D.R., Wrighton K.C, Biddle J.F., Denis E.H., Frederickson J.K., Kieft T.L., Onstott T.C., Peterson L., Pfiffner S.M., Phelps T.J., Schrenk M.O. Trends and future challenges in sampling the deep terrestrial biosphere. *Frontiers in Microbiology*, 5(SEP) (2014). doi:10.3389/fmicb.2014.00481

51. Crespo-Medina M., Twing K.I., Kubo M.D.Y., Hoehler T.M., Cardace D., McCollom T., Schrenk M.O. Insights into environmental controls on microbial communities in a

continental serpentinite aquifer using a microcosm-based approach. *Frontiers in Microbiology*, 5:604 (2014). doi:10.3389/fmicb.2014.00604

52. Jousset A., Bienhold C., Chatzinotas A., Gallien L., Gobet A., Kurm V., Küsel K., Rillig M.C., Rivett D.W., Salles J.F., van der Heijden M.G.A., Youssef N.H., Zhang X., Wei Z., Gera Hol W.H. Where less may be more: how the rare biosphere pulls ecosystems strings. *The ISME Journal*, 11:853–62 (2017). doi:10.1038/ismej.2016.174

53. Shade A., Jones S.E., Caporaso J.G., Handelsman J., Knight R., Fierer N., Gilbert J.A. Conditionally Rare Taxa Disproportionately Contribute to Temporal Changes in Microbial Diversity. *mBio*, (2014). doi:10.1128/mBio.01371-14.Editor

54. Bjornstad B.N., McKinley J.P., Stevens T.O., Rawson S.A., Fredrickson J.K., Long P.E. Generation of Hydrogen Gas as a Result of Drilling Within the Saturated Zone. Vol. 14, *Groundwater Monitoring & Remediation*, 14;140–7 (1994). doi:10.1111/j.1745-6592.1994.tb00492.x

55. Mayhew L.E., Ellison E.T., McCollom T.M., Trainor T.P., Templeton A.S. Hydrogen generation from low-temperature water-rock reactions. *Nature Geoscience*, 6(6):478–84 (2013). doi:10.1038/ngeo1825

56. Preiner M., Igarashi K., Muchowska K.B., Yu M., Varma S.J., Kleinermanns K., Nobu M.K., Kamagata Y., Tüysüz H., Moran J., Martin W.F. A hydrogen-dependent geochemical analogue of primordial carbon and energy metabolism. *Nature Ecology & Evolution*, 4(April) (2020). doi:10.1038/s41559-020-1125-6

57. McCollom T.M. Laboratory Simulations of Abiotic Hydrocarbon Formation in Earth's Deep Subsurface. *Reviews in Mineralogy & Geochemistry*, 75:467–94 (2013). doi:10.2138/rmg.2013.75.15

58. Merino N., Kawai M., Boyd E.S., Colman D.R., McGlynn S.E., Nealson K.H., Kurokawa K., Hongoh Y. Single-Cell Genomics of Novel Actinobacteria with the Wood–Ljungdahl Pathway Discovered in a Serpentinizing System. *Frontiers in Microbiology*, 11(June):1–21 (2020). doi:10.3389/fmicb.2020.01031

59. Miller H.M., Matter J.M., Kelemen P., Ellison E.T., Conrad M.E., Fierer N., Ruchala T., Tominaga M., Templeton A.S. Modern water/rock reactions in Oman hyperalkaline peridotite aquifers and implications for microbial habitability. *Geochimica et Cosmochimica Acta*, 179:217–41 (2016). doi:10.1016/j.gca.2016.01.033

60. Tiago I., Veríssimo A. Microbial and functional diversity of a subterrestrial high pH groundwater associated to serpentinization. *Environmental Microbiology*, 15(6):1687–706 (2013). doi:10.1111/1462-2920.12034

61. Melton E.D., Sorokin D.Y., Overmars L., Lapidus A.L., Pillay M., Ivanova N., Glavina del Rio T., Kyrpides N.C., Woyke T., Muyzer G. Draft genome sequence of *Dethiobacter alkaliphilus* strain AHT1^{T}, a gram-positive sulfidogenic polyextremophile. *Standards in Genomic Sciences*, 12(57):1–9 (2017). doi:10.1186/s40793-017-0268-9

62. Lee Y.-J., Romanek C.S., Mills G.L., Davis R.C., Whitman W.B., Wiegel J. *Gracilibacter thermotolerans* gen. nov., sp. nov., an anaerobic , thermotolerant bacterium from a constructed wetland receiving acid sulfate water. *International Journal of Systematic and Evolutionary Microbiology*, 56:2089–93 (2006). doi:10.1099/ijs.0.64040-0

63. Watanabe M., Kojima H., Fukui M. Review of Desulfotomaculum species and proposal of the genera Desulfallas gen. nov., Desulfofundulus gen. nov., Desulfofarcimen gen. nov. and Desulfohalotomaculum gen. nov. *International Journal of Systematic and Evolutionary Microbiology*, 68:2891–9 (2018). doi:10.1099/ijsem.0.002915

64. Sun L., Toyonaga M., Ohashi A., Tourlousse D.M., Matsuura N., Meng X.-Y., Tamaki H., Hanada S, Cruz R., Yamaguchi T., Sekiguchi Y. *Lentimicrobium saccharophilum* gen. nov., sp. nov., a strictly anaerobic bacterium representing a new family in the phylum Bacteroidetes, and proposal of *Lentimicrobiaceae* fam. nov. *International Journal of Systematic and Evolutionary Microbiology*, 66:2635–42 (2016). doi:10.1099/ijsem.0.001103

65. Jones SE, Lennon JT. Dormancy contributes to the maintenance of microbial diversity. Proceedings of the National Academy of Sciences [Internet]. 2010;107(13):5881–6. Available from: http://www.pnas.org/cgi/doi/10.1073/pnas.0912765107

66. Lennon J.T., Jones S.E. Microbial seed banks: The ecological and evolutionary implications of dormancy. *Nature Reviews Microbiology*, 9(2):119–30 (2011). doi:10.1038/nrmicro2504

67. Ivanova N., Rohde C., Munk C., Nolan M., Lucas S., Glavina Del Rio T., Tice H., Deshpande S., Cheng J.-F., Tapia R., Han C., Goodwin L., Pitluck S., Liolios K., Mavromatis K., Mikhailova N., Pati A., Chen A., Palaniappan K., Land M., Hauser L., Chang Y.-J., Jeffries C.D., Brambilla E., Rohde M., Göker M., Tindall B.J., Woyke T., Bristow J., Eisen J.A., Markowitz V., Hugenholtz P., Kyrpides N.C., Klenk H.-P., Lapidus A. Complete genome sequence of *Truepera radiovictrix* type strain (RQ-24^{T}). *Standards in Genomic Sciences*, 4:91–9 (2011). doi:10.4056/sigs.1563919

68. Hoefman S., Heylen K., De Vos P. *Methylomonas lenta* sp. nov., a methanotroph isolated from manure and a denitrification tank. *International Journal of Systematic and Evolutionary Microbiology*, 64:1210–7 (2014). doi:10.1099/ijs.0.057794-0

69. Tiago I., Mendes V., Pires C., Morais P.V., Veríssimo A. *Phenylobacterium falsum* sp. nov., an Alphaproteobacterium isolated from a nonsaline alkaline groundwater , and emended description of the genus Phenylobacterium. *Systematic and Applied Microbiology*, 28:295–302 (2005). doi:10.1016/j.syapm.2005.02.005

70. Ishii S., Ashida N., Ohno H., Segawa T., Yabe S., Otsuka S., Yokota A., Senoo K. *Noviherbaspirillum denitrificans* sp. nov., a denitrifying bacterium isolated from rice paddy soil and *Noviherbaspirillum autotrophicum* sp. nov., a denitrifying , facultatively autotrophic bacterium isolated from rice paddy soil and proposal to reclassify *Herbaspirillum massiliense* as *Noviherbaspirillum massiliense* comb. nov. *International Journal of Systematic and Evolutionary Microbiology*, 67:1841–8 (2017). doi:10.1099/ijsem.0.001875

71. Herold M., Martínez Arbas S., Narayanasamy S., Sheik A.R., Kleine-Borgmann L.A.K., Lebrun L.A., Kunath B.J., Roume H., Bessarab I., Williams R.B.H., Gillece J.D., Schupp J.M., Keim P.S., Jäger C., Hoopmann M.R., Moritz R.L., Ye Y., Li S., Tang H., Heintz-Buschart A., May P., Muller E.E.L., Laczny C.C. Wilmes P. Integration of time-series meta-omics data reveals how microbial ecosystems respond to disturbance. *Nature Communications,* 11 (2020). doi:10.1038/s41467-020-19006-2

72. Jiao S., Wang J., Wei G., Chen W., Lu Y. Dominant role of abundant rather than rare bacterial taxa in maintaining agro-soil microbiomes under environmental disturbances. *Chemosphere*, 235:248–59 (2019). doi: 10.1016/j.chemosphere.2019.06.174

73. Chen Y.-J., Leung P.M., Wood J.L., Bay S.K., Hugenholtz P., Kessler A.J., Shelley G., Waite D.W., Franks A.E., Cook P.L.M., Greening C. Metabolic flexibility allows bacterial habitat generalists to become dominant in a frequently disturbed ecosystem. *The ISME Journal*, (2021). doi:10.1038/s41396-021-00988-w

74. Kurm V., Geisen S., Gera Hol W.H. A low proportion of rare bacterial taxa responds to abiotic changes compared with dominant taxa. *Environmental Microbiology*, 21(2):750–8 (2019). doi:10.1111/1462-2920.14492

75. Shade A. Understanding Microbiome Stability in a Changing World. *MSystems,* 3(2):e00157-17 (2018). doi:10.1128/mSystems.00157-17

76. Shade A., Read J.S., Welkie D.G., Kratz T.K., Wu C.H., McMahon K.D. Resistance, resilience and recovery: aquatic bacterial dynamics after water column disturbance. *Environmental Microbiology,* 13:2752–67 (2011). doi:10.1111/j.1462-2920.2011.02546.x

77. Ortiz E., Tominaga M., Cardace D., Schrenk M.O., Hoehler T.M., Kubo M.D., Rucker D.F. Geophysical Characterization of Serpentinite Hosted Hydrogeology at the McLaughlin Natural Reserve, Coast Range Ophiolite. *Geochemistry, Geophysics, Geosystems*, 19(1):114–31 (2018). doi:10.1002/2017GC007001

78. Schloss P.D., Westcott S.L., Ryabin T., Hall J.R., Hartmann M., Hollister E.B., Lesniewski R.A., Oakley B.B., Parks D.H., Robinson C.J., Sahl J.W., Stres B., Thallinger G.G., Van Horn D.J., Weber C.F. Introducing mothur: Open-source, platform-independent, community-supported software for describing and comparing microbial communities. *Applied and Environmental Microbiology*, 75(23):7537–41 (2009). doi:10.1128/AEM.01541-09

79. Sheik C.S., Reese B.K., Twing K.I., Sylvan J.B., Grim S.L., Schrenk M.O., Sogin M.L., Colwell F.S. Identification and removal of contaminant sequences from ribosomal gene databases: Lessons from the Census of Deep Life. *Frontiers in Microbiology,* 9(APR):1–14 (2018). doi:10.3389/fmicb.2018.00840

80. Fullerton K.M., Schrenk M.O., Yücel M., Manini E., Basili M., Rogers T.J., Fattorini D., Di Carlo M., d'Errico G., Regoli F., Nakagawa M., Vetriani C., Smedile F., Ramírez C., Miller H., Morrison S.M., Buongiorno J., Jessen G.L., Steen A.D., Martínez, M., Maarten de Moor J., Barry P.H., Giovannelli D., Lloyd K.G. Effect of tectonic processes on

biosphere-geosphere feedbacks across a convergent margin. *Nature Geoscience*, 14(May) (2021). doi:10.1038/s41561-021-00725-0

81. Zhang Z., Schwartz S., Wagner L., Miller W. A Greedy Algorithm for Aligning DNA Sequences. *Journal of Computational Biology*, 7:203–14 (2000). doi:10.1089/10665270050081478

82. R Core Team. R: A language and environment for statistical computing. *R Foundation for Statistical Computing, Vienna, Austria*, (2014). url:http://www.R-project.org/

83. McMurdie P.J., Holmes S. Phyloseq: An R Package for Reproducible Interactive Analysis and Graphics of Microbiome Census Data. *PLoS ONE*, 8(4) (2013). doi:10.1371/journal.pone.0061217

84. Oksanen J., Blanchet F.G., Friendly M., Kindt R., Legendre P., McGlinn D., Minchin P.R., O'Hara R.B., Simpson G.L., Solymos P., Stevens M.H.H., Szoecs E., Wagner H. vegan: Community Ecology Package. R package version 25-5 (2019). Available from: https://cran.r-project.org/package=vegan

85. Wickham H. ggplot2: Elegant Graphics for Data Analysis. *Springer-Verlag New York*, (2016). url:https://ggplot2.tidyverse.org

CHAPTER 4

Experimental insights into drilling-induced changes in microbial community structure and geochemistry in a serpentinizing aquifer

Abstract

Environmental perturbations are known to alter microbial community composition, function, and biogeochemical cycling. Here, we report a series of experiments performed using ultrabasic groundwater from the serpentinizing Coast Range Ophiolite that were conducted to understand patterns of increased hydrogen and acetate consumption observed *in situ* following the installation of boreholes using sterile oxygenated water as the drilling fluid. The response of microbial populations to elevated oxygen, hydrogen, and acetate concentrations in experimental microcosms was evaluated to better characterize community dynamics related to these geochemical changes. Here we illustrate that elevated hydrogen concentrations were actively consumed by resident populations of the candidate genus *Serpentinomonas*, while increased acetate concentrations were the result of biological activity, likely the product of acetogenesis by members of the genus *Dethiobacter*. Microbial community data reveal that *Serpentinomonas* were predominant under all experimental conditions, indicating that these organisms initially bloomed under more oxygen-rich conditions in the subsurface and subsequently utilized increased concentrations of hydrogen and acetate while continuing to flourish. The experimental treatments also demonstrated that a significant fraction of organisms in the oligotrophic groundwater pass through filters traditionally used in biomolecular surveys, potentially underestimating the contributions of ultra-small organisms. These findings elucidate the complex biogeochemistry and microbial community responses that occurred *in situ* following drilling and highlight impressive

versatility and opportunistic behavior of *Serpentinomonas* during periods of stress in the serpentinizing subsurface.

Introduction

A massive amount of microbial biomass and biodiversity is harbored within the subsurface (1) where microbial communities play central roles in mediating biogeochemical cycles of carbon, nitrogen, sulfur, and other inorganic and organic chemical species (2–6). Microbial communities are subject to a variety of seasonal (5,7,8) and episodic or isolated changes in their environment related to natural events (9–11) or anthropogenic change (12–16). As the effects of anthropogenic change become more pronounced it is important that we can anticipate changes in microbial community composition, function, and large scale biogeochemical cycles (6,17–22). One environment where our ability to anticipate change is of vital importance is in groundwater, where depletion (23) and contamination of subsurface reservoirs is altering the biogeochemistry and potability of groundwater resources. These observations have spurred efforts to access and utilize deep groundwater resources that are likely less susceptible to contamination and recharge issues than their shallower counterparts (24). One major challenge is that access to deep groundwater is relatively sparse, making our understanding of the current state of these resources and our ability to model and manage them into the future somewhat limited (24).

Serpentinized peridotites are common and diverse environments on Earth (25,26) occurring in both marine and terrestrial settings (27). In these settings, water reacts with iron-rich minerals in peridotite, resulting in the formation of serpentine minerals and abundant molecular hydrogen (H_2). This H_2 can further react with dissolved carbon in the presence of iron/nickel minerals to generate small organic compounds such as methane (CH_4) and acetate (28–30). These

reactions also produce high pH fluids with limited available dissolved inorganic carbon (27,30,31). Microbial communities uniquely adapted to this extreme environment (32,33) have been previously characterized, revealing active microbial populations that utilize available H_2, CH_4, carbon monoxide, small organic acids, and sulfur compounds for autotrophic and heterotrophic metabolisms (32,34–43). The drilling and establishment of the Coast Range Ophiolite Microbial Observatory (CROMO) in 2011 provided direct access to serpentinized fluids in the subsurface for the first time (44) and served as a template for scientific drilling operations carried out at the Samail Ophiolite, Sultanate of Oman (45) and Atlantis Massif (46). Time series geochemical and microbiological data collected from CROMO in the years following drilling revealed substantial changes in redox conditions, dissolved H_2, and acetate concentrations in the first two years after drilling (**Ch. 3**). Microbial community responses were assessed in the *in situ* dataset, but the mechanisms behind the generation of increased concentrations of H_2 and acetate remained ambiguous, and functional responses of microbial populations could not be determined with the existing data (**Ch. 3**). Since the disturbance was relatively recent and groundwater microbial community resilience responses to hydrologic perturbations appear to have a historical contingency (a.k.a ecological memory) component (47) we anticipated that experimental exposure to the same geochemical changes that occurred after drilling would elicit the same responses from microbial populations that were employed *in situ* after the perturbation.

Here I describe a series of experiments that investigate the biogeochemical dynamics and microbial community responses to the major geochemical changes observed *in situ* following drilling activity at CROMO in 2011 (**Ch. 3**). Fluids were collected from the N08-B and QV1.1 wells at CROMO for microcosm experiments and subjected to three different experimental treatments. The first treatment was the addition of sterile oxygenated water as was used for drilling

fluid (44), leading to increased dissolved oxygen concentrations and oxidation reduction potential conditions within the subsurface (**Ch. 3**). The second and third treatments were the addition of H_2 and acetate, respectively, which were observed at increased concentrations (> 0.25 μM H_2 and > 5 μM acetate) following drilling relative to normally observed conditions (< 0.25 μM H_2 and < 1 μM acetate) (**Ch. 3**). Our data show that increased H_2 concentrations observed following drilling were likely produced via water-rock reactions in the subsurface, and that acetate was likely produced by organisms from the genus *Dethiobacter* via the Wood-Ljungdahl pathway. Microbial community data reveal that organisms from the candidate genus *Serpentinomonas* (32) thrived under all experimental conditions and dominated microbial community composition in experiments. This versatile organism is capable of aerobic respiration, autotrophy using H_2 oxidation, and heterotrophy using acetate (32) and seems to have initially flourished under more oxic conditions and continued to bloom grow using H_2 and acetate, outcompeting other hydrogenotrophs and heterotrophs for these increased available resources.

Results

Population Growth in Microcosm Experiments

Samples for the determination of microbial cell abundances were collected from microcosms once every two weeks over the course of two months (**Fig. 4.1; Table C.1**). Initial timepoint (T0) samples were collected the same day that experimental treatments were started, prior to the amendment of microcosms with substrate. Microbial cell abundance was approximately 3×10^5 cells/mL in the T0 timepoints of experimental samples (**Fig. 4.2 A-F; Table C.2**). Steady growth was seen in most microcosms, reaching approximate maxima of 10×10^5 cells/mL in experimental microcosms (**Fig. 4.2 A-F; Table C.2**) Exceptions were the N08-B

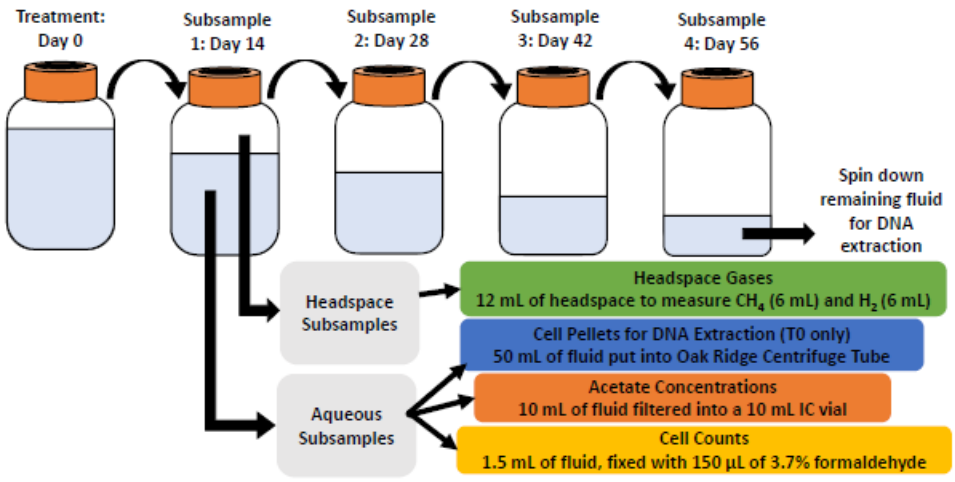

Figure 4.1. Subsampling Schematic Cartoon.

Cartoon showing microcosms with well fluid in a stoppered 0.5 L Pyrex bottle. Experiments began with 50 mL of headspace. Microcosm bottles were sampled once every two weeks for the aqueous and headspace samples described in the bottom right of the figure.

treatments amended with H_2 (**Fig. 4.2 B**), which showed relatively consistent cell abundances throughout experiments. N08-B microcosms amended with sterile oxygenated water as well as N08-B and QV1.1 microcosms amended with acetate increased in cell abundances during the initial six weeks of experiments but showed decreasing cell abundances in the final two weeks between T3 and T4 (**Fig. 4.2 A, C, F**). N08-B filtered treatments amended with water and all QV1.1 filtered treatments displayed almost no growth (**Fig. 4.2 A, D-F**). Curiously, microbial growth was observed in N08-B 0.1 µm filtered treatments amended with H_2 and sterile sodium acetate (**Fig. 4.2 B & C**). Discussion of potential sources of microorganisms within the filtered experiments is explored more below. Microbial cell abundance measurements from experimental blanks and live control (unfiltered well fluid that received no additional amendments) microcosms are plotted in the **Appendix** (**Fig. C.1 A & E**).

The excel file and R code used to generate **Figure 4.2** are published on Figshare (https://figshare.com/projects/Microcosm_Drilling_Experiments/113787).

Microcosm Geochemistry

Geochemical samples were collected according to the schedule described in the previous section (**Fig. 4.1; Table C.1**). Headspace gas samples to measure H_2 and CH_4 and aqueous samples to measure acetate were collected and analyzed as described below. These data were tracked in all experimental microcosm treatments to investigate the role microbial communities may have

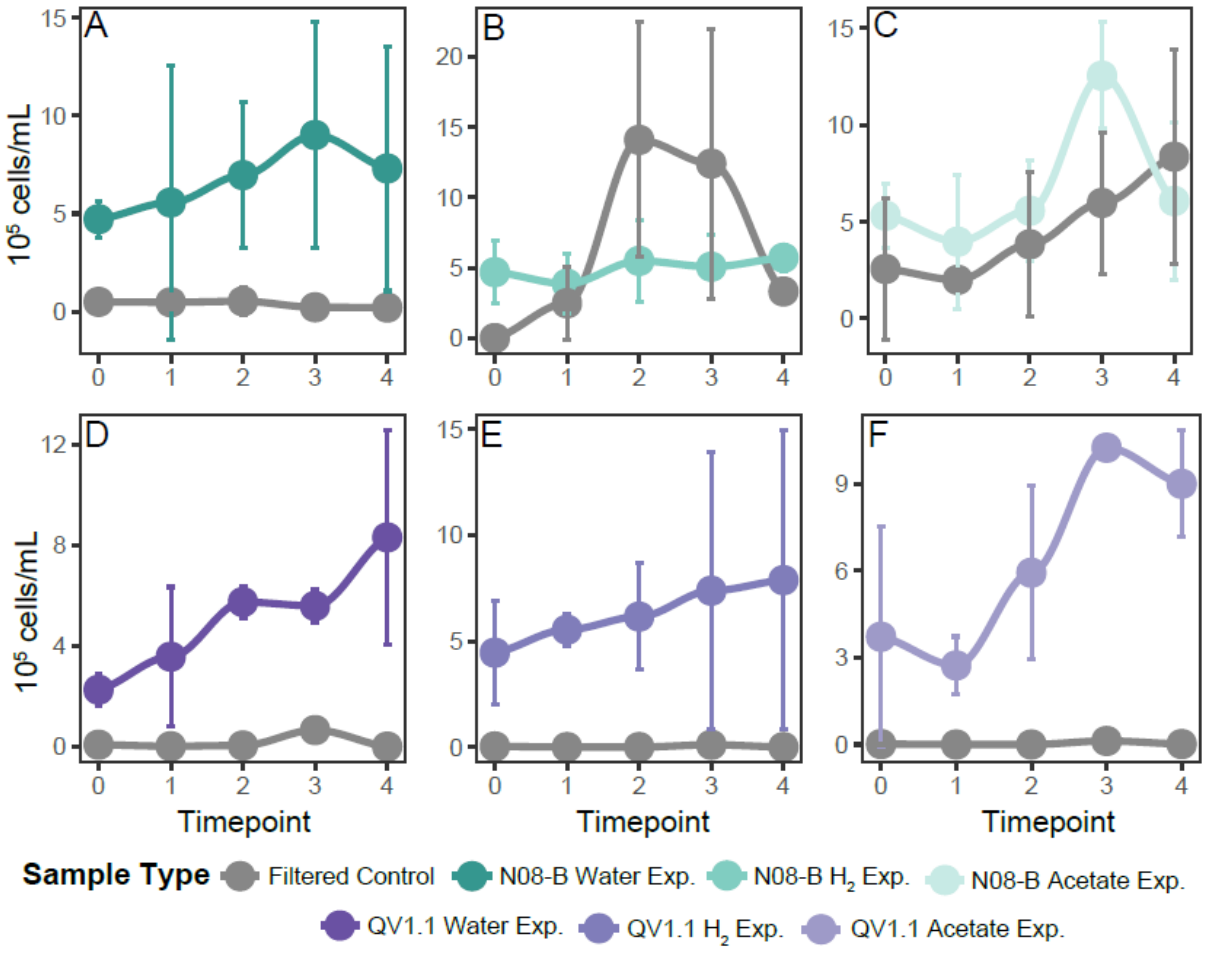

Figure 4.2. Cell Abundance Over Time.

Plots showing microbial abundance in 10^5 cells/mL in filtered and unfiltered microcosms at each of the sampling time points (T0, T1, T2, T3, T4) for N08-B microcosms treated with sterile oxygenated water (A), hydrogen (B), and acetate (C), and for QV1.1 microcosms treated with sterile oxygenated water (D), hydrogen (E), and acetate (F). Error bars display the standard deviation of cell abundance above and below the mean obtained from averaging data from experimental replicates. Samples were collected every 2 weeks (Fig. 4.1).

played in producing and/or consuming higher available concentrations of oxygen, H_2, and acetate following drilling activity at CROMO (**Ch. 3**). Geochemical data obtained from live controls is visualized in the **Appendix** (**Fig. C.1 B-D & F-H**).

Microcosms treated with sterile oxygenated water were set up to investigate which microbial taxa could withstand more oxygen-rich conditions and whether the increase in observed H_2 concentrations were the result of biological activity or water-rock reactions that can occur during drilling activity (48). N08-B microcosms treated with sterile oxygenated water showed in general a decrease in available acetate (**Fig. 4.3 A**), a decrease in H_2 (**Fig. 4.3 B**) and a decrease in available CH_4 (**Fig. 4.3 C**). H_2 appeared to be more abundant in experimental treatments than in controls, but still showed a general decrease in concentration over time (**Fig. 4.3 B**). Decreases in CH_4 and acetate concentrations in unfiltered treatments were indistinguishable from changes in concentration in the filtered treatments (**Fig. 4.3 A & C**). QV1.1 microcosms treated with sterile oxygenated water showed clear decreases in available H_2 and CH_4 (**Fig. 4.3 K & L**), while acetate concentrations showed a slight decrease in concentration between T0 and T4 with variable concentrations during intermediate timepoints (**Fig. 4.3 J**). Changes in acetate and CH_4 concentrations in the unfiltered treatments were indistinguishable from changes in concentration in the filtered treatments (**Fig. 4.3 J & L**). When compared to the filtered treatments, H_2 concentrations decreased substantially in the unfiltered microcosms, providing strong evidence that H_2 is being consumed by microorganisms in the QV1.1 experiments (**Fig. 4.3 K**). A lack of growth in QV1.1 0.1 um-filtered treatments further supports this interpretation (**Fig. 4.2 D-F**). Data from both N08-B and QV1.1 microcosms treated with sterile oxygenated water showed overall consumption (or loss) of H_2 (**Fig. 4.3 B & K**). These data provide strong evidence that increased H_2 concentrations observed at the CROMO wells following drilling was likely not the

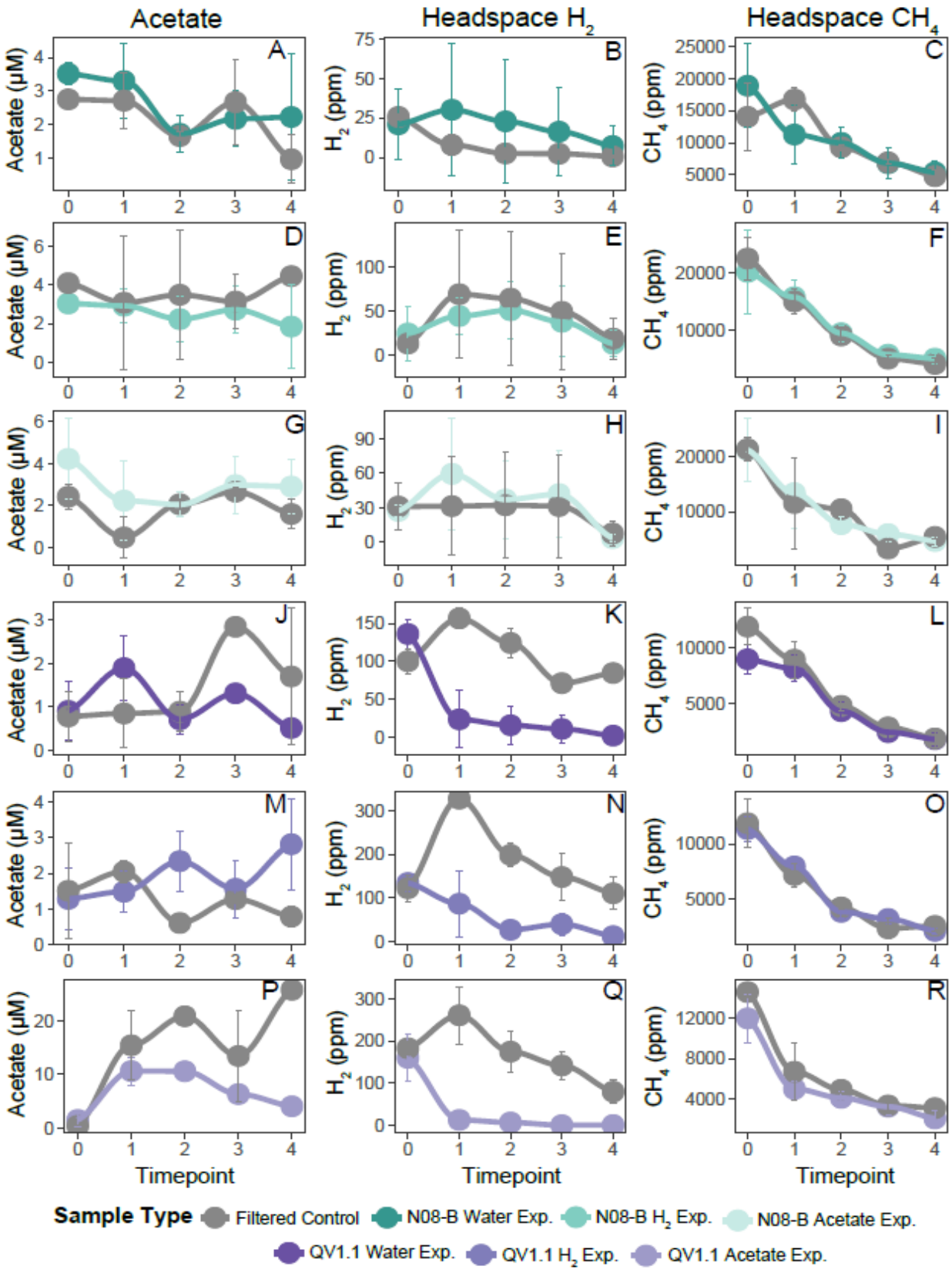

Figure 4.3. Gas and Aqueous Geochemistry Over Time.

Figure 4.3. (cont'd).

Plots showing the concentration of acetate, hydrogen, and methane at each of the sampling time points (T0, T1, T2, T3, T4) for N08-B microcosms treated with sterile oxygenated water (A-C), N08-B microcosms treated with hydrogen (D-F), N08-B microcosms treated with acetate (G-I), QV1.1 microcosms treated with sterile oxygenated water (J-L), QV1.1 microcosms treated with hydrogen (M-O), and QV1.1 microcosms treated with acetate (P-R). Standard error bars display the standard deviation of geochemical species above and below the mean obtained from averaging data from experimental replicates. Samples were collected every two weeks (Fig. 4.1).

result of biological H_2 production. This result fits well with our current understanding of [FeFe] hydrogenase enzymes, which tend to be extremely sensitive to oxygen (49,50).

Treatments with H_2 were set up to mimic the concentrations observed *in situ* following drilling (**Ch. 3**) and to determine if microbial community members used excess available H_2 for acetogenesis (51), resulting in increased acetate concentrations observed following drilling (**Ch. 3**). Alternatively, more abundant H_2 could have reacted with available dissolved inorganic carbon (DIC) in Fischer-Tropsch type reactions that could generate acetate and other small organic compounds including CH_4 (28–30,52). N08-B microcosms treated with H_2 showed an initial increase in H_2 concentrations at T1 (H_2 was added after T0 samples were collected) and then H_2 concentrations in both filtered and unfiltered treatments steadily decreased over time (**Fig. 4.3 E**). H_2 concentrations were slightly lower in whole water treatments than in filtered treatments but were not distinctly different. Microbial growth present in the filtered N08-B H_2 microcosms likely explain the similar trends in H_2 consumption (**Fig. 4.2 B**). Acetate concentrations stay relatively consistent over time, with a drop in concentration between T3 and T4 (**Fig. 4.3 D**). Again, concentrations very similar to those observed in the filtered experiments are likely related to the microbial growth observed in these experiments (**Fig. 4.2 B**). CH_4 concentrations steadily decreased over time and are not distinguishable from concentrations observed in the filtered microcosms (**Fig. 4.2 F**). QV1.1 microcosms treated with H_2 did not have microbial growth in

controls (**Fig. 4.2 E**) and show more distinct geochemical trends in the H_2 and acetate data. H_2 concentrations increased at T1 (H_2 addition occurred after T0 samples were collected) and gradually decreased in filtered treatments (**Fig. 4.3 N**). Steady consumption of H_2 is seen in experimental microcosms, with no increase seen at all in T1 measurements, despite the addition of H_2 to the experiments (**Fig. 4.3 N**). Decreases in H_2 concentrations in whole-water microcosms are substantially greater than those observed in filtered treatments, providing strong evidence of microbial H_2 consumption (**Fig. 4.3 N**). Acetate concentrations are comparable at T0 and T1 in QV1.1 microcosms treated with H_2. Following this steady state, acetate concentrations gradually increase in experimental microcosms and gradually decrease in filtered treatments (**Fig. 4.3 M**). These data suggest that microbial production of acetate occurred in QV1.1 microcosms treated with H_2. The presence and transcription of genes involved in the Wood-Ljungdahl pathway have previously been observed in numerous CROMO wells, including the QV1.1 well (38,43). CH_4 concentrations gradually decreased over time in QV1.1 microcosms treated with H_2 (**Fig. 4.3 O**). Changes in concentration were indistinguishable between filtered and unfiltered treatments (**Fig. 4.3 O**). Overall, results indicate that microbial communities in both N08-B and QV1.1 were able to respond to excess concentrations of H_2 following drilling for metabolism (**Fig. 4.3 E & N**) and that excess H_2 may have then been used to perform acetogenesis in QV1.1 fluids (**Fig. 4.3 M**).

Microcosms treated with acetate were set up to mimic increased concentrations of acetate observed following drilling *in situ* (**Ch. 3**). Acetate is an extremely important carbon source in the oligotrophic deep subsurface (51,53–55) where acetate produced abiotically (28–30,52) or biotically by acetogens (51,54) can fuel heterotrophy and metabolisms of sulfate reducing bacteria and methanogens in the carbon limited deep subsurface (51,55,56). Numerous CROMO microbial community members should be able to easily metabolize acetate (32,38,57). As such, we were

curious which taxa would be able to most effectively compete for and utilize increased acetate concentrations following an increase in concentration after drilling. N08-B microcosms treated with acetate show steady concentrations of H_2 that decrease between T3 and T4 in both filtered and unfiltered treatments (**Fig. 4.3 H**). Despite the addition of acetate following T0 samples, acetate concentrations are not higher at T1, but instead decrease from concentrations observed at T0 and remain at steady concentrations during following time points (**Fig. 4.3 G**). Acetate concentrations are comparable in experimental and control microcosms (**Fig. 4.3 G**). CH_4 concentrations gradually decrease in both experimental and control microcosms (**Fig. 4.3 I**). Geochemical measurements in N08-B experimental microcosms treated with acetate were not distinguishable from data measured in controls (**Fig. 4.3 G-I**). Nearly identical changes in geochemistry observed in filtered and unfiltered treatments are likely due to microbial growth observed in filtered N08-B microcosms treated with acetate (**Fig. 4.2 C**). QV1.1 microcosms treated with acetate show distinct changes in H_2 and acetate concentrations (**Fig. 4.3 P & Q**) and a gradual loss of CH_4 over time that cannot be differentiated from CH_4 loss in filtered treatments (**Fig. 4.3 R**). H_2 concentrations were nearly identical between whole water and filtered treatments at T0 (**Fig. 4.3 Q**). Following the addition of acetate (after T0 sampling), H_2 was rapidly consumed in the initial two weeks and remained near or below the detection limit for the remainder of the experiment (**Fig. 4.3 Q**). This result contrasts with H_2 measurements in filtered samples which remain quite high despite a gradual loss of H_2 over time (**Fig. 4.3 Q**). Acetate concentrations remained close to zero in all T0 samples (**Fig. 4.3 P**). Acetate concentrations increased in T1 samples following the addition of acetate after T0 subsampling and decreased in subsequent time points in experimental microcosms (**Fig. 4.3 P**). Acetate remained relatively steady at elevated concentrations in filtered treatments (**Fig. 4.3 P**). Overall, geochemical results provide strong

evidence for microbial consumption of H_2 and acetate in QV1.1 microcosms treated with acetate. It also appears that microbial consumption of H_2 occurred in N08-B 0.1-μm-filtered treatments (**Fig. 4.2 C**), and that acetate may have been utilized in a more limited capacity (**Fig. 4.3 G & H**). Results from microbial community analyses revealed which microbial community members were enriched under these conditions, and therefore most likely utilizing available H_2 and acetate.

The excel file and R code used to generate **Figure 4.3** are published on Figshare (https://figshare.com/projects/Microcosm_Drilling_Experiments/113787).

Microbial Community Composition

Total genomic DNA was extracted from microbial cells that were harvested from T0 and from fluids remaining at the end of experiments as described below. Microbial community diversity and taxonomic assessments are based on a dataset generated from gene amplicon sequencing of the V4 region of the 16S rRNA gene. The dataset used for analyses consists of 31 samples, 5,947,999 sequence reads, and 366 operational taxonomic units (OTUs) clustered at 97% similarity as described below. The OTU count table and associated taxonomy table and metadata are published on FigShare along with the R code used for the following analyses (https://figshare.com/projects/Microcosm_Drilling_Experiments/113787).

Microbial communities in experimental microcosms are composed of approximately 50-75 OTUs on average, with a large amount of variability observed in experimental treatments using water and acetate and less variability observed in microcosms treated with H_2 (**Fig. 4.4 A**). Microcosms treated with acetate contain the greatest mean diversity of OTUs, followed by microcosms treated with water and then H_2 (**Fig. 4.4 A**). Fluids sampled directly from N08-B and QV1.1 generally contained 300-550 OTUs and 50-150 OTUs, respectively (33**; Fig. 2.3 A**).

Evenness (measured by Pielou's evenness index), or the extent to which taxa in a community are equal in numerical abundance, is quite low throughout all experimental microcosms, with the highest mean evenness observed in microcosms treated with acetate, followed by those treated with H_2 and water (**Fig. 4.4 B**). As was observed in microbial community richness data (**Fig. 4.4**

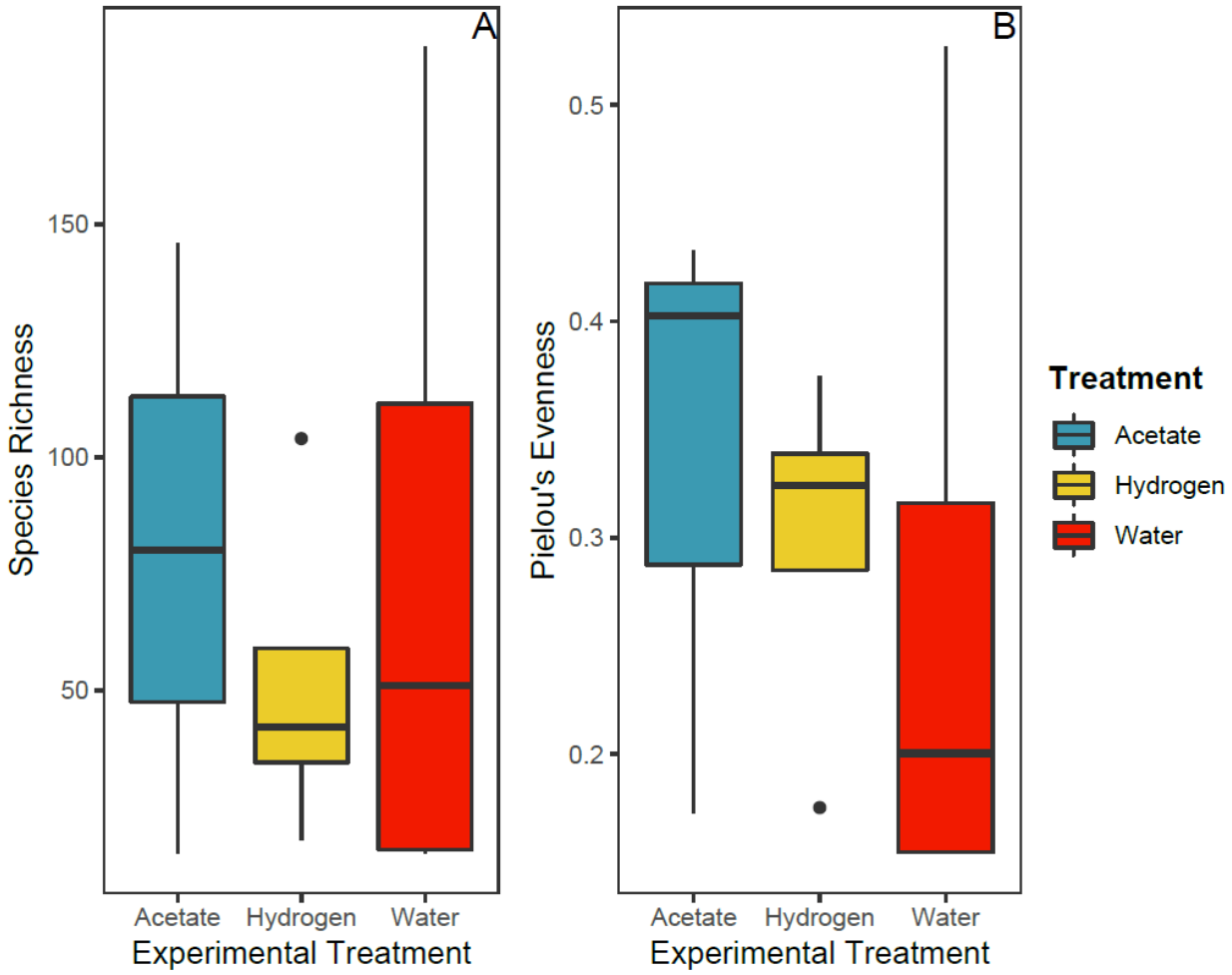

Figure 4.4. Richness and Pielou's Evenness Index of Microcosm Microbial Communities.

Boxplots showing richness (A) and Pielou's evenness index (B) for microbial communities sampled from microcosms treated with sterile oxygenated water, hydrogen, and acetate. Boxplots display the distribution of data within each treatment, where the main colored box displays the interquartile range (25th to 75th percentile) of the data. Solid lines within the boxes represent the median of the data. Whiskers on the plot display the maximum and minimum expected values of the data distribution, and black colored points represent outlier data points with respect to the plotted distribution.

A), the greatest variability in evenness was observed in microcosms treated with acetate and water (**Fig. 4.4 B**). Fluids sampled directly from N08-B and QV1.1 generally have similar measures of evenness (33**; Fig. 2.3 B**). Interestingly, microbial richness increases from T0 to the end of experiments treated with acetate and water and decreases for experiments treated with H_2, while Pielou's evenness index decreases for all experimental treatments. The increase observed in microbial richness from T0 to the end of experiments could be related to the difference in volume collected for T0 (50 mL) and final samples (200 mL) collected to assess microbial community composition (**Fig 4.1**; see Materials and Methods). The decrease in evenness over time is likely associated with the enrichment of a few OTUs in each experimental treatment and examination of these OTUs will indicate which populations flourished under each experimental condition.

To assess how microcosm experiment microbial communities changed over time and according to observed geochemical changes (H_2, CH_4, and acetate concentrations) a PERMANOVA analysis was performed on Bray-Curtis dissimilarities and microcosm geochemical data (**Table C.3**). PERMANOVA results indicate how much variance in community composition can be explained by measured experimental data. Bray-Curtis dissimilarities were visualized using a non-metric multidimensional scaling (NMDS) plot with significant variables identified in the PERMANOVA analyses overlain as vectors (**Fig. 4.5**). Results from this analysis show that the well location from which the fluids were originally sampled (R^2=0.387) is the primary driver of observed differences in microbial community composition, followed by changes seen over time (R^2=0.241) and with changing concentrations of H_2 (R^2=0.183). Overall, measured environmental data (Time, fluid source, H_2, CH_4, and acetate concentrations) explain observed variance in microbial community composition well, accounting for 91.8% of observed variance in PERMANOVA analyses (**Table C.3**). Statistical ellipses were not drawn around samples

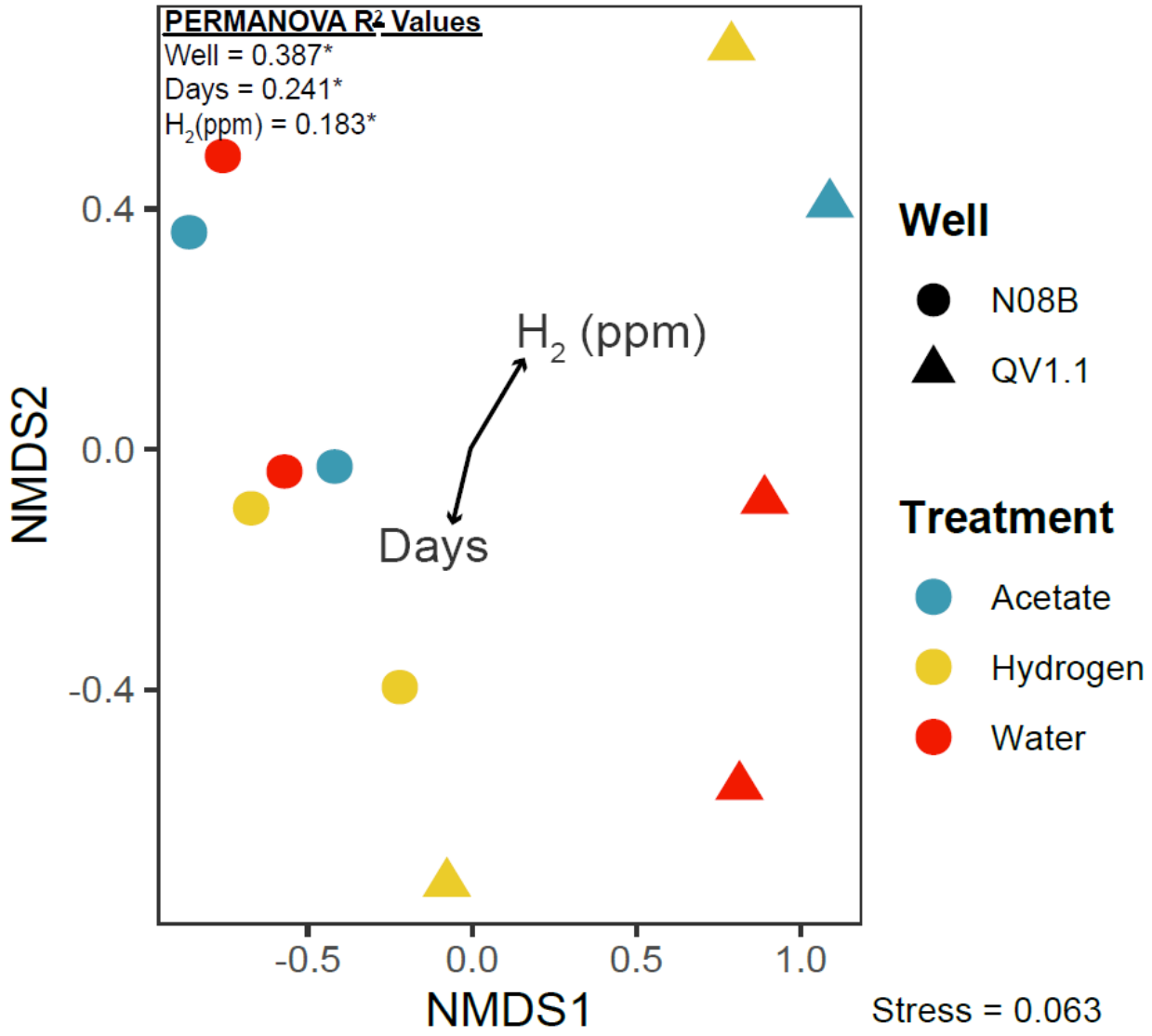

Figure 4.5. NMDS Plot Microcosm Microbial Communities.

Non-metric multidimensional scaling (NMDS) plot of 16S rRNA gene relative abundances using a Bray-Curtis dissimilarity. Environmental variables identified in a PERMANOVA analysis that are significantly correlated with changes in community composition ($(p \leq 0.05)$ are overlain on the plot as vectors. Points on the plot represent individual microbial community samples. Point shape is representative of the fluid source and points are colored based on experimental treatment. Points that lie close together are more similar in community composition, while points that lie far apart are less similar in community composition.

originating from each well to maintain visibility. N08-B samples can easily be seen on the west side of the plot and QV1.1 samples on the east side, with sample separation associated with time and H_2 concentrations occurring in the north-south axis of the plot for samples from each well

(**Fig. 4.5**). The fact that vectors for time and change in H_2 concentration lie almost exactly opposite of each other fits with observations of microcosm geochemistry. H_2 concentrations were greatest in initial time points and gradually decreased in all microcosms, regardless of treatment (**Fig. 4.3 B, E, H, K, N, & Q**). Microbial community members capable of hydrogenotrophic metabolisms were likely enriched during experiments, changing community composition in the microcosms over time (**Fig. 4.5**).

Finally, the taxonomy of dominant OTUs in microcosm microbial communities was assessed in samples collected from initial and final time points (**Fig. 4.6**). OTUs that were enriched by the experimental conditions were assessed by investigating changes in the relative abundance of OTUs from initial to final time points. Assessment of the 25 most abundant OTUs in initial and final time points is effective for understanding microbial community composition in these samples as these OTUs account for 96.87-99.84% of community composition in T0 samples and 99.17-99.81% of community composition in samples at the end of experiments. N08-B initial time point samples contain greater diversity than those observed in QV1.1 (**Fig. 4.6 A**). N08-B initial time point communities were primarily composed of organisms from the candidate genus *Serpentinomonas* (52.24-78.25%) (32), followed by a close relative of *Sulfuritalea hydrogenivorans* (5.41-7.66%) and a distant relative of *Lentimicrobium saccharophilum* (3.76-8.50%). Methanotrophic, methylotrophic, and fermentative organisms are also present in N08-B samples (**Fig. 4.6 A**). QV1.1 initial time point microbial communities contain markedly lower diversity and are composed primarily of organisms related to *Dethiobacter alkaliphilus* (18.16-59.21%), *Serpentinomonas* strain B1 (5.40-39.95%), *Delftia tsuruhatensis* (11.99-34.54%), and a relative of *Truepera radiovictrix* (8.92-22.96%) (**Fig. 4.6 A**).

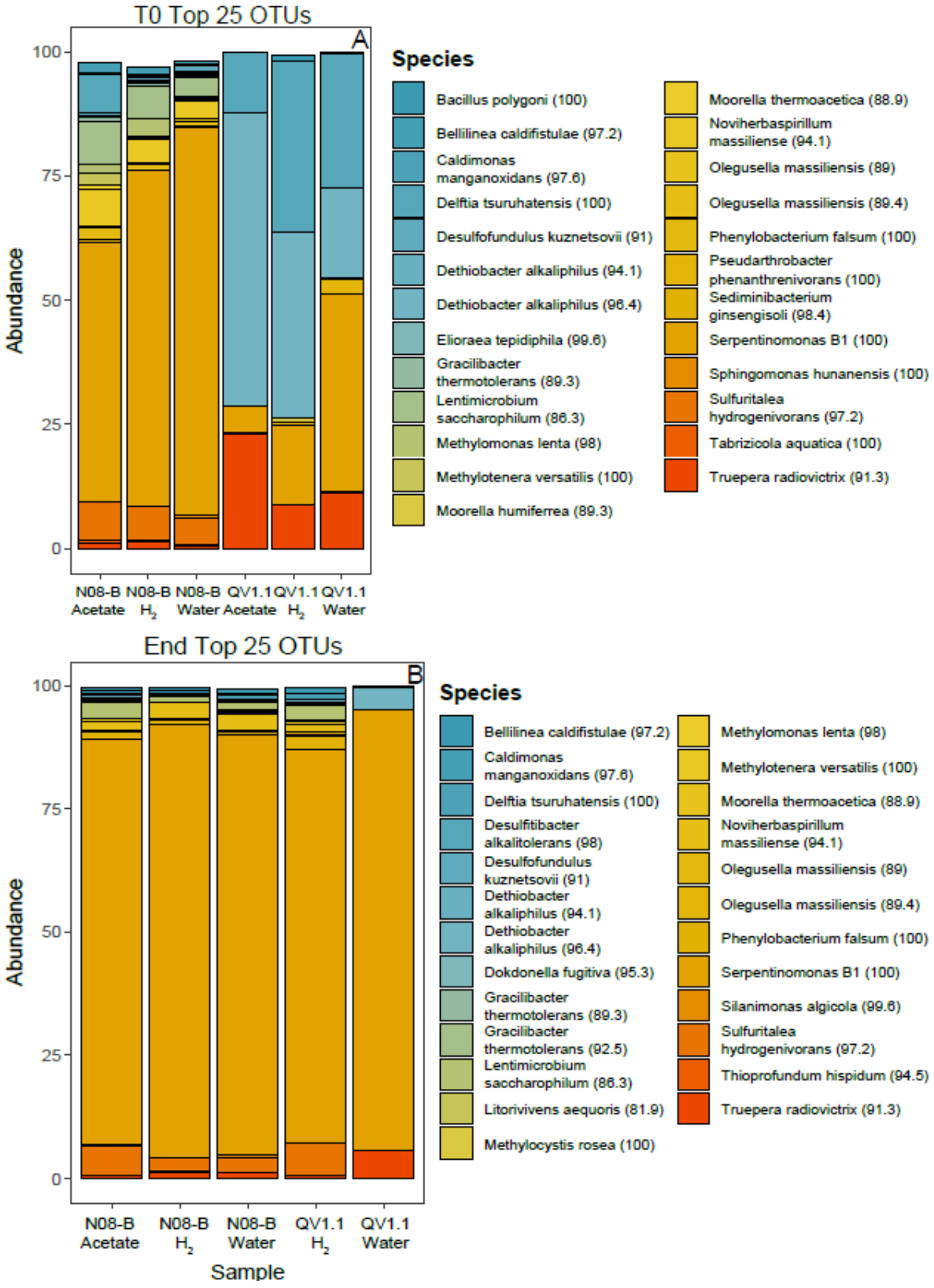

Figure 4.6. Taxonomy of Dominant OTUs in T0 and Final Time Point Microbial Communities.

Figure 4.6. (cont'd).

Stacked bar plots showing the closest known species taxonomic classifications for the 25 most abundant OTUs in initial (A) and final (B) time point samples as determined by assessing the normalized abundance of OTUs in the 16S rRNA gene amplicon dataset. Species classifications were determined using MegaBLAST. The closest known species name classification is listed for each OTU along with the percent pairwise identity of the sequence in question in parentheses following the species name.

Microbial community composition was assessed again at the end of experiments following treatment with sterile oxygenated water, H_2, or acetate. Interestingly, regardless of the source fluid and experimental treatment microbial community compositions became dominated by *Serpentinomonas* strain B1 (79.87-89.40%) (**Fig. 4.6 B**). The abundance of a close relative to *Sulfuritalea hydrogenivorans* remained at relatively stable concentrations in N08-B microcosms and increased in abundance in QV1.1 microcosms treated with H_2 from <1% abundance to 6.44% relative abundance (**Fig. 4.6 B**). The relative abundance of *Dethiobacter alkaliphilus,* and *Delftia tsuruhatensis,* which were dominant community members in T0 samples, decreased substantially in QV1.1 microcosms treated with H_2 and water (**Fig. 4.6 B**). A relative of *Truepera radiovictrix* that was present at high abundances in T0 samples from QV1.1 microcosms (8.92-22.96%), maintained somewhat stable abundance in the QV1.1 microcosms treated with sterile oxygenated water (5.64%) while falling to <1% abundance in microcosms treated with H_2 after constituting close to 9% or of community composition in the initial samples (**Fig. 4.6**). Other dominant taxa in the final time point samples were primarily present at abundances < 1%, with a few lying between 1-2% relative abundance (**Fig. 4.6 B**).

The taxonomy and relative abundance of OTUs detected in samples collected from blanks and experimental controls is plotted in **Fig. C.2** in the **Appendix**. Overall, organisms detected in filtered treatments were primarily organisms commonly identified in bulk fluids sampled from CROMO.

Spreadsheets with the full taxonomic classifications and normalized abundances of the 25 most abundant OTUs in T0 samples (https://doi.org/10.6084/m9.figshare.14669769), final time point samples (https://doi.org/10.6084/m9.figshare.14669784.v1), and filtered treatments (https://doi.org/10.6084/m9.figshare.14677167) are available on FigShare (https://figshare.com/projects/Microcosm_Drilling_Experiments/113787).

Discussion

Overall, the results of microcosm experiments using CROMO groundwater are consistent with the interpretation that a bloom of *Serpentinomonas* strain B1 likely occurred following drilling activity at CROMO in 2011. This interpretation corresponds well with results reported in **Chapter 3**, where an OTU identified as *Serpentinomonas* strain B1 (**Ch. 3**) was identified at extremely high relative abundances in the first two years after drilling and gradually decreased in abundance over time (**Ch. 3**). Additionally, a decrease in the relative abundance of fermentative organisms and CH_4 cycling organisms was observed in the initial two years after drilling in the *in situ* dataset, which is also observed in the experiments reported here (**Ch. 3**). Experimental data show substantial decreases in the relative abundance of sulfur cycling, fermentative, methanotrophic, and methylotrophic organisms such as organisms from the genus *Moorella*, *Methylomonas lenta*, *Methylotenera versatilis*, and sulfur cycling organisms from the Firmicutes phylum including *Dethiobacter alkaliphilus* (**Fig. 4.6 B**). An exception to this trend was the maintained or increased relative abundance of a close relative of the sulfur and H_2 oxidizing organism *Sulfuritalea hydrogenivorans* (58) in all treatments. The capacity of *Serpentinomonas* to flourish and dominate microbial community composition in all experimental treatments and

following drilling at the site (**Ch. 3**), is likely due to their physiological and metabolic versatility (32) which will be further explored here.

Serpentinomonas is a flagellated organism that appears to flourish at oxic-anoxic interfaces in serpentinizing environments (38,42,59). A highly versatile organism, this facultative anaerobe and obligate alkaliphile was originally isolated from serpentinizing springs to the west of the CROMO site at The Cedars, CA (32). *Serpentinomonas* is capable of autotrophic growth using H_2 and calcium carbonate or bicarbonate, aerobic respiration, and heterotrophic growth using a variety of fatty acids and sugars, including acetate (32,42). *Serpentinomonas* can also perform nitrate reduction, thiosulfate oxidation and reduction, and carbon monoxide oxidation (32,42). Interestingly, compared to close relatives within Betaproteobacteria, *Serpentinomonas* has a very small genome (~2.5 Mb) and also contains genes for polyhydroxyalkanoic acid (PHA) synthesis (32). Isolated strains were found to accumulate polyhydroxybutyrate (PHB) when grown mixotrophically on acetate (32).

Given what is known about *Serpentinomonas* from metagenomics and the study of isolates, it is not surprising that these organisms were able to thrive under all three experimental conditions (addition of sterile oxygenated water, H_2, and acetate). In experiments where sterile oxygenated water was added, *Serpentinomonas* was likely able to utilize aerobic respiration, as well as available H_2, for metabolic processes (32,42), whereas dominant community members that are obligate anaerobes likely struggled to handle more oxygen rich conditions, such as close relatives of *Dethiobacter alkaliphilus* (42,60), and more distant relatives of fermentative organisms in the genus *Moorella* (61,62). A close relative to *Truepera radiovictrix* that is commonly observed at CROMO and was abundant in QV1.1 microcosm initial timepoint samples, remained at relatively high abundances (5.64%) at the end of experiments in the QV1.1 microcosms treated with sterile

oxygenated water. The relative of *Truepera radiovictrix* at CROMO has previously been described and is capable of oxygen respiration, as well as H_2 oxidation (42), which would allow these organisms to persist within the QV1.1 microcosms treated with sterile oxygenated water. The type strain of *Truepera radiovictrix* is a non-motile organism (63). If the close relative at CROMO is also non-motile this situation would likely allow for the motile *Serpentinomonas* to access available oxygen and H_2 in solution more effectively than *Truepera.* This notion may explain why *Serpentinomonas* grew substantially more than *Truepera* in QV1.1 microcosms treated with water even though metagenomic information from both organisms indicate that they are both well suited to experimental conditions in water treated microcosms (32,42,63).

Given the close relationship of *Serpentinomonas* to other H_2 oxidizing Betaproteobacteria (32,42) it is not surprising that *Serpentinomonas* thrived in N08-B and QV1.1 microcosms treated with H_2. Additionally, a relative of *Sulfuritalea hydrogenivorans* maintained a relative abundance of ~ 6% in N08-B microcosms treated with H_2 and increased in abundance from <1% to 6.44% relative abundance in QV1.1 microcosms treated with H_2 (**Fig. 4.6 B**). Despite the maintenance of anaerobic conditions and additional H_2 added to experiments, fermentative acetogens present in N08-B fluids and relatives of *Dethiobacter alkaliphilus* did not grow well and instead decreased in relative abundance in microcosms treated with H_2. *Dethiobacter alkaliphilus*, a thiosulfate, sulfur, and polysulfide reducer (60), and *Sulfuritalea hydrogenivorans*, a sulfur oxidizing organism are also both capable of nitrate reduction (42,58,64). While both *Dethiobacter alkaliphilus* and *Sulfuritalea hydrogenivorans* are motile organisms (58,60), nitrate is not often detected in CROMO fluids (< 1 µM) (41) and elemental sulfur and sulfide species (measured as HS^-) are present at <1 - 10 µM concentrations (41). Low availability and sluggish cycling of these chemical species in the microcosm fluids could have limited growth of the relatives of

Dethiobacter alkaliphilus and *Sulfuritalea hydrogenivorans* resulting in their low relative abundances at the end of experiments. Additionally, *Serpentinomonas* may have been able to outcompete these organisms for available H_2. QV1.1 microcosms treated with H_2 showed increased concentrations of acetate over time with respect to controls (**Fig. 4.3 N**). While *Serpentinomonas* is not capable of acetogenesis, other organisms present at lower relative abundances in final samples of the QV1.1 microcosms treated with H_2 are likely capable of producing acetate. *Dethiobacter alkaliphilus* is known to utilize the Wood-Ljungdahl pathway (60), and close relatives of the species present at CROMO are also capable of performing this metabolism (42). A close relative of *Dethiobacter alkaliphilus* was present at 0.67% relative abundance in QV1.1 microcosms treated with H_2. While this organism was not present at high abundances in final samples from these microcosms, they still could have produced the increased acetate concentrations measured in these microcosms, especially when considering that rarer microbial community members can often be implicated in mediating major biogeochemical cycles in natural environments (41,56,65,66). Interestingly, a microbial population related to *Dethiobacter alkaliphilus* was found to flourish and increased in abundance substantially following drilling activity *in situ*, differing from the decrease in relative abundance observed here (**Ch. 3**). *Dethiobacter alkaliphilus* was also present at <0.1% relative abundance in N08-B microcosms treated with H_2, where neither the production nor consumption of acetate was clear (**Fig. 4.3 D**).

Acetate is a small organic compound that is extremely important for sustaining life and carbon cycling in the oligotrophic subsurface (51,53–55). It is an easy substrate for most microorganisms to use in heterotrophic metabolisms (51,55,56). As was seen in all other experimental treatments, *Serpentinomonas* dominated the microbial community composition of

final samples collected from N08-B and QV1.1 microcosms treated with acetate (**Fig. 4.6 B**). Consumption of acetate was clear in QV1.1 microcosms treated with acetate (**Fig. 4.3 P**), while results in N08-B microcosms were more ambiguous, initially showing a decrease in acetate that leveled off from T2 to the end of experiments (**Fig. 4.3 G**). Outside of obligate autotrophs, most organisms in the microbial communities are likely capable of utilizing acetate. While there is not an obvious reason why *Serpentinomonas* dominated as compared to other organisms capable of heterotrophy using acetate, the fact that *Serpentinomonas* was able to dominate microbial community composition in other treatments indicates that these organisms are highly adapted and able to quickly respond to and take advantage of changes in their environment. One interesting aspect of the physiology of *Serpentinomonas* is the formation of PHB granules while growing mixotrophically on acetate (32). Organisms that can form PHB granules form them when carbon is abundant in the environment and some other nutrient such as nitrogen or phosphorus is limited (67). If carbon becomes unavailable in the future, microorganisms can use PHB from the granules as a carbon source, allowing them to continue to persist even under carbon limitation (67). Work done in the last decade has shown that PHB granules play a large role in the capacity to manage cellular stress and extreme conditions, and polyhydroxyalkanoate synthase deletion mutants often fail to survive the harsh conditions where they normally persist (67). Serpentinizing environments have extreme pH and have limited available inorganic carbon and electron acceptors (38,39), requiring a variety of unique physiological adaptations that have previously been described (33). *Serpentinomonas* is metabolically diverse and is also likely better able to deal with environmental stress due to the formation and use of PHB granules (32,67). This versatility potentially gives these organisms a competitive advantage in the environment, allowing them to quickly respond to and benefit from changes in environmental conditions.

While not an initial goal of this study, the observation of microbial growth in 0.1-micron-filtered treatments (**Fig. 4.2 A-C**) required further investigation of filterable microorganisms and methods for setting up experimental controls using environmental fluid samples. Killed controls were not used in this study, as acidifying CROMO fluids or adding a fixative alters the fluid chemistry, which would make chemistry results difficult to assess. Filtered controls using 0.1-micron syringe filters (polyvinylidene fluoride (PVDF) membrane) were chosen over the conventional use of 0.2-micron filters since ultra-small bacteria can pass through the larger pore filters and persist within the filtrate (68–71). Additionally, microorganisms capable of passing through 0.1 micron filters have been identified (72–74) and 0.1 micron PVDF and polyethersulfone filters have been identified as materials more likely to allow ultra-small microorganisms to pass through the filter (74). Ultra-small cells are common in oligotrophic groundwater environments (70,71,75) and in candidate phyla within the candidate phyla radiation (69,70,76). Given the prevalence of ultra-small microorganisms in groundwater environments, future experimental studies using groundwater should consider utilizing 0.1 micron filters constructed of polycarbonate or mixed cellulose esters, which were found to capture more ultra-small cells (74). Another contributing factor could be that microbial biomass for molecular extractions was collected using centrifugation (see Materials and Methods). If samples had been collected using filtration (using a 0.2 micron PES Sterivex filter), filterable bacteria may have passed through the filter and never been detected within blank and control samples.

Overall, results from this study reveal mechanisms behind geochemical changes observed *in situ* at CROMO following drilling activity in 2011 (**Ch. 3**). Following the injection of oxygenated water during drilling, organisms from the candidate genus *Serpentinomonas* flourished under more aerobic conditions, utilizing aerobic respiration (32) (**Fig. 4.6 B**). Additionally, water

injected into the subsurface likely reacted with ultramafic lithologies generating H_2 during serpentinization (30,31,77). Alternatively, injected water may have mobilized and flushed H_2 trapped within microscopic pore spaces in the hard rock aquifer. Biological production of H_2 did not occur in microcosms treated with sterile oxygenated water (**Fig. 4.3 B & K**). This finding is not surprising seeing as [FeFe] hydrogenase enzymes require anaerobic conditions and can easily be inactivated by trace amounts of oxygen (49). Increased concentrations of H_2, likely produced through water rock reactions (30,31,77), were utilized by *Serpentinomonas* as these organisms continued to flourish and was potentially used to a lesser extent in wells with abundant populations of *Dethiobacter alkaliphilus* to fuel acetate production via the Wood Ljungdahl pathway (42,60) (**Fig. 4.3 D, E, M, & N; Fig. 4.6 B**). *Serpentinomonas*, which was already present at a high abundance, was then able to use acetate for heterotrophic growth, likely outcompeting other facultative and obligate heterotrophs in the system for this easily metabolized source of organic carbon (**Fig. 4.3 G & P; Fig. 4.6 B**). These results corroborate observations from the *in situ* dataset (**Ch. 3**) and highlight the versatility of *Serpentinomonas* and its capability to respond to and thrive under the altered environmental conditions explored here. These results provide a basis for improving our understanding of geochemical and microbial community datasets obtained from recently drilled serpentinizing systems (45,46) and will inform future decisions related to drilling into and accessing the deep subsurface to sample and experiment on the microbial communities hosted there.

Materials and Methods

Sample Collection

Fluids used in experiments were collected from two different CROMO wells, QV1.1 and N08-B. The N08-B well (26.2 m) was drilled >30 years ago, while the QV1.1 well (23 m) was drilled nearby in August of 2011 (33,44). The sampled wells are drilled into the serpentinite mélange of the Coast Range Ophiolite along with a series of ten other wells drilled to various depths (7-76 m) (33,38,41,44). Well fluids are sampled from the subsurface using permanently emplaced positive displacement Teflon bladder pumps (Geotech Environmental Equipment, Denver, CO, USA) (38,41,57). Fluids pass through a YSI 3059 flow-through cell attached to a YSI multiprobe (Yellowsprings, OH, USA) that measures pH, ORP, DO, specific conductance, and temperature (38,41,57). Well fluids are purged until fluid temperature and DO stabilizes, after which fluids are sampled from tubing attached directly to the flow-through cell.

Fluids for microcosm experiments were collected during August of 2019. Fluids were collected anoxically in 60 mL syringes via a series of 3-way stopcocks attached directly to the pump tubing via a luer lock attachment. Syringes were field rinsed using well fluid to avoid contamination of anoxic well fluids with air. Fluids were injected into sterilized, nitrogen flushed, 0.5 L Pyrex bottles containing nitrogen at a pressure of 1 atm with sterile butyl rubber stoppers. A vent needle with a 0.2 µm syringe filter attached was used to allow nitrogen gas to escape the bottle as fluid displaced gas in the bottle. Water was added to bottles until all gas was displaced and fluid began to come out of the vent needle. To minimize contamination, butyl rubber stoppers were wiped with 70% ethanol prior to being pierced by a needle. Three experimental treatments were planned for fluids from the QV1.1 and N08-B wells. Sixteen 0.5 L bottles were filled completely (zero available headspace) with fluid at each well, providing a single live control, triplicate

experimental replicates, and duplicate 0.1 µm filtered (0.1 µm Millex© PVDF syringe filter (MilliporeSigma, Burlington, MA, USA)) controls for each experimental treatment. While triplicate filtered and live controls would be ideal, available fluid for sampling at CROMO wells is limited. Wells are occasionally pumped dry during sampling. Normally, 8-12 L of fluid are removed from wells in total during normal geochemical and molecular microbiology sampling. Based on this limitation we were conservative (8 additional liters) in the additional amount of water collected from the wells for experiments to ensure that there would be enough fluid for experiments as well as annually collected geochemical and molecular biology samples. Filled bottles were placed in a cooler with ice packs and stored in the dark at 4℃ prior to the start of experiments upon return to the lab.

Microcosm Experiment Set-Up and Subsampling Procedures

Microcosm experimental treatments were set up to mimic the three primary geochemical changes observed *in situ* following drilling activity at the site in August of 2011 (**Ch. 3**). The use of sterile oxygenated water as a drilling fluid increased DO concentrations and ORP conditions within the subsurface. Following the injection of water into the subsurface, increased H_2 (> 0.25 µM) and acetate (> 5 µM) concentrations were observed, which then decreased back to normally observed concentrations (< 0.25 µM H_2 and < 1 µM acetate) approximately two years after drilling (**Ch. 3**). Experimental treatments were set up to mimic the estimated subsurface volume that injected drilling fluid saturated and the maximum H_2 and acetate concentrations observed *in situ* following drilling. Calculations performed by Ortiz and colleagues (78) indicate that 70.04 m^3 of injected fluid at each new well saturated on average 4,200 m^3 of the subsurface. This volume results in a 1:60 ratio of injected to saturated volume which was used to calculate the amount of

water (7.5 mL) added to experimental water treatment microcosms (500 mL). Instrument grade H_2 was added to experimental H_2 treatment microcosms at 1 atm pressure to match peak measured H_2 concentrations in QV1.1 (1.08 µM) and N08-B (0.4 µM). A sterile 1 mM solution of sodium acetate was added to experimental acetate treatment microcosms to match peak measured acetate concentrations in QV1.1 (16.05 µM) and N08-B (0.67 µM).

Bottles for microcosm experiments were stored in the dark at 4°C upon return to the lab. The day before T0 samples were collected and experimental treatments were started, experimental and control bottles collected at each well were randomly assigned to experimental treatments. Bottles were also moved to a dark, room temperature cabinet and 50 mL of water was removed from all bottles using sterile nitrogen flushed syringes to allow dissolved gases to equilibrate with the headspace volume. Instrument grade nitrogen was used to displace fluid volume in the bottles. Microcosms were sampled prior to the addition of treatments to collect data on starting conditions in the microcosm bottles. Following the addition of treatments, microcosms were subsampled once every two weeks for two months to collect headspace H_2 and CH_4 samples, acetate samples, and samples for cell enumeration (**Fig. 4.1**). Biomass samples for DNA extraction were collected prior to the addition of treatments (T0) and after the final time point at 2 months (**Fig. 4.1**).

Headspace gas samples were collected using a sterile 20 mL syringe fitted with a one-way luer lock attachment stopcock. The syringe and sampling needle were flushed with instrument grade nitrogen prior to sampling. With the stopcock closed, the needle was pushed through the stopper of the upright bottle. The stopcock was then opened allowing gas to fill the syringe until 15 mL of gas had been sampled. The stopcock was then closed, and the syringe was removed. Gas samples were transferred to exetainers containing 20% v/v sodium chloride solution, displacing a

portion of the solution through a vent needle (66). Exetainers were stored upside down at room temperature to minimize the loss of gas via diffusion prior to analysis (66). Aqueous samples for acetate analyses and cell enumeration were collected using a sterile 30 mL syringe with a one-way luer lock attachment stopcock. The syringe and stopcock were flushed and then filled 30 mL of instrument grade nitrogen. Holding the bottles upside down, nitrogen gas was injected into the bottle (to displace the volume of fluid and gas sampled from the bottle) and then 15 mL of fluid was collected in the syringe. 1.5 mL of fluid for cell enumeration was added directly to a 2 mL microcentrifuge tube containing 150 µL of 37% formalin (38). Then a 0.2 µm syringe filter was attached to the syringe and primed by pushing 2 mL of fluid through it. 10 mL of 0.2 µm filtered fluid was collected for acetate analyses (57) in ion chromatography (IC) vials that had been washed and triple rinsed in MilliQ water. Cell enumeration samples were vortexed to disperse formalin through the sample and stored at room temperature. Acetate samples were stored at -20°C.

Biomass for DNA extraction from T0 samples was collected using a sterile 60 mL syringe fitted with a one-way luer lock attachment stopcock. Syringes were flushed and then filled with instrument grade nitrogen. Holding the microcosm bottles upside down, 50 mL of nitrogen gas was injected into the bottle to displace the volume of fluid being sampled and 50 mL of fluid was allowed to fill the syringe. Sampled fluid was transferred to sterilized 50 mL Oak Ridge centrifuge tubes and centrifuged at 10,000 × *g* for 20 min. at 4°C. Following centrifugation fluid was decanted from the Oak Ridge tubes and 1.8 mL of sterile phosphate buffered saline (PBS) was added to the tube. Tubes were vortexed for 1 min. to resuspend the biomass in PBS and then transferred to a 2 mL microcentrifuge tube. Samples were centrifuged again at 10,000 × *g* for 20 min. at 4°C. PBS was decanted from the microcentrifuge tubes. Cell pellets were flash frozen on dry ice and then stored at -80°C. Biomass samples collected from remaining fluid (200 mL) at the end of

experiments were poured into sterile 50 mL Oak Ridge tubes after butyl rubber stoppers were removed from microcosm bottles. Samples were centrifuged and resuspended in PBS as described above. Resuspended biomass from the 200 mL (separated into 4 Oak Ridge tubes) was pelleted into a single 2 mL microcentrifuge tube by pelleting 1.8 mL of the resuspended biomass at a time (pelleting and then decanting 1.8 mL of PBS suspended biomass from the 4 Oak Ridge centrifuge tubes needed to collect 200 mL from a single microcosm bottle in series in a single 2 mL microcentrifuge tube). Cell pellets were flash frozen on dry ice and stored at -80°C. During all subsampling, butyl rubber stoppers on microcosm bottles were cleaned with 70% ethanol prior to being pierced by a sampling needle to minimize contamination.

Geochemical Analyses

Headspace gas samples were analyzed using gas chromatography (GC). H_2 samples were measured using a Trace Analytical RGA3 Reduced Gas Analyzer with a reduced gas detector and CH_4 samples were analyzed using an SRI 8610C GC (SRI Instruments, Torrance, CA, USA) equipped with a flame ionizing detector (FID) (38,41,57).

Acetate samples were sent to the University of Michigan Biological Station Analytical Lab (Pellston, MI, USA) for analysis using IC. A Dionex high-performance IC (Dionex, Sunnyvale, CA, USA) paired with a UV/VIS detector was used to measure acetate concentrations. Due to the high salinity of CROMO fluids (41) a Dionex™ InGuard™ Ag Cartridge (Dionex, Sunnyvale, CA, USA) was used to strip chloride from the samples prior to injection onto the IC column.

Cell Enumeration

Cell enumeration was performed as previously described (38,79). Briefly, fluids preserved in 37% formalin were filtered through 0.2 µm black polycarbonate filters (Millipore, Billerica, MA, USA), stained with 1 µg/mL 4',6-diamidino-2-phenylindole (DAPI), and mounted onto microscope slides (38,79). Cells captured on the slide were counted using epifluorescence microscopy according to previously published protocols (79).

Extraction of DNA

DNA extractions from cell pellets were performed as previously described (33,38,41,42)with slight modifications (microbial cells were pelleted not captured on 0.2 µm Sterivex filters). Briefly, cell pellets were lysed using freeze/thaw cycles paired with chemical and physical lysis. DNA was purified through a series of phenol/chloroform extractions, precipitated with ethanol, and resuspended in Tris low-ethylenediaminetetraacetic acid. DNA was purified using the Genomic DNA Clean & Concentrate Kit (Zymo Research, Irvine, CA, USA) and quantified using the High Sensitivity dsDNA Assay Kit on a Qubit fluorometer (Invitrogen, Carlsbad, CA, USA) as previously described (33,41,42).

16S rRNA Gene Amplicon Sequencing

Total genomic DNA was submitted to the Michigan State University (MSU) Genomics Core for sequencing of the V4 region of the 16S rRNA gene (515F/806R primers) using an Illumina MiSeq instrument (Illumina, San Diego, CA, USA) as previously described (41). Procedures for amplification, quantification, and sequencing of the 16S rRNA gene performed by the MSU Genomics Core were previously described by Sabuda and colleagues (41).

16S rRNA Sequence Processing

Sequences generated by the MSU Genomics Core were processed using mothur v1.39.5 (80) as previously described (41). Briefly, VSEARCH v2.6.2 (81) was used to filter and merge paired-end sequence reads. Additional filtering of chimeric sequences and sequences with ambiguous bases and homopolymers was performed in mothur as previously described (41). Pre-clustering of sequences to remove rare sequences that are most likely the result of sequencing errors (82) was performed as previously described (41). Pre-clustered sequences were then clustered into OTUs at a 3% distance threshold using mothur's implementation of the *de novo* distance-based greedy clustering method (83). Clustered OTUs were aligned to the SILVA SSURef alignment (v138) and taxonomic classifications were performed in mothur.

16S rRNA gene amplicon sequence data from the microcosm experiments were processed and clustered into OTUs with samples collected from 2011-2017 that directly assessed fluid microbial community composition changes observed following drilling. After clustering the sequences (19,155 OTUs and 10,847,024 reads) basic filtering of sequences classified as eukaryotes, archaea, unknown, mitochondria, and chloroplasts was performed. Additionally, sequences were screened for potential contaminants associated with human skin and feces, and DNA extraction reagents that are commonly identified in deep subsurface samples (84) as previously described (33,42,85). A detailed description of the contaminant filtering process is described in **Chapter 3**. After contaminant filtering, the final 16S rRNA dataset consisted of 9,762 OTUs and 10,614,878 reads (retained 97.86% of reads). Samples from the microcosm experiments analyzed here account for 366 OTUs and 5,947,999 of the reads (56.03%) in the total dataset. Species classifications were performed using MegaBLAST (86) as described in **Chapter 3**. Initial exploration of the microbial community data revealed that biological replicates sequenced to

similar depths and displayed similar alpha and beta diversity. Based on this similarity, replicates were collapsed into a single sample to provide a more comprehensive picture of the microbial communities in each experimental treatment (14).

Data files and R scripts used to contaminant filter the 16S rRNA sequence dataset are available on FigShare (https://figshare.com/projects/Drilling_Disturbance_in_a_Serpentinizing_Ophiolite/113898).

Statistical Analyses

Statistical analyses and visualization of geochemical data, cell abundance data, and microbial community data were performed using the R computing environment (87). Geochemistry and cell abundance data were visualized and plotted using the R package ggplot2 (88). Exploration and analysis of microbial community data and associated metadata were performed using the R packages vegan (89) and phyloseq (90). R scripts, excel and csv files used in analyses are available on FigShare (https://figshare.com/projects/Microcosm_Drilling_Experiments/113787). PERMANOVA analyses were performed using the adonis() function in vegan (89). Bray-Curtis dissimilarities were ordinated using NMDS in phyloseq (90). Plotting of the NMDS ordination, fitting of environmental vectors, and scaling of vectors based on significant PERMANOVA results was performed as previously described (33). Sample richness and Pielou's evenness index were calculated as previously described (33). Phylogeny bar plots plotting the normalized abundance of OTUs based on their taxonomic classification were created using the plot_bar() function in phyloseq (90).

Acknowledgements

Thank you to Cathy Koehler and Paul Aigner, Co-directors of the University of California - Davis McLaughlin Reserve for their support and help in establishing CROMO and continued field work at the site. Special thanks to the summer of 2019 CROMO field sampling team including Mike Kubo and students, Dawn Cardace and students, and Dylan Mankel who helped anoxically fill experimental bottles used in this work. This work was supported by the NASA Astrobiology Institute CAN-7 Rock Powered Life Grant #NNA15BB02A and the Dr. Marvin Hensley Endowed Fellowship in Science (Michigan State University College of Natural Science).

APPENDIX

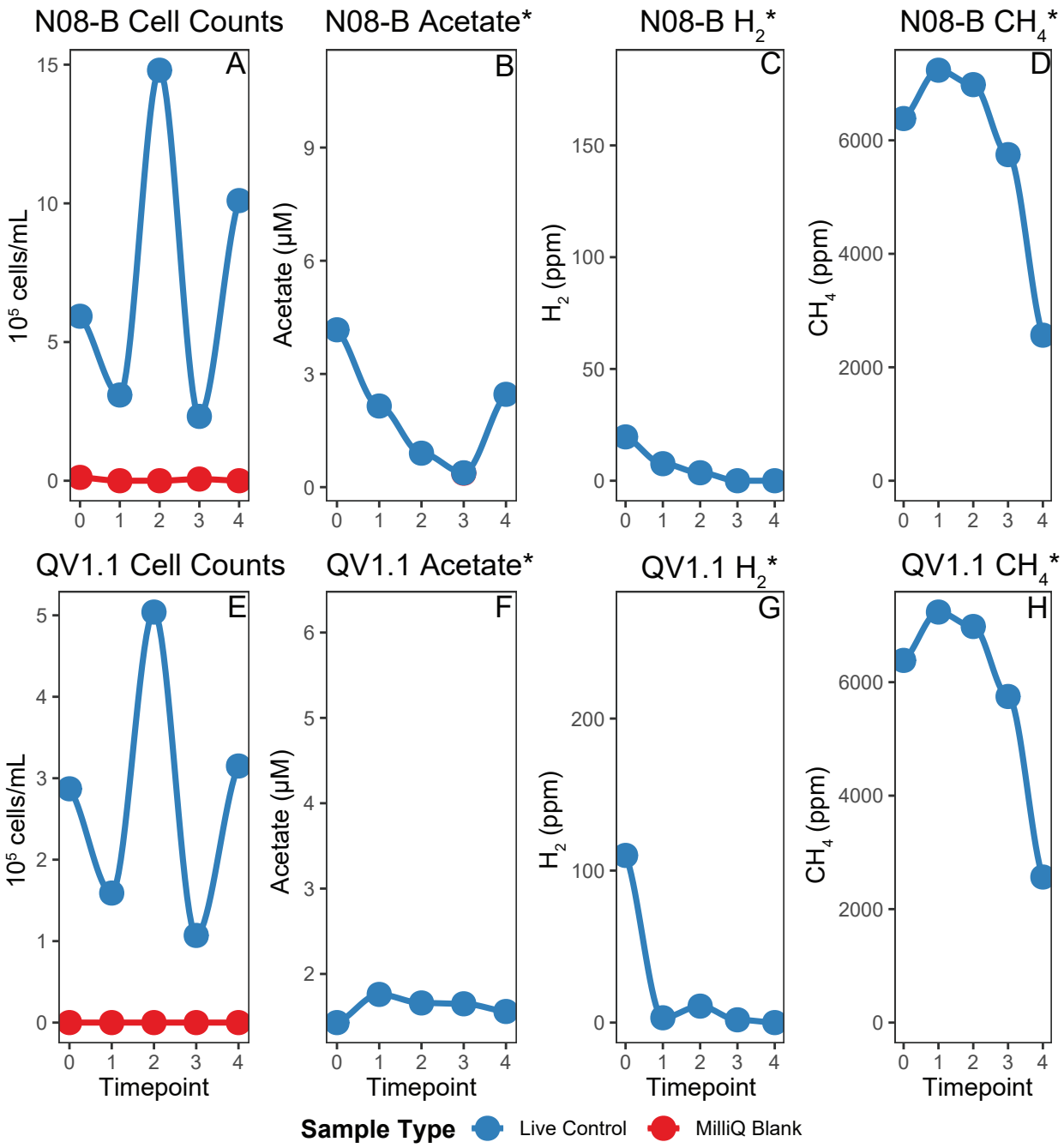

*Blank data not plotted for geochemical measures, sample data was adjusted where necessary based on blanks

Figure C.1. Control Cell Abundance and Geochemistry Plots.

Plots showing microbial abundance in 105 cells/mL (A, E), the concentration of acetate (B, F), hydrogen (C, G), and methane (D, H) at each of the sampling time points (T0, T1, T2, T3, T4) for N08-B (A-D) and QV1.1 (E-H) blank and live control microcosms. Samples were collected every two weeks (Fig. 4.1).

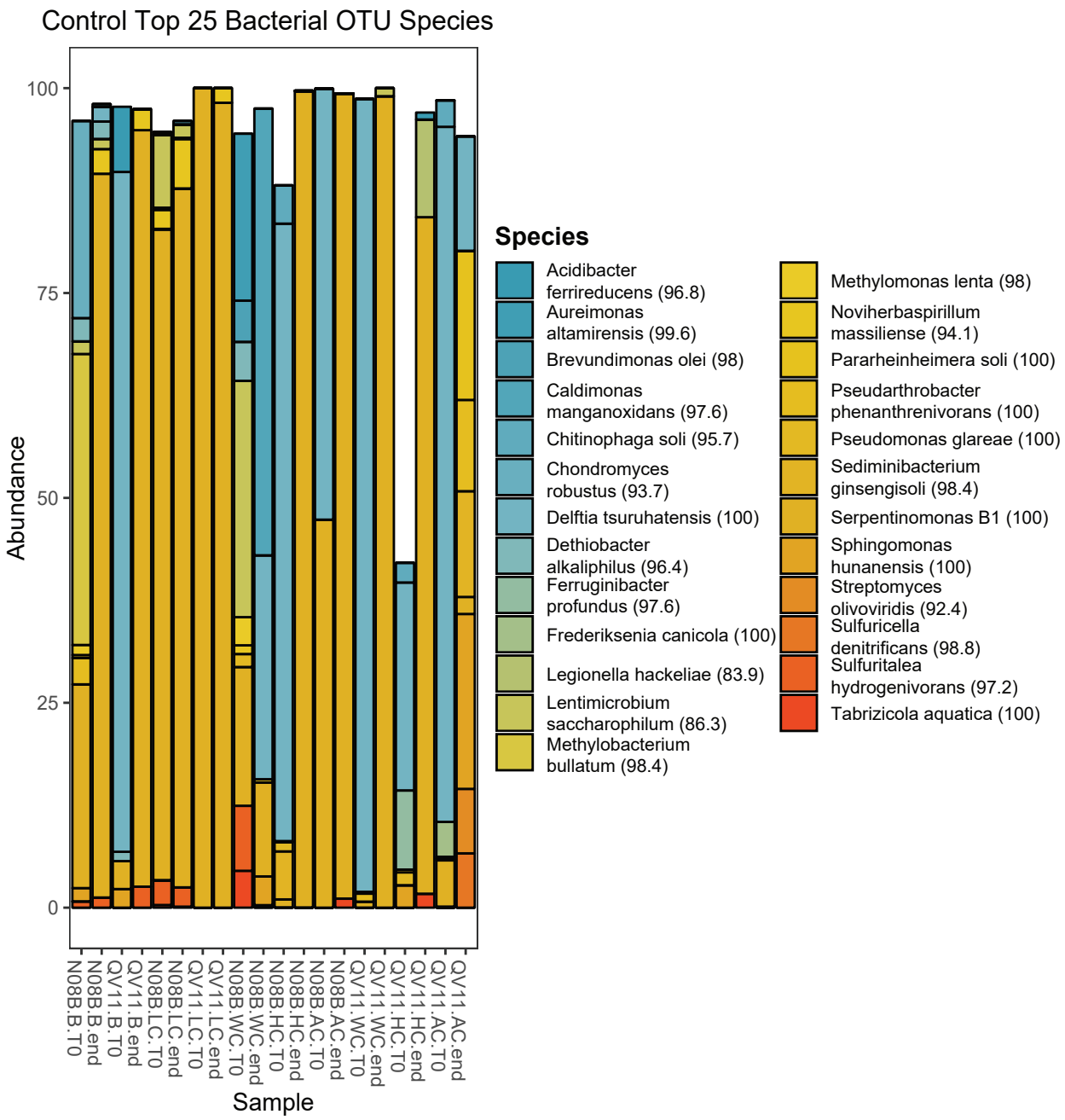

Figure C.2. Taxonomy of Dominant OTUs in T0 and Final Time Point Controls.

Stacked bar plot showing the closest known species taxonomic classifications for the 25 most abundant OTUs in initial and final time point samples from blanks, live controls, and 0.1 micron filtered treatments as determined by assessing the normalized abundance of OTUs in the 16S rRNA gene amplicon dataset. Species classifications were determined using MegaBLAST. The closest known species name classification is listed for each OTU along with the percent pairwise identity of the sequence in question in parentheses following the species name.

Table C.1. Averaged Microcosm Metadata.

Well	Treatment	Timepoint	Cell Abundance (10^5 cells/mL)*	Headspace H_2 (ppm)	Headspace CH_4 (ppm)	Acetate (μM)
N08B	Water	0	4.72	20.99	18863.96	3.52
N08B	Water	1	5.57	30.21	11266.16	3.30
N08B	Water	2	6.97	22.87	9964.93	1.72
N08B	Water	3	9.02	16.33	6802.16	2.17
N08B	Water	4	7.31	7.24	5373.35	2.23
N08B	Water Control	0	0.49	25.70	14009.60	2.75
N08B	Water Control	1	0.47	7.93	16719.78	2.71
N08B	Water Control	2	0.52	2.53	9287.32	1.65
N08B	Water Control	3	0.21	2.34	6938.63	2.67
N08B	Water Control	4	0.20	0.60	4778.70	0.96
N08B	Hydrogen	0	4.69	25.01	20249.60	3.05
N08B	Hydrogen	1	3.86	44.56	15834.02	2.93
N08B	Hydrogen	2	5.49	51.13	9570.30	2.24
N08B	Hydrogen	3	5.07	38.14	5833.31	2.72
N08B	Hydrogen	4	5.71	13.47	5147.65	1.86
N08B	Hydrogen Control	0	0.00	13.77	22573.73	4.09
N08B	Hydrogen Control	1	2.48	69.12	15108.97	3.09
N08B	Hydrogen Control	2	14.10	64.12	9180.23	3.49
N08B	Hydrogen Control	3	12.41	49.26	5138.01	3.14
N08B	Hydrogen Control	4	3.32	19.25	4232.94	4.46
N08B	Acetate	0	5.32	27.40	21270.27	4.22
N08B	Acetate	1	3.97	59.46	13359.30	2.23
N08B	Acetate	2	5.57	37.18	7715.10	2.05
N08B	Acetate	3	12.54	41.84	5891.91	2.97
N08B	Acetate	4	6.07	3.75	4630.47	2.90
N08B	Acetate Control	0	2.57	31.10	21388.98	2.42
N08B	Acetate Control	1	2.00	31.48	11565.80	0.49
N08B	Acetate Control	2	3.84	32.22	10435.29	2.07
N08B	Acetate Control	3	5.98	31.54	3253.71	2.66
N08B	Acetate Control	4	8.37	7.80	5375.21	1.60

Table C.1. (cont'd).

Well	Treatment	Timepoint	Cell Abundance (10^5 cells/mL)*	Headspace H_2 (ppm)	Headspace CH_4 (ppm)	Acetate (μM)
QV1.1	Water	0	2.26	136.21	8996.09	0.91
QV1.1	Water	1	3.57	23.35	8156.03	1.89
QV1.1	Water	2	5.74	15.57	4317.02	0.71
QV1.1	Water	3	5.59	10.71	2427.69	1.31
QV1.1	Water	4	8.31	1.86	1793.94	0.51
QV1.1	Water Control	0	0.08	100.27	11932.13	0.78
QV1.1	Water Control	1	0.02	156.84	8958.04	0.85
QV1.1	Water Control	2	0.05	124.37	4797.16	0.89
QV1.1	Water Control	3	0.66	71.24	2862.63	2.84
QV1.1	Water Control	4	0.00	84.67	1861.43	1.70
QV1.1	Hydrogen	0	4.45	134.62	11338.19	1.28
QV1.1	Hydrogen	1	5.53	87.20	7941.14	1.48
QV1.1	Hydrogen	2	6.15	27.59	3814.90	2.34
QV1.1	Hydrogen	3	7.37	40.31	3164.71	1.56
QV1.1	Hydrogen	4	7.87	13.04	2084.70	2.81
QV1.1	Hydrogen Control	0	0.03	122.54	11866.61	1.51
QV1.1	Hydrogen Control	1	0.00	327.46	7163.49	2.04
QV1.1	Hydrogen Control	2	0.00	198.89	4212.44	0.61
QV1.1	Hydrogen Control	3	0.11	148.22	2314.51	1.27
QV1.1	Hydrogen Control	4	0.00	111.08	2534.98	0.79
QV1.1	Acetate	0	3.72	160.12	11974.36	1.50
QV1.1	Acetate	1	2.73	13.72	5012.23	10.59
QV1.1	Acetate	2	5.93	7.65	4127.83	10.56
QV1.1	Acetate	3	10.25	1.30	3253.30	6.30
QV1.1	Acetate	4	9.00	1.59	2094.87	4.04
QV1.1	Acetate Control	0	0.02	182.80	14566.68	0.38
QV1.1	Acetate Control	1	0.00	260.51	6706.53	15.39
QV1.1	Acetate Control	2	0.00	174.76	4928.93	20.80
QV1.1	Acetate Control	3	0.12	142.08	3375.87	13.40
QV1.1	Acetate Control	4	0.02	80.40	3117.24	25.72

* = cell count data was converted from cells/mL to 10^5 cells/mL for averaged data to improve readability of plot axes.

Table C.2. Raw Microcosm Metadata.

Well	Treatment	Biological Replicate	Timepoint	Cell Abundance (cells/mL)	Headspace H_2 (ppm)	Headspace CH_4 (ppm)	Acetate (μM)
N08-B	Water	1	0	5.04E+05	44.73	26275.61	3.75
N08-B	Water	2	0	5.44E+05	1.21	14186.11	3.66
N08-B	Water	3	0	3.67E+05	17.04	16130.17	3.15
N08-B	Water Control	1	0	6.11E+03	24.14	17763.12	2.95
N08-B	Water Control	2	0	9.17E+04	27.26	10256.08	2.56
N08-B	Water	1	1	3.30E+05	8.56	14689.75	3.27
N08-B	Water	2	1	0.00E+00	78.28	6165.07	4.42
N08-B	Water	3	1	1.34E+06	3.78	12943.67	2.20
N08-B	Water Control	1	1	3.06E+04	12.39	18021.24	3.29
N08-B	Water Control	2	1	7.33E+04	3.48	15418.32	2.14
N08-B	Water	1	2	1.13E+06	0.22	12808.16	1.31
N08-B	Water	2	2	4.92E+05	68.40	8790.45	2.36
N08-B	Water	3	2	4.68E+05	0.00[a]	8296.17	1.51
N08-B	Water Control	1	2	3.06E+03	5.06	8950.33	1.75
N08-B	Water Control	2	2	1.01E+05	0.00[a]	9624.31	1.56
N08-B	Water	1	3	9.69E+05	0.00[a]	9498.22	1.92
N08-B	Water	2	3	1.44E+06	48.99	5278.34	3.10
N08-B	Water	3	3	2.96E+05	0.00[a]	5629.91	1.49
N08-B	Water Control	1	3	1.22E+04	4.67	7168.48	3.56
N08-B	Water Control	2	3	3.06E+04	0.00[a]	6708.78	1.78
N08-B	Water	1	4	1.44E+06	0.00[a]	7361.96	1.39
N08-B	Water	2	4	2.57E+05	21.72	4154.41	4.39
N08-B	Water	3	4	4.95E+05	0.00[a]	4603.69	0.90
N08-B	Water Control	1	4	3.06E+03	1.21	5466.34	1.48
N08-B	Water Control	2	4	3.67E+04	0.00[a]	4091.06	0.45
N08-B	Hydrogen	1	0	7.06E+05	60.06	13762.79	2.66
N08-B	Hydrogen	2	0	2.72E+05	4.87	18888.58	3.25
N08-B	Hydrogen	3	0	4.28E+05	10.09	28097.45	3.22
N08-B	Hydrogen Control	1	0	0.00E+00	10.40	25141.52	4.08
N08-B	Hydrogen Control	2	0	0.00E+00	17.14	20005.93	4.10
N08-B	Hydrogen	1	1	2.08E+05	43.77	13001.12	3.92
N08-B	Hydrogen	2	1	6.17E+05	24.02	15780.11	2.20
N08-B	Hydrogen	3	1	3.33E+05	65.90	18720.84	2.66
N08-B	Hydrogen Control	1	1	6.72E+04	18.29	16718.97	0.64
N08-B	Hydrogen Control	2	1	4.28E+05	119.94	13498.98	5.53
N08-B	Hydrogen	1	2	4.22E+05	84.72	8060.58	3.61
N08-B	Hydrogen	2	2	8.80E+05	19.16	9761.14	1.70

Table C.2. (cont'd).

Well	Treatment	Biological Replicate	Timepoint	Cell Abundance (cells/mL)	Headspace H_2 (ppm)	Headspace CH_4 (ppm)	Acetate (μM)
N08-B	Hydrogen	3	2	3.45E+05	49.51	10889.19	1.41
N08-B	Hydrogen Control	1	2	8.19E+05	10.69	10277.59	1.14
N08-B	Hydrogen Control	2	2	2.00E+06	117.55	8082.86	5.85
N08-B	Hydrogen	1	3	2.51E+05	80.74	5889.35	4.14
N08-B	Hydrogen	2	3	6.97E+05	2.69	5777.27	1.88
N08-B	Hydrogen	3	3	5.74E+05	31.01	**broken**	2.15
N08-B	Hydrogen Control	1	3	5.62E+05	3.37	4762.11	2.17
N08-B	Hydrogen Control	2	3	1.92E+06	95.15	5513.92	4.12
N08-B	Hydrogen	1	4	4.64E+05	30.14	4310.96	4.29
N08-B	Hydrogen	2	4	6.26E+05	2.25	5086.85	0.21
N08-B	Hydrogen	3	4	6.23E+05	8.01	6045.14	1.07
N08-B	Hydrogen Control	1	4	3.39E+05	3.02	4945.09	4.32
N08-B	Hydrogen Control	2	4	3.24E+05	35.47	3520.79	4.59
N08-B	Acetate	1	0	7.21E+05	22.63	26307.32	3.27
N08-B	Acetate	2	0	4.19E+05	27.54	22519.94	2.95
N08-B	Acetate	3	0	4.55E+05	32.04	14983.56	6.44
N08-B	Acetate Control	1	0	5.13E+05	16.41	19810.56	2.00
N08-B	Acetate Control	2	0	0.00E+00	45.79	22967.41	2.85
N08-B	Acetate	1	1	7.79E+05	7.72	16713.58	0.18
N08-B	Acetate	2	1	1.04E+05	67.46	17513.79	2.59
N08-B	Acetate	3	1	3.09E+05	103.21	5850.53	3.93
N08-B	Acetate Control	1	1	2.35E+05	61.80	17468.87	0.20
N08-B	Acetate Control	2	1	1.65E+05	1.16	5662.72	1.17
N08-B	Acetate	1	2	7.46E+05	0.00[a]	9128.63	1.56
N08-B	Acetate	2	2	6.63E+05	46.07	7021.41	1.85
N08-B	Acetate	3	2	2.63E+05	65.47	6995.24	2.73
N08-B	Acetate Control	1	2	6.45E+05	64.45	10575.63	2.22
N08-B	Acetate Control	2	2	1.22E+06	0.00[a]	10294.96	1.92
N08-B	Acetate	1	3	9.63E+05	0.00[a]	6105.32	1.46
N08-B	Acetate	2	3	1.29E+06	53.72	7224.67	3.34
N08-B	Acetate	3	3	1.51E+06	71.81	4345.75	4.12
N08-B	Acetate Control	1	3	8.56E+05	63.08	4445.52	2.83
N08-B	Acetate Control	2	3	3.39E+05	0.00[a]	2061.90	2.49
N08-B	Acetate	1	4	9.08E+05	0.00[a]	5298.09	1.48
N08-B	Acetate	2	4	7.70E+05	6.09	4857.47	3.34
N08-B	Acetate	3	4	1.44E+05	5.17	3735.85	3.90
N08-B	Acetate Control	1	4	1.23E+06	15.60	5661.14	2.09
N08-B	Acetate Control	2	4	4.43E+05	0.00[a]	5089.27	1.12

Table C.2. (cont'd).

Well	Treatment	Biological Replicate	Timepoint	Cell Abundance (cells/mL)	Headspace H_2 (ppm)	Headspace CH_4 (ppm)	Acetate (μM)
QV1.1	Water	1	0	2.14E+05	155.77	9221.17	0.2853
QV1.1	Water	2	0	1.68E+05	116.72	7531.12	1.62
QV1.1	Water	3	0	2.96E+05	136.15	10235.97	0.81
QV1.1	Water Control	1	0	3.06E+03	111.88	10768.04	1.18
QV1.1	Water Control	2	0	1.22E+04	88.66	13096.22	0.37
QV1.1	Water	1	1	6.75E+05	0.00[a]	9306.72	1.09
QV1.1	Water	2	1	2.29E+05	3.16	6938.17	2.05
QV1.1	Water	3	1	1.68E+05	66.88	8223.20	2.54
QV1.1	Water Control	1	1	0.00E+00	147.44	7809.11	1.41
QV1.1	Water Control	2	1	3.06E+03	166.24	10106.97	0.29
QV1.1	Water	1	2	6.29E+05	0.00[a]	4864.25	0.95
QV1.1	Water	2	2	5.87E+05	2.07	3292.39	0.32
QV1.1	Water	3	2	5.07E+05	44.65	4794.42	0.86
QV1.1	Water Control	1	2	0.00E+00	138.31	4447.34	0.56
QV1.1	Water Control	2	2	9.17E+03	110.43	5146.98	1.22
QV1.1	Water	1	3	5.62E+05	0.00[a]	2934.07	1.43
QV1.1	Water	2	3	6.26E+05	0.00[a]	1678.18	1.39
QV1.1	Water	3	3	4.89E+05	32.13	2670.81	1.12
QV1.1	Water Control	1	3	7.03E+04	69.69	2785.68	**broken**
QV1.1	Water Control	2	3	6.11E+04	72.78	2939.58	2.84
QV1.1	Water	1	4	6.23E+05	0.00[a]	1260.38	0.49
QV1.1	Water	2	4	1.32E+06	0.00[a]	1649.66	0.32
QV1.1	Water	3	4	5.50E+05	5.59	2471.79	0.73
QV1.1	Water Control	1	4	0.00E+00	76.03	2464.52	0.59
QV1.1	Water Control	2	4	0.00E+00	93.31	1258.35	2.81
QV1.1	Hydrogen	1	0	1.89E+05	120.19	12602.45	0.54
QV1.1	Hydrogen	2	0	4.68E+05	126.05	11076.30	1.10
QV1.1	Hydrogen	3	0	6.78E+05	157.61	10335.81	2.20
QV1.1	Hydrogen Control	1	0	3.06E+03	143.78	10273.21	0.57
QV1.1	Hydrogen Control	2	0	3.06E+03	101.29	13460.00	2.44
QV1.1	Hydrogen	1	1	6.11E+05	114.75	7831.04	1.68
QV1.1	Hydrogen	2	1	5.81E+05	145.20	7723.07	1.93
QV1.1	Hydrogen	3	1	4.68E+05	1.65	8269.31	0.83
QV1.1	Hydrogen Control	1	1	0.00E+00	327.08	6417.36	1.83
QV1.1	Hydrogen Control	2	1	0.00E+00	327.85	7909.61	2.26
QV1.1	Hydrogen	1	2	8.53E+05	13.29	4073.20	2.49
QV1.1	Hydrogen	2	2	6.51E+05	46.05	3165.11	1.44

Table C.2. (cont'd).

Well	Treatment	Biological Replicate	Timepoint	Cell Abundance (cells/mL)	Headspace H_2 (ppm)	Headspace CH_4 (ppm)	Acetate (μM)
QV1.1	Hydrogen	3	2	3.51E+05	23.44	4206.39	3.08
QV1.1	Hydrogen Control	1	2	0.00E+00	180.77	4330.29	0.74
QV1.1	Hydrogen Control	2	2	0.00E+00	217.01	4094.59	0.47
QV1.1	Hydrogen	1	3	5.19E+05	59.78	3031.24	0.86
QV1.1	Hydrogen	2	3	2.23E+05	12.10	3696.10	1.39
QV1.1	Hydrogen	3	3	1.47E+06	49.05	2766.80	2.44
QV1.1	Hydrogen Control	1	3	3.06E+03	186.94	2936.86	1.19
QV1.1	Hydrogen Control	2	3	1.83E+04	109.51	1692.16	1.36
QV1.1	Hydrogen	1	4	3.30E+05	8.76	1829.50	1.52
QV1.1	Hydrogen	2	4	4.31E+05	12.89	2111.50	2.83
QV1.1	Hydrogen	3	4	1.60E+06	17.46	2313.10	4.08
QV1.1	Hydrogen Control	1	4	0.00E+00	137.87	2164.54	1.00
QV1.1	Hydrogen Control	2	4	0.00E+00	84.29	2905.42	0.57
QV1.1	Acetate	1	0	7.98E+05	104.49	12751.75	2.05
QV1.1	Acetate	2	0	2.54E+05	159.04	9284.88	0.17
QV1.1	Acetate	3	0	6.42E+04	216.84	13886.45	2.29
QV1.1	Acetate Control	1	0	3.06E+03	194.21	14180.89	0.37
QV1.1	Acetate Control	2	0	0.00E+00	171.39	14952.46	0.39
QV1.1	Acetate	1	1	3.70E+05	16.31	5073.41	13.16
QV1.1	Acetate	2	1	2.78E+05	8.97	5745.73	10.64
QV1.1	Acetate	3	1	1.71E+05	15.87	4217.54	7.98
QV1.1	Acetate Control	1	1	0.00E+00	212.66	4705.36	10.877
QV1.1	Acetate Control	2	1	0.00E+00	308.36	8707.70	19.91
QV1.1	Acetate	1	2	5.29E+05	7.10	4527.24	11.16
QV1.1	Acetate	2	2	3.30E+05	10.22	3443.60	9.96
QV1.1	Acetate	3	2	9.20E+05	5.65	4412.65	**broken**
QV1.1	Acetate Control	1	2	0.00E+00	141.43	4660.57	20.03
QV1.1	Acetate Control	2	2	0.00E+00	208.09	5197.29	21.57
QV1.1	Acetate	1	3	1.04E+06	0.03	2996.41	6.93
QV1.1	Acetate	2	3	1.05E+06	3.88	2546.33	4.28
QV1.1	Acetate	3	3	9.84E+05	0.00[a]	4217.15	7.69
QV1.1	Acetate Control	1	3	1.53E+04	119.33	2817.43	19.38
QV1.1	Acetate Control	2	3	9.17E+03	164.83	3934.32	7.42
QV1.1	Acetate	1	4	9.69E+05	0.64	2904.42	4.57
QV1.1	Acetate	2	4	1.04E+06	3.18	1394.17	3.74
QV1.1	Acetate	3	4	6.91E+05	0.94	1986.02	3.79
QV1.1	Acetate Control	1	4	0.00E+00	99.95	3118.20	25.30

Table C.2. (cont'd).

Well	Treatment	Biological Replicate	Timepoint	Cell Abundance (cells/mL)	Headspace H_2 (ppm)	Headspace CH_4 (ppm)	Acetate (μM)
QV1.1	Acetate Control	2	4	3.06E+03	60.85	3116.28	26.15
N08-B	Live Control	1	0	5.93E+05	19.61	18986.43	4.17
N08-B	Live Control	1	1	3.09E+05	7.62	12734.97	2.15
N08-B	Live Control	1	2	1.48E+06	3.57	5251.73	0.9
N08-B	Live Control	1	3	2.32E+05	0.00[a]	2106.19	0.38
N08-B	Live Control	1	4	1.01E+06	0.00[a]	707.54	2.46
QV1.1	Live Control	1	0	2.87E+05	109.97	18986.43	1.43
QV1.1	Live Control	1	1	1.59E+05	3.16	12734.97	1.76
QV1.1	Live Control	1	2	5.04E+05	10.82	5251.73	1.66
QV1.1	Live Control	1	3	1.07E+05	1.82	2106.19	1.65
QV1.1	Live Control	1	4	3.15E+05	0.00[a]	707.54	1.56

[a] =sample below detection limit. Concentration assumed to be zero.

broken = sample container was broken. Sample could not be analyzed.

Table C.3. Drilling Experiment PERMANOVA Results.

Variable	Degrees of Freedom	Sum of Squares	Mean Squares	F Score	R^2	p-value
Well	1	0.571	0.571	23.674	0.387	0.001
Days	1	0.355	0.355		0.241	0.001
CH_4 (ppm)	1	0.128	0.128	5.328	0.087	0.057
H_2 (ppm)	1	0.271	0.271	11.221	0.183	0.001
Acetate (μM)	1	0.029	0.029	1.222	0.020	0.307
Residuals	5	0.121	0.024		0.082	
Total	10	1.475			1.000	

REFERENCES

REFERENCES

1. Bar-On Y.M., Phillips R., Milo R. The biomass distribution on Earth. *Proc Natl Acad Sci USA*, (2018). doi:10.1073/pnas.1711842115

2. Lin C., Larsen E.I., Larsen G.R., Cox M.E., Smith J.J. Bacterially mediated iron cycling and associated biogeochemical processes in a subtropical shallow coastal aquifer: implications for groundwater quality. *Hydrobiologia*, (2012). doi:10.1007/s10750-012-1184-z

3. Anantharaman K., Brown C.T., Hug L.A., Sharon I., Castelle C.J., Probst A.J., Thomas B.C., Singh A., Wilkins M.J., Karaoz U., Brodie E.L., Williams K.H., Hubbard S.S., Banfield J.F. Thousands of microbial genomes shed light on interconnected biogeochemical processes in an aquifer system. *Nature Communications*, 7 (2016). doi:10.1038/ncomms13219

4. Lau M.C.Y., Kieft T.L., Kuloyo O., Linage-Alvarez B., van Heerden E., Lindsay M.R., Magnabosco C., Wang W., Wiggins J.B., Guo L., Perlman D.H., Kyin S., Shwe H.H., Harris R.L., Oh Y., Yi M.J., Purtschert R., Slater G.F., Ono S., Wei S., Li L., Lollar B.S., Onstott T.C. An oligotrophic deep-subsurface community dependent on syntrophy is dominated by sulfur-driven autotrophic denitrifiers. *Proc Natl Acad Sci USA*, (2016). doi:10.1073/pnas.1612244113

5. Stegen J.C., Fredrickson J.K., Wilkins M.J., Konopka A.E., Nelson W.C., Arntzen E.V., Chrisler W.B., Chu R.K., Danczak R.E., Fansler S.J., Kennedy D.W., Resch C.T., Tfaily M. Groundwater–surface water mixing shifts ecological assembly processes and stimulates organic carbon turnover. *Nature Communications*, 7 (2016). doi:10.1038/ncomms11237

6. Hall E.K., Bernhardt E.S., Bier R.L., Bradford M.A., Boot C.M., Cotner J.B., del Giorgio P.A., Evans S.E., Graham E.B., Jones S.E., Lennon J.T., Locey K.J., Nemergut D., Osborne B.B., Rocca J.D., Schimel J.P., Waldrop M.P., Wallenstein M.D. Understanding how microbiomes influence the systems they inhabit. *Nature Microbiology*, 3(September):977–82 (2018). doi:10.1038/s41564-018-0201-z

7. Fuhrman J.A., Hewson I., Schwalbach M.S., Steele J.A., Brown M.V., Naeem S. Annually reoccurring bacterial communities are predictable from ocean conditions. *Proc Natl Acad Sci USA*, 103(35):13104–9 (2006). doi:10.1073/pnas.0602399103

8. Cermeño P., de Vargas C., Abrantes F., Falkowski P.G. Phytoplankton Biogeography and Community Stability in the Ocean. *PLoS ONE*, 5(4) (2010). doi:10.1371/journal.pone.0010037

9. Creamer C.A., de Menezes A.B., Krull E.S., Sanderman J., Newton-Walters R., Farrell M. Microbial community structure mediates response of soil C decomposition to litter addition

and warming. *Soil Biology and Biochemistry*, 80:175–88 (2015). doi:10.1016/j.soilbio.2014.10.008

10. Bastida F., Torres I.F., Hernández T., García C. The impacts of organic amendments: Do they confer stability against drought on the soil microbial community? *Soil Biology and Biochemistry*, 113:173–83 (2017). doi:10.1016/j.soilbio.2017.06.012

11. Gravuer K., Eskelinen A. Nutrient and rainfall additions shift phylogenetically estimated traits of soil microbial communities. *Frontiers in Microbiology*, 8(JUL):1–16 (2017). doi:10.3389/fmicb.2017.01271

12. de Vries F.T., Shade A. Controls on soil microbial community stability under climate change. *Frontiers in Microbiology*, 4(September):1–16 (2013). doi:10.3389/fmicb.2013.00265

13. Evans S.E., Wallenstein M.D. Climate change alters ecological strategies of soil bacteria. *Ecology Letters*, 17:155–64 (2014). doi:10.1111/ele.12206

14. Lee S.-H., Sorensen J.W., Grady K.L., Tobin T.C., Shade A. Divergent extremes but convergent recovery of bacterial and archaeal soil communities to an ongoing subterranean coal mine fire. *The ISME Journal*, 11(6):1447–59 (2017). doi:10.1038/ismej.2017.1

15. Trias R., Ménez B., le Campion P., Zivanovic Y., Lecourt L., Lecoeuvre A., Schmitt-Kopplin P., Uhl J., Gislason S.R., Alfredsson H.A., Mesfin K.G., Snaebjörnsdóttir S.O., Aradóttir E.S., Gunnarsson I., Matter J.M., Stute M., Oelkers E.H., Gérard E. High reactivity of deep biota under anthropogenic CO_2 injection into basalt. *Nature Communications*, 8(1) (2017). doi:10.1038/s41467-017-01288-8

16. Sorensen J.W., Shade A. Dormancy dynamics and dispersal contribute to soil microbiome resilience. *Philosophical Transactions of the Royal Society B*, 375 (2020). doi:10.1098/rstb.2019.0255

17. Allison S.D., Martiny J.B.H. Resistance, resilience, and redundancy in microbial communities. *Proc Natl Acad Sci USA*, 105 (2008). doi:10.1073/pnas.0801925105.

18. Shade A., Peter H., Allison S.D., Baho D.L., Berga M., Bürgmann H., Huber D.H., Langenheder S., Lennon J.T., Martiny J.B.H., Matulich K.L., Schmidt T.M., Handelsman J. Fundamentals of microbial community resistance and resilience. *Frontiers in Microbiology*, 3(DEC):1–19 (2012). doi:10.3389/fmicb.2012.00417

19. Knelman J.E., Nemergut D.R. Changes in community assembly may shift the relationship between biodiversity and ecosystem function. *Frontiers in Microbiology*, 5(August):1–4 (2014). doi:.3389/fmicb.2014.00424

20. Graham E.B., Knelman E.K., Schindlbacher A., Siciliano S., Breulmann M., Yannarell A., Beman J.M., Abell G., Philippot L., Prosser J., Foulquier A., Yuste J.C., Glanville H.C., Jones D.L., Angel R., Salminen J., Newton R.J., Bürgmann H., Ingram L.J., Hamer U., Siljanen H.M.P., Peltoniemi K., Potthast K., Bañeras L., Hartmann M., Banerjee S., Yu R-

Q., Nogaro G., Richter A., Koranda M., Castle S.C., Goberna M., Song B., Chatterjee A., Nunes O.C., Lopes A.R., Cao Y., Kaisermann A., Hallin S., Strickland M.S., Garcia-Pausas J., Barba J., Kang H., Isobe K., Papaspyrou S., Pastorelli R., Lagomarsino A., Lindström E.S., Basiliko N., Nemergut D.R. Microbes as Engines of Ecosystem Function: When Does Community Structure Enhance Predictions of Ecosystem Processes? *Frontiers in Microbiology*, 7(February):1–10 (2016). doi:10.3389/fmicb.2016.00214

21. Shade A. Understanding Microbiome Stability in a Changing World. *MSystems*, 3(2):e00157-17 (2018). doi:10.1128/mSystems.00157-17

22. Widder S., Allen R.J., Pfeiffer T., Curtis T.P., Wiuf C., Sloan W.T., Cordero O.X., Brown S.P., Momeni B., Shou W., Kettle H., Flint H.J., Haas A.F., Laroche B., Kreft J-U., Rainey P.B., Freilich S., Schuster S., Milferstedt K., van der Meer J.R., Groβkopf T., Huisman J., Free A., Picioreanu C., Quince C., Klapper I., Labarthe S., Smets B.F., Wang H., Isaac Newton Institute Fellows, Soyer O.S. Challenges in microbial ecology: building predictive understanding of community function and dynamics. *The ISME Journal*, 10(November 2015):2557–68 (2016). doi:10.1038/ismej.2016.45

23. Aeschbach-Hertig W., Gleeson T. Regional strategies for the accelerating global problem of groundwater depletion. *Nature Geoscience*, 5(December) (2012). doi:10.1038/ngeo1617

24. Lall U., Josset L., Russo T. A Snapshot of the World's Groundwater Challenges. *Annu. Rev. Environ. Resour.*, 45:171–96 (2020). doi:10.1146/annurev-environ-102017-025800

25. Vaughan A.P.M., Scarrow J.H. Ophiolite obduction pulses as a proxy indicator of superplume events? *Earth and Planetary Science Letters*, 213 (2003). doi:10.1016/S0012-821X(03)00330-3

26. Vithanage M., Kumarathilaka P., Oze C., Karunatilake S., Seneviratne M., Hseu Z-Y., Gunarathne V., Dassanayake M., Sik Ok Y., Rinklebe J. Occurrence and cycling of trace elements in ultramafic soils and their impacts on human health: A critical review. *Environment International*, 131(August 2018) (2019). doi:10.1016/j.envint.2019.104974

27. Schrenk M.O., Brazelton W.J., Lang S.Q. Serpentinization, carbon, and deep life. *Reviews in Mineralogy and Geochemistry*, 75:575–606 (2013). doi:10.2138/rmg.2013.75.18

28. Sleep N.H., Meibom A., Fridriksson Th., Coleman R.G., Bird D.K. H_2-rich fluids from serpentinization: Geochemical and biotic implications. *Proc Natl Acad Sci USA*, 101(35):12818–23 (2004). doi:10.1073/pnas.0405289101

29. McCollom T.M. Laboratory Simulations of Abiotic Hydrocarbon Formation in Earth's Deep Subsurface. *Reviews in Mineralogy & Geochemistry*, 75:467–94 (2013). doi:10.2138/rmg.2013.75.15

30. Preiner M., Xavier J.C., Sousa F.L., Zimorski V., Neubeck A., Lang S.Q., Greenwell H.C., Kleinermanns K., Tüysüz H., McCollom T.M., Holm N.G., Martin W.F. Serpentinization: Connecting Geochemistry, Ancient Metabolism and Industrial Hydrogenation. *Life*, 8(4) (2018). doi:10.3390/life8040041

31. McCollom T.M., Bach W. Thermodynamic constraints on hydrogen generation during serpentinization of ultramafic rocks. *Geochimica et Cosmochimica Acta*, 73(3):856–75 (2009). doi: 10.1016/j.gca.2008.10.032

32. Suzuki S., Kuenen J.G., Schipper K., van der Velde S., Ishii S., Wu A., Sorokin D.Y., Tenney A., Meng X., Morrill P.L., Kamagata Y., Muyzer G., Nealson K.H. Physiological and genomic features of highly alkaliphilic hydrogen-utilizing Betaproteobacteria from a continental serpentinizing site. *Nature Communications*, 5 (2014). doi:10.1038/ncomms4900

33. Putman L.I., Sabuda M.C., Brazelton W.J., Kubo M.D., Hoehler T.M., McCollom T.M., Cardace D., Schrenk M.O. Microbial communities in a serpentinizing aquifer are assembled through strong concurrent dispersal limitation and selection. *mSystems*, (2021). doi:10.1128/mSystems.00300-21

34. Brazelton W.J., Nelson B., Schrenk M.O. Metagenomic evidence for H_2 oxidation and H_2 production by serpentinite-hosted subsurface microbial communities. *Frontiers in Microbiology*, 2 (2012). doi:10.3389/fmicb.2011.00268

35. Kohl L., Cumming E., Cox A., Rietze A., Morrissey L., Lang S.Q., Richter A., Suzuki S., Nealson K.H., Morrill P.L. Exploring the metabolic potential of microbial communities in ultra-basic, reducing springs at The Cedars, CA, USA: Experimental evidence of microbial methanogenesis and heterotrophic acetogenesis. *Journal of Geophysical Research: Biogeosciences*, 121(4):1203–20 (2016). doi: 10.1002/2015JG003233

36. Brazelton W.J., Thornton C.N., Hyer A., Twing K.I., Longino A.A., Lang S.Q., Lilley M.D., Früh-Green G.L., Schrenk M.O. Metagenomic identification of active methanogens and methanotrophs in serpentinite springs of the Voltri Massif, Italy. *PeerJ*, (2017). doi:10.7717/peerj.2945

37. Crespo-Medina M., Twing K.I., Sánchez-Murillo R., Brazelton W.J., McCollom T.M., Schrenk M.O. Methane dynamics in a tropical serpentinizing environment: The Santa Elena Ophiolite, Costa Rica. *Frontiers in Microbiology*, 8(MAY):1–14 (2017). doi:10.3389/fmicb.2017.00916

38. Twing K.I., Brazelton W.J., Kubo M.D.Y., Hyer A.J., Cardace D., Hoehler T.M., McCollom T.M., Schrenk M.O. Serpentinization-Influenced Groundwater Harbors Extremely Low Diversity Microbial Communities Adapted to High pH. *Frontiers in Microbiology*, 8:308 (2017). doi:10.3389/fmicb.2017.00308

39. Rempfert K.R., Miller H.M., Bompard N., Nothaft D., Matter J.M., Kelemen P., Fierer N., Templeton A.S. Geological and geochemical controls on subsurface microbial life in the Samail Ophiolite, Oman. *Frontiers in Microbiology*, 8 (2017). doi:10.3389/fmicb.2017.00056

40. Fones E.M., Colman D.R., Kraus E.A., Nothaft D.B., Poudel S., Rempfert K.R., Spear J.R., Templeton A.S., Boyd E.S. Physiological adaptations to serpentinization in the Samail Ophiolite, Oman. *The ISME Journal* (2019). doi:10.1038/s41396-019-0391-2

41. Sabuda M.C., Brazelton W.J., Putman L.I., McCollom T.M., Hoehler T.M., Kubo M.D.Y., Cardace D., Schrenk M.O. A dynamic microbial sulfur cycle in a serpentinizing continental ophiolite. *Environmental Microbiology*, 22:2329–45 (2020). doi:10.1111/1462-2920.15006

42. Sabuda M.C., Putman L.I., Hoehler T.M., Kubo M.D., Brazelton W.J., Schrenk M.O. Biogeochemical Gradients in a Serpentinization-Influenced Aquifer: Implications for Gas Exchange between the Subsurface and Atmosphere. *Journal of Geophysical Research: Biogeosciences*, 126, e2020JG006209 (2021). doi:10.1029/2020JG006209

43. Seyler L.M., Brazelton W.J., McLean C., Putman L.I., Hyer A., Kubo M.D.Y., Hoehler T., Cardace D., Schrenk M.O. Carbon Assimilation Strategies in Ultrabasic Groundwater: Clues from the Integrated Study of a Serpentinization-Influenced Aquifer. *mSystems*, 5(2):1–17 (2020. doi:10.1128/mSystems.00607-19

44. Cardace D., Hoehler T., Mccollom T., Schrenk M., Carnevale D., Kubo M., Twing, K. Establishment of the Coast Range ophiolite microbial observatory (CROMO): drilling objectives and preliminary outcomes. *Scientific Drilling*, 16:45–55 (2013). doi:10.5194/sd-16-45-2013

45. Conze R., Coggon J.A., Matter J. ICDP Oman Drilling Project: News from the Scientific Drilling in the Samail Ophiolite Sultanate of Oman. *ECORD Newsletter*, 28 (2017). doi:10.14379/OmanDP.proc.2020

46. Früh-Green G.L., Orcutt B.N., Green S., Cotterill C., Expedition 357 Scientists. Expedition 357 Preliminary Report: Atlantis Massif Serpentinization and Life. *International Ocean Discovery Program*, (2016). doi:10.14379/iodp.pr.357.2016

47. Song H-S., Stegen J.C., Graham E.B., Scheibe T.D. Historical Contingency in Microbial Resilience to Hydrologic Perturbations. *Frontiers in Water*, 3(February):1–10 (2021). doi:10.3389/frwa.2021.590378

48. Bjornstad B.N., McKinley J.P., Stevens T.O., Rawson S.A., Fredrickson J.K., Long P.E. Generation of Hydrogen Gas as a Result of Drilling Within the Saturated Zone. Vol. 14, *Groundwater Monitoring & Remediation*, 14;140–7 (1994). doi:10.1111/j.1745-6592.1994.tb00492.x

49. Fritsch J., Scheerer P., Frielingsdorf S., Kroschinsky S., Friedrich B., Lenz O., Spahn C.M.T. The crystal structure of an oxygen-tolerant hydrogenase uncovers a novel iron-sulphur centre. *Nature*, 479:3–7 (2011). doi:10.1038/nature10505

50. Peters J.W., Schut G.J., Boyd E.S., Mulder D.W., Shepard E.M., Broderick J.B., King P.W., Adams M.W.W. [FeFe]- and [NiFe]- hydrogenase diversity, mechanism, and maturation. *Biochimica et Biophysica Acta*, 1853(6):1350–69 (2015). doi:10.1016/j.bbamcr.2014.11.021

51. Lever M.A. Acetogenesis in the energy-starved deep biosphere-a paradox? *Frontiers in Microbiology*, 2(JAN):1–18 (2012). doi:10.3389/fmicb.2011.00284

52. Preiner M., Igarashi K., Muchowska K.B., Yu M., Varma S.J., Kleinermanns K., Nobu M.K., Kamagata Y., Tüysüz H., Moran J., Martin W.F. A hydrogen-dependent geochemical analogue of primordial carbon and energy metabolism. *Nature Ecology & Evolution*, 4(April) (2020). doi:10.1038/s41559-020-1125-6

53. Lovley D.R., Chapelle F.H. Deep Subsurface Microbial Processes. *Reviews of Geophysics*, (1995). doi:10.1029/95RG01305

54. Pedersen K. Microbial life in deep granitic rock. *FEMS Microbiology Reviews*, 20:399–414 (1997). doi:10.1111/j.1574-6976.1997.tb00325.x

55. Purkamo L., Bomberg M., Nyyssönen M., Ahonen L., Kukkonen I., Itävaara M. Response of Deep Subsurface Microbial Community to Different Carbon Sources and Electron Acceptors during ~ 2 months Incubation in Microcosms. *Frontiers in Microbiology*, 8(February) (2017). doi:10.3389/fmicb.2017.00232

56. Nuppunen-Puputti M., Purkamo L., Kietäväinen R., Nyyssönen M., Itävaara M., Ahonen L., Kukkonen I., Bomberg M. Rare Biosphere Archaea Assimilate Acetate in Precambrian Terrestrial Subsurface at 2.2 km Depth. *geosciences*, (2018). doi:10.3390/geosciences8110418

57. Crespo-Medina M., Twing K.I., Kubo M.D.Y., Hoehler T.M., Cardace D., McCollom T., Schrenk M.O. Insights into environmental controls on microbial communities in a continental serpentinite aquifer using a microcosm-based approach. *Frontiers in Microbiology*, 5:604 (2014). doi:10.3389/fmicb.2014.00604

58. Kojima H., Fukui M. *Sulfuritalea hydrogenivorans* gen. nov., sp. nov., a facultative autotroph isolated from a freshwater lake. *International Journal of Systematic and Evolutionary Microbiology*, 61:1651–5 (2011). doi:10.1099/ijs.0.024968-0

59. Brazelton W.J., Morrill P.L., Szponar N., Schrenk M.O. Bacterial communities associated with subsurface geochemical processes in continental serpentinite springs. *Applied and Environmental Microbiology*, 79(13):3906–16 (2013). doi:10.1128/AEM.00330-13

60. Melton E.D., Sorokin D.Y., Overmars L., Lapidus A.L., Pillay M., Ivanova N., Glavina del Rio T., Kyrpides N.C., Woyke T., Muyzer G. Draft genome sequence of *Dethiobacter alkaliphilus* strain AHT1^{T}, a gram-positive sulfidogenic polyextremophile. *Standards in Genomic Sciences*, 12(57):1–9 (2017). doi:10.1186/s40793-017-0268-9

61. Pierce E., Xie G., Barabote R.D., Saunders E., Han C.S., Detter J.C., Richardson P., Brettin T.S., Das A., Ljungdahl L.G., Ragsdale S.W. The complete genome sequence of *Moorella thermoacetica* (f. *Clostridium thermoaceticum*). *Environmental Microbiology*, 10(10):2550–73 (2008). doi:10.1111/j.1462-2920.2008.01679.x

62. Poehlein A., Keyl A., Milsch J.C., Daniel R. Draft Genome Sequence of the Thermophilic Acetogen *Moorella humiferrea* DSM 23265. *Genome Announcements*, 6(17):1–2 (2018). doi:10.1128/genomeA.00357-18

63. Ivanova N., Rohde C., Munk C., Nolan M., Lucas S., Glavina Del Rio T., Tice H., Deshpande S., Cheng J.-F., Tapia R., Han C., Goodwin L., Pitluck S., Liolios K., Mavromatis K., Mikhailova N., Pati A., Chen A., Palaniappan K., Land M., Hauser L., Chang Y.-J., Jeffries C.D., Brambilla E., Rohde M., Göker M., Tindall B.J., Woyke T., Bristow J., Eisen J.A., Markowitz V., Hugenholtz P., Kyrpides N.C., Klenk H.-P., Lapidus A. Complete genome sequence of *Truepera radiovictrix* type strain (RQ-24^{T}). *Standards in Genomic Sciences*, 4:91–9 (2011). doi:10.4056/sigs.1563919

64. Watanabe T., Kojima H., Fukui M. Complete genomes of freshwater sulfur oxidizers *Sulfuricella denitrificans* skB26 and *Sulfuritalea hydrogenivorans* sk43H: Genetic insights into the sulfur oxidation pathway of betaproteobacteria. *Systematic and Applied Microbiology*, 37(6):387–95 (2014). doi:10.1016/j.syapm.2014.05.010

65. Jousset A., Bienhold C., Chatzinotas A., Gallien L., Gobet A., Kurm V., Küsel K., Rillig M.C., Rivett D.W., Salles J.F., van der Heijden M.G.A., Youssef N.H., Zhang X., Wei Z., Gera Hol W.H. Where less may be more: how the rare biosphere pulls ecosystems strings. *The ISME Journal*, 11:853–62 (2017). doi:10.1038/ismej.2016.174

66. Glombitza C., Putman L.I., Rempfert K.R., Kubo M.D., Schrenk M.O., Templeton A.S., Hoehler T.M. Active microbial sulfate reduction in fluids of serpentinizing peridotites of the continental subsurface. *Communications Earth & Environment*, 2(84):1-9 (2021). doi:10.1038/s43247-021-00157-z

67. Müller-Santos M., Koskimäki J.J., Alves L.P.S., de Sousa E.M., Jendrossek D., Pirttilä A.M. The protective role of PHB and its degradation products against stress situations in bacteria. *FEMS Microbiology Reviews*, 45(October 2020):1–13 (2021). doi:10.1093/femsre/fuaa058

68. Hahn M.W., Lünsdorf H., Wu Q., Schauer M., Höfle M.G., Boenigk J., Stadler P. Isolation of Novel Ultramicrobacteria Classified as Actinobacteria from Five Freshwater Habitats in Europe and Asia. *Applied and Environmental Microbiology*, 69(3):1442–51 (2003). doi:10.1128/AEM.69.3.1442

69. Brown C.T., Hug L.A., Thomas B.C., Sharon I., Castelle C.J., Singh A., Wilkins M.J., Wrighton K.C., Williams K.H., Banfield J.F. Unusual biology across a group comprising more than 15% of domain Bacteria. *Nature*, 523 (2015). doi:10.1038/nature14486

70. Luef B., Frischkorn K.R., Wrighton K.C., Holman H.-Y.N., Birarda G., Thomas B.C., Singh A., Williams K.H., Siegerist C.E., Tringe S.G., Downing K.H., Comolli L.R., Banfield J.F. Diverse uncultivated ultra-small bacterial cells in groundwater. *Nature Communications*, 6(6372) (2015). doi:10.1038/ncomms7372

71. Nakai R. Size Matters: Ultra-small and Filterable Microorganisms in the Environment. *Microbes and Environments*, 35(2):1–11 (2020). doi:10.1264/jsme2.ME20025

72. Wang Y., Hammes F., Boon N., Egli T. Quantification of the Filterability of Freshwater Bacteria through 0.45, 0.22, and 0.1 µm Pore Size Filters and Shape-Dependent Enrichment of Filterable Bacterial Communities. *Environmental Science and Technology*, 41(20):7080–6 (2007). doi:10.1021/es0707198

73. Park J.W., Young J.L., Meyer A.S., Douterelo I., Maeng S.K. Bacterial growth through microfiltration membranes and NOM characteristics in an MF-RO integrated membrane system: Lab-scale and full-scale studies. *Water Research*, 144:36–45 (2018). doi:10.1016/j.watres.2018.07.027

74. Liu J., Li B., Wang Y., Zhang G., Jiang X., Li X. Passage and community changes of filterable bacteria during microfiltration of a surface water supply. *Environment International*, 131(March) (2019). doi:10.1016/j.envint.2019.104998

75. Tian R., Ning D., He Z., Zhang P., Spencer S.J., Gao S., Shi W., Wu L., Zhang Y., Yang Y., Adams B.G., Rocha A.M., Detienne B.L., Lowe K.A., Joyner D.C., Klingeman D.M., Arkin A.P., Fields M.W., Hazen T.C., Stahl D.A., Alm E.J., Zhou J. Small and mighty: adaptation of superphylum *Patescibacteria* to groundwater environment drives their genome simplicity. *Microbiome*, 8(51) (2020). doi:10.1186/s40168-020-00825-w

76. Proctor C.R., Besmer M.D., Langenegger T., Beck K., Walser J.-C., Ackermann M., Bürgmann H., Hammes F. Phylogenetic clustering of small low nucleic acid-content bacteria across diverse freshwater ecosystems. *The ISME Journal*, 12:1344–59 (2018). doi:

77. Mayhew L.E., Ellison E.T., McCollom T.M., Trainor T.P., Templeton A.S. Hydrogen generation from low-temperature water-rock reactions. *Nature Geoscience*, 6(6):478–84 (2013). doi:10.1038/ngeo1825

78. Ortiz E., Tominaga M., Cardace D., Schrenk M.O., Hoehler T.M., Kubo M.D., Rucker D.F. Geophysical Characterization of Serpentinite Hosted Hydrogeology at the McLaughlin Natural Reserve, Coast Range Ophiolite. *Geochemistry, Geophysics, Geosystems*, 19(1):114–31 (2018). doi:10.1002/2017GC007001

79. Schrenk M.O., Kelley D.S., Delaney J.R., Baross J.A. Incidence and Diversity of Microorganisms within the Walls of an Active Deep-Sea Sulfide Chimney. *Applied and Environmental Microbiology*, 69(6):3580–92 (2003). doi:10.1128/AEM.69.6.3580

80. Schloss P.D., Westcott S.L., Ryabin T., Hall J.R., Hartmann M., Hollister E.B., Lesniewski R.A., Oakley B.B., Parks D.H., Robinson C.J., Sahl J.W., Stres B., Thallinger G.G., Van Horn D.J., Weber C.F. Introducing mothur: Open-source, platform-independent, community-supported software for describing and comparing microbial communities. *Applied and Environmental Microbiology*, 75(23):7537–41 (2009). doi:10.1128/AEM.01541-09

81. Rognes T., Flouri T., Nichols B., Quince C., Mahé F. VSEARCH: A versatile open source tool for metagenomics. *PeerJ*, (10):1–22 (2016). doi:10.7717/peerj.2584

82. Schloss P.D., Westcott S.L. Assessing and Improving Methods Used in Operational Taxonomic Unit-Based Approaches for 16S rRNA Gene Sequence Analysis. *Applied and Environmental Microbiology*, 77(10):3219–26 (2011). doi:10.1128/AEM.02810-10

83. Westcott S.L., Schloss P.D. De novo clustering methods outperform reference-based methods for assigning 16S rRNA gene sequences to operational taxonomic units. *PeerJ*, 3:e1487 (2015). doi:10.7717/peerj.1487

84. Sheik C.S., Reese B.K., Twing K.I., Sylvan J.B., Grim S.L., Schrenk M.O., Sogin M.L., Colwell F.S. Identification and removal of contaminant sequences from ribosomal gene databases: Lessons from the Census of Deep Life. *Frontiers in Microbiology*, 9(APR):1–14 (2018). doi:10.3389/fmicb.2018.00840

85. Fullerton K.M., Schrenk M.O., Yücel M., Manini E., Basili M., Rogers T.J., Fattorini D., Di Carlo M., d'Errico G., Regoli F., Nakagawa M., Vetriani C., Smedile F., Ramírez C., Miller H., Morrison S.M., Buongiorno J., Jessen G.L., Steen A.D., Martínez, M., Maarten de Moor J., Barry P.H., Giovannelli D., Lloyd K.G. Effect of tectonic processes on biosphere-geosphere feedbacks across a convergent margin. *Nature Geoscience*, 14(May) (2021). doi:10.1038/s41561-021-00725-0

86. Zhang Z., Schwartz S., Wagner L., Miller W. A Greedy Algorithm for Aligning DNA Sequences. *Journal of Computational Biology*, 7:203–14 (2000). doi:10.1089/10665270050081478

87. R Core Team. R: A language and environment for statistical computing. *R Foundation for Statistical Computing, Vienna, Austria*, (2014). url:http://www.R-project.org/

88. Wickham H. ggplot2: Elegant Graphics for Data Analysis. *Springer-Verlag New York*, (2016). url:https://ggplot2.tidyverse.org

89. Oksanen J., Blanchet F.G., Friendly M., Kindt R., Legendre P., McGlinn D., Minchin P.R., O'Hara R.B., Simpson G.L., Solymos P., Stevens M.H.H., Szoecs E., Wagner H. vegan: Community Ecology Package. R package version 25-5 (2019). Available from: https://cran.r-project.org/package=vegan

90. McMurdie P.J., Holmes S. Phyloseq: An R Package for Reproducible Interactive Analysis and Graphics of Microbiome Census Data. *PLoS ONE*, 8(4) (2013). doi:10.1371/journal.pone.0061217

CHAPTER 5

Summary and Future Directions

Summary

The establishment of CROMO in 2011 provided direct access to the serpentinizing subsurface and served as a template for drilling and accessing subsurface fluids within ophiolites (1) and ultramafic massifs (2). Additionally, the convenient location and well-maintained field station at McLaughlin Reserve, Lower Lake, CA, USA allowed for easy access and relatively affordable long-term sampling of fluids from the site by an interdisciplinary team of researchers. This accessibility resulted in the large time series dataset that was used to assess community assembly (3) and microbial community responses to the injection of drilling fluid into the subsurface (**Ch. 3**). In the last decade, serpentinite microbial communities have primarily been investigated to understand the physiological adaptations that allow these populations to persist under carbon limited and extreme pH conditions (4–7) and to determine the role these microbial communities play in biogeochemical cycling in these systems (8–12). Despite great advances in our understanding of the composition and function of serpentinite microbial communities, our knowledge of the ecological processes that structure these communities and the capacity of microbial populations to respond to changes in their environment has been lacking.

This dissertation assessed community assembly processes (13,14) in the serpentinizing subsurface using a null ecological modeling technique (15) paired with assessments of microbial physiology and site hydrogeology and geochemistry (3; **Ch. 2**). Results revealed that slow fluid movement in the low permeability aquifer introduces significant stochasticity (ecological drift due to dispersal limitation) into the system, and that pH imposes a strong selective force on microbial populations, resulting in highly similar communities that utilize a variety of physiological

adaptations to manage pH homeostasis and carbon limitation (3; **Ch.2**). These findings highlight the important role that stochastic processes can play, even under extreme conditions where selection processes would be expected to dominate assembly (16).

This dissertation also assessed the impact of the injection of drilling fluid (sterile water) (17) on subsurface geochemistry and microbial community composition and function. This assessment used geochemistry and molecular biology samples collected directly from the site in the first five years following drilling (**Ch. 3**) as well as through a series of microcosm experiments performed on fluids from the site to assess microbial community responses to geochemical changes that were observed in the *in situ* dataset following drilling (**Ch. 4**). Results from the *in situ* dataset revealed that microbial populations from the candidate genus *Serpentinomonas* and the genus *Dethiobacter* flourished in the first two years after drilling activity and gradually decreased in abundance over time as dissolved oxygen concentrations decreased and fluids became more reducing (**Ch. 3**). Results from experimental microcosms showed a similar result, revealing that *Serpentinomonas,* a mixotrophic, facultative anaerobe, flourished under increased concentrations of oxygen, hydrogen, and acetate that occurred following drilling (**Ch. 4**). Additionally, a population of organisms related to *Dethiobacter alkaliphilus* persisted in one set of experiments, potentially performing acetogenesis under increased concentrations of hydrogen (**Ch. 4**). These findings highlight the impressive versatility of *Serpentinomonas,* which is a dominant microbial community member at most terrestrial sites of serpentinization, and demonstrate how substantial changes in subsurface geochemistry following a disturbance can alter microbial community composition and function for a substantial amount of time (**Ch. 4**). Results from **Chapter 3** and **Chapter 4** indicate that *Serpentinomonas* is an opportunistic r-strategist, taking advantage of favorable conditions and growing to extremely high abundances. This versatility and behavior

could explain why highly similar populations of *Serpentinomonas* are present at sites of serpentinization distributed throughout the globe. Finally, these results can inform the scientific design and assessment of geochemical and microbial community data collected from newly drilled wells into mafic and ultramafic lithologies.

Future Directions

A methodological improvement that could be made in the future as sequencing technology continues to improve and decrease in cost would be the incorporation of consistent metatranscriptomic or proteomic surveys of serpentinizing environments over time. Given the low biomass of these systems, obtaining enough genetic material from samples for gene amplicon sequencing can prove to be difficult in some cases (18). The increased required concentrations of genetic material needed for metagenomics and metatranscriptomics can make this effort even more difficult. Due to these challenges, metatranscriptomic data from serpentinizing ophiolites have only been published in the last two years, including data presented in **Chapter 2** (3,8,9,12). The metatranscriptomic data presented in **Chapter 2** (3) provided extremely useful information that supported interpretations of community assembly dynamics obtained from null modeling techniques employed on the 16S rRNA gene amplicon dataset. Had functional 'omics' data been collected from wells throughout the long-term sampling campaign, differences in the functional activity of microbial populations could have been assessed in response to the drilling disturbance (**Ch. 3**). Direct and quantitative evidence of the functional responses of populations from the genera *Serpentinomonas* and *Dethiobacter* would have been invaluable to the work presented here. Future investigations into the ecology and response of serpentinite microbial communities should

include a functional ‘omics’ component if sufficient RNA or protein can be extracted from collected samples.

With the addition of the study in **Chapter 2**, microbial community assembly in the deep subsurface in hard rock aquifers has only been assessed in three studies to date (3,19,20). Given the abundance of ophiolites on Earth (21) and importance of deep groundwater as a potable water source for future generations (22) it is critical that community assembly processes continue to be assessed in ophiolites and other hard rock aquifers (23). Differences in subsurface geochemistry, hydrology, and connectivity to the surface at different ophiolites likely alter assembly processes, resulting in observed differences in microbial community composition and function. Understanding the differing forces that structure these communities around the world will improve our capacity to manage and anticipate changes in microbial community composition and biogeochemical cycling associated with drilling activity, injection of water or substrate associated with fracking, carbon capture and sequestration or deep well injection (22,24).

Alterations to geochemical conditions and microbial community composition and function in the deep subsurface should continue to be assessed in response to environmental disturbances. Characterizing the response of microbial communities to different disturbances will be extremely important as new drilling projects into ophiolites are being proposed (25) and ophiolites continue to be considered as candidates for carbon capture and sequestration (24). The ability to anticipate the timeline and different types of responses from microbial populations will be vital for planning effective experimentation and monitoring after site establishment, and for determining the stability and longevity of mineralized carbon dioxide in the subsurface in the case of carbon sequestration.

Finally, community assembly processes and microbial responses to drilling activity observed in this dissertation can be used to inform current and future investigations of the Martian

subsurface by the current Mars rover, Perseverance. Perseverance landed on Mars in February of 2021 and is equipped to sample rock and regolith to search for signs of ancient life (26,27). The updated scientific payload on Perseverance, and potentially improved geophysical and drilling equipment on future rovers could help to detect signatures of past microbial activity associated with serpentinization (28) and sporadic groundwater upwelling from the subsurface to the surface (29). Sporadic groundwater upwelling in the past on Mars certainly could have stimulated growth and metabolism from ancient microbial-like life that could have existed in the ancient Martian subsurface (30). Evidence of this activity could potentially be detected by Perseverance in future expeditions or by future scientific investigations capable of sampling deeper into the subsurface of Mars.

REFERENCES

REFERENCES

1. Conze R., Coggon J.A., Matter J. ICDP Oman Drilling Project: News from the Scientific Drilling in the Samail Ophiolite Sultanate of Oman. *ECORD Newsletter*, 28 (2017). doi:10.14379/OmanDP.proc.2020

2. Früh-Green G.L., Orcutt B.N., Green S., Cotterill C., Expedition 357 Scientists. Expedition 357 Preliminary Report: Atlantis Massif Serpentinization and Life. *International Ocean Discovery Program*, (2016). doi:10.14379/iodp.pr.357.2016

3. Putman L.I., Sabuda M.C., Brazelton W.J., Kubo M.D., Hoehler T.M., McCollom T.M., Cardace D., Schrenk M.O. Microbial communities in a serpentinizing aquifer are assembled through strong concurrent dispersal limitation and selection. *mSystems*, (2021). doi:10.1128/mSystems.00300-21

4. Miller H.M., Matter J.M., Kelemen P., Ellison E.T., Conrad M.E., Fierer N., Ruchala T., Tominaga M., Templeton A.S. Modern water/rock reactions in Oman hyperalkaline peridotite aquifers and implications for microbial habitability. *Geochimica et Cosmochimica Acta*, 179:217–41 (2016). doi:10.1016/j.gca.2016.01.033

5. Rempfert K.R., Miller H.M., Bompard N., Nothaft D., Matter J.M., Kelemen P., Fierer N., Templeton A.S. Geological and geochemical controls on subsurface microbial life in the Samail Ophiolite, Oman. *Frontiers in Microbiology*, 8 (2017). doi:10.3389/fmicb.2017.00056

6. Twing K.I., Brazelton W.J., Kubo M.D.Y., Hyer A.J., Cardace D., Hoehler T.M., McCollom T.M., Schrenk M.O. Serpentinization-Influenced Groundwater Harbors Extremely Low Diversity Microbial Communities Adapted to High pH. *Frontiers in Microbiology*, 8:308 (2017). doi:10.3389/fmicb.2017.00308

7. Suzuki S., Kuenen J.G., Schipper K., van der Velde S., Ishii S., Wu A., Sorokin D.Y., Tenney A., Meng X., Morrill P.L., Kamagata Y., Muyzer G., Nealson K.H. Physiological and genomic features of highly alkaliphilic hydrogen-utilizing Betaproteobacteria from a continental serpentinizing site. *Nature Communications*, 5 (2014). doi:10.1038/ncomms4900

8. Sabuda M.C., Brazelton W.J., Putman L.I., McCollom T.M., Hoehler T.M., Kubo M.D.Y., Cardace D., Schrenk M.O. A dynamic microbial sulfur cycle in a serpentinizing continental ophiolite. *Environmental Microbiology*, 22:2329–45 (2020). doi:10.1111/1462-2920.15006

9. Seyler L.M., Brazelton W.J., McLean C., Putman L.I., Hyer A., Kubo M.D.Y., Hoehler T., Cardace D., Schrenk M.O. Carbon Assimilation Strategies in Ultrabasic Groundwater: Clues from the Integrated Study of a Serpentinization-Influenced Aquifer. *mSystems*, 5(2):1–17 (2020. doi:10.1128/mSystems.00607-19

10. Brazelton W.J., Nelson B., Schrenk M.O. Metagenomic evidence for H_2 oxidation and H_2 production by serpentinite-hosted subsurface microbial communities. *Frontiers in Microbiology*, 2 (2012). doi:10.3389/fmicb.2011.00268

11. Fones E.M., Colman D.R., Kraus E.A., Nothaft D.B., Poudel S., Rempfert K.R., Spear J.R., Templeton A.S., Boyd E.S. Physiological adaptations to serpentinization in the Samail Ophiolite, Oman. *The ISME Journal* (2019). doi:10.1038/s41396-019-0391-2

12. Kraus E.A., Nothaft D., Stamps B.W., Rempfert K.R., Ellison E.T., Matter J.M., Templeton A.S., Boyd E.S., Spear J.R. Molecular Evidence for an Active Microbial Methane Cycle in Subsurface Serpentinite-Hosted Groundwaters in the Samail Ophiolite, Oman. *Applied and Environmental Microbiology*, (August 2020):1–18 (2021). doi:10.1128/AEM.02068-20

13. Vellend M. Conceptual synthesis in community ecology. *The Quarterly Review of Biology*, 85(2):183–206 (2010). doi:10.1086/652373

14. Nemergut D.R., Schmidt S.K., Fukami T., O'Neill S.P., Bilinski T.M., Stanish L.F., Knelman J.E., Darcy J.L., Lynch R.C., Wickey P., Ferrenberg S. Patterns and Processes of Microbial Community Assembly. *Microbiology and Molecular Biology Reviews*, 77(3):342–56 (2013). doi:10.1128/MMBR.00051-12

15. Stegen J.C., Lin X., Fredrickson J.K., Konopka A.E. Estimating and mapping ecological processes influencing microbial community assembly. *Frontiers in Microbiology*, 6(MAY):1–15 (2015). doi:10.3389/fmicb.2015.00370

16. Tripathi B.M., Stegen J.C., Kim M., Dong K., Adams J.M., Lee Y.K. Soil pH mediates the balance between stochastic and deterministic assembly of bacteria. *The ISME Journal* (2018). doi:10.1038/s41396-018-0082-4

17. Cardace D., Hoehler T., Mccollom T., Schrenk M., Carnevale D., Kubo M., Twing, K. Establishment of the Coast Range ophiolite microbial observatory (CROMO): drilling objectives and preliminary outcomes. *Scientific Drilling*, 16:45–55 (2013). doi:10.5194/sd-16-45-2013

18. Wilkins M.J., Daly R.A., Mouser P.J., Trexler R., Sharma S., Cole D.R., Wrighton K.C, Biddle J.F., Denis E.H., Frederickson J.K., Kieft T.L., Onstott T.C., Peterson L., Pfiffner S.M., Phelps T.J., Schrenk M.O. Trends and future challenges in sampling the deep terrestrial biosphere. *Frontiers in Microbiology*, 5(SEP) (2014). doi:10.3389/fmicb.2014.00481

19. Beaton E.D., Stevenson B.S., King-Sharp K.J., Stamps B.W., Nunn H.S., Stuart M. Local and Regional Diversity Reveals Dispersal Limitation and Drift as Drivers for Groundwater Bacterial Communities from a Fractured Granite Formation. *Frontiers in Microbiology*, 7 (2016). doi:10.3389/fmicb.2016.01933

20. Danczak R.E., Daly R.A., Borton M.A., Stegen J.C., Roux S., Wrighton K.C., Wilkins M.J. Ecological assembly processes are coordinated between bacterial and viral communities in fractured shale ecosystems. *mSystems*, 5(2):1–13 (2020). doi:10.1128/mSystems.00098-20

21. Vaughan A.P.M., Scarrow J.H. Ophiolite obduction pulses as a proxy indicator of superplume events? *Earth and Planetary Science Letters*, 213 (2003). doi:10.1016/S0012-821X(03)00330-3

22. Lall U., Josset L., Russo T. A Snapshot of the World's Groundwater Challenges. *Annu. Rev. Environ. Resour.*, 45:171–96 (2020). doi:10.1146/annurev-environ-102017-025800

23. Pedersen K. Microbial life in deep granitic rock. *FEMS Microbiology Reviews*, 20:399–414 (1997). doi:10.1111/j.1574-6976.1997.tb00325.x

24. Kelemen P.B., Matter J., Streit E.E., Rudge J.F., Curry W.B., Blusztajn J. Rates and Mechanisms of Mineral Carbonation in Peridotite: Natural Processes and Recipes for Enhanced, in situ CO2 Capture and Storage. *Annual Review of Earth and Planetary Sciences*, (2011). doi:10.1146/annurev-earth-092010-152509

24. New Caledonia Peridotite Amphibious Drilling Workshop – Montpellier, France. 22-24 January 2019. Available from: https://newcaledoniadp.wordpress.com/

26. Williford K.H., Farley K.A., Stack K.M., Allwood A.C., Beaty D., Beegle L.W., Bhartia R., Brown A.J., de la Torre Juarez M., Hamran S.-E., Hecht M.H., Hurowitz J.A., Rodriguez-Manfredi J.A., Maurice S., Milkovich S., Wiens R.C. Chapter 11: The NASA Mars 2020 Rover Mission and the Search for Extraterrestrial Life. From Habitability to Life on Mars. *Elsevier Inc.*, 275–308 (2020). doi:10.1016/B978-0-12-809935-3.00010-4

27. Bosak T., Moore K.R., Gong J., Grotzinger J.P. Searching for biosignatures in sedimentary rocks from early Earth and Mars. *Nature Reviews Earth & Environment*, (2021). doi:10.1038/s43017-021-00169-5

28. Ehlmann B.L., Mustard J.F., Murchie S.L. Geologic setting of serpentine deposits on Mars. *Geophysical Research Letters*, 37 (2010). doi:10.1029/2010GL042596

29. Michalski J.R., Cuadros J., Niles P.B., Parnell J., Rogers A.D., Wright S.P. Groundwater activity on Mars and implications for a deep biosphere. *Nature Geoscience*, 6(2):133–8 (2013). doi:10.1038/ngeo1706

30. Michalski J.R., Onstott T.C., Mojzsis S.J., Mustard J., Chan Q.H.S., Niles P.B., Johnson S.S. The Martian subsurface as a potential window into the origin of life. *Nature Geoscience*, (2017). doi:10.1038/s41561-017-0015-2